National Technical University of Athens

School of Naval Architecture and Marine Engineering

Division of Marine Structures

Interdisciplinary Postgraduate Program

“Naval and Marine Technology and Science”

Master Thesis

“Study of metallic ship structure response subjected to thermomechanical loads”

Author

Stamatios D. Fanourgakis

Supervisor

Prof. Emmanuel S. Samuelides

Athens, Greece 2019

National Technical University of Athens

School of Naval Architecture and Marine Engineering

Division of Marine Structures

Interdisciplinary Postgraduate Program

"Naval and Marine Technology and Science"

Master Thesis

"Study of metallic ship structure response subjected to thermomechanical loads"

Author

Stamatios D. Fanourgakis

Dipl. Mechanical & Aeronautical Engineering

Examination Committee:

1. **Professor Emmanuel S. Samouelides (Supervisor)**
2. **Professor George Zaraphonitis**
3. **Professor Nicholas Tsouvalis**

Athens, Greece 09/05/2019

Acknowledgments

Foremost, I would like to express my sincere gratitude to my advisor Prof. Emmanuel S. Samuelides for the continuous support, patience, motivation and enthusiasm. His advice and insightful comments were invaluable and helped me improve not only the present thesis but also my academic skills. I would also like to thank Ph.D. candidate, Dimitrio Georgiadi for his support and for the discussions in marine engineering topics. Finally, but by no means least, I am hugely appreciative to my family and Antigoni for the unbelievable support and continuous encouragement throughout my years of study. I would like to dedicate this thesis to my beloved grandparents.

Stamatios D. Fanourgakis

Athens, September 2019

Table of Contents

List of Tables

List of Figures

Περίληψη

Τα ατυχήματα στον διαρκώς αυξανόμενο τομέα των θαλάσσιων μεταφορών είναι ένα συχνό φαινόμενο. Ατυχήματα, όπως σύγκρουση, βύθιση, φωτιά, έκρηξη κλπ., οφείλονται συχνά σε ένα ή περισσότερους παράγοντες ή στην αλληλεπίδραση αυτών. Η φωτιά αποτελεί μία σημαντική απειλή τόσο για τους ανθρώπους (επιβάτες, ναυτικούς) όσο και για το πλοίο. Το αντικείμενο της παρούσας εργασίας είναι ο προσδιορισμός της μέγιστης αντοχής του πλοίου όταν σε αυτό επιβάλλονται υψηλές θερμοκρασίες. Πιο αναλυτικά, εξετάζεται η μέγιστη αντοχή της γάστρας ενός πλοίου χημικού φορτίου και φορτίου προϊόντων πετρελαίου σε άθικτη κατάσταση και σε κατάσταση υψηλών θερμοκρασιών. Για τον υπολογισμό της μέγιστης αντοχής της γάστρας χρησιμοποιήθηκε η μέθοδος Smith, όπως περιγράφεται από τους κανονισμούς του IACS, και η μη γραμμική μέθοδος πεπερασμένων στοιχείων μέσω του υπολογιστικού πακέτου ABAQUS. Για την περίπτωση των υψηλών θερμοκρασιών προτάθηκε και εφαρμόστηκε μεθοδολογία τροποποιημένης μεθόδου Smith για τον υπολογισμό της μέγιστης αντοχής της γάστρας. Στο πρόγραμμα ABAQUS το υλικό θεωρήθηκε ως ελαστικό – τέλειο πλαστικό για θερμοκρασίες μικρότερες των 100°C ενώ για υψηλότερες θερμοκρασίες η συμπεριφορά του υλικού περιγράφεται από τις καμπύλες που έχουν παρουσιαστεί από τον Ευρωκώδικα (Eurocode). Η δημιουργία του θερμοκρασιακού προφίλ που εξετάστηκε βασίστηκε στην μείωση των μηχανικών ιδιοτήτων του υλικού με την θερμοκρασία, λόγω έλλειψης δεδομένων για περιπτώσεις φωτιάς σε πλοία. Η αντοχή του υπό μελέτη πλοίου ελέγχθηκε μέσω του κριτηρίου των CSR – Η που αναφέρεται σε δεξαμενόπλοια (tankers).

Στο 1ο κεφάλαιο της εργασίας παρουσιάζεται μια εκτενής βιβλιογραφική έρευνα σε θέματα που άπτονται στο αντικείμενο της εργασίας, ενώ στο 2ο κεφάλαιο γίνεται αναφορά στο θεωρητικό υπόβαθρο που είναι απαραίτητο για την παρακολούθηση και την κατανόηση της εργασίας από τον αναγνώστη. Στα κεφάλαια 3 και 4 παρουσιάζονται αναλύσεις αναφοράς που πραγματοποιήθηκαν με σκοπό την αξιολόγηση της λειτουργίας του προγράμματος ABAQUS, την στάθμιση των αποτελεσμάτων και την ορθή υπολογιστική μοντελοποίηση του προβλήματος. Στο 5ο κεφάλαιο γίνεται ανάλυση των παραμέτρων της μη γραμμικής ανάλυσης των πεπερασμένων στοιχείων, με σκοπό την ορθή μοντελοποίηση του προβλήματος και την ελαχιστοποίηση και γνώση των σφαλμάτων των αποτελεσμάτων. Στο 6ο κεφάλαιο παρουσιάζονται τα αποτελέσματα της μη γραμμικής ανάλυσης των πεπερασμένων στοιχείων που προέκυψαν βάση των αναλύσεων που παρουσιάστηκαν στο κεφάλαιο 5. Στο κεφάλαιο 7, παρουσιάζεται η εφαρμογή και τα αποτελέσματα της μεθόδου Smith και της τροποποιημένης μεθόδου Smith για τον προσδιορισμό της μέγιστης αντοχής της γάστρας σε άθικτη κατάσταση και σε κατάσταση υψηλών θερμοκρασιών, αντίστοιχα. Τέλος, στο 8ο κεφάλαιο, συγκρίνονται οι δύο μέθοδοι που χρησιμοποιήθηκαν, γίνεται μία συνοπτική αναφορά στα ευρήματα της εργασίας και παρουσιάζονται προτάσεις για μελλοντική μελέτη.

Τα αποτελέσματα της μεθόδου Smith (άθικτη κατάσταση) ικανοποιούν το κριτήριο των CSR – Η για καταστάσεις hogging και sagging, ενώ τα αποτελέσματα της τροποποιημένης μεθόδου Smith, για την περίπτωση των υψηλών θερμοκρασιών, δεν ικανοποιούν το κριτήριο. Τα αποτελέσματα που προκύπτουν από το πρόγραμμα ABAQUS για την άθικτη κατάσταση ικανοποιούν το κριτήριο των CSR – Η για κατάσταση

hogging ενώ δεν το ικανοποιούν για κατάσταση sagging. Στην κατάσταση των υψηλών θερμοκρασιών τα αποτελέσματα του προγράμματος ABAQUS ικανοποιούν το κριτήριο των CSR – H στην κατάσταση hogging και δεν το ικανοποιούν στην κατάσταση sagging. Η ικανοποίηση του κριτηρίου των CSR – H είναι αλληλένδετη με τις παραμέτρους μοντελοποίησης της μεθόδου των πεπερασμένων στοιχείων. Συγκρίνοντας, τα αποτελέσματα των δύο μεθόδων, παρατηρείται ότι υπάρχουν μικρές διαφορές οι οποίες οφείλονται κατά κύριο λόγο στις παραδοχές που έχουν πραγματοποιηθεί στην εφαρμογή των δύο μεθόδων. Τέλος, το θερμικό σενάριο το οποίο εξετάστηκε οδηγεί στην οριακή μη ικανοποίηση του κριτηρίου των CSR – H και για αυτό το λόγο μπορεί να λεχθεί ότι θερμικά σενάρια με την ίδια γεωμετρική έκταση αλλά με διαφορετικές υψηλότερες θερμικές συνοριακές συνθήκες οδηγούν και αυτά στην μη ικανοποίηση του κριτηρίου.

Abstract

Accidents in shipping industry is a frequent phenomenon. Accidents such as collision, foundering, fire, explosion etc. are caused by more than one contributing factors. Fire is a significant threat for humans (passengers, seafarers) but also for the ship structure. The scope of the present master thesis is the estimation of hull girder bending moment capacity at elevated temperatures. Specifically, the bending moment capacity of a chemical/ oil product carrier hull girder at intact and at elevated temperature conditions is examined. Smith method, as described from IACS, and nonlinear finite element method (ABAQUS) were used for the analyses. A methodology for modified Smith method was proposed and applied for the bending moment capacity estimation at elevated temperatures. Material was assumed as elastic – perfectly plastic at lower temperatures, while for higher temperature the material's mechanical properties are described from Eurocode. The creation of the examined temperature profile was based in mechanical properties of steel, due to the lack of relevant studies and ship fire data. The ship's ultimate bending moment was compared to CSR – H criterion, which is referred to tankers.

An extensive literature review is presented in chapter 1. Chapter 2 presents the theoretical background needed for the comprehension of the thesis. Benchmark analyses are presented in chapters 3 and 4, in order to evaluate ABAQUS execution and correct finite element modelling of the examined problem. Chapter 5 presents the examination of the nonlinear finite element analysis parameters in order to define the correct finite element modelling but also to minimize the results error. The results of the nonlinear finite element analysis are presented in chapter 6. Chapter 7 presents the application and the results of Smith method (intact condition) and modified Smith method (elevated temperature condition). Finally, in chapter 8 a comparison between the examined methods is presented. Moreover, there is a briefly presentation of the study results and proposals for future work are mentioned.

Smith method results for ultimate bending moment capacity satisfy the CSR – H criterion. Modified Smith method, for elevated temperature condition, results for ultimate bending moment capacity do not satisfy the CSR – H criterion. According to ABAQUS results for intact ship case, it was obtained that the CSR – H criterion is satisfied for hogging condition only. ABAQUS results of ultimate bending moment capacity for elevated temperatures satisfy the CSR – H criterion for hogging condition only. Satisfaction or not of CSR – H criterion by NLFEA method is strongly related to finite element modelling parameters. Compering the results of the two examined methods, it is observed that there are small differences due to the assumptions, which have been made in the two methods application. Finally, the examined thermal scenario lead to lack of satisfaction of the CSR – H criterion. This means that the examination of greater temperatures with the same thermal boundary conditions will lead to the same results.

Chapter 1: Introduction

The globally expanding shipping industry has several hazards such as collision, capsizing, foundering, grounding, fire and explosion. Accidents are often caused by more than one contributing factor through complex interaction. In the safety and shipping review of 2018 [1] analytical statistical data on marine accidents and incidents are presented. Figure 1 shows the top 5 causes of ship loss from 2008 to 2017. The most common type of loss is foundering. Fire and explosion is also a crucial type of accident in ship loss. Moreover, the review presents statistical data on the losses by the type of the vessel and losses by region. Baalisampang et al. [2] present a detailed review and analysis of fire and explosion accidents that occurred in the maritime transportation industry during 1990 – 2015. In this study the underlying causes of fire and explosion accidents are identified and analyzed. The contributing factors in fire and explosion accidents are human error, mechanical failure, electrical fault and thermal reaction. In a 9% of fire and explosion accidents the cause is unknown (Figure 2). Additionally, they present a prevention procedure for all the causes of fire and explosion accidents and propose alternative fuels in order to reduce the risk of ignition during accidental leakage.

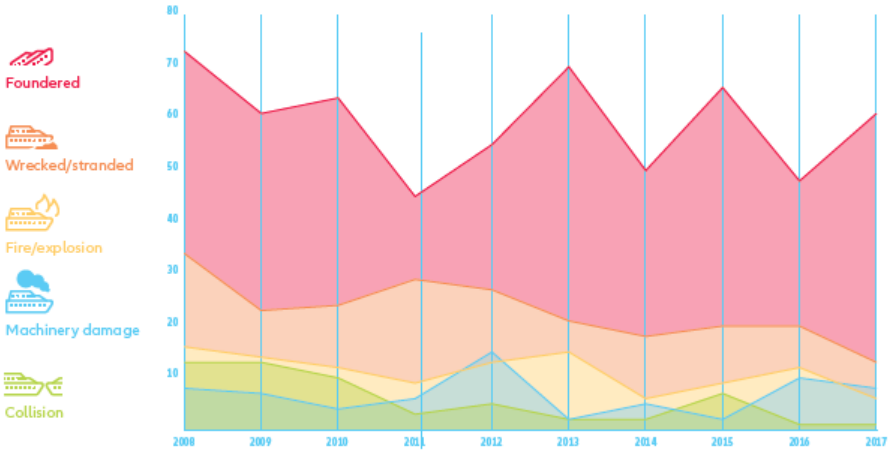

Figure 1: Losses by type cause (2008 – 2017) [1]

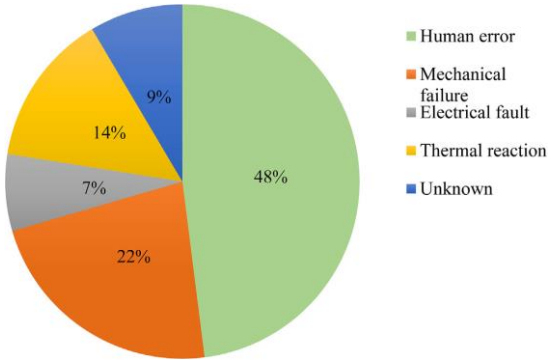

Figure 2: Percentages of fire and explosion accidents [2]

1.1 Purpose

As shown above fire and explosion accidents is a common type of accidents in marine transportation industry. The elimination of the risk of this type of accidents is infeasible due to the nature of causes. For this reason, the structural response in these type of accidents should be known, in order to minimize the fatalities and the environmental impact from the accident. Furthermore, the fire or explosion structural response should be known for design purposes. The scope of this master thesis is to examine the metallic ship structure response subjected to thermal and mechanical loads. This achieved by obtaining the ultimate bending moment capacity for intact and elevated temperature conditions. Specifically, the bending moment capacity of a chemical/ oil product carrier hull girder at intact and at elevated temperature conditions is examined using Smith method (intact condition), modified Smith method (elevated temperature conditions) and nonlinear finite element method (ABAQUS, for intact and elevated temperature conditions).

1.2 Literature Review

In this subchapter, studies relative to structural response under thermomechanical loads, fire modelling, thermal fluid – structure interaction, buckling analysis and ultimate state assessment will be presented. Paik el al. [3] developed a practical procedure for the nonlinear structural consequence analysis of structures under fire. Specifically, thermal and structural response analysis for I type steel beam have been performed using commercial code LS – DYNA and the computational results compared to experimental results. For this case diagrams of beam deflection relative to increasing temperature are presented. The paper concludes with a collapse study of a steel member under fire loading, in which analytical and computational calculations for the collapse strength of the beam in different temperatures, are presented. Lien et al. [4] examined the nonlinear behavior of steel structures considering the heating and the cooling phases of a fire by the Vector Form Intrinsic Finite Element (VFIFE) method. The results from their numerical model compared to analytical and experimental results. They also use the numerical model to examine several applications, concluding that the proposed numerical model can predict effectively the nonlinear behavior of the steel structure in both the heating and cooling phases. Gillie, in his study [5], identifies the key phenomena needed for accurate high temperature structural modelling and highlights their importance by reference to a conceptually simply but structurally complex problem. A structural analysis at high temperature is necessary to consider material non – linearity, geometric non – linearity, and time – and temperature – varying strength. Moreover, the structural behavior is proposed to being established through a full heating – cooling cycle when designing for fire loading. Soares and Texeira [6] presented a parametric study for quantifying the effect of localized heat loads on the collapse of steel plates through numerical calculations. The results showed that the compressive strength of the plates depends significantly on the size of the heated area. Also, they shown that the strength decreases rapidly due to a degradation of the material properties when the heated area increases beyond 50% of the total plate area.

Paik et al. [7] focused on the development of a program which can transfer the computed pressures for FLACS CFD gas explosion simulations to an input file that may be used for the calculation of the structural

response of an object structure under explosive pressure loading, using the finite element codes ANSYS or LS – DYNA. The developed interface program applied to two examples, on pressure vessels structure and on a simplified module of FPSO topsides. Paik et al. [8] developed an interface program for automation of thermal load mapping between fluid and solid. Temperature distributions are obtained by CFD simulations, using Kameleon FireEX, while the consequence analysis is performed using the LS – DYNA. In the study, the interface program procedure is analytically described and the accuracy and methodology of the interface program are verified through the application of two sample problems. Also, in the developed interface program the effects of Passive Fire Protection (PFP) are well considered. Samuelides et al. [9] presented a computational modelling of accidental fire actions in the topside structures of a floating, production, storage and offloading (FPSO) unit. The assumed scenario implements a jet fire which loads the structure by temperature increments and pressures generation on their exposed surfaces. Temperature distributions were obtained by computational fluid dynamic simulations (ANSYS CFX) and the consequent structural analyses employed on LS – DYNA. Results from CFD code were directly assigned as an input file in FEM code.

A two – way fluid structure interaction analysis of structures subjected to jet fire is presented by Paik et al. [10]. The aim of the study is to investigate the effect of the time increments of the analysis and to suggest a proper time increment. An interface program (KFX2DYNA) between CFD (Kameleon FireEX) and NLFEA (LS – DYNA) was used. The results showed that the examined case was time increment independent and as the structural consequences grow more severe with time, the differences between the one – way and multi – way methods become more significant. Hofmeyer et al., in their work report [11], proposed an automated two – way coupling procedure between CFD and FEM codes using external scripts written in C++ and Python languages. They also highlighted the importance of a two – way coupled analysis, due to the fact that it considers the effect of the structural response on the fire propagation. Paajanen et al. [12] presented a simulation framework for the fire – response of composite structures. They developed a one – way coupled analysis between CFD code (Fire Dynamics Simulator) and FEM code (ABAQUS/ ANSYS) using a coupling tool called FDS2FEM. FDS2FEM transfers time – dependent thermal boundary conditions. A similar study is presented by Malendowski and Glema [13]. In their study a one – way coupled numerical analysis of steel structures under natural fire is implemented. Coupling between CFD and FEM codes is done by dedicated scripts, which utilize developed methods and compute the heat transfer between gas and solid phase. A thermal fluid – structure interaction and a coupled thermal – stress analysis in a cable stayed bridge exposed to fire are presented by Nariman [14]. The analyses were utilized to identify the effected of transient and steady – state heat – transfer on the vortex induced vibration and fatigue of a segmental bridge deck due to fire incidents and were employed on ABAQUS. Table 1 presents briefly the used methods of the above discussed studies. One – way coupling method states for semi coupled analysis while two – way coupling method states for fully coupled analysis.

Kang et al. [15] explored a framework for using computational fire simulations during the early phases of ship design. Additionally, they highlighted the difficulties is such simulations due to the numerous fire scenarios and fire safety schemes for ship design. Hulin et al. [16] carry out full – scale tests of A – 60 steel,

FRD – 60 aluminum and FRP bulkheads exposed to fire in order to compare their respective behaviors in terms of their ultimate load – carrying capacity beyond the prescribed 60 minutes threshold under thermomechanical loadings. Two time – temperature curves were used in the tests: the standard prescribed in ISO834 and the NFC50, which represents exposure to natural fire. Steel specimens pass the prescribed threshold and they did not experience structural failure. The study focuses on the structural behavior of FRP bulkheads and showed that designing structural elements for a SOLAS vessel using FRP material and complying with the existing regulations could be possible. The application of sophisticated simulation and risk analysis methods in fire safety design of ships has been studied in SURSHIP – FIRE research project [17].

Study	Fem Code	CFD Code	Coupling
Paik el al. [8]	LS - DYNA	Kameleon FireEX	1 way method using developed interface program
Samuelides et al.[9]	LS - DYNA	ANSYS CFX	1 way method using developed interface program
Paik et al. [10]	LS - DYNA	Kameleon FireEX	2 way method using KFX2DYNA
Hofmeyer et al. [11]	ABAQUS	FDS	1 way and 2 way methods using C++ and Python scripts
Paajanen et al. [12]	ABAQUS/ ANSYS	FDS	1 way method using FDS2FEM
Malendowski et al. [13]	ABAQUS	FDS	1 way method using Scilab scripts

Table 1: Literature methods on 1 way and 2 way thermal fluid structure interaction

Methods for the ultimate limit state assessment of marine structures presented by Paik et al. [18–20] in a series of 3 papers. The aim of the papers are to conduct benchmark studies on methods for ultimate limit state assessment of plates, stiffened panels and hull girders of ship and ship – shaped structures, using FEA, DNV PULS, ALPS/ULSAP, ALPS/HULL and CSR methods. The first part deals with the ultimate limit state assessment of unstiffened plates under combined biaxial compression and lateral pressure loads. The candidate methods results compared and it was concluded that the plate ultimate strength behavior is significantly affected by various parameters such as plate initial deflection shape, boundary and loading conditions. The second part is focused on methods for the ultimate limit state assessment of stiffened plate structures under combined biaxial compression and lateral pressure actions. In this study, four types of initial geometric deflection were used, the plate deflection, the stiffener wed deflection, the column type deflection and the sideways deflection. The plate deflection was assumed to be equivalent to the plate buckling mode which may give the lowest resistance against the actions. The two later deflection types are fabrication – related and their type was supposed to be the buckling mode that results in the minimum buckling strength of the stiffener. The consideration of the above initial distortions is important, because the stiffener beam – column initial deflection can significantly affect the beam – column – type collapse mode, while the stiffener sideways deflection can significantly affect the flexural –

torsional buckling mode. Once again the candidate methods results compared and the results are strongly related to the magnitude and shape of initial geometrical imperfections and to the boundary and loading conditions. In the third part, a method for the progressive collapse analysis of hull girder under bending moments is presented, based on the previous parts. For the FEA a single hull cross – section model between two adjacent transverse frames at mid – ship was adopted. The ultimate hull girder strength predictions from the candidate methods compared for the results accuracy identification and the applicability of the candidate methods.

Similarly to Paik's works other researcher have perform studies for plates, stiffened panels and hull girders. Gordo [21] examined the effect of the initial imperfections on the strength of restrained plates. Analytically, he examined the effect of the number of half waves (m) in the initial imperfection equation and the effect of the amplitude (w_0) of the initial imperfection. He concluded that there is a convergence in the shape of load end shortening curve of the plate with the increase of m value (m>4) and there is a decrease in the ultimate strength of the plate with the increase of the initial imperfection amplitude. Soares et al. [22] presented a collapse assessment of uniaxially load plates and stiffened panels of ship structures. The results from nonlinear finite element analysis compared with equivalent results from CSR. The differences between the two methods are significant in the post – collapse region and the one reason for this response is the strain hardening effect which did not included in the analysis. Soares et al. [23] investigated the influence of the initial imperfections in the ultimate strength of stiffened panels. Three types of initial imperfections were compared, plate deflection, beam – column deflection and sideways deflection. The ultimate strength of the stiffened panel with the three imperfection types applied simultaneously is significantly smaller than that of each initial imperfection type. The stiffened panel with the beam – column deflection presents the higher ultimate strength. An extensive study for the parameters that affect the ultimate strength of stiffened panels was presented in 2009 at 17th International Ship and Offshore Structures congress [24]. In this study, the effect of boundary conditions, lateral pressure, mesh density, material hardening, geometrical imperfections and residual stress were investigated. The use of 5% hardening in the material stress – strain curve can affect significantly the post buckling region of the load end shortening curve diagram. Xu et al. [25] presented a nonlinear finite element analysis for the ultimate bending moment of hull girder. They examined several parameters such as boundary conditions, geometric ranges of finite element models, elements types, loading methods, loading time and finite element analysis procedure. The results from FEA compared with the analytical methods (CSR). The use of nonlinear finite element method to predict the ultimate strength of hull girder is also presented by [26,27]. Considering, the above studies for ultimate hull girder strength, one can notice that the finite element modelling method (boundary & loading condition, geometric imperfection, mesh parameters etc.) for the ultimate hull girder strength analysis presented in each paper is different. This can cause a confusion as there is difficult to obtain experimental data.

Ioannidis [28] examined the ultimate strength of a bulk carrier in intact and damaged condition using Smith method. He developed MatLab codes for the two conditions and the results from the code for the intact

condition compared with the results from MARS 2000. Pollalis in 2012 [29] presented computational methods and results for ultimate strength analysis of ship – shaped structures using Abaqus Implicit.

1.3 Fire Accident Case

Stolt Valor was a Hong – Kong flagged, chemical tanker, built in 2004 by Shimanami Shipyard. The overall length of the ship was 158.83 m, the breadth was 25.53 and the draught was 10.5 m (Figure 3). The deadweight of the ship was 25269 tonnes and the gross tonnage was 15732 tonnes. On March 15, 2012, an explosion and subsequent fire occurred on board, while it was 27 nautical miles off Jubail, Saudi Arabia. The fire lasted 5 days (Figure 4). The ship was carrying 13000 tonnes of methyl tertiary – butyl ether (MTBE), 1300 tonnes of isobutyraldehyde (IBAL) and 430 tonnes of intermediate fuel oil (IFO 380). Stolt Valor was deemed too badly damaged for repairs to be economically viable and the ship owners and managers decided to scrap it (Figure 5).

Figure 3: Stolt Valor

Figure 4: Stolt Valor under fire

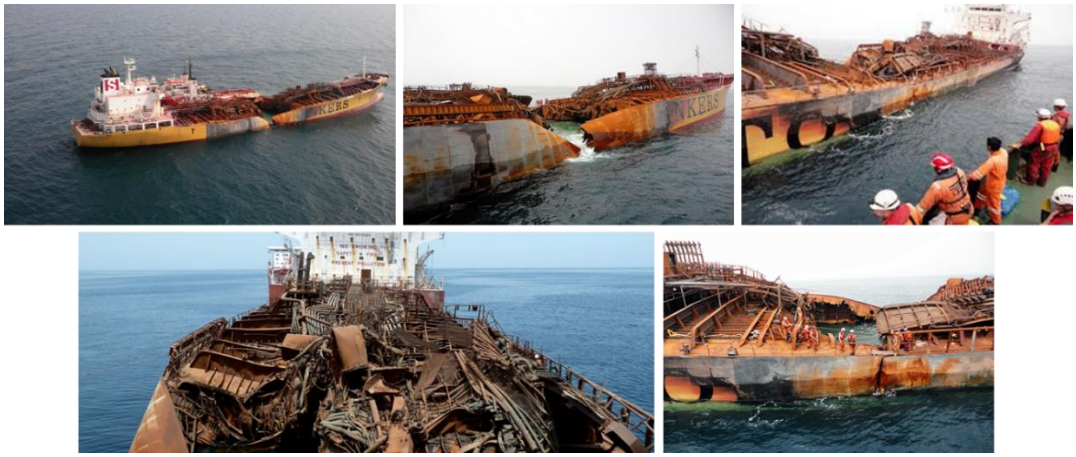

Figure 5: Damaged Stolt Valor after fire & explosion

Chapter 2: Theoretical Background

In this chapter there will be a reference to the theoretical background, needed for the following analyses. There will be references in loads on ship, the structural response and design of ship, common structural rules criterion, finite element method, plasticity theory, buckling, heat transfer, combustion theory and pool fire dynamics.

2.1 Loads, Structural Response & Design

A ship is a long, slender structure with thin walls. For the stiffness increase, transverse and longitudinal stiffeners are used. A ship is divided in compartments with longitudinal and transverse bulkheads. There are different ways of classifying the loads which acting on ships. A common way of classifying loads is according to how they vary with time: static, slowly varying or rapidly varying. In static loads there are all "Stillwater" loads (external and internal pressures, weights), drydocking loads and thermal loads. In category of slowly varying loads, there are the wave – induced dynamic pressure distribution in the hull resulting from the combination of wave encounter and the resulting ship motion (hogging & sagging, (Figure 6)), the sloshing of liquid cargoes, the inertia loads etc. Slamming and forced mechanical vibrations can be characterized as rapidly varying loads [30]. In practice, the structure's response under the prescribed critical loads is a combination of the basic types of failure. The basic types of failure are large local plasticity, instability (bifurcation) and fracture (direct, fatigue, brittle) [30].

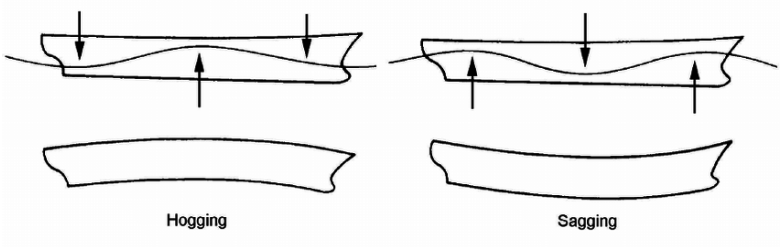

Figure 6: Hogging and sagging

For the evaluation of a ship structure behavior, there is an examination of four critical states: Serviceability Limit State, Ultimate Limit State, Fatigue Limit State and Accidental Limit State. Serviceability Limit State refers to the operational conditions of the ship. The ship is tested in expected operational loads and under these loads the ship should be useful and operational. During the Ultimate Limit State, the ship is tested under extreme loads and there is a calculation of maximum strength of the ship. In Fatigue Limit State, the ship is tested if can safely carry the estimated periodical loads. Accidental Limit State refers to accidental loads from collision, explosion etc. [31].

2.2 CSR – H Criterion

When ship structure behavior is determined at Ultimate Limit State, hull girder ultimate bending capacity has to be checked to ensure that it satisfies the checking criteria described in Part 1, Chapter 5, Section 2 of IACS [32]. In particular for oil tankers there are two design load scenarios: A and B. The first is referred to seagoing and harbor/sheltered water conditions and the second is for the operational seagoing homogeneous full load condition. The vertical hull girder ultimate bending capacity at any hull transverse section and at any conditions has to satisfy the following criteria:

$$M \leq \frac{M_U}{\gamma_R} \tag{1}$$

Where: M is the vertical bending moment, M_U is the vertical hull girder ultimate bending capacity obtained from FEM, Smith Method etc., γ_R is a partial safety factor for the vertical hull girder ultimate bending capacity, taken as: $\gamma_R = \gamma_M * \gamma_{DB}$, γ_M is a partial safety factor for the vertical hull girder ultimate bending capacity, covering material, geometric and strength prediction uncertainties, taken equal to 1.1 and γ_{DB} is a partial safety factor for the vertical hull girder ultimate bending capacity, covering the effect of double bottom bending, taken equal to 1.1 for oil tankers in hogging condition, 1 in sagging condition except flooded condition and 1 in hogging and sagging condition for flooded condition.

The vertical hull girder bending moment in hogging and sagging condition has to be calculated from the below equation:

$$\mathrm{M} = \gamma_s \mathrm{M}_{sw-U} + \gamma_w f_\beta \mathrm{M}_{wv} \tag{2}$$

Where: M_{sw-U} is the permissible still water bending moment in hogging and sagging conditions at the hull transverse section, M_{wv} is the vertical wave bending moment in hogging and sagging conditions at the hull transverse section, γ_s is a partial safety factor for the still water bending moment taken equal to 1 for the two design load scenarios, γ_w is a partial safety factor for the vertical wave bending moment taken equal to 1.2 for design load scenario A and equal to 1.3 for design load scenario B and f_β is a heading correction factor taken as 1.05 for seagoing conditions and 1 for ballast water exchange at sea, harbor/sheltered water and accidental flooded design load scenarios.

The vertical wave bending moments at any longitudinal position are to be taken as (Part 1, Chapter 4, Section 4, Paragraph 3.1.1 of IACS [32]):

$$\begin{aligned} Hogging:\ M_{wv-h} &= 0.19 f_{nl-vh} f_m f_p C_w L^2 B C_B \\ Sagging:\ M_{wv-s} &= -0.19 f_{nl-vs} f_m f_p C_w L^2 B C_B \end{aligned} \tag{3}$$

Where: f_{nl-vh} is a coefficient considering nonlinear effects applied to hogging, taken equal to 1 for strength and fatigue assessment, f_{nl-vs} is a coefficient considering nonlinear effects applied to sagging, taken equal to $0.58\left(\frac{C_B+0.7}{C_B}\right)$ for strength assessment and equal to 1 for fatigue assessmevnt, f_p is a coefficient taken as $f_p = f_{ps}$ for strength assessment and $f_p = 0.9[0.27 - (6 + 4f_T)L * 10^{-5}]$ for fatigue assessment, f_m is a distribution

factor for vertical wave bending moment along the ship's length taken as $f_m = \begin{matrix} 0\ for\ x \le 0 \\ 1\ for\ 0.4L \le x \le 0.65L \\ 0\ for\ x \ge L \end{matrix}$ and f_{ps} is a coefficient for strength assessments which is dependent on the applicable design load scenario, taken equal to 1 for extreme sea loads design load scenario, equal to 0.8 for the ballast water exchange design load scenario, equal to 0.8 for the accidental flooded design load scenario at sea and equal to 0.4 for the harbor/sheltered water design load scenario. The permissible still water bending moment in hogging and sagging conditions at the hull transverse section can be calculated from the rules [32] or it may be provided with the capacity plan or the ship drawings.

In addition to the above criteria the values of the net moment inertia about the horizontal axis and of the vertical hull girder net section modulus at the deck and the bottom has be greater from reference values. The net moment inertia about the horizontal axis has not to be less than the value calculated from equation (4) and the vertical hull girder net section modulus at deck and bottom have not to be less than the value calculated from equation (5)[32].

$$I_{yR} = 2.7 C_w L^3 B (C_B + 0.7) 10^{-8} \quad (4)$$

$$Z_R = 0.9 k C_w L^2 B (C_B + 0.7) 10^{-6} \quad (5)$$

Furthermore, the normal stress σ_L at any point of the hull transverse section has to comply with the following formula: Normal Stress $\sigma_L \le$ Permissible Stress σ_{perm}. The permissible stress and the normal stress are presented in tables in Part 1, Chapter 5, Section 1, Paragraph 2.2 of IACS [32]. From the above formula the permissible net section modulus at deck and bottom can be calculated for the different operational conditions.

2.3 Finite Element Method

Finite element method has become a powerful tool for the numerical solution of a wide range of engineering problems. Applications range from deformation and stress analysis of automotive, aircraft, building and bridge structures to field analysis of heat flux, fluid flow, magnetic flux and other flow problems. Basic ideas of the finite element method originated from advances in aircraft structure analysis. In the early 1960s, engineers used the method for approximate solution of problems in stress analysis, fluid flow and other cases [33,34].

Finite element method is based on two approaches, potential energy and virtual work. Principle of Minimum Potential Energy states that for conservative systems, of all the kinematically admissible displacement fields, those corresponding to equilibrium extremize the total potential energy. If the extremum condition is a minimum, the equilibrium state is stable. The Galerkin's method can be stated as follows: choose basis functions G_i. Determine the coefficients Q_i, in $\tilde{u} = \sum_{i=1}^{n} Q_i G_i$ such that $\int_v \varphi(L\tilde{u} - P)dV = 0$ for every φ of the type $\varphi = \sum_{i=1}^{n} \varphi_i G_i$, where coefficients φ_i are arbitrary except for requiring that φ satisfy homogenous (zero) boundary conditions. The solution of the resulting equations for Q_i then yields the approximate solution for $\tilde{u}$.

Principle of Virtual Work states that a body is in equilibrium if the internal virtual work equals the external virtual work for every kinematically admissible displacement field $(\varphi, \varepsilon(\varphi))$ [33].

The motion of a structure in matrix form can be described from equation (6), where [M] denotes the mass matrix of the structure, [C] represents the damping matrix (which include the material and structural damping), [K] is the stiffness matrix of the structure and $x, \dot{x}, \ddot{x}$ are displacement, velocity and acceleration, respectively. The vector $\{F(t)\}$ denotes the external forces applied in structure. In case of a static structural analysis, the two first terms of the equation (6) are neglected. The stiffness matrix is material and geometry depended. In case of a thermal analysis, stiffness matrix includes terms which describe thermal properties [35]. The equilibrium equation which includes the stiffness matrix, the displacements vector and the external forces vector can be solved directly (Direct Stiffness Method) or iteratively (i.e. Newton – Raphson Method) [33,34,36–38].

$$[M]\{\ddot{x}\} + [C]\{\dot{x}\} + [K]\{x\} = \{F(t)\} \tag{6}$$

2.3.1 Newton Raphson Method

Newton Raphson method is the most frequently used iteration scheme for the solution of nonlinear problems. Newton gave a version of the method in 1669 and Raphson generalized and presented the method in 1690. Both mathematician used the same concept, and both algorithms gave the same numerical results. The basic approach in an incremental step – by – step solution is to assume that the solution for the discrete time t is known and that the solution for the discrete time $t + \Delta t$ is required, where Δt is a suitably chosen time increment. The force equilibrium at time $t + \Delta t$ is described from the equation (7).

$$^{t+\Delta t}R + {}^{t+\Delta t}F = 0 \tag{7}$$

Assume that $^{t+\Delta t}R$ is independent of the deformations and the solution of the internal forces is known at time t, we can write:

$$^{t+\Delta t}F = {}^{t}F + F \tag{8}$$

Where F is the increment in nodal point forces corresponding to the increment in element displacements and stresses from time t to time $t + \Delta t$. This vector can be approximated using a tangent stiffness matrix ^{t}K which corresponds to the geometric and material conditions at time t.

$$F = {}^{t}KU \Rightarrow {}^{t}K = \frac{\partial {}^{t}F}{\partial {}^{t}U} \tag{9}$$

Where U is a vector of incremental nodal point displacements. From the above equations (7) – (9), we obtain:

$$^{t}KU = {}^{t+\Delta t}R + {}^{t}F \tag{10}$$

Solving the equation (10) for U, we can calculate an approximation to the displacements at time $t + \Delta t$. The exact displacements at time $t + \Delta t$ are those that correspond to the applied loads $^{t+\Delta t}R$. Having evaluated an approximation to the displacements corresponding to time $t + \Delta t$, we could now solve for an approximation to the stresses and corresponding nodal forces at time $t + \Delta t$, and then proceed to the next time increment

calculations. In summary, the equations used in the Newton Raphson iteration, for $i = 1,2,3, \ldots$ are described from equation (11) [36]. Figure 7 presents a graphical representation of the N – R method.

$$
\begin{aligned}
{}^{t+\Delta t}K^{i-1}\Delta U^{i} &= {}^{t+\Delta t}R + {}^{t+\Delta t}F^{i-1} \\
{}^{t+\Delta t}U^{i} &= {}^{t+\Delta t}U^{i-1} + \Delta U^{i} \\
{}^{t+\Delta t}U^{0} = {}^{t}U, {}^{t+\Delta t}K^{0} &= {}^{t}K, {}^{t+\Delta t}F^{0} = {}^{t}F
\end{aligned}
\tag{11}
$$

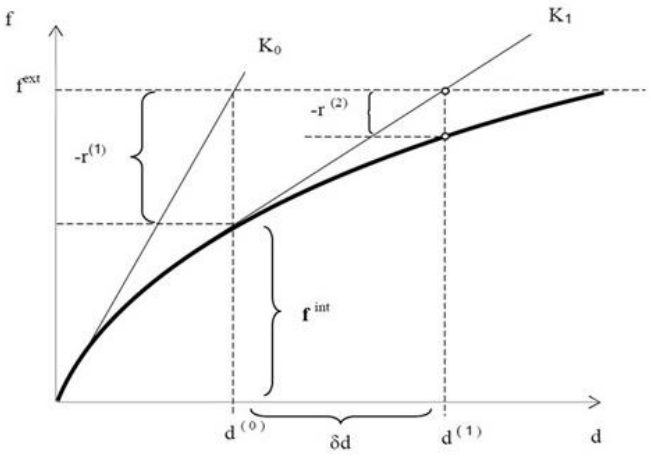

Figure 7: Newton – Raphson iterative process

2.3.2 Riks Method (Arc Length Method)

Riks method provided from several finite element analysis softwares is used to obtain nonlinear static equilibrium solutions for unstable problems. Unstable problems can be characterized problems with material and geometric nonlinearity or generally the load – displacement response can exhibit the type of behavior as presented in Figure 8 [35].

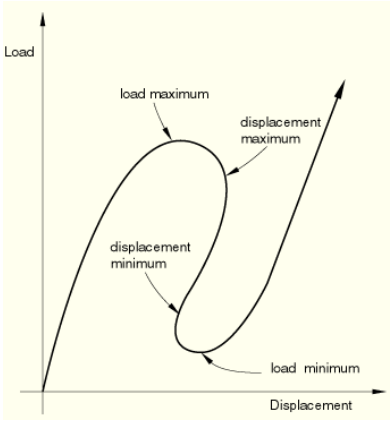

Figure 8: Load – displacement response of nonlinear problems [35]

ABAQUS is using the modified Riks algorithm. Unlike the Newton Raphson method, the Arc Length method postulates a simultaneous variation in both the displacements Δu and the load vector coefficient Δλ, hence in Arc Length method there are two unknowns in contrast with Netwon – Raphson method in which there is one unknown Δu [39]. ABAQUS provides an initial control over the load magnitude but for subsequent

iterations and increments load magnitude is computed automatically. Moreover, minimum and maximum arc length increments can be used to control the automatic incrementation. ABAQUS theory manual presents analytically the iterative algorithm for the modified Riks method [40].

2.3.3 Explicit Methods

Direct integration methods are divided in implicit and explicit methods. In explicit method the displacement vector is defined by the known displacement vector and its derivatives in previous time t. Writing the equation (6) for time increment t:

$$[M]\{\ddot{x}\}^t + [C]\{\dot{x}\}^t + [K]\{x\}^t = \{F(t)\}^t \tag{12}$$

Using the central difference method we obtain velocity and acceleration:

$$\ddot{x}^t = \frac{1}{\Delta t^2}({}^{t-\Delta t}x - 2\ {}^{t}x + {}^{t+\Delta t}x)$$
$$\dot{x}^t = \frac{1}{2\Delta t}({}^{t+\Delta t}x - {}^{t-\Delta t}x) \tag{13}$$

Using the above equation to the equation of motion (12) we obtain the final equation:

$$\left(\frac{1}{\Delta t^2}[M] + \frac{1}{\Delta t}[C]\right)\{x\}^{t+\Delta t} = \{F(t)\}^t - \left([K] - \frac{2}{\Delta t^2}[M]\right)\{x\}^t - \left(\frac{1}{\Delta t^2}[M] + \frac{1}{2\Delta t}[C]\right)\{x\}^{t-\Delta t} \tag{14}$$

Explicit method is more efficient than implicit methods for lumped mass and damping matrices and there is no need for stiffness matrix inversion. The main drawback of the method is that is stable under a specific time increment condition: $\Delta t \leq \Delta t_{ct} = \frac{T_n}{\pi}$, where T_n is the smallest period in the finite element system [36,38].

2.3.4 Shell Elements

Shell elements are used in structure where the thickness of a surface is significant small compared to the other dimensions and the stresses normal to the direction of the thickness are negligible. S4 and S4R elements are presented in Figure 9 which are part of the "shell" family. Each node has six degrees of freedom, three displacements and three rotations (3D elements). The S4R element uses reduced integration to form the element stiffness. In the reduced integration technique, the order of in – plane integration is one integration order less than that which would require performing the stiffness matrix integration exactly [35,36].

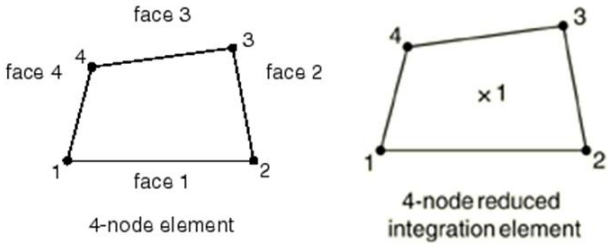

Figure 9: S4 and S4R elements [35]

Shear locking is characterized by a sharp increase in the element stiffness as the length to thickness ratio becomes larger (Figure 10). To address the shear locking and to increase computational efficiency, a

reduced integration scheme is proposed in FEA codes. Reduced integration usually provides results that are more accurate (as means of overcoming some over stiffness elements in the shell, relieves shear locking provided the elements are not distorted or loaded in – plane bending) and reduces running time. S4R element is computationally less expensive since the integration is executed at one Gauss point per element. Reduced integration first order element suffers from its own numerical difficulty called hourglassing since it tends to be excessively flexible (Figure 10). However, FEA codes overcome this difficulty by using an additional artificial stiffness which is added to the elements (Hourglass control) [35,36,38,41].

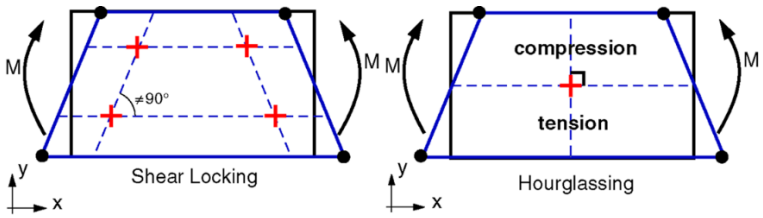

Figure 10: Shear locking and hourglassing

A two – dimensional 4 – node isoparametric element is presented in Figure 11. The four shape functions are described in equation (15). The stiffness matrix for the quadrilateral element can be derived from the strain energy in the body (equations (16) and (17)). The calculating process of stiffness matrix is analytically presented in Chandrupatla's and Belegundu's book [33].

$$N_1 = 1/4(1-\xi)(1-n) \quad N_3 = 1/4(1+\xi)(1+n)$$
$$N_2 = 1/4(1+\xi)(1-n) \quad N_4 = 1/4(1-\xi)(1+n) \tag{15}$$

$$U = \int_v 1/2\sigma^T \varepsilon dV \tag{16}$$

$$k^e = t^e \int_{-1}^{1}\int_{-1}^{1} B^T DBdetJd\xi dn \tag{17}$$

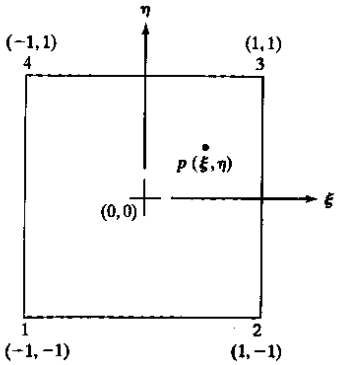

Figure 11: The quadrilateral element in ξ, n space [33]

2.4 Plasticity

Plasticity describes the deformation of a material undergoing non – reversible changes of shape in response to applied forces. Significant permanent deformations will usually occur when the stress reaches some

critical value, called yield stress. The classical theory of plasticity grew out of the study of metals in the late nineteenth century from Tresca. Plastic deformation are normally rate independent [42].

The following analysis is based on observations in standard tension tests, with small, cylindrical specimen and a given rate of stretching. A typical force – displacement diagram is given in Figure 12. In the elastic range the force – displacement behavior for the most engineering materials is linear. After passing the elastic limit (point A) the material is said to undergo plastic flow. Further increases in load are usually required to maintain the plastic flow and an increase in displacement. This phenomenon is known as work – hardening. In some cases, after the initial plastic flow and hardening, the force – displacement curve decreases and the material is said to be softening. If the specimen is unloaded from a plastic state (point B), it will return along the path BC. This is elastic recovery. The strain which remains upon unloading is the permanent plastic deformation. If the material in now loaded again, the force – displacement curve will retrace the unloading path CB until it again reaches the plastic state. Further increases in stress will cause the curve to follow BD. A compression test will lead to similar results as the tensile test [43].

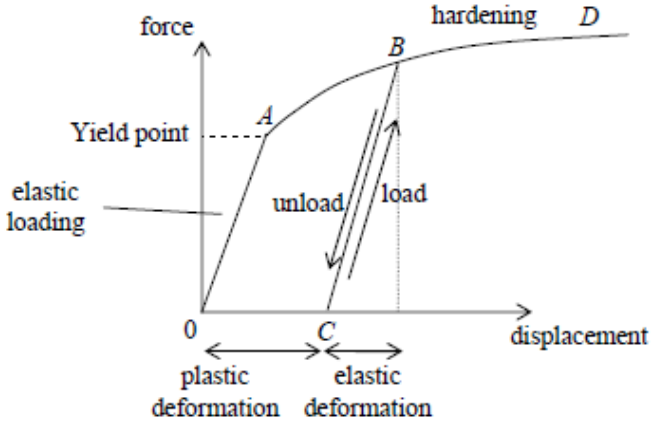

Figure 12: Force – displacement curve for the tension test [43]

2.4.1 Engineering (Nominal) and True Stress and Strain

There are two different ways of describing the force F which acts in a tension test (**Error! Reference ource not found.**). Engineering (nominal) stress (σ) is calculated with respect to the original cross sectional area A_o of the tension test specimen (equation (18)). True stress (σ´) is calculated with respect to the current cross sectional area A (equation (19)). Similarly, deformation can be described by two alternative ways. The engineering strain (ε) (equation (20)) and the true (logarithmic) strain (ε´) (equation (21)) where l_o is the original specimen length and l is the current length. The relation between the two stresses and the two strains are described by equations (22) [43].

$$\sigma = \frac{F}{A_o} \tag{18}$$

$$\sigma' = \frac{F}{A} \tag{19}$$

$$\varepsilon = \frac{l - l_o}{l_o} \tag{20}$$

$$\varepsilon' = \ln\left(\frac{l_o}{l_o}\right) \tag{21}$$

$$\sigma' = \sigma(1 + \varepsilon)$$
$$\varepsilon' = \ln(1 + \varepsilon) \tag{22}$$

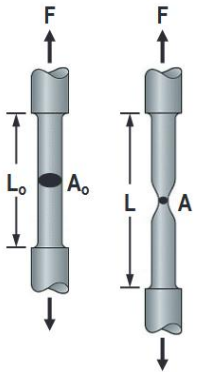

Figure 13: Tensile test force

2.4.2 The Bauschinger Effect

It is a common observation that the plastic deformation in one direction effects the plastic deformation in another direction. For instance, loading in tension a virgin sample into the plastic range and then unloading with consequently compression, one finds that the yield stress in compression is not the same as the yield stress in tension. In fact the yield point in this case will be significantly less than the corresponding yield stress in tension. This reduction in yield stress is known as the Bauschinger effect. In Figure 14 the solid line depicts the response of a real material. In isotropic hardening model, the yield stress in tension and compression are maintained equal. In kinematic hardening model, the total elastic range is maintained constant throughout the deformation [42,43].

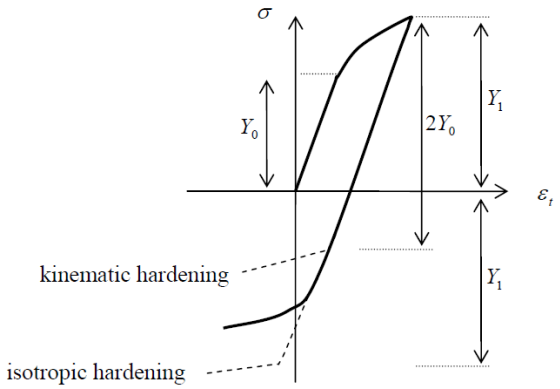

Figure 14: Bauschinger effect

2.4.3 Assumptions of Plasticity Theory

In order to formulate a basic plasticity theory the following assumptions are usually made: 1) the response is independent of rate effects, 2) the material is incompressible in the plastic range, 3) there is no Bauschinger effect, 4) the yield stress is independent of hydrostatic pressure and 5) the material is isotropic. Assumptions can be made on the type of hardening and on whether elastic deformations are significant (Figure 15). In Figure 15 (a) both the elastic and plastic curves are assumed linear. In Figure 15 (b) work – hardening is neglected and the yield stress is constant after initial yield. In Figure 15 (c) and (d) the elastic strains are neglected and these models are used in specific applications (i.e. metal working processes) [43].

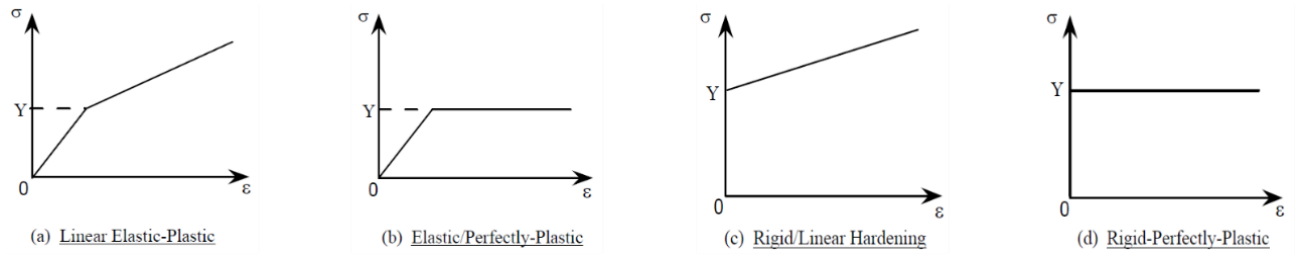

Figure 15: Simple models of elastic and plastic deformation [43]

Analytical equations have been developed in order to describe the material plastic behavior, including work – hardening phenomenon. The most common representation for the plastic behavior of material the Lidwik – Hollomon equations (23) (Figure 16). Where n is the work – hardening coefficient ($0.2 < n < 0.5$) and K constant ($G/100 < K < G/1000$). Both parameters are material depended and for n = 0 there is a perfectly plastic behavior [42].

$$\sigma = K\varepsilon^n$$
$$\sigma = \sigma_0 + K\varepsilon^n \tag{23}$$

Voce introduced a different equation for material plastic behavior. Equation (24) uses empirical parameters σ_s, σ_0 and ε_c which are material, temperature and deformation rate depended [42].

$$\frac{\sigma_s - \sigma}{\sigma_s - \sigma_0} = \exp\left(-\frac{\varepsilon}{\varepsilon_c}\right) \tag{24}$$

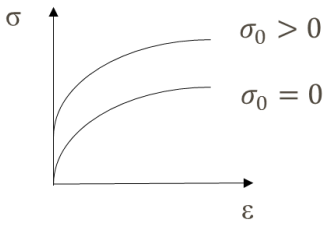

Figure 16: Lidwik – Hollomon plastic behavior model

The most known constitutive equation called Johnson – Cook (equation (25)). The first term stands for work – hardening, the second term stands for deformation rate and third term stands for temperature rate. Constants K, n and m are material depended, T_r is the reference temperature, T_m is the melting point and $\dot{\varepsilon}$ is the deformation rate [42].

$$\sigma = (\sigma_0 + \mathrm{K}\varepsilon^{\mathrm{n}})\left(1 + \mathrm{Cln}\frac{\dot{\varepsilon}}{\dot{\varepsilon}_0}\right)\left[1 - \left(\frac{\mathrm{T} - \mathrm{T}_r}{T_m - T_r}\right)^m\right] \quad (25)$$

2.4.4 Tangent and Plastic Modulus

In the elastic region stress and strains are related with Young's modulus (E). The tangent modulus K is the slope of the stress – strain curve in the plastic region and will in general change during the deformation (equation (26), Figure 17). After yield, the strain increment consists of both elastic ε^e and plastic ε^p strains (equation (27)). The stress and plastic strain increments are related by the plastic modulus H (equation (28)).

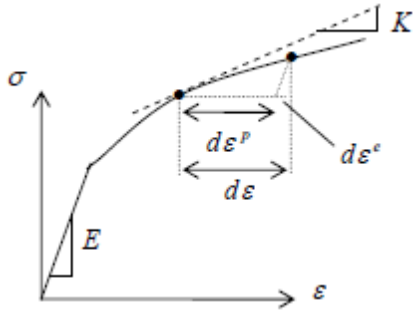

Figure 17: Tangent modulus [43]

$$d\sigma = Kd\varepsilon \quad (26)$$

$$d\varepsilon = d\varepsilon^e + d\varepsilon^p \quad (27)$$

$$d\sigma = Hd\varepsilon^p \quad (28)$$

$$\frac{1}{K} = \frac{1}{E} + \frac{1}{H} \quad (29)$$

2.4.5 Plastic Analysis of a Beam

For better understanding the plasticity mechanism, the plastic behavior of a beam is being presented. For the analysis 3 assumptions are made for the material: 1) Elastic – Perfectly Plastic deformations, 2) Isotropic hardening model and 3) No work – hardening. With the above assumptions the beam behavior beyond elastic region and the critical state in which the cross section of the beam undergoes plastic yield will be examined. The boundary conditions and the load case are presented in Figure 18. The distribution of bending stress in the cross section are presented for different values of bending moment in Figure 19. In Figure 19 (a) bending moment has reach a critical value in which the outer zones stress is equivalent to yield stress. This critical state can be described by the following equation (30) [44].

$$\sigma_F = \frac{M_{cr}}{W_z} = \frac{M_{cr}}{\frac{bh^2}{6}} \Leftrightarrow M_{cr} = \sigma_F * \frac{bh^2}{6} \quad (30)$$

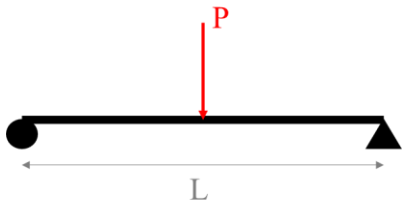

Figure 18: Examined beam

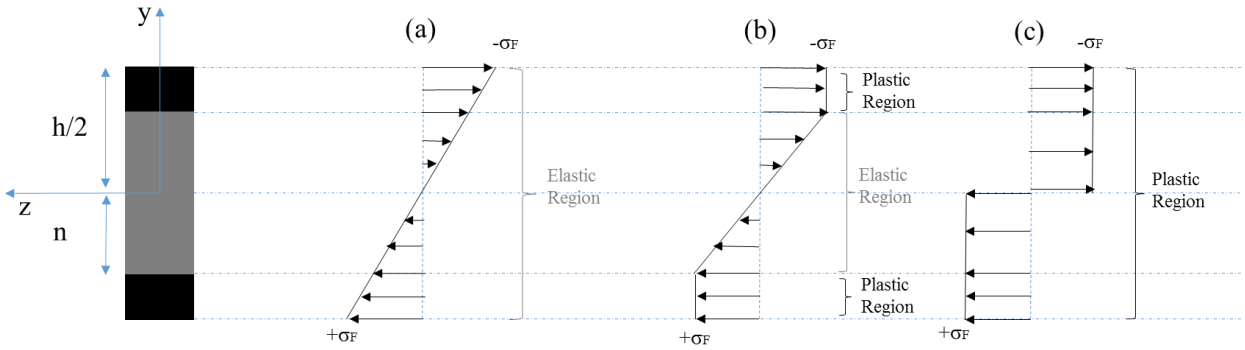

Figure 19: Beam plastic bending with square cross section [44]

Increasing the external loads, bending moment exceeds the critical value M_{cr}. In this case, plastic deformation propagates towards the centerline of the cross section, until the whole cross section undergo plastic yield (Figure 19 (b) and (c)). The bending moment for this state can be calculated from the static equilibrium [44]:

$$M_z = \int_{(F)} \sigma(y) y dE = -\int_{(F_{el})} \sigma(y) y dF - \int_{(F_{pl})} \sigma_F y dF \tag{31}$$

Where F_{el} and F_{pl} refer to cross section area in elastic and plastic region, respectively. Inserting Hooke's law in elastic region and based on assumption of Navier – Bernoulli (plane cross sections) the equation (31) transforms to equation (32).

$$M_z = \left[\frac{2E}{\rho} \int_0^n y^2 dF + \sigma_F \int_n^{\frac{h}{2}} y dF \right] \begin{matrix} dF = bdy \\ \Leftrightarrow \end{matrix} M_z = \frac{2E}{3\rho} n^3 b + \sigma_F b \left(\frac{h^2}{4} - n^2 \right) \tag{32}$$

At the point where $y = n$, $\sigma_F = \frac{E}{\rho} n$ applied to the above equation:

$$M_z = 2\sigma_F b \left(\frac{h^2}{8} - \frac{n^2}{6} \right) \Leftrightarrow M_z = \frac{2E}{\rho} bn \left(\frac{h^2}{8} - \frac{n^2}{6} \right) \tag{33}$$

When $n \longrightarrow 0$, the above equation gives the maximum bending moment in which the whole cross section undergoes plastic yield (equation (34)) [44].

$$M_z = \sigma_F b \frac{h^2}{4} \tag{34}$$

2.5 Temperature Effect

Temperature change in a structure can lead to strain growth. Temperature change effects the material's elastic constants and can contract and dilate the structure. Strains due to temperature change in different directions are equivalent in homogenous and isotropic materials. Generally, strains due to temperature change are experimentally calculated and for the most material the thermal strain described from equation (35). Thermal strain is linearly related with small temperature changes (equation (36)). Thermal expansion coefficient (α) depends on material and temperature [45].

$$\varepsilon_T = \frac{\Delta L}{L} \tag{35}$$

$$\varepsilon_T = \alpha(T - T_0) \tag{36}$$

Total strains of a body with homogenous and isotropic material, subjected to external mechanical loads and temperature changes, are given by equation (37). Shear strains are independent of temperature changes [45].

$$\varepsilon_x = \frac{\partial u}{\partial x} - a * \Delta T, \varepsilon_y = \frac{\partial v}{\partial y} - a * \Delta T, \varepsilon_z = \frac{\partial w}{\partial z} - a * \Delta T \tag{37}$$

An example will be presented in order to determine the stress created by temperature change. A rod fixed in both ends subjected to temperature change ΔT (Figure 20). The elongation from the temperature change is described from equation (38) and the elongation from the force P which represents the redundant reaction is described from equation (39).

$$\delta_T = \alpha(\Delta T)L \tag{38}$$

$$\delta_P = \frac{PL}{AE} \tag{39}$$

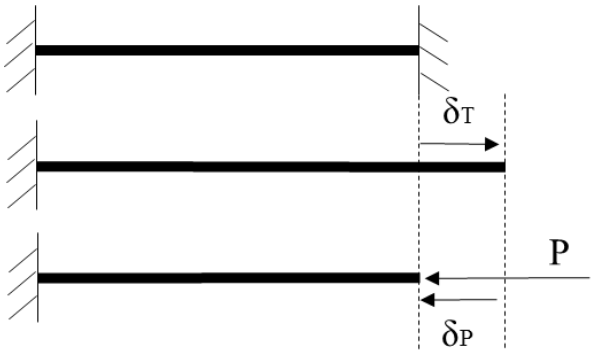

Figure 20: Rod with ends restrained against thermal expansion

The total deformation δ must be zero (equation (40)), consequently, the stress in the rod due to temperature change ΔT can be calculated (equation (41)) [45,46].

$$\delta = \delta_T + \delta_P = \alpha(\Delta T)L - \frac{PL}{AE} = 0 \tag{40}$$

$$\sigma = \frac{P}{A} = E\alpha(\Delta T) \tag{41}$$

Temperature differences in a structure can lead to deformation. The response of a rod will be examined subjected to two different temperatures in upper (T1) and lower (T2) surface (Figure 21). Uniform temperature

profile along the cross sectional height was assumed. The rod is fixed in one end and there are no external mechanical loads. The gradient of the neutral axis of rod is given by equation (42) where h is the cross sectional height [44].

$$\frac{d^2y}{dx^2} = \frac{\alpha(T_2 - T_1)}{h} \tag{42}$$

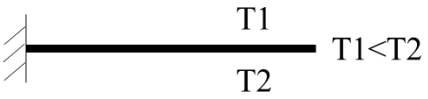

Figure 21: Rod with temperature difference

Integrating equation (42), using as boundary conditions $x = 0, \theta = 0$ and $x = 0, y = 0$ the bending deformation is given by equation (43) [44].

$$y(x) = \frac{\alpha(T_2 - T_1)}{2h} x^2 \tag{43}$$

2.6 Buckling

Buckling or structural instability is one of the two major categories which lead to the sudden failure of a mechanical component. The other category is the material failure. Buckling may occur when the structure is subjected to compressive stress. Specifically, a structural member, such as a plate, a stiffened plate, a stiffener etc., under thrust load deflect in an out – of – plane direction when the load reaches to a certain critical value.

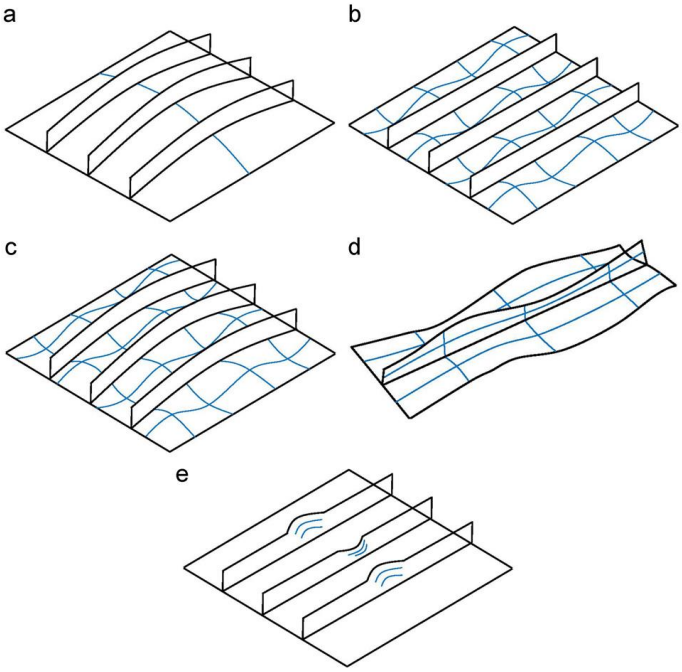

Figure 22: Buckling behavior of stiffened plate [47]

The critical buckling load or bifurcation load can be calculated analytically or through finite element analysis and is dependent from the material properties, the geometry and the boundary conditions. The structural

problem caused by buckling is the reduction in in – plane stiffness. Moreover, buckling leads to earlier occurrence of yielding than the yield stress, due to out of plane deflections. Figure 22 presents different modes of buckling behavior of stiffened plate subjected to compressive loads ((a) global buckling mode, (b) local buckling mode of the plate segment between the stiffeners, (c) beam – column type buckling, (d) local buckling of the stiffener web and (e) lateral – torsional buckling of the stiffener web) [47,48].

Figure 23 presents the buckling behavior of column under axial compression. Deflection increases with no increase in the applied axial load for a while beyond buckling. However, the capacity again starts to increase and a column can sustain further load if its behavior is perfectly elastic. This is called Elastica. On the other hand, an actual column member undergoes yielding by bending after buckling has occurred, and soon its capacity starts to decrease with an increase in the deflection. In case of a simply supported plate subjected to uniaxial thrust, buckling collapse behavior is indicated in Figure 23 A and B in terms of average stress – central deflection and average stress – average strain relationships, respectively [48].

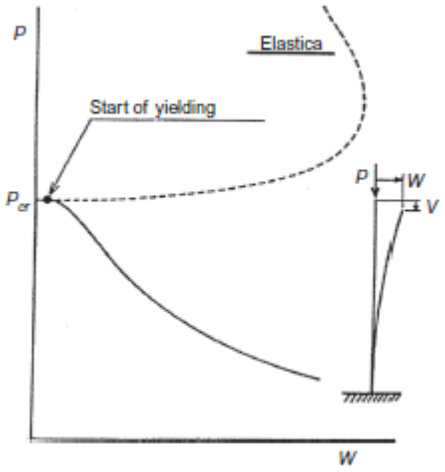

Figure 23: Buckling behavior of a column under thrust load [48]

Buckling behavior of both thin and thick plates is indicated in Figure 24. In case of a thin plate, lateral deflection starts to develop beyond the buckling point A. Beyond the buckling, capacity further increases in buckling deflection until the stiffness becomes zero and the ultimate strength is attained. Then, the capacity starts to decrease beyond the ultimate strength. The buckling collapse behavior of a stiffened plate is presented in Figure 25, which is a fundamental structural unit composing a ship's hull girder. Curve A describes the average stress – average strain relationship for a stiffened plate with high slenderness ratio of the local panel (thin local panel). In this case, buckling takes place locally at point 1. At point 3, yielding starts to takes place and point 2 stands for the ultimate strength. Curve B describes the average stress – average strain relationship for a stiffened plate with lower slenderness ratio of the local panel. In this case, initial yielding takes place at point 3 and the ultimate strength is attained at point 4. Finally, Curve C describes the average stress – average strain relationship for a stiffened plate with much lower slenderness ratio of the local panel. In this case, yielding starts at point 5 and at point 6 the panel or the stiffener undergoes buckling [48].

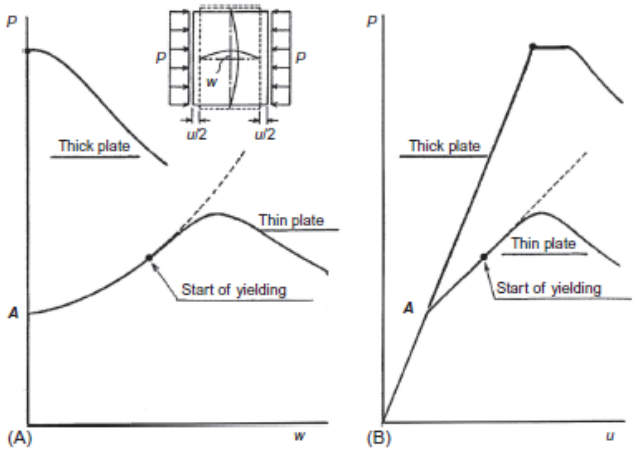

Figure 24: Buckling behavior of thick and thin plates [48]

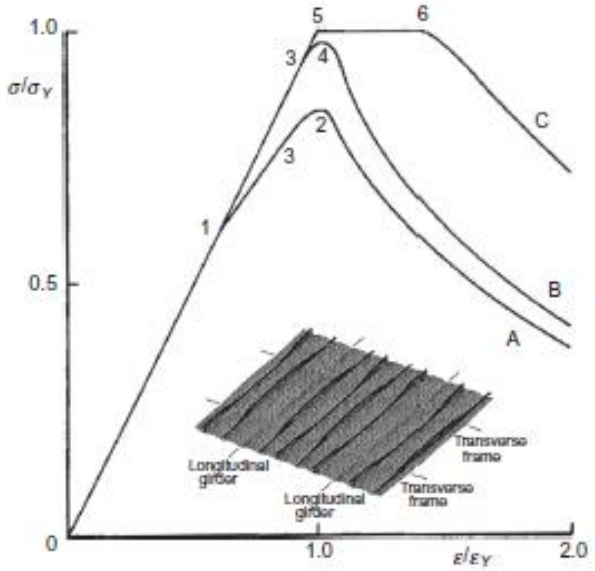

Figure 25: Buckling behavior of stiffened plates [48]

2.6.1 Analytical Solutions

The analytical solution for beam column buckling, pure torsional buckling and plate buckling will be presented in this chapter. Let assume a pinned beam column subjected to axial load P as presented in Figure 26.

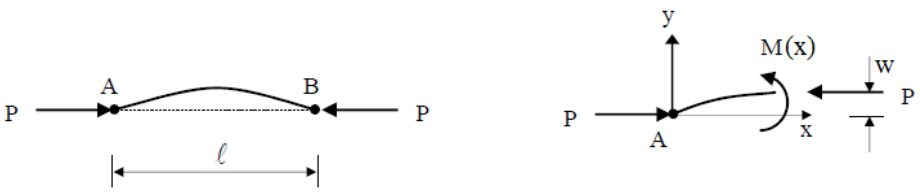

Figure 26: Pin column [49]

Using the moment equilibrium about point A and according to Euler – Bernoulli beam theory (equation (44)):

$$\Sigma M_A = 0 \Rightarrow M(x) + Pw = 0$$
$$M = -EI\frac{\partial^2 w}{\partial x^2} \qquad \Rightarrow EI\frac{\partial^2 w}{\partial x^2} + Pw = 0 \tag{44}$$

Let $\lambda^2 = \frac{P}{EI}$

$$\frac{\partial^2 w}{\partial x^2} + \lambda^2 w = 0 \tag{45}$$

The general solution can be described from: $w(x) = Acos(\lambda x) + \mathrm{Bsin}(\lambda \mathrm{x})$ and applying the boundary conditions for the pin – pin beam: $w(0) = 0 \longrightarrow A = 0$, $w(L) = 0 \longrightarrow \mathrm{Bsin}(\lambda \mathrm{x}) = 0 \longrightarrow \sin(\lambda \mathrm{x}) = 0 \longrightarrow \lambda \mathrm{x} = \mathrm{n}\pi$. Substituting the above to equation (45):

$$\lambda^2 = \frac{P}{EI} \Longrightarrow \left(\frac{n\pi}{L}\right)^2 = \frac{P}{EI} \Longrightarrow P = \frac{EIn^2\pi^2}{L^2} \tag{46}$$

The first critical load can be calculated for $n = 1$: $P_{cr} = \frac{EI\pi^2}{\mathrm{L}^2}$ and the first buckling mode: $w_1(x) = \mathrm{Bsin}\left(\frac{\pi}{\mathrm{L}}\mathrm{x}\right)$ [49].

In pure torsional buckling of a thin – walled bar, the longitudinal axis of the bar remains straight when subjected to axial compressive load. Considering a doubly symmetric bar as presented in Figure 27. In order to determine the compressive force which produces torsional buckling, it is necessary to consider deflection of the flanges during buckling [49]. The differential equation for torsional buckling of a bar of thin – walled open section is presented in equation (47).

$$\frac{dM_t}{dz} = C\frac{d^2\varphi}{dz^2} - C_1\frac{d^4\varphi}{dz^4} \tag{47}$$

The equilibrium of the element torque m_z can be expressed as: $m_z = -\frac{d\mathrm{M}_t}{dz} = -\sigma\frac{d^2\varphi}{dz^2}\mathrm{I}_o$. Therefore the equation (47) takes the form:

$$C_1\frac{d^4\varphi}{dz^4} - C\frac{d^2\varphi}{dz^2} = m_z \Longrightarrow C_1\frac{d^4\varphi}{dz^4} - (C - \sigma I_o)\frac{d^2\varphi}{dz^2} = 0 \tag{48}$$

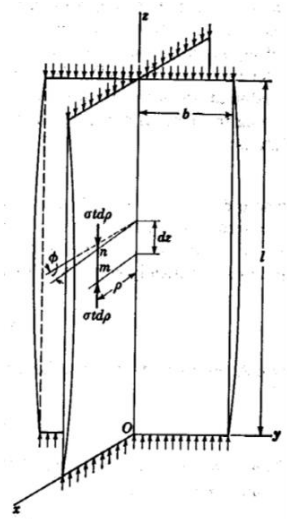

Figure 27: Doubly symmetric bar [49]

The critical value of the compressive stress σ, and hence also the critical load, can be calculated from the above equation. Let $\rho^2 = \frac{\sigma I_o - C}{C_1}$ and the general solution is described by $\varphi = A_1 \sin(\rho z) + A_2 \cos(\rho z) + A_3 z + A_4$. In case of a bar with simply supports for which the ends cannot rotate about z axis but are free to warp, the boundary conditions are stated: $\varphi(0) = \varphi(L) = 0, \frac{d\varphi}{dz}|_0 = \frac{d\varphi}{dz}|_L = 0, \frac{d^2\varphi}{dz^2}|_0 = \frac{d^2\varphi}{dz^2}|_L = 0$. Applying the boundary conditions to the general solution: $A_2 = A_3 = A_4 = 0,\ sin\rho L = 0 \Longrightarrow \rho L = n\pi$. Thus, the critical compressive stress and the critical buckling mode are described from the equation (49).

$$\sigma_{cr} = \frac{1}{I_0}\left(C + \frac{n^2\pi^2}{L^2} C_1\right)$$
$$\varphi = A_1 sin\left(\frac{\pi z}{L}\right) \tag{49}$$

Where $C = GJ$ (Torsional Rigidity), $C_1 = EC_w$ (Warping Rigidity) and C_w (Warping Constant).

Assume a rectangular plate which is compressed in its middle plane by forces uniformly distributed along the sides $x = 0$ and $x = a$ (Figure 28). Let the magnitude of this compressive force per unit length of the edge be denoted by N_x. The equation for a buckled plate with no body forces is described by equation (50) [49].

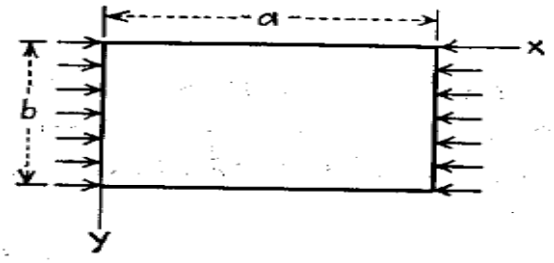

Figure 28: Simply supported rectangular plate [49]

$$\frac{\partial^4 w}{\partial x^4} + 2\frac{\partial^4 w}{\partial x^2 \partial y^2} + \frac{\partial^4 w}{\partial y^4} = \frac{1}{D}\left(N_x \frac{\partial^2 w}{\partial x^2} + N_y \frac{\partial^2 w}{\partial y^2} + 2N_{xy}\frac{\partial^2 w}{\partial x \partial y}\right) \tag{50}$$

The deflection surface (general solution) of the buckled plate in case of simply supported edges can be represented by equation (51).

$$w = \sum_{m=1}^{\infty}\sum_{n=1}^{\infty} a_{mn}\, sin\left(\frac{m\pi x}{a}\right) sin\left(\frac{n\pi y}{b}\right) \tag{51}$$

For a simply supported plate the boundary conditions are defined as: $w(0,y) = 0,\ w(a,y) = 0,\ w(x,0) = 0, w(x,b) = 0,\ M_{xx}(0,y) = 0, M_{xx}(a,y) = 0, M_{yy}(x,0) = 0, M_{yy}(x,b) = 0$. The equilibrium between the strain energy and the work done by the compressive forces is presented in equation (52)

$$\frac{\pi^4 ab}{8} D \sum_{m=1}^{\infty}\sum_{n=1}^{\infty} a_{mn}^2 \left(\frac{m^2}{a^2} + \frac{n^2}{b^2}\right)^2 = \frac{\pi^2 b}{8} N_x \sum_{m=1}^{\infty}\sum_{n=1}^{\infty} m^2 a_{mn}^2 \Rightarrow \cdots \Rightarrow$$
$$N_x = \frac{\pi^2 a^2 D}{m^2}\left(\frac{m^2}{a^2} + \frac{n^2}{b^2}\right)^2 \tag{52}$$

For $n = 1$ we obtain the critical load: $N_{x,cr} = \frac{\pi^2 D}{a^2}\left(m + \frac{1}{m}\frac{a^2}{b^2}\right)^2$ where $D = \frac{Eh^3}{12(1-\nu^2)}$.

2.7 Heat Transfer

The transfer of energy as heat is always from the higher – temperature medium to the lower – temperature one, and heat transfer stops when the two mediums reach the same temperature. Heat can be transferred in three different modes: conduction, convection and radiation (Figure 29). All modes of heat transfer require the existence of a temperature difference, and all modes are from the high – temperature medium to a lower – temperature one [50].

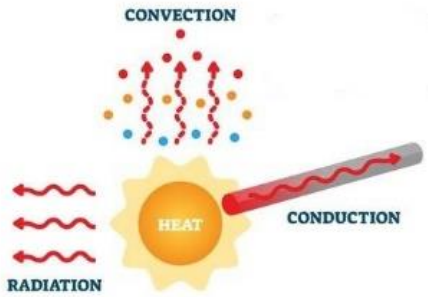

Figure 29: Heat transfer mechanisms

2.7.1 Conduction

Conduction is the transfer of energy from the more energetic particles of a substance to the adjacent less energetic ones as a result of interaction between the particles. Conduction can take place in solids, liquids, or gases. Rate of conduction heat transfer can be described from equation (53) which is called Fourier's law of heat conduction. Where k is the thermal conductivity of the material, A is the heat conduction area and $\frac{\mathrm{d}T}{\mathrm{d}x}$ is the temperature gradient [50].

$$\dot{Q}_{cond} = k * A * \frac{\mathrm{d}T}{\mathrm{d}x} \tag{53}$$

2.7.2 Convection

Convection is the mode of energy transfer between a solid surface and the adjacent liquid or gas that is in motion, and it involves the combined effects of conduction and fluid motion. Convection is called forced convection if the fluid is forced to flow over the surface by external means such as fan, pump, or the wind. In contrast, convection is called natural (or free) convection if the fluid motion is caused by buoyancy forces that are induced by density differences due to the variation of temperature in the fluid. Despite the complexity of convection, the rate of convection heat transfer is conveniently expressed by Newton's law of cooling (equation (54)) where h is the convection heat transfer coefficient, A_s is the surface area through which convection heat transfer takes place, T_s is the surface temperature and T_∞ is the temperature of the fluid sufficiently far from the surface [50].

$$\dot{Q}_{conv} = h * A_s * (T_s - T_\infty) \tag{54}$$

2.7.3 Radiation

Radiation is the energy emitted by matter in the form of electromagnetic waves as a results of the changes in the electronic configurations of the atoms or molecules. Unlike conduction and convection, the transfer of energy by radiation does not require the presence of an intervening medium. The maximum rate of radiation that can be emitted from a real surface at an absolute temperature can be expressed from equation (55) where ε is the emissivity of the surface, $\sigma = 5{,}67 * 10^{-8}\ W/m^2K^4$ is the Stefan – Boltzmann constant, A_s is the area of the surface and T_s is the surface temperature [50].

$$\dot{Q}_{rad} = \varepsilon * \sigma * A_s * T_s^4 \tag{55}$$

2.8 Combustion

Combustion is a high – temperature exothermic chemical reaction between a fuel and an oxidant that produces oxidized, often gaseous products, in a mixture termed as smoke. In complete combustion, the reactant burns in oxygen and produces a limited number of products. When a hydrocarbon burns in oxygen, the reaction will primarily yield carbon dioxide and water. Incomplete combustion will occur when there is not enough oxygen to allow the fuel to react completely. It also happens when there is sufficient amount of oxygen but the combustion cannot use the proper amount of oxygen due to its nature. The products of the incomplete combustion are not clearly defined, however, carbon, carbon monoxide, hydroxide and NO_x are some of the products except from carbon dioxide and water. Combustion theory includes chemistry, chemical thermodynamics, chemical kinetics and other theories, which cannot be presented and analyzed in the framework of this master thesis. In this chapter, specific definitions and essential theories will be presented.

A mole is defined as the quantity of a given substance that contains as many molecules or formula unit as the number of atoms in exactly 12 g of carbon. The number of atoms in a 12 g sample of carbon is called Avogadro's number ($6.0221367 * 10^{23}$). The molar mass of a substance is the mass of one mole of the substance. From equation (56), the moles of a substance can be calculated with a given mass and molar mass [51].

$$n = m/M_r \tag{56}$$

The heat of reaction or heat evolved can be calculated from the given heats of formation of the substances which are comprised in reaction. The heat of reaction is calculated in reference temperature T_0 (equation (57)). Heat release rate can be calculated from the heat of reaction and the fuel mass burning rate (equation (58)) [51,52]. For a combustion process that takes place adiabatically with no shaft work, the temperature of the products is referred to as the adiabatic flame temperature. Excess air will reduce the adiabatic flame temperature [53].

$$\Delta H_{T_0} = \Delta H_c = \sum_{i,\,prod} n_i (\Delta H_f)_{T_0,i} - \sum_{j,react} n_j \left(\Delta H_f\right)_{T_0,j} = -Q_p \tag{57}$$

$$\dot{Q}_c = \Delta H_c * \dot{m}_{fuel} \tag{58}$$

2.9 Pool Fires

Pool fires concern flames developed over horizontal fuel surfaces. Typically, pool fire can be determined as a fire in an open – topped, circular flammable liquid tank or a bounded spill of combustible liquid. Pool fires can be categorized based on type of the flame in: premixed flame, when the fuel and the oxidizer are mixed before reacting each other and diffusion flame, when only the fuel is supplied to the burner and the oxidizer is supplied from the ambient air. Based on the ventilation quality they can be categorized into open pool fires (well ventilation) and enclosure pool fires (poor ventilation). Some significant parameters of a pool fire are: the pool geometry, the fuel composition, the duration of the fire, the ventilation conditions and the surrounding geometry [54], [55].

Intensive research has been carried over decades. The review study of Steinhaus [54] presents a discussion of the different physical factors affecting the behavior of large pool fires. Special attention is given to large pool fires ensuing form spills. Also, describes the challenges in pool fire modelling due to the complex and highly coupled nature of the problem. Computational Fluid Dynamics (CFD) are used to model pool fires. Most common techniques for turbulence representation are RANS (Reynolds Average Navier Stokes) and LES (Large Eddy Simulation). The review has clearly shown that despite the enormous body of work on large – scale pool fires there are still significant uncertainties in our understanding of such fires and capabilities to predict their behavior.

Chapter 11 in section 3 of Handbook of Fire Protection Engineering [55] presents detailed techniques for calculating impacts from large, open hydrocarbon fires. The state of the art of predicting the thermal environment of hydrocarbon pool fires consists essentially of semiempirical methods, some of which are based on experimental data. These semiempirical methods are always subject to uncertainties. Several correlations for pool fire geometry have been developed from researchers (equations (59)), where $\dot{m}$ is the mass burning rate per unit pool area (kg/m^{2}sec), ρ_α is the ambient air density (kg/m^3), H is the height of the flame (m), D is the diameter of the flame (m) and $\dot{Q}$ is the heat release rate (kW). Furthermore, this chapter presents screening methods and detailed methods for the thermal radiation from large pool fires to external targets. A screening method was proposed by Shorki and Beyler in 1989 [56].

$$Thomas: \frac{H}{D} = 42\left(\frac{\dot{m}}{\rho_\alpha\sqrt{gD}}\right)^{0.61}$$
$$Heskestad: \frac{H}{D} = 0.235\frac{\dot{Q}^{\frac{2}{5}}}{D} - 1.02 \quad (59)$$

Burning rate of a pool fire is significant parameter since it is depended from the pool fire diameter and the fuel composition. Babrauskas [57] made a distinction in pool fires relative to diameter and summarized the available information for the burning rate. Moreover, he presented burning rate relative to pool diameter for gasoline and LNG. With the increase of pool diameter the burning rate of the fuel remain constant. He proposed an equation for estimating the burning rates for pools with diameter greater form 0.2 m (equations (60)), where $\dot{m}_\infty$ is the infinite – diameter pool mass loss rate (kg/m^{2}sec), k is the extinction coefficient (m^{-1}), β is the mean

beam length corrector, Δh_c is the lower heat of combustion (kJ/kg) and A is the pool area (m^2). The factor $k\beta$ is given from tables of experimental data for each fuel. A simple curve of fire heat release rate is presented in Figure 30 [58].

$$\dot{m} = \dot{m}_{\infty}\left(1 - e^{-k\beta D}\right)$$
$$\dot{q} = \Delta h_c \dot{m} A \tag{60}$$

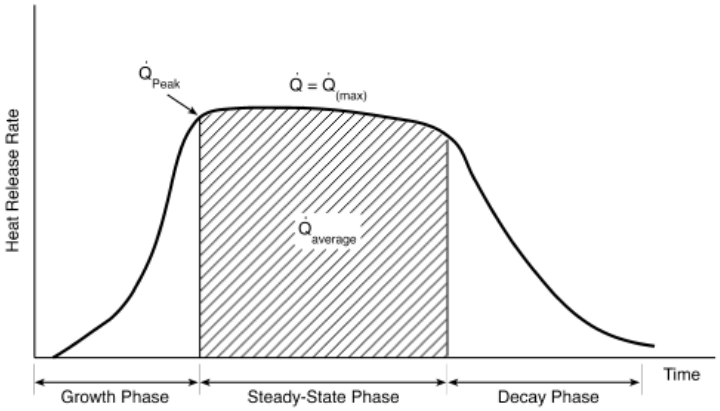

Figure 30: A simple design fire curve [58]

Chapter 14 in section 2 of Handbook of Fire Protection Engineering [55] presents empirical correlations for predicting heat transfer from flames. However, their use is usually limited to a particular type of fire or the geometry of the surface being heated. Heat fluxes from exposure fires adjacent to flat walls can be calculated by experimentally generated equation (61). The equation includes convection and radiation heat transfer.

$$q_{peak} = 200 * \left[1 - e^{-0.09Q^{\frac{1}{3}}}\right] \left(\frac{kW}{m^2}\right),\ Q\ in\ kW \tag{61}$$

Chapter 3: Benchmark Analysis – Bending

The benchmark analysis presented in present chapter assists in evaluation of ABAQUS structural analysis, in comparison of computational results and experimental results, in results consistency and in correct finite element modelling (mesh density and topology, force and boundary condition application, assumptions) of the examined problem. The computational analysis results compared to equivalent results from Paik's study [3].

3.1 Benchmark Analysis Parameters

Figure 31 shows the length of the beam, the boundary conditions and the load application of the analysis. Figure 32 shows the dimensions of steel beam used in the analysis. Figure 33 describes the mechanical load profile and Figure 34 shows the analysis temperature profile. The beam temperature is calculated from the heat transfer equation method from EN 1993 – 1 – 2 as described in paper. The temperature curve received from the paper using the Graph Grabber program. The temperature was applied as predefined field on the beam surfaces and the line mechanical load modeled with 7 concentrated loads. The material properties have been discussed extensively in the reference paper [3] and are presented in Appendix A. The boundary condition at first end was pin and at second was roller. Total step time was 3500 in static general step. For the mesh generation shell elements (S4R) were used with global mesh size equal to 0.06 m [3].

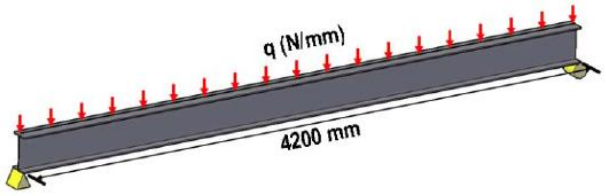

Figure 31: Loading and boundary conditions of steel beam [3]

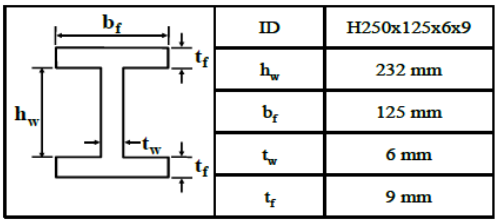

ID	H250x125x6x9
h_w	232 mm
b_f	125 mm
t_w	6 mm
t_f	9 mm

Figure 32: Dimensions of steel beam [3]

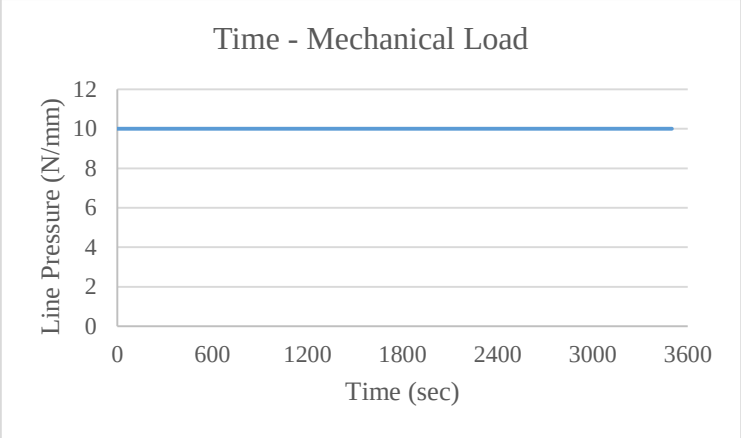

Figure 33: Mechanical load profile [3]

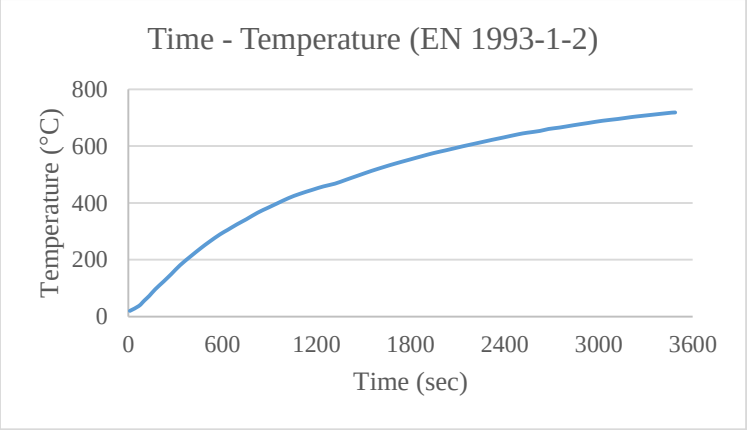

Figure 34: Temperature profile [3]

3.2 Mesh Convergence Analysis

In order to specify the amount and the topology of elements a mesh convergence study was conducted. For the mesh convergence analysis a beam with roller boundary conditions and point load equal to 100 kN in the middle was used. The geometry and the material of the beam were the same as described above. Figure 35 shows the load and the BCs. Global mesh size parameter was examined in the analysis.

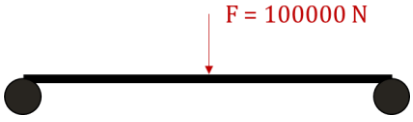

Figure 35: Mesh convergence analysis load and BCs

The displacement in the middle of the beam can be calculated from analytical solution [45]. The middle displacement is given form the equation (62).

$$v\left(x=\frac{L}{2}\right)=-\frac{\mathrm{F}L^3}{48EI_z}=-0{,}01888036\,m \tag{62}$$

In Table 2 the decrease of global mesh size (G.S.) is presented, relative to the increasing total number of elements (No.E.) in the beam. Figure 36 shows the convergence in the middle vertical displacement with the

decrease of global mesh size. Also, the figure presents a comparison between computational and analytical results. The convergence is obvious after the global mesh size reach the value of 0.06 m $\left(\frac{s}{t_w} = 10\right)$. Good results are also presented in greater global mesh sizes such as 0.1 m and 0.09 m.

G.S. (m)	1	0.75	0.5	0.3	0.2	0.15	0.1	0.09	0.08	0.07	0.06	0.05	0.04	0.03	0.02	0.01
No.E.	20	30	40	70	110	168	252	322	364	420	560	756	1484	2240	5040	19740

Table 2: Global mesh size relative to total number of elements

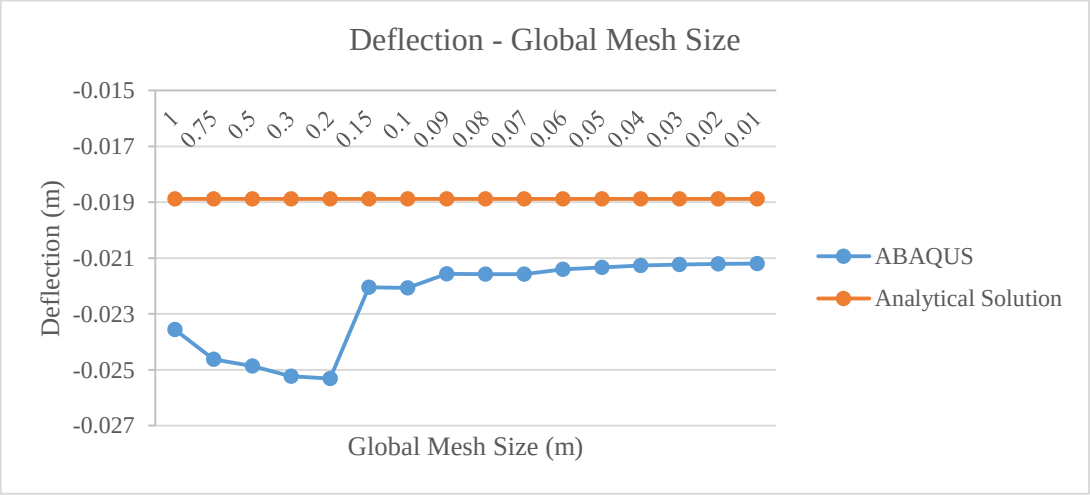

Figure 36: Deflection relative to global mesh size

3.3 Load Validation

The line load presented in paper used for benchmark analysis is inapplicable in 3D ABAQUS geometries. Consequently, the line load should be transformed in n – point loads. The analysis concept is presented in Figure 37. Beam geometry and material were the same as Paik's paper [3].

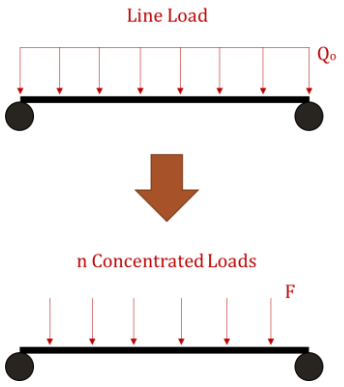

Figure 37: Load validation analysis concept

The displacement in the middle of the beam can be calculated from analytical solution [45]. The middle displacement is given form the equation (63). Figure 38 shows the middle vertical displacement relative to number of concentrated loads. Moreover, the figure shows the displacement from the analytical solution and

from computational analysis of line load applied to 1D geometry. The difference between the curves minimizes as the number of concentrated loads rises. When the number of concentrated loads is equal to 7 the difference for the 1D line load analysis is below 1%.

$$v_{max} = -\frac{5Q_oL^4}{384EI_z} = -0{,}0049561\ m\ (Q_o = 10000N) \quad (63)$$

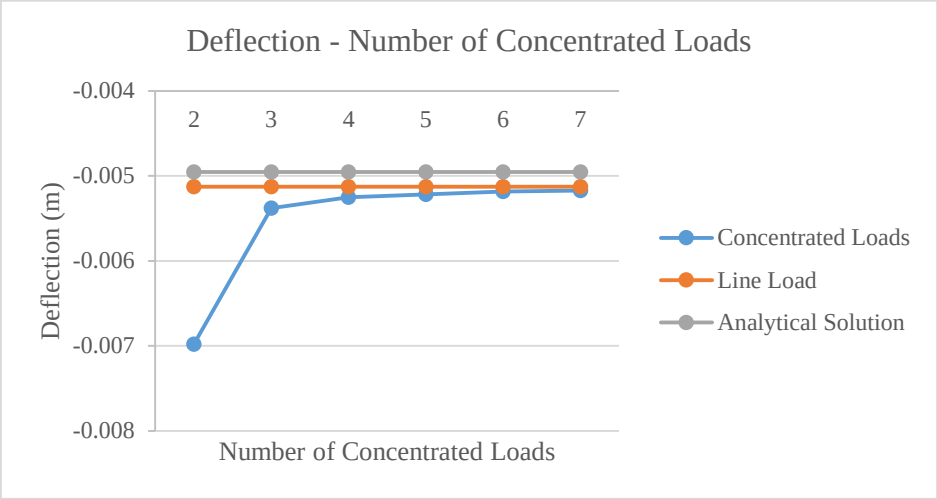

Figure 38: Deflection relative to number of concentrated loads and comparison with 1D line load and analytical solution

3.4 Benchmark Analysis Results

Figure 39 shows the structural response in ABAQUS compared to structural responses from the paper (computational & experimental)[3]. Deflection at upper flange from ABAQUS analysis seems to be very close to experimental and computational results from the reference paper.

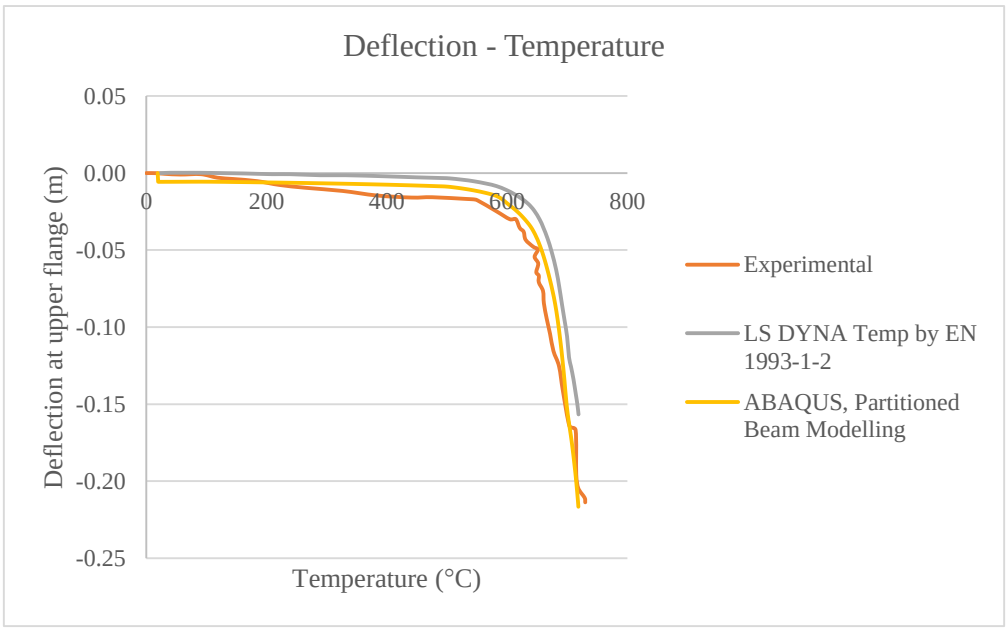

Figure 39: Structural response in ABAQUS and comparison

Beam's middle deflection is significant large after 600°C. This is due to material properties degradation at elevated temperatures as described from Eurocode. It can be noted that steel strength at 500°C is 50% lower than the strength at 20°C. Differences between experimental and ABAQUS results are based on the material properties such as true stress – strain relations and hardening phenomenon and on temperature differences. Differences between LS – DYNA and ABAQUS results are based on solution step and on the temperature modelling as there is no reference in the paper for these parameters. Figure 40 depicts the beam temperature in 3500 step time and Figure 41 depicts the vertical displacements (U2) at the same step time.

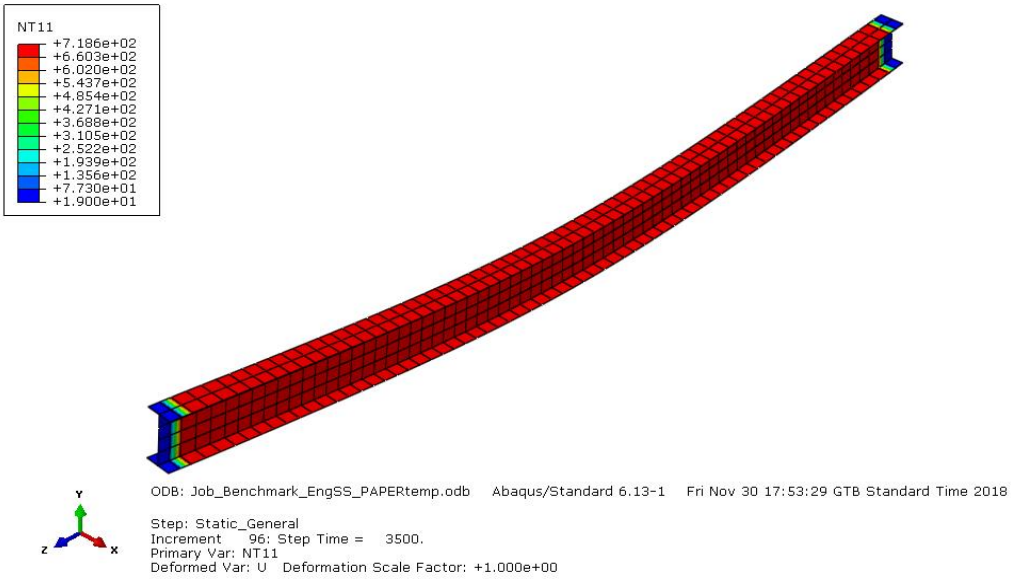

Figure 40: Beam temperature in 3500 step time

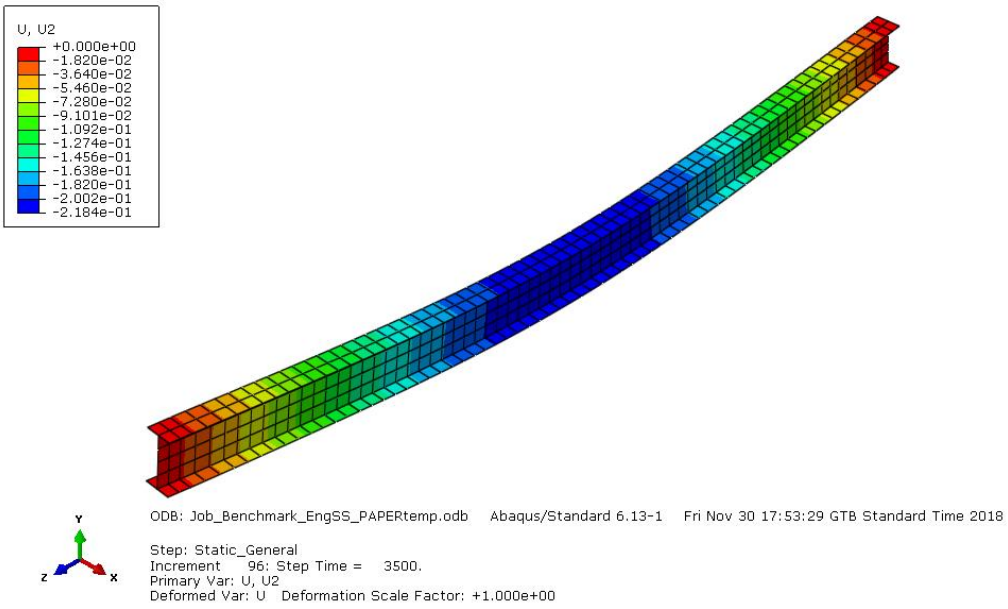

Figure 41: Beam vertical displacement in 3500 step time

Chapter 4: Benchmark Analysis – Buckling

Another benchmark study was executed in order to verify and evaluate the procedure of the nonlinear buckling analysis of unstiffened and stiffened panels in ABAQUS. As it has been mentioned before, a benchmark analysis assists in correct finite element modeling of the problem and in results consistency. The ultimate strength of unstiffened panel and stiffened plates was examined. The result from the unstiffened panel analysis was compared with equivalent results presented by Paik et al. [18], while the results from the stiffened plates were compared with the results of the study from Soares et al. [22]. The present reference studies do not include experimental results so the comparison will be between the computational results. For the following analyses the arc length method (Static Riks Step) was used.

4.1 Unstiffened Panel

One bay plate model was used for the present benchmark analysis. This specific model represents the plate between the longitudinal and transverse stiffeners of the outer bottom stiffened plate structure of an AFRAMAX – class hypothetical double hull oil tanker designed by CSR method [18]. The material and geometric characteristics of the unstiffened panel are presented in Table 3.

Yield Stress	315 MPa
Young's Modulus	205.8 GPa
v	0.3
a	4300 mm
b	815 mm
t	17.8 mm

Table 3: Material properties and geometric characteristics of unstiffened panel

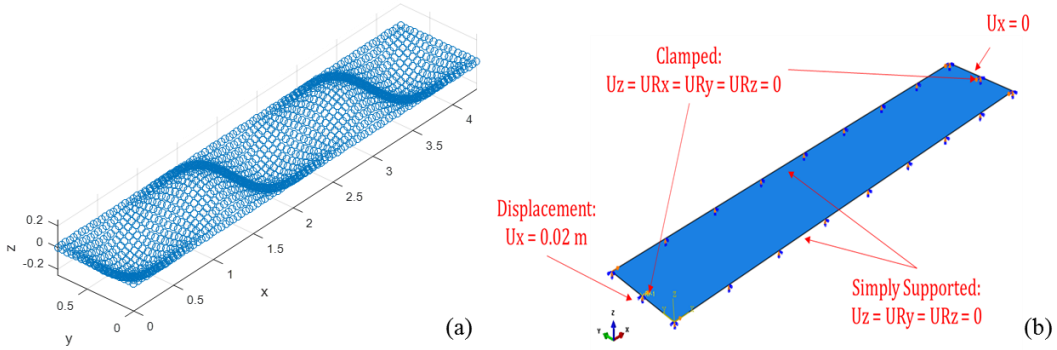

Figure 42: (a) Initial geometric imperfections of unstiffened panel, (b) Boundary and loading conditions of unstiffened panel

The material was assumed as elastic – perfectly plastic. For the mesh generation S4R elements were used with a size of $50\ mm * 50\ mm$ as proposed in the reference study. The maximum plate initial deflection w_{opl} was calculated from the following formula: $w_{opl} = b/200$ and the deflection pattern expressed by the following formula: $w_p = w_{opl} * \sin\left(\frac{m\pi x}{a}\right) * \sin\left(\frac{n\pi y}{b}\right)$, where a and b is the length and breadth of the plate,

respectively. Figure 42 (a) presents the initial deflection pattern where m is equal to 5 and n is equal to 1. The procedure for the initial deflection pattern in MatLab is presented in Appendix C. The boundary and loading conditions are presented in Figure 42 (b).

Figure 43 presents the comparison between the load end shortening curves from Paik's study [18] and the present study (ABAQUS). It can be seen that the value of ultimate strength of the unstiffened panel is almost the same in the two studies, but there is a significant difference in the post buckling region. This difference is based on the implicit and explicit analysis procedures. The explicit method is capable to obtain better the post buckling behavior than implicit method. The ultimate strength value presented by Paik is equal to 0.7240 while in the present study is equal to 0.7211 and there is a small difference in the equivalent ultimate strength strains. Figure 44 presents the deformed meshed unstiffened plate with stress contour at the ultimate strength.

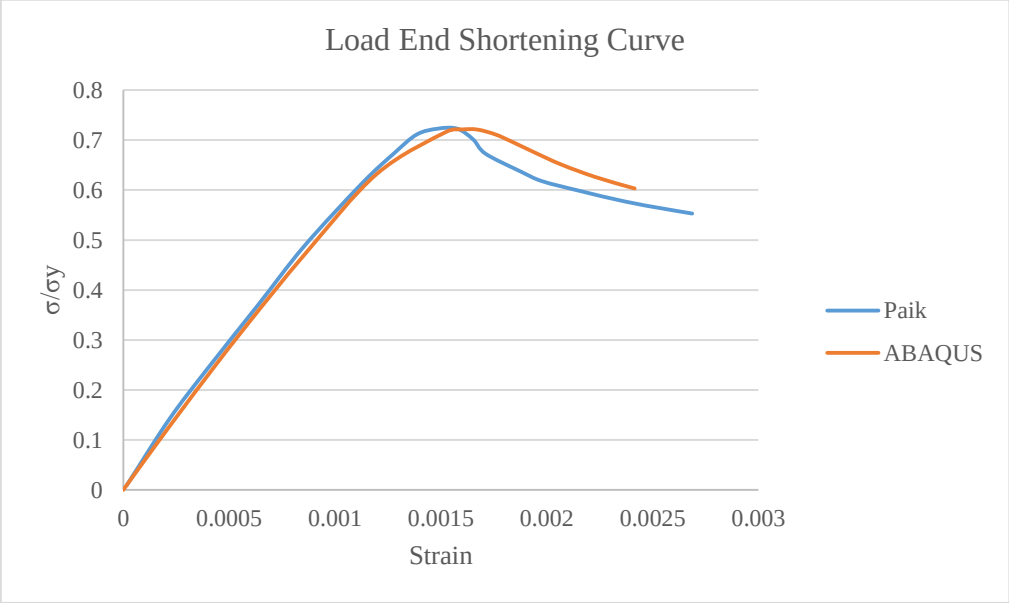

Figure 43: Load end shortening curves of unstiffened panel (reference & present study)

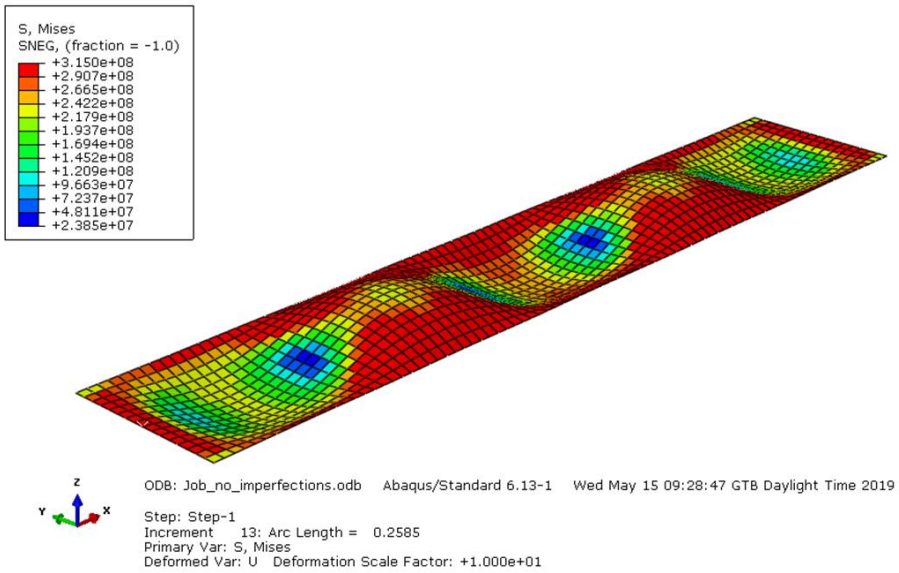

Figure 44: Stress contour of unstiffened panel at ultimate strength

4.2 Stiffened Plates

Two 1/2 + 1/2 bay stiffened plate model with different stiffener profiles were examined in the present benchmark analysis. This model extent is suitable for uniaxial load, while for biaxial stresses and lateral pressure model should be extended both in longitudinal and transverse direction [19,22] Analytically, a stiffened plate with T stiffener profile and a stiffened plate with L stiffener profile were examined. The geometric properties of the stiffened plates are presented in Table 4. For the present analyses the material assumed as elastic – perfectly plastic and the material properties are presented in Table 5. Boundary conditions were the same for the two types of stiffened plates. Boundary conditions are presented in Figure 45 for the stiffened plate with L stiffener profile. For the mesh generation S4R elements were used with size $40\ mm * 40\ mm$, as stated in the reference study [22].

Profile	a (mm)	B (mm)	t_p (mm)	h_w (mm)	t_w (mm)	b_f (mm)	t_f (mm)
T	4300	815	17.8	463.0	8.0	172.0	17.0
L	3840	820	17.5	223.2	11.0	50.8	28.4

Table 4: Geometric characteristics of the two types of stiffened plates [22]

Yield Stress	315 MPa
Young's Modulus	205.8 GPa
v	0.3

Table 5: Material properties of stiffened plates [22]

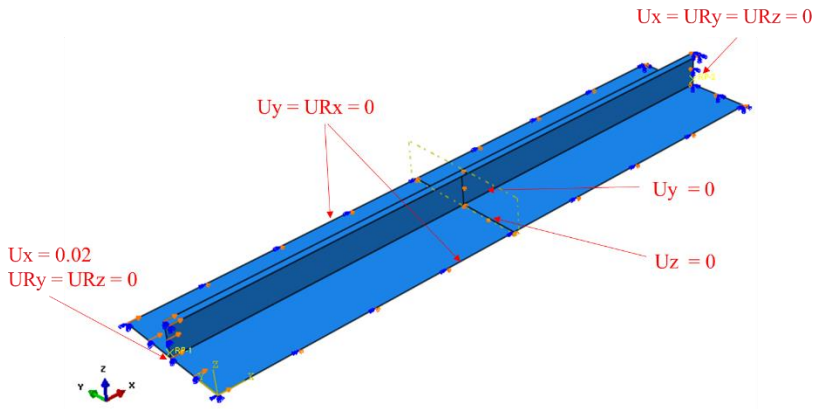

Figure 45: Boundary and loading conditions of stiffened plates

Three types of initial geometric deflections were used: plate deflection, beam column deflection and sideways deflection as described in the reference study [22]. The initial deflections were the same for the two types of stiffened plates, thus they will be presented only for the stiffened plate with T stiffener profile. The procedure for the initial deflection pattern in MatLab is presented in Appendix C. Figure 46 presents the initial and deformed stiffened plate with plate deflection and the formula describing the plate deflection. Figure 47 presents the initial and deformed stiffened plate with beam column deflection and the formula describing the beam column deflection. Figure 48 presents the initial and deformed stiffened plate with sideways deflection and the formula describing the sideways deflection. Figure 49 presents the initial and deformed stiffened plate

with the combination of all above deflections. The magnitudes for the above initial deflections are presented in Table 6. The formulas describing the initial imperfections are not clearly defined in the reference paper, so the below formulas are based on formulas presented at [48] and were modified properly in order to describe better the initial imperfection figures presented by reference study [22].

Maximum plate deflection	$w_p = b/200$
Maximum beam column deflection	$w_{oc} = a/1000$
Maximum sideways deflection	$w_{os} = a/1000$

Table 6: Magnitudes of the 3 types of initial deflections

$$w_{pl} = w_p * \sin\left(\frac{5\pi(x+0.43)}{a}\right) * \sin\left(\frac{1\pi(y-\frac{b}{2})}{b}\right)$$

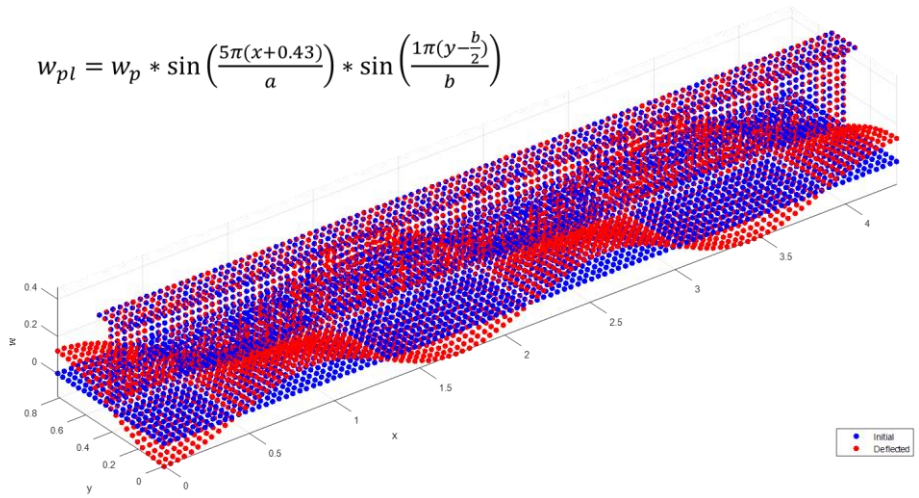

Figure 46: Plate initial geometric imperfection (amplitude 30)

$$w_{cl} = 2 * w_{oc} * \sin\left(\frac{1\pi(x-\frac{a}{2})}{a}\right) + w_{oc} * \sin\left(\frac{1\pi(x+\frac{a}{2})}{a}\right) * \sin\left(\frac{1\pi\left(y-\frac{b}{2}\right)}{b}\right)$$

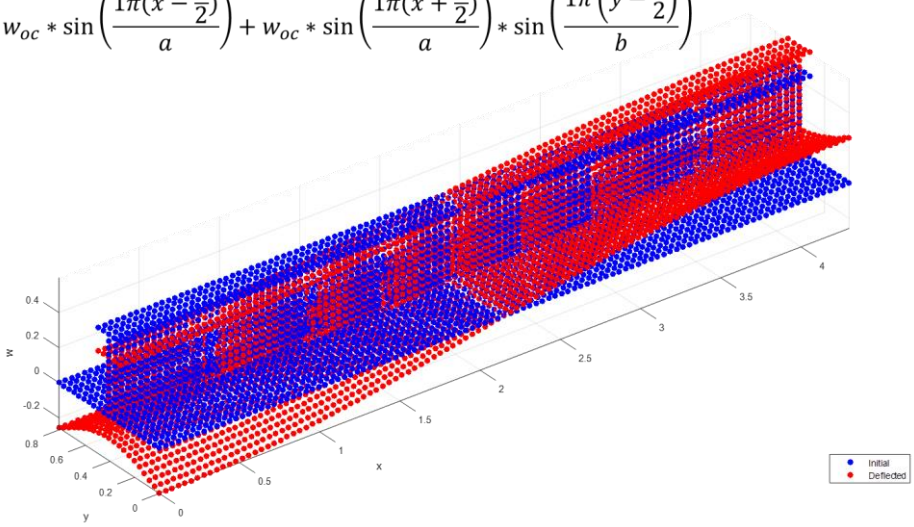

Figure 47: Beam column initial geometric imperfection (amplitude 30)

$$w_{flange} = dz = \frac{w_{os}}{h_w} * \sin\left(\frac{1\pi\left(x + \frac{a}{2}\right)}{a}\right) * \frac{(y - b/2)}{b}$$

$$w_{ss} = dy = \frac{w_{os}}{h_w} * z * \sin\left(\frac{1\pi(x - \frac{a}{2})}{a}\right)$$

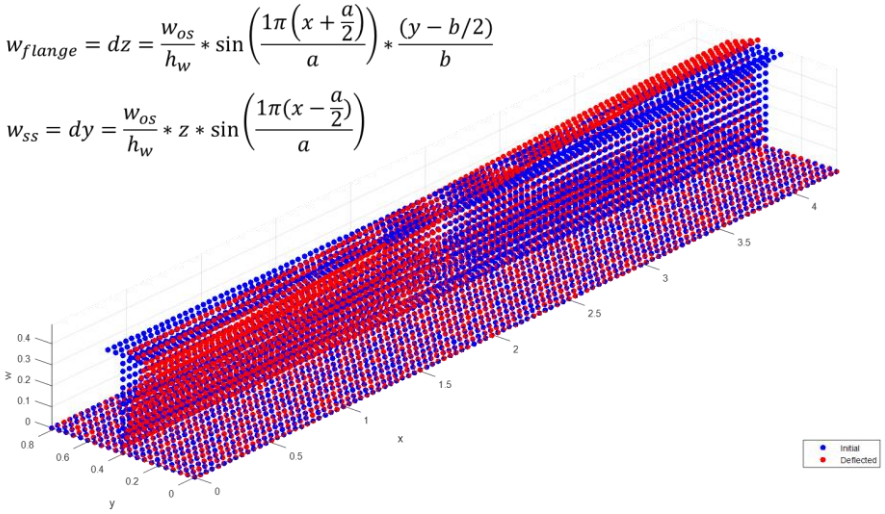

Figure 48: Sideways initial geometric imperfection (amplitude 30)

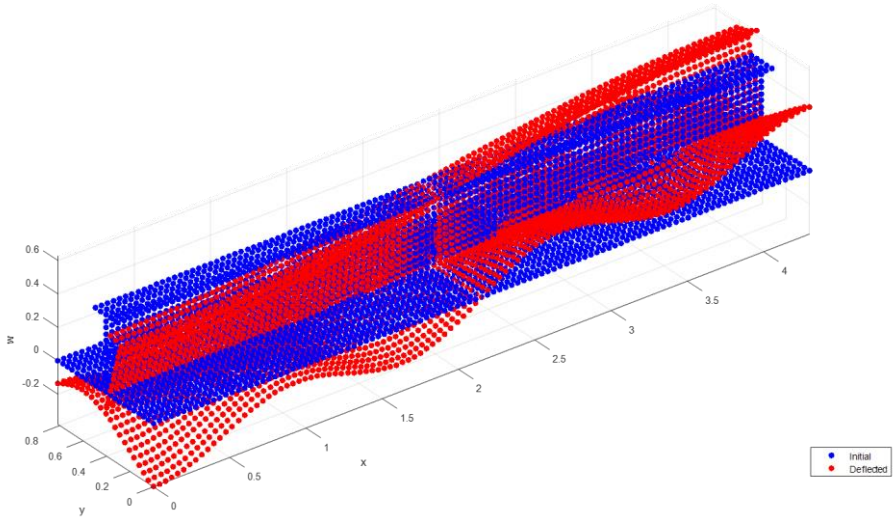

Figure 49: Total (3 types combined) initial geometric imperfection (amplitude 30)

4.2.1 Stiffened Plate with T Stiffener Profile

Figure 50 presents the results for the stiffened plate with T stiffener profile from the present study (ABAQUS) compared with the reference study [22]. The value of the ultimate strength of the stiffened plate (0.8527) is greater in the present study than the results from the reference study. The ultimate strength value presented by Soares et al. is equal to 0.7677, while Paik et al. equivalent value is 0.81. This is due to the differences in initial geometric imperfection. As stated before, the initial deflections are not clearly described in the reference study. The value of the ultimate strength of the stiffened plate obtained from the present study is closer to the equivalent value from CSR (0.8544). There are differences in the post buckling region, due to the analysis methods (implicit or explicit). Figure 51 presents the stress contour at the ultimate strength of the deformed stiffened plate with T stiffener profile from the reference study and the present study, respectively. There are differences on buckling mode, the reference model present plate and torsional buckling while the

present study model presents plate and web local buckling. The stress contours are the same at the plate region and different at stiffener region due to the difference in buckling mode. Furthermore, the ultimate strength of the stiffened plate without using initial deflections is greater than 1 (specifically 1.084) which means that in this case the model is stiffer. The difference between the value of ultimate strength in case of no initial deflection and the critical value 1 is small therefore can be neglected. Figure 52 presents the stress contour at the ultimate strength in case of no initial deflection. It can be obtained that the stresses do not overcome the value of yield stress.

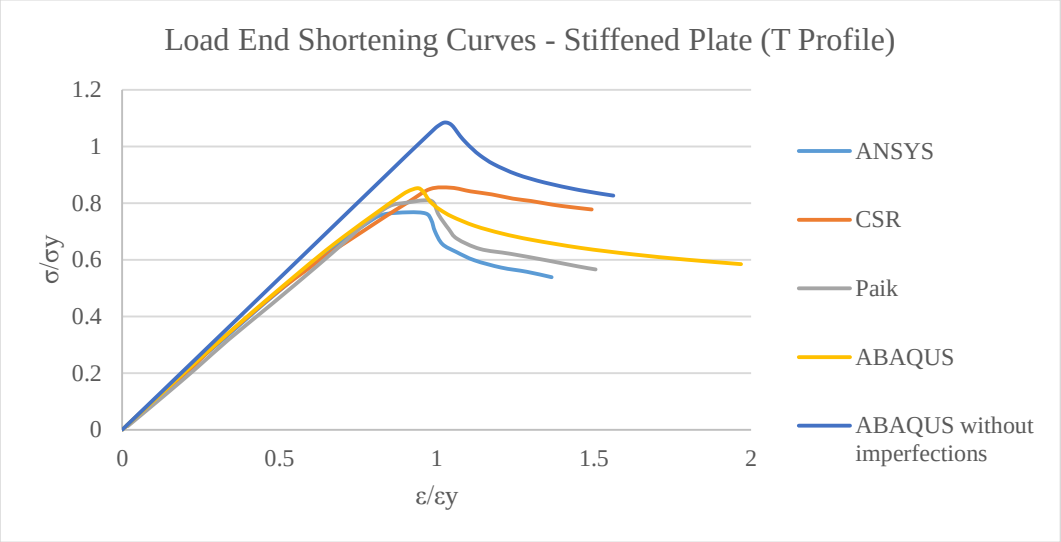

Figure 50: Load end shortening curves of stiffened plate with T stiffener profile

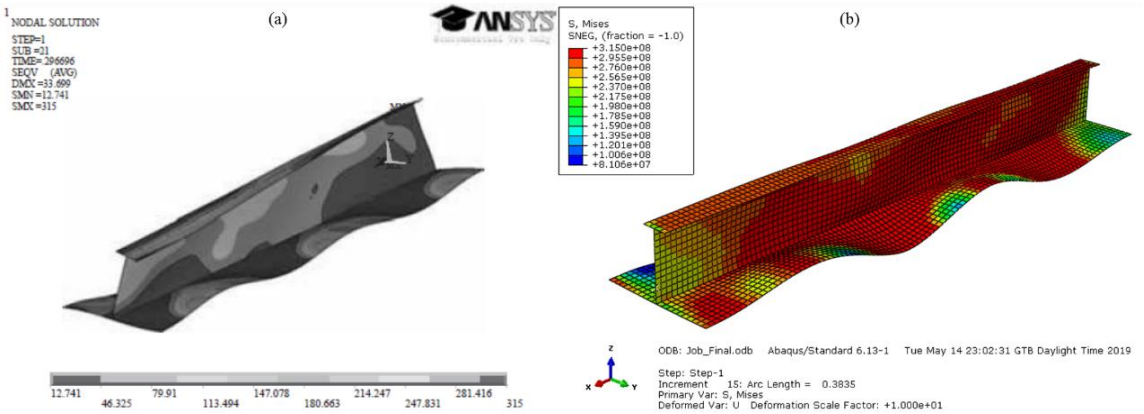

Figure 51: Stress contours of stiffened plate with T stiffener profile ((a) reference study, (b) present study)

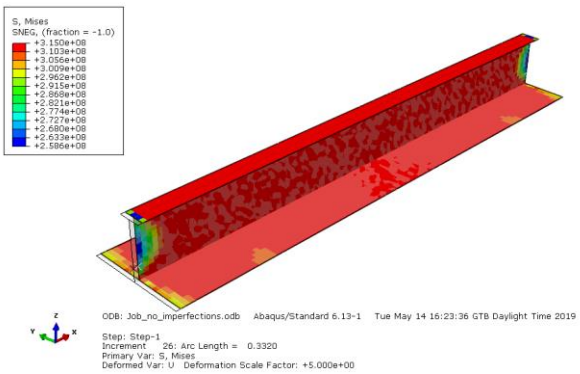

Figure 52: Stress contour on ultimate stress in case of no initial deflections

4.2.2 Stiffened Plate with L Stiffener Profile

Figure 53 presents the results for the stiffened plate with L stiffener profile from the present study (ABAQUS) compared with the reference study [22]. The value of the maximum ultimate strength of the stiffened plate is almost the same between the two studies. The value of the maximum ultimate strength presented by Soares et al. is equal to 0.7494 while the equivalent value from the present study is 0.7487. There are differences in the post buckling region, which are due to the analysis methods (implicit or explicit). The developed MatLab code for the calculation of the load shortening curves of stiffened plates [28,32] displays same results as the CSR results from the reference study. The value of the maximum ultimate strength of the stiffened plate presented by MatLab code is 0.8013 for beam column failure mode. Figure 54 shows the load end shortening curves for the 4 failure modes calculated from MatLab code. The developed MatLab code was based on the equations presented in section 7.1.1 and the code is presented in Appendix D. Figure 55 presents the stress contour at the ultimate strength of the deformed stiffened plate with L stiffener profile from the reference study and the present study, respectively. Both models present plate buckling and web local buckling. The stress contours are identical in plate region and slightly different in web region.

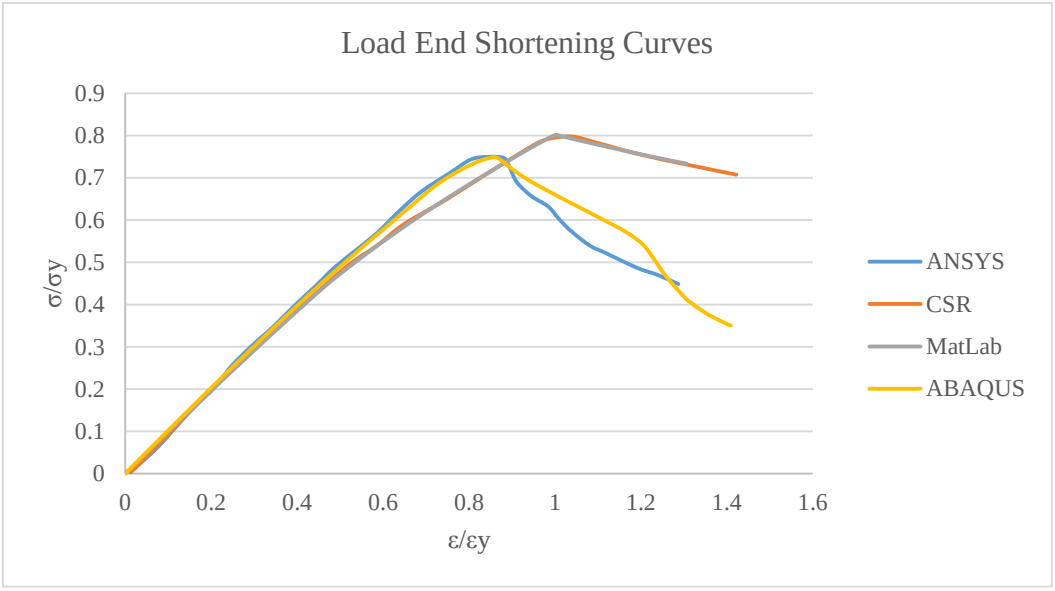

Figure 53: Load end shortening curves of stiffened plate with L stiffener profile

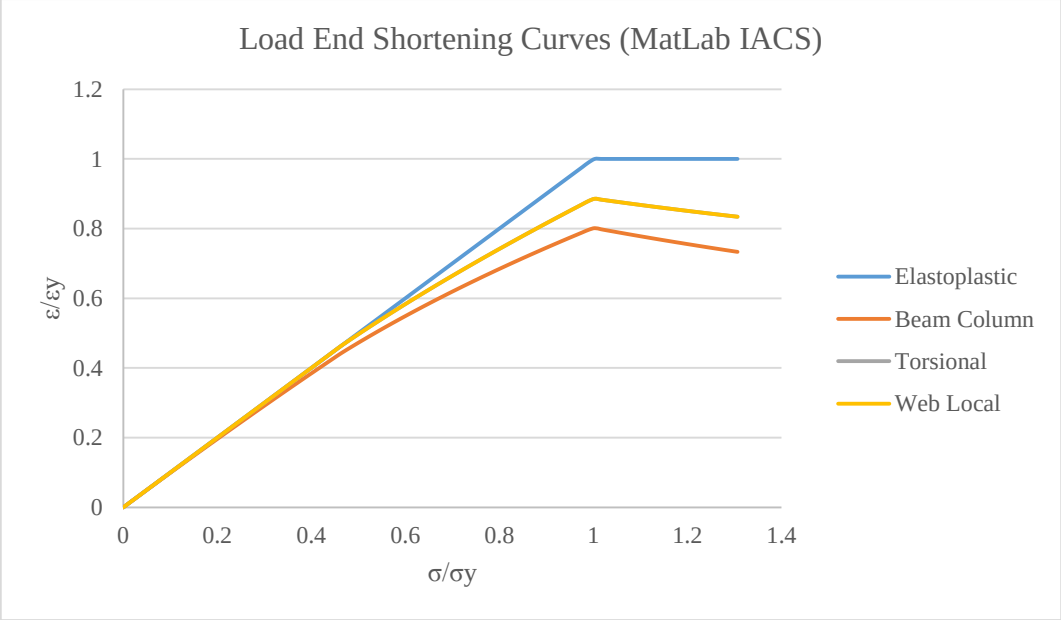

Figure 54: Load end shortening curves of stiffened plate with L stiffener profile calculated from MatLab code

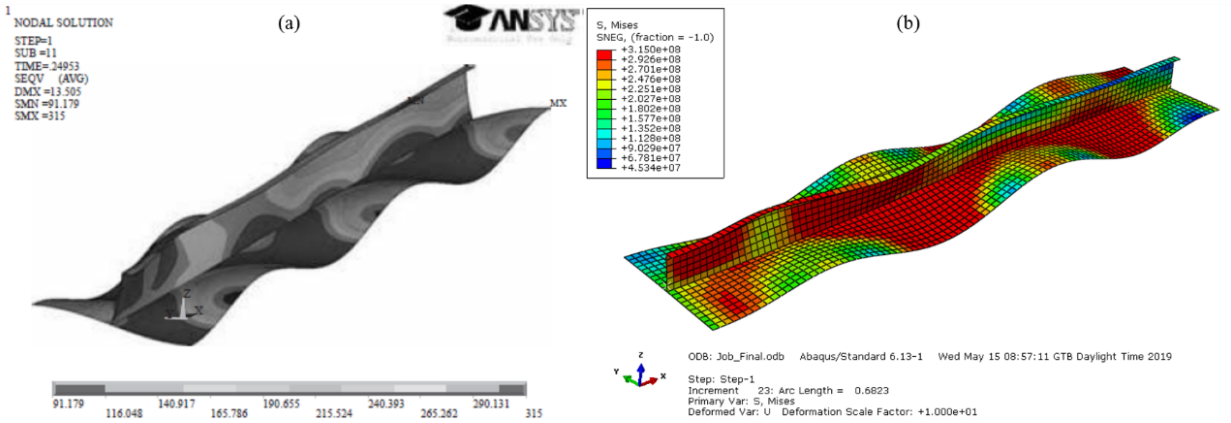

Figure 55: Stress contour of stiffened plate with L stiffener profile ((a) reference study, (b) present study)

Chapter 5: Finite Element Modelling Parameters

Computational analysis parameters have to be studied and examined before the analysis. This study is very significant not only for the reliability of the results but also for the correct physical modelling of the examined problem. According to that point of view, in this chapter studies on step, temperature profiles, load and boundary conditions for beam will be introduced. The impact of initial geometric imperfections in buckling analysis of stiffened plates will be presented. Mesh convergence and buckling at elevated temperature for a stiffened plate will be also presented. Furthermore, a thermal analysis on ship model used as input data in NLFEA analysis of ultimate strength and in modified Smith method will be introduced. Finally, for the examined ship model several analysis parameters studies were performed. Analytically, studies related the effect of initial geometric imperfection topology, the effect of the longitudinal bulkhead existence at the finite element model, the effect of boundary conditions, the effect of analysis method and finally the effect of the model geometric range were performed.

5.1 Step Examination for Thermomechanical Analysis

The purpose of this examination is to obtain the analysis step features on thermomechanical analysis. The examined steps are: Static General, Dynamic Implicit, Coupled Temperature – Displacement Steady and Coupled Temperature – Displacement Transient (Implicit) [35]. Prior to results presentation, examined step features are worth mentioned for better comprehension of the present examination. Static General step solves iteratively (NR Method) the equation (6) neglecting the first two terms, the mass and damping matrices. Static General step is used for time – independent structural analyses. Regarding temperature application, it is accomplished through the direct specification on the structure as a predefined field. Dynamic Implicit solves iteratively the equation (6) taking under consideration all the terms. Dynamic Implicit step is used for time – dependent structural analyses. Regarding temperature application, it is accomplished through the direct specification on the structure as a predefined field [40]. Both steps cannot describe heat transfer phenomena. Hence, when temperature is applied on structure, with Static General step we can obtain the static structural response under specific temperature states, while with Dynamic Implicit step we can obtain the dynamic structural response under specific temperature states.

Coupled Temperature – Displacement procedure is used to perform a coupled thermomechanical analysis. A thermomechanical analysis is a nonlinear calculation in which the displacements and temperature are simultaneously solved. In this way the reciprocal action of the temperature on the displacements and the displacements on the temperature can be taken into account. The influence of the temperature on the displacements is calculated through the thermal expansion and the effect of the displacements on the temperature is limited to radiation effects. Elements with temperature and displacement degrees of freedom required when Coupled Temperature – Displacement procedure is performed. Thermal terms referring to the temperature

degrees of freedom are added in the stiffness matrix. The thermal terms are related to material's thermal properties such as thermal expansion coefficient. Coupled Temperature – Displacement Steady step normally neglects time – dependent heat transfer phenomena. Regarding the mechanical analysis Coupled Temperature – Displacement Steady step solves iteratively the equation (6), neglecting the first two terms and taking under account additional terms for temperature degrees of freedom on stiffness matrix. Coupled Temperature – Displacement Transient step can model time – dependent heat transfer phenomena. Regarding the mechanical analysis Coupled Temperature – Displacement Transient step solves iteratively the equation (6), neglecting the first two terms and taking under account additional terms for temperature degrees of freedom on stiffness matrix. The main difference between the Coupled Temperature – Displacement Steady step and Coupled Temperature – Displacement Transient step is that the second one uses real time. In general, Coupled Temperature – Displacement procedure in the sector of mechanical analysis is identical to Static General step but it takes under account additional thermal related terms on stiffness matrix, in order to perform the thermomechanical analysis.

The examined total step times are 35, 350, 3500, 35000 and 350000 for Static General and Coupled Temperature – Displacement Steady steps and the examined analysis times are 35, 350, 3500, 35000 and 350000 seconds for Dynamic Implicit and Coupled Temperature – Displacement Transient steps. For Coupled Temperature – Displacement Transient one more analysis time was examined, 3.5 seconds. Beam from the bending benchmark analysis (geometry, material, mechanical and thermal loads and BCs) (Chapter 3) was used for this examination study. Loading profile and temperature profile have been applied according to the total step/analysis time of each case. Temperature profile was applied as a predefined field in Static General and Dynamic Implicit steps and as boundary condition in Coupled Temperature – Displacement steps.

Figure 56 and 57 present beam's middle vertical displacement relative to increasing temperature for Static General step and Dynamic Implicit step, respectively. It is observed that there is no difference between the examined total step times (Dynamic) or the examined total analysis times (Static). Figure 58 shows a comparison between Static General step and Dynamic Implicit step for 3500 step time and 3500 analysis time, respectively. The beam's response is identical in the two examined steps for the greater analysis time. In early time increments of Dynamic Implicit analysis beam presents a damped oscillatory response due to the steady load amplitude. It can be said that both Static General and Dynamic Implicit steps solve steady and dynamic structural states with given thermal conditions, respectively. Moreover, in both examined steps heat transfer time – dependent methods are not implemented, because the solution was independent of step or analysis time as it can been seen from Figures 56 and 57.

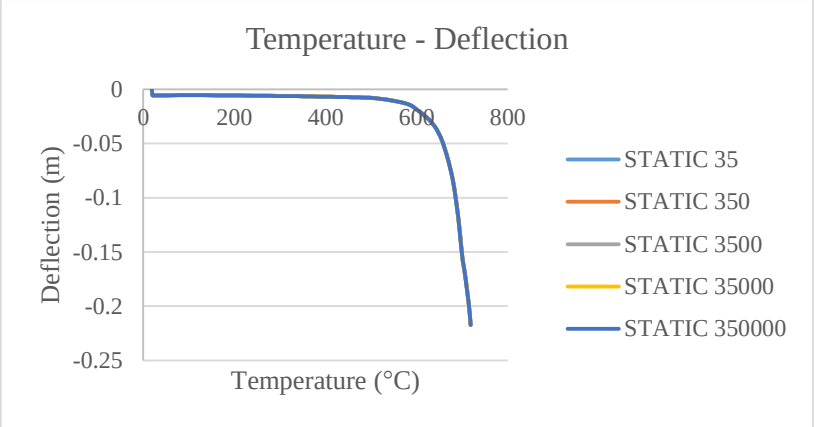

Figure 56: Beam response on static general step

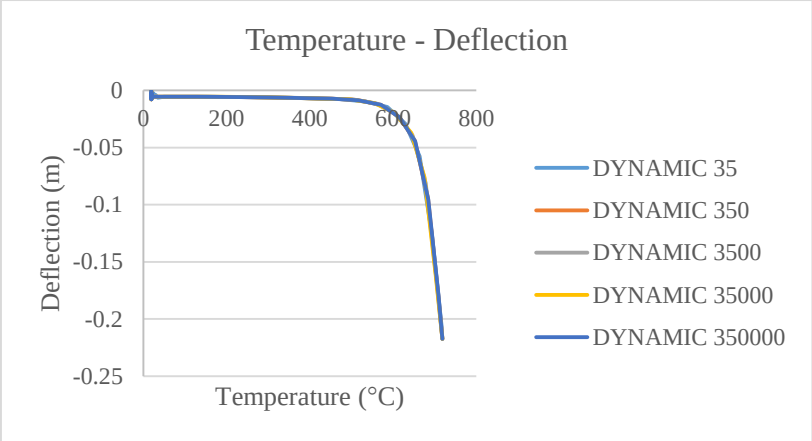

Figure 57: Beam response on dynamic implicit step

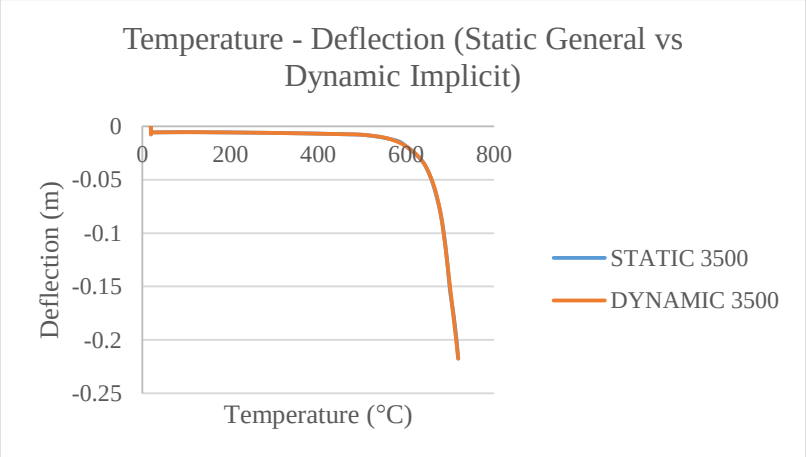

Figure 58: Beam response comparison static general – dynamic implicit

Figure 59 and 60 present beam's middle vertical displacement relative to increasing temperature for Coupled Temperature – Displacement Steady step and Coupled Temperature – Displacement Transient step, respectively. Different total step times in Coupled Temperature – Displacement Steady step has no effect on beam response, in contrast with Coupled Temperature – Displacement Transient step. In Coupled Temperature – Displacement Transient step heat transfer is analysis time – dependent. For lower analysis time, beam surface

temperature is equal to temperature profile but beam volume temperature has minor difference from the initial ambient temperature. On greater analysis time, beam temperature has reach an equilibrium state in which the total beam volume temperature follows temperature profile.

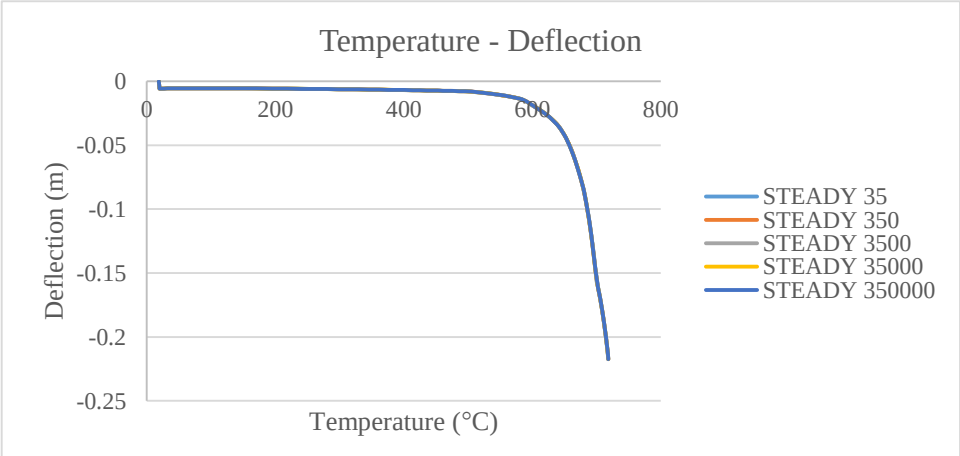

Figure 59: Beam response on coupled temperature – displacement steady step

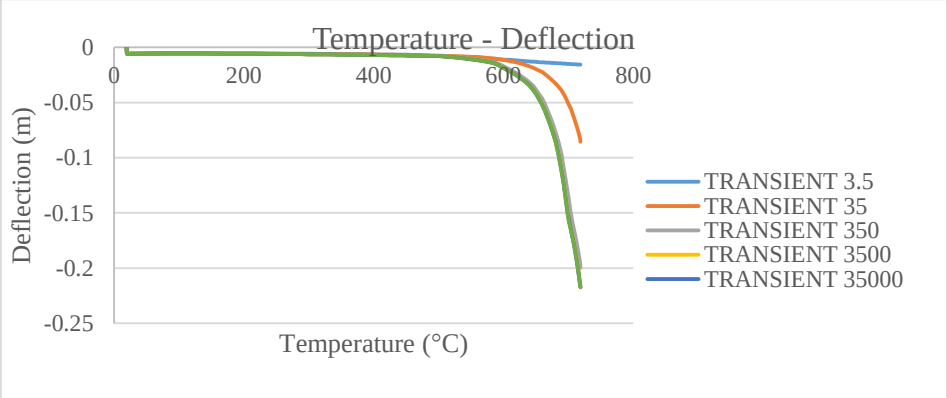

Figure 60: Beam response on coupled temperature – displacement transient step

Figure 61 shows a comparison on beam response between Coupled Temperature – Displacement Steady and Transient steps for 3500 step/analysis time. Figures 60 and 61 show that for greater analysis time the thermal response of the beam can be mentioned as pseudostatic and there is no dependency on analysis time for heat transfer. Figure 62 depicts a comparison on beam response between Static General step and Coupled Temperature – Displacement Transient step for 3500 step/analysis time. The thermomechanical response of the beam is identical between the two steps with a minor differences on the final value of middle vertical displacement.

The main purpose of the present section was to examine the step heat transfer features. It concluded that Static General and Dynamic Implicit steps do not include heat transfer phenomena and they solve static or dynamic structural states with a given temperature. Additionally, beam response in Coupled Temperature – Displacement steps obtained to be identical to beam response obtained from Static General step for greater analysis time. Hence, for a thermal analysis with greater analysis time time dependent heat transfer phenomena

can be neglected and Static General step can be used instead of Coupled Temperature – Displacement step which has the need for greater computational resources.

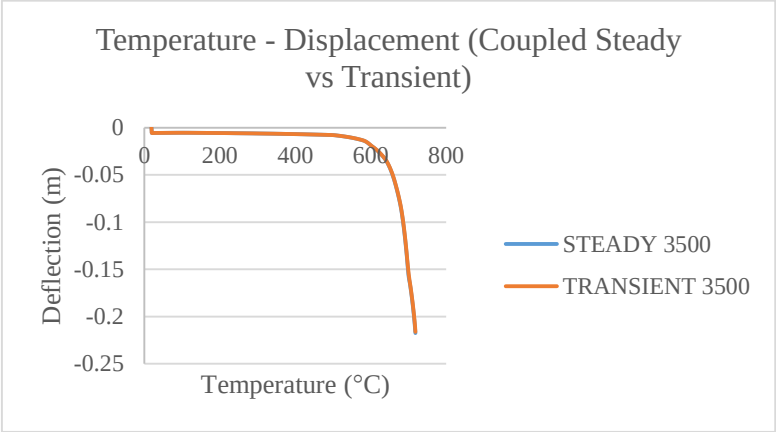

Figure 61: Beam response comparison coupled temperature – displacement steady – transient

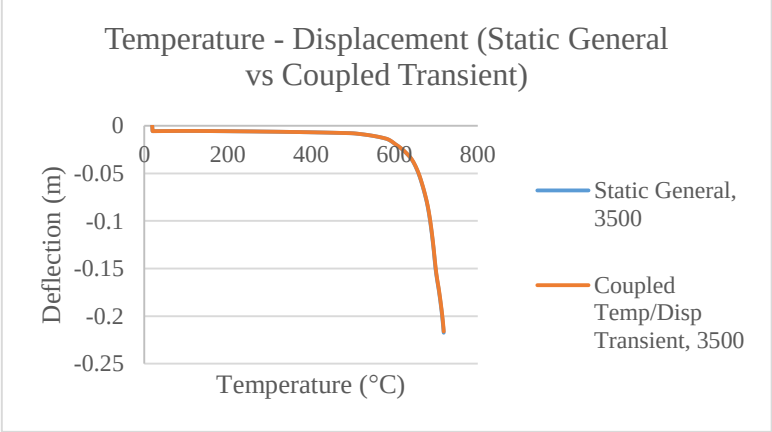

Figure 62: Beam response comparison static general – coupled temperature – displacement transient

5.2 Temperature Profiles Examination

Previous section examination indicated the effect of analysis step in thermal analysis with a given temperature profile. The impact of temperature profile in thermal analysis with two analysis steps will be examined in the present section. Three different temperature profiles were examined with two different step, Static General and Coupled Temperature – Displacement Transient. The examined temperature profiles were generated according to the temperature increase rate. They are presented in Figure 63 and described from equations (64). TP1 presents an early steep temperature increase rate, TP2 presents a steady temperature increase rate and TP3 presents a late steep temperature increase rate. Bending benchmark analysis beam (geometry, material, mechanical load and BCs) (Chapter 3) was used for this examination study. For the Static General step, total step time was equal to 1 and for the Coupled Temperature – Displacement Transient step the examined step analysis times were: 10, 100 and 10000 seconds.

$$TP1 = 672.1768 * (\log(t + 0.1) + 1)$$
$$TP2 = 700 * t \quad (64)$$
$$TP3 = 700 * t^4$$

Regarding to Static General step, beam response for 3 different temperature profiles are presented in Figure 64. There is no difference in beam response between 3 temperature profiles. Figure 64 confirms the previous observation related to the Static General step function.

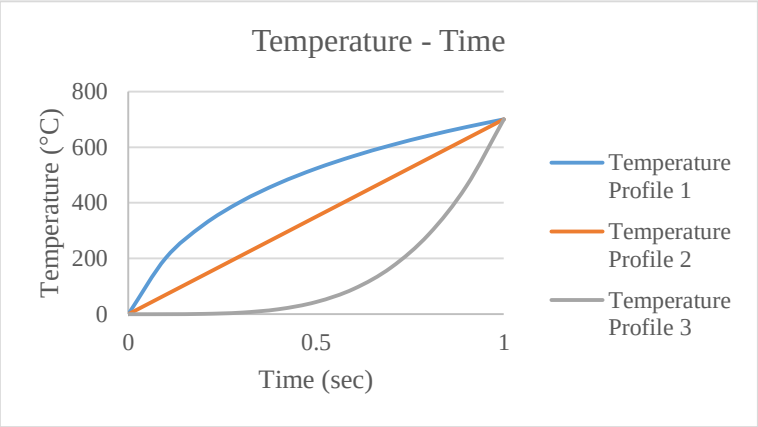

Figure 63: Temperature profiles

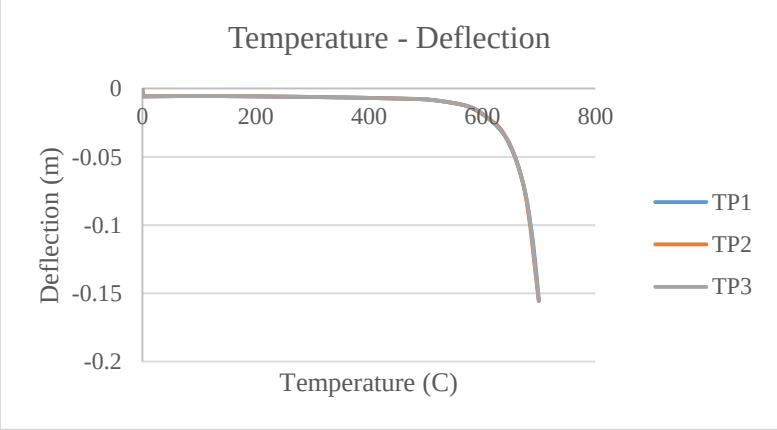

Figure 64: Beam response at 3 temperature profiles (Static General Step)

Figures 65, 66 and 67 show beam response at 3 temperature profiles for analysis time 10, 100 and 10000 seconds, respectively. At lower analysis time, there are minor differences on beam response due to the fact that the final beam volume temperature is very close to initial ambient temperature. In addition to that, the middle vertical displacement of the beam is relatively small. At medium analysis time, beam response in temperature profile 1 presents the greater middle vertical displacement. This response is because of the rapid increase of temperature. At greater analysis time, beam responses are identical. Thus, for greater analysis time heat transfer phenomena can be considered as pseudostatic.

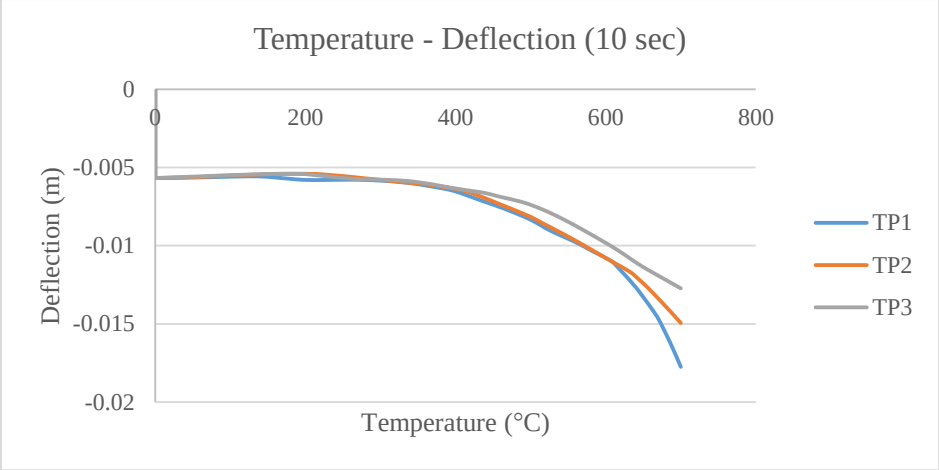

Figure 65: Beam response at 3 temperature profiles (Coupled Temperature – Displacement Transient Step, 10 sec)

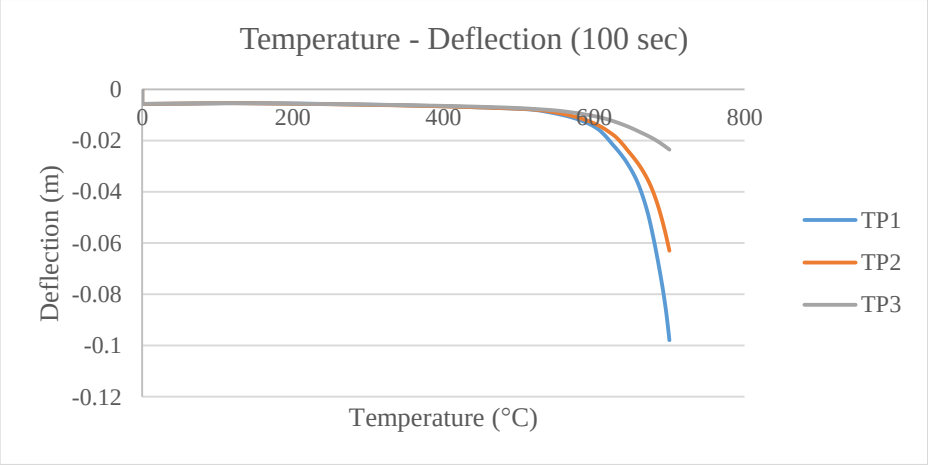

Figure 66: Beam response at 3 temperature profiles (Coupled Temperature – Displacement Transient Step, 100 sec)

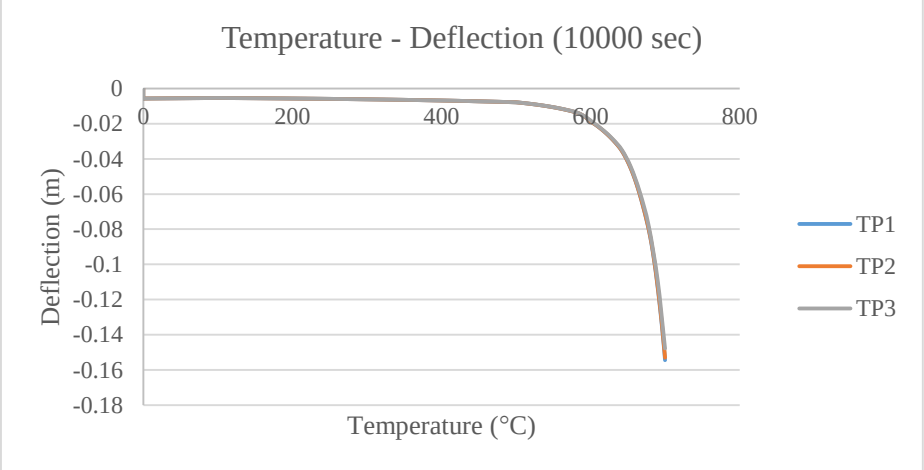

Figure 67: Beam response at 3 temperature profiles (Coupled Temperature – Displacement Transient Step, 10000 sec)

To sum up, it is obvious that Coupled Temperature – Displacement Transient step have the time – dependent heat transfer feature and provides a fully coupled thermal stress analysis [35]. For greater analysis time, beam thermal response can be stated as pseudostatic but in lower analysis time the heat transfer phenomena are significant and cannot be neglected. The above analyses confirmed that Static General step solves steady

structural states with a given temperature. Thus, Static General step can be used instead of Coupled Temperature – Displacement Transient step.

5.3 Square Beam Analysis

A ship can be modelled as a thin walled beam with longitudinal and transverse stiffeners. Hence, in the present section a square thin walled beam with transverse stiffeners is introduced. The present beam model consists a premature ship model. The scope of the present examination is to obtain the structural response of a ship shaped structure subjected to thermomechanical loads. Specifically, examination studies on thermal load application topology, boundary conditions, thermal expansion and critical load will be presented.

5.3.1 Geometry, Material & Analysis Parameters

Square beam geometry was generated in CATIA and then imported in ABAQUS. The wall and transverse stiffeners thickness is 0.02 m. Figure 68 shows the geometry and the dimensions of the beam. The beam material is carbon steel, modelled with engineering stress – strain relationship and without hardening, as presented in Appendix A.

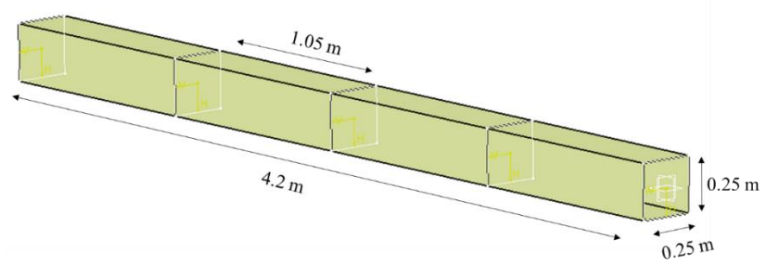

Figure 68: Square beam dimensions

Square beam in ABAQUS was modelled with shell elements (S4R). The global mesh size was based in the previous mesh convergence study and it is equal to 0.06 m. Standard (ISO) and hydrocarbon (HC) temperature – time curves were used (Appendix B). Static General step was used for the analyses. Temperature profiles were modelled as predefined field.

5.3.3 Thermal Load Topology

A four point bending was modelled in ABAQUS, with pressure load at each surface equal to 840 kPa (Figure 69). Each surface area was 0.025 m^2. The load value was based on the benchmark analysis load. A pin and a roller boundary conditions were used. The beam was divided in 4 parts as Figure 69 shows. Three cases of thermal load application were studied as presented in Figure 70. In Case ALL, the thermal load applied in the whole beam internal surface. In Case 23, the thermal applied in sections 2 and 3 internal surfaces and in Case 2, the thermal load applied in section 2 internal surface.

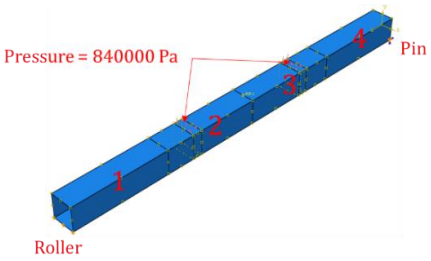

Figure 69: Sections, BCs and load of square beam

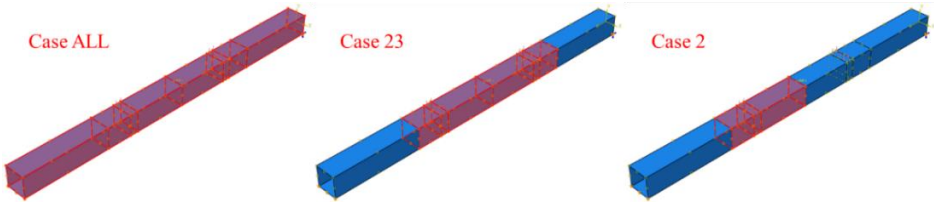

Figure 70: Thermal load cases of square beam bending analysis

Figure 71 shows the middle vertical displacement of the beam with the increasing temperature (ISO curve) for the three examined cases. Beam's middle vertical displacement in Case ALL is greater than the other two cases. Figure 72 shows the equivalent plastic strain contour for Case ALL in final step time 3600. The maximum value of equivalent plastic strain appears in load application surfaces.

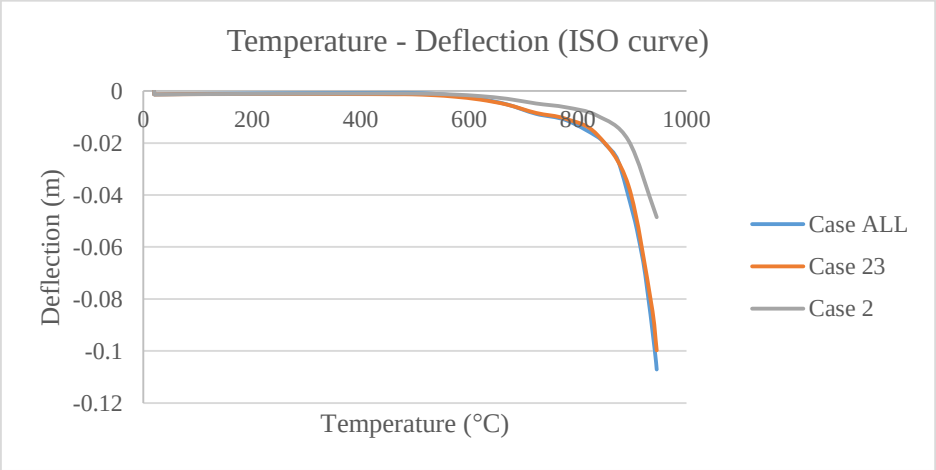

Figure 71: Temperature – middle defection, bending and predefined temperature (ISO), square beam

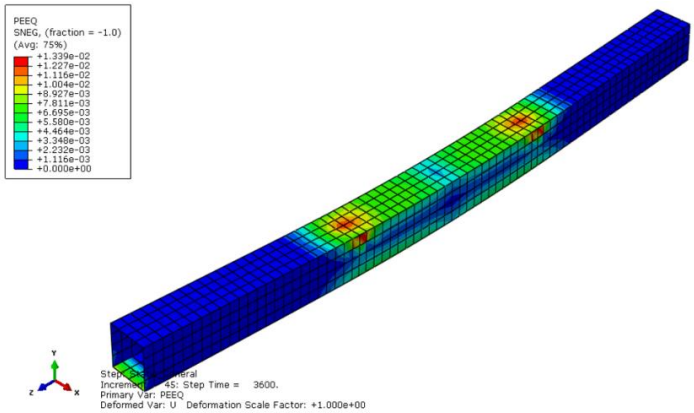

Figure 72: Equivalent plastic strain, Case ALL, bending and predefined temperature (ISO), square beam

Figure 73 shows the middle vertical displacement of the beam with the increasing temperature (HC curve) for the three examined cases. Beam's middle vertical displacement in Case ALL is greater than the other two cases. Compare with the ISO curve cases, beam's middle displacements are greater in cases with HC curve. Figure 74 shows the equivalent plastic strain contour for Case ALL in final step time 3600. The maximum value of equivalent plastic strain appears near the surfaces of load application.

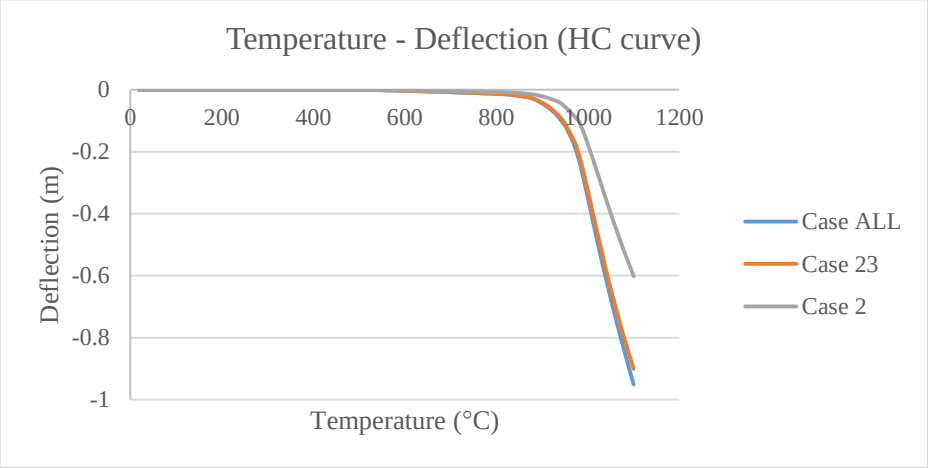

Figure 73: Temperature – middle deflection, bending and predefined temperature (HC), square beam

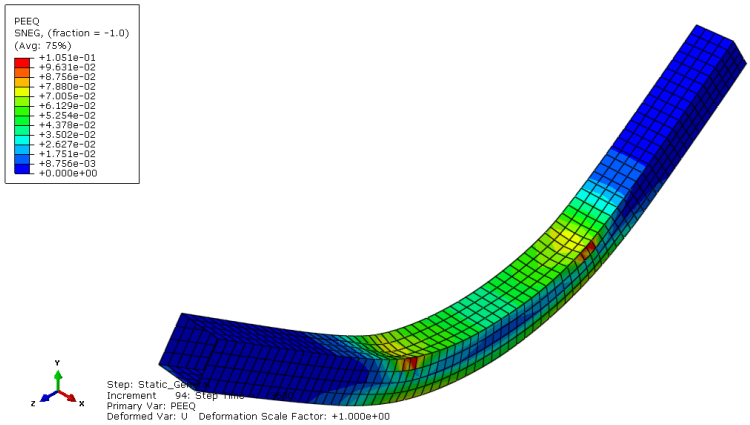

Figure 74: Equivalent plastic strain, Case ALL, bending and predefined temperature (HC), square beam

The results show that the application topology of thermal loads can affect beam structural response. The greater thermal load application topology lead to greater deflections.

5.3.4 Boundary Conditions Examination

Structural response depends on the boundary conditions. For that reason the examination of the boundary conditions and their correct application to the structure is very significant for a structural analysis. For this examination Static General step was used, with total step time equal to 3600. ISO curve was used for temperature description and the temperature was modelled as predefined field in the internal beam surfaces in the examined cases. Case ALL as described previously was used (section 5.3.3). Three different cases of

boundary conditions were examined, fix – fix (1 edge), fix – fix (4 edge) and roller – pin (Figure 75). Pressure load applied in two surfaces as described above and is equal to 840 kPa at each surface.

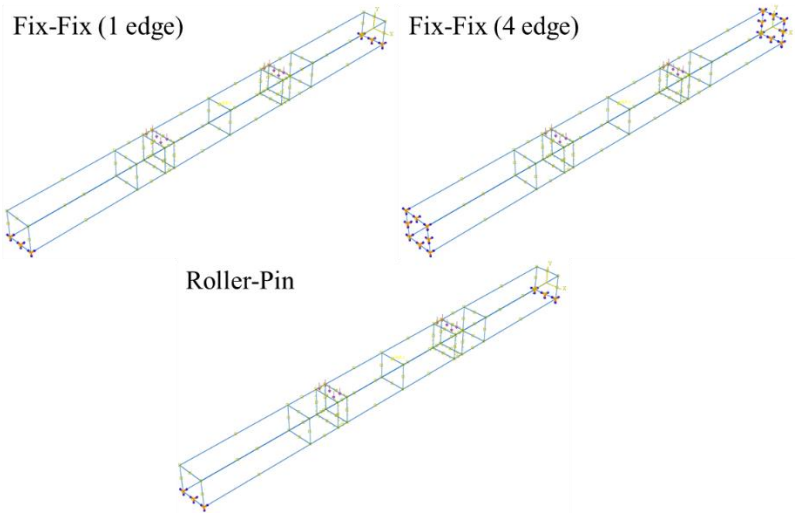

Figure 75: Examined boundary conditions

Figure 76 shows the middle vertical displacement of the beam relative to increasing temperature and for the three different boundary conditions. In case of fix – fix (1 edge) boundary condition, the middle vertical displacement is positive. Beam structural response is a result of boundary condition type and structural thermal expansion. More analytically, the applied mechanical load is significant small and the mechanical strains cannot overcome the thermal strains. The value of pressure load should be near the value of 11000 kPa at each surface in order the middle displacement is negative only. Fix – fix (4 edges) boundary condition type displays the maximum negative middle displacement. All the above observations suggests that structural response is related to boundary conditions but also the thermal expansion has a significant role in structural response.

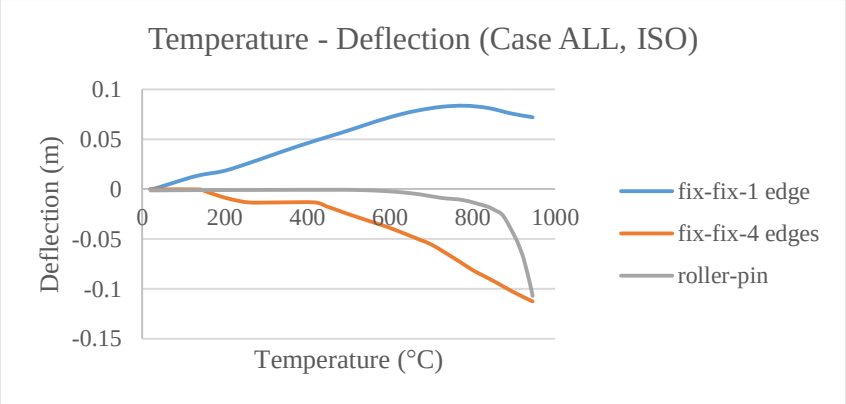

Figure 76: Beam response relative to boundary conditions, Case ALL, ISO curve

5.3.5 Thermal Expansion Examination

Previous chapter reveal the significant role of thermal expansion in structural response. Two examples will be presented as they have been described analytically in section 2.5. In the first example, the developed stresses in a square beam with restrained ends will be examined with computational methods. In the second

example, the tip displacement in a square beam with temperature difference between upper and lower surface will be examined. Static General step was used for the two analyses with total step time equal to 1.

Regarding the first example, the initial beam temperature was 20 °C and the final 1000 °C. The boundary condition is fix at both ends in order to simulate the theory example (section 2.5) [45]. Figure 77 shows the stress contours in step times 0.25, 0.5, 0.75 and 1, and Figure 78 shows a typical relationship between the stress and temperature. The stress initially increases with the temperature increase and consequently decreases with the increasing temperature. It can be said that stress follows the reduction of Young's modulus with the increasing temperature. Stress can be analytically calculated from equation (41) for small temperature changes.

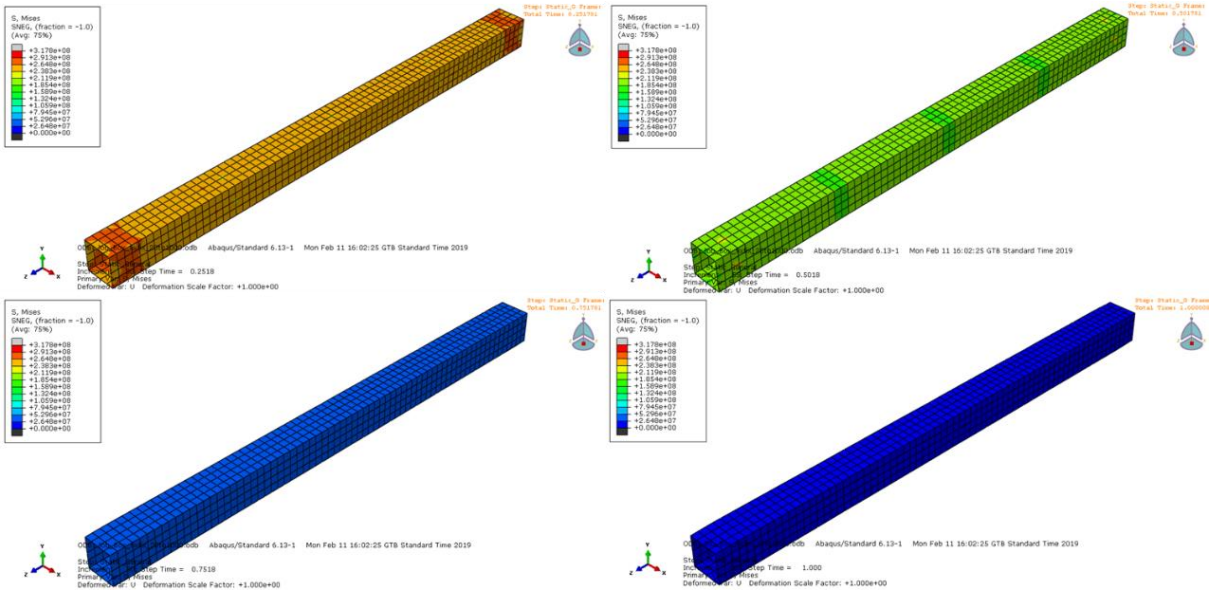

Figure 77: Stress contours at 0.25, 0.5, 0.75 and 1 step time, 1st example

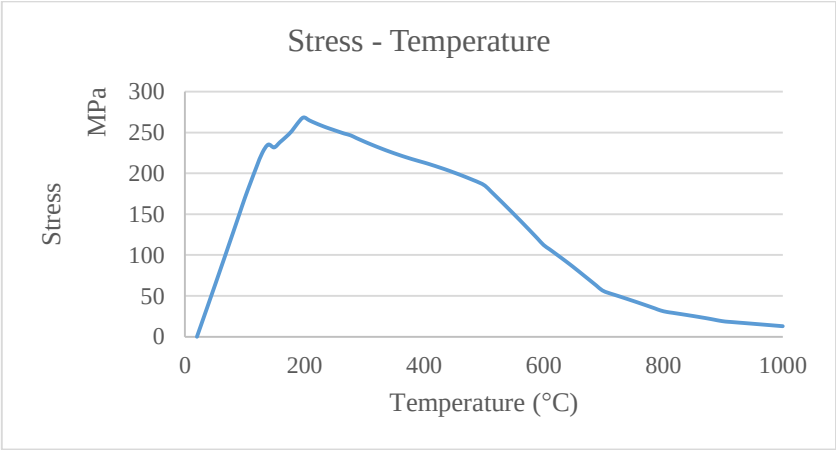

Figure 78: Typical stress – temperature relationship, 1st example

Regarding the second example, the initial beam temperature was 20 °C and at the upper surface the temperature was 500 °C as presented in theory (section 2.5) [44]. The beam has one fixed end and one free end. Using the analytical equation (43) for $x = L$, the maximum tip displacement is 0.2218 m. Figures 79 and 80

show the vertical displacement contours and the stress contours on beam at the final step time, respectively. The maximum tip deflection presented by ABAQUS is 0.1577 m. Comparing the analytical with the computational results there is a difference based on temperature application surfaces and on differences between analytical method and finite element method.

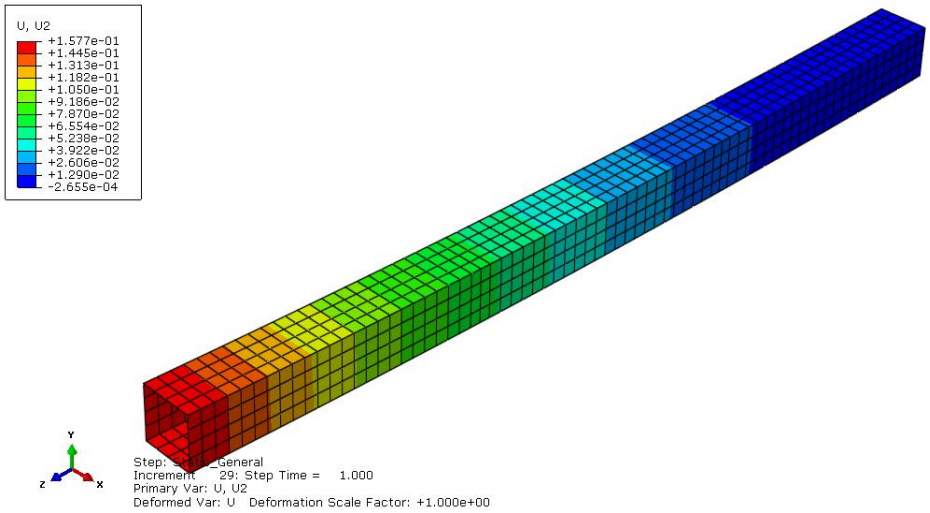

Figure 79: Vertical displacement contours on square beam, 2nd example

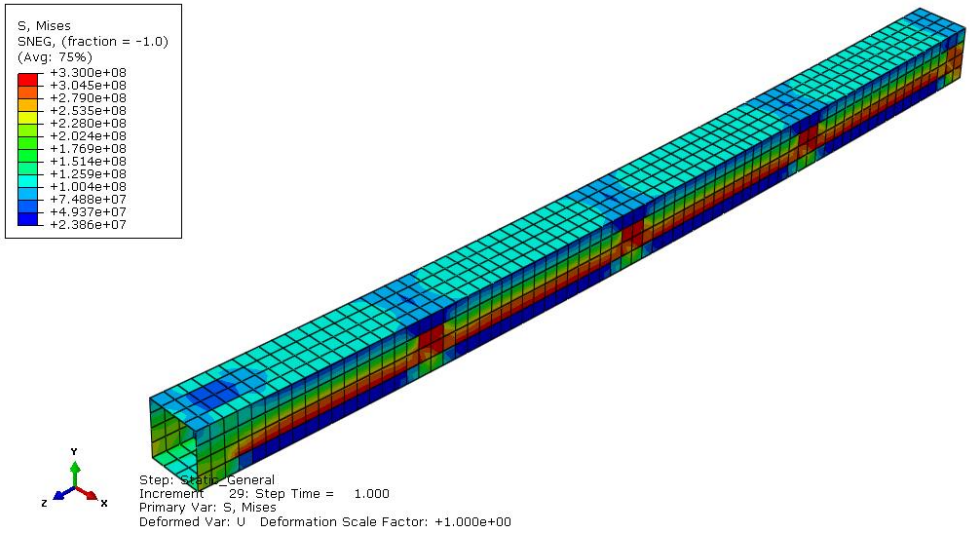

Figure 80: Stress contours on square beam, 2nd example

5.3.6 Bending Critical Load Examination

The load value, in which all the cross section areas of a beam are in elastic region before undergo plastic yield, is determined as bending critical load (section 2.4.5) [44]. For this analysis Static General step was used with total step time equal to 1. Beam's boundary conditions were roller and pin and the maximum pressure load was 15 MPa at each surface. The load value which leads to the initialization of plastic strains was determined as computational critical load in the structure for the specific parameters. Temperatures from 20 °C to 1100 °C were examined. The computational critical load transformed from Pa to N and the comparison with the

theoretical critical load is presented in Figure 81. There is a good correlation between the computational and the theoretical values. Differences between values are due to critical load definition between the two analyses.

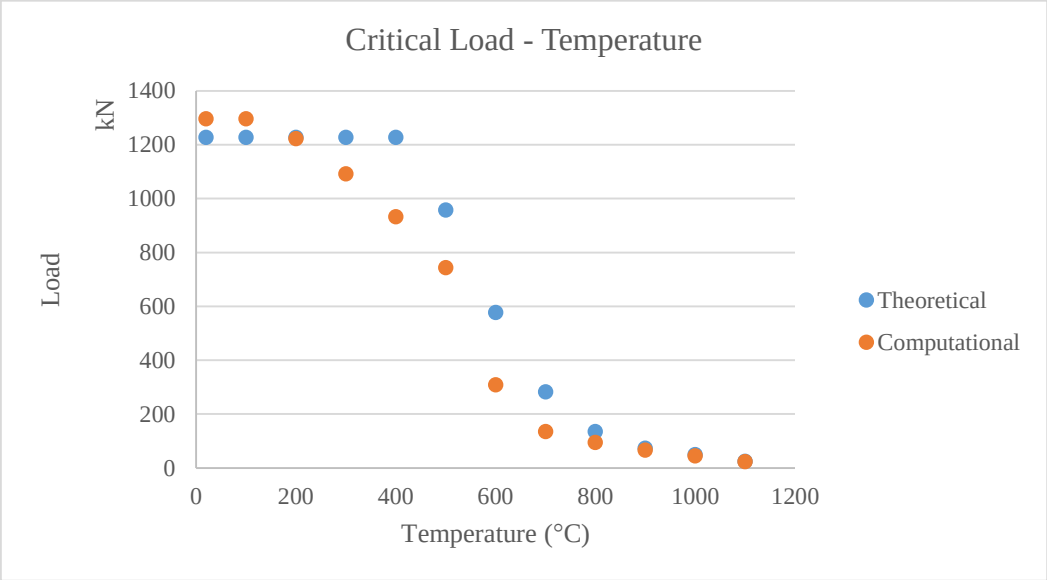

Figure 81: Critical load examination

5.4 Ship Model

NLFEA, Smith and modified Smith methods were applied on a 35000 DWT product oil/ chemical carrier design in 1999. The principal dimensions of the ship are presented in Table 7. Figure 82 presents the principal dimensions of the longitudinal stiffeners. Figures 83 and 84 depict the web frame section and the ordinary section, respectively. The max allowable design still water bending moments at seagoing conditions are given at the notes of the ship drawing report. For hogging condition the max allowable design still water bending moment is equal to 838000 kNm and for sagging condition is equal to 756000 kNm.

Length O.A.	183 m
Length B.P.	174.5 m
Length Scant.	172.66 m
Breadth Mld.	27.4 m
Depth Mld.	17.6 m
Draft (Design)	9.8 m
Draft (Scant.)	11 m
C_B (Scantling)	0.828
Service Speed	14.2 knots

Table 7: Principal dimensions of product oil/ chemical carrier

SIZE OF LONGITUDINAL

LOCATION	NO.	SIZE
UPPER DECK	0	150 X 14 F.B
	2 ~ 10	300 X 90 X 11/16 I.A
	11 ~ 12	350 X 100 X 12/17 I.A
	14 ~ 17	250 X 90 X 10/15 I.A
INNER BOTTOM & INNER HULL	0	150 X 90 X 12 U.A
	2 ~ 12	350 X 100 X 12/17 I.A
	17 ~ 19	300 X 90 X 11/16 I.A
	21 ~ 27	250 X 90 X 10/15 I.A
	29 ~ 35	200 X 90 X 9/14 I.A
	37 ~ 38	150 X 90 X 12 U.A
BOTTOM SHELL & SIDE SHELL	1 ~ 15	300 X 90 X 13/17 I.A
	16 ~ 17	300 X 90 X 11/16 I.A
	18 ~ 27	250 X 90 X 10/15 I.A
	29 ~ 31	200 X 90 X 9/14 I.A
	32 ~ 35	150 X 90 X 12 U.A
	37 ~ 38	250 X 90 X 12/18 I.A
STOOL STIFF	LOWER	250 X 90 X 12/16 I.A "AH"
	UPPER	150 X 90 X 12 U.A "AH"

Figure 82: Dimensions of longitudinal stiffeners

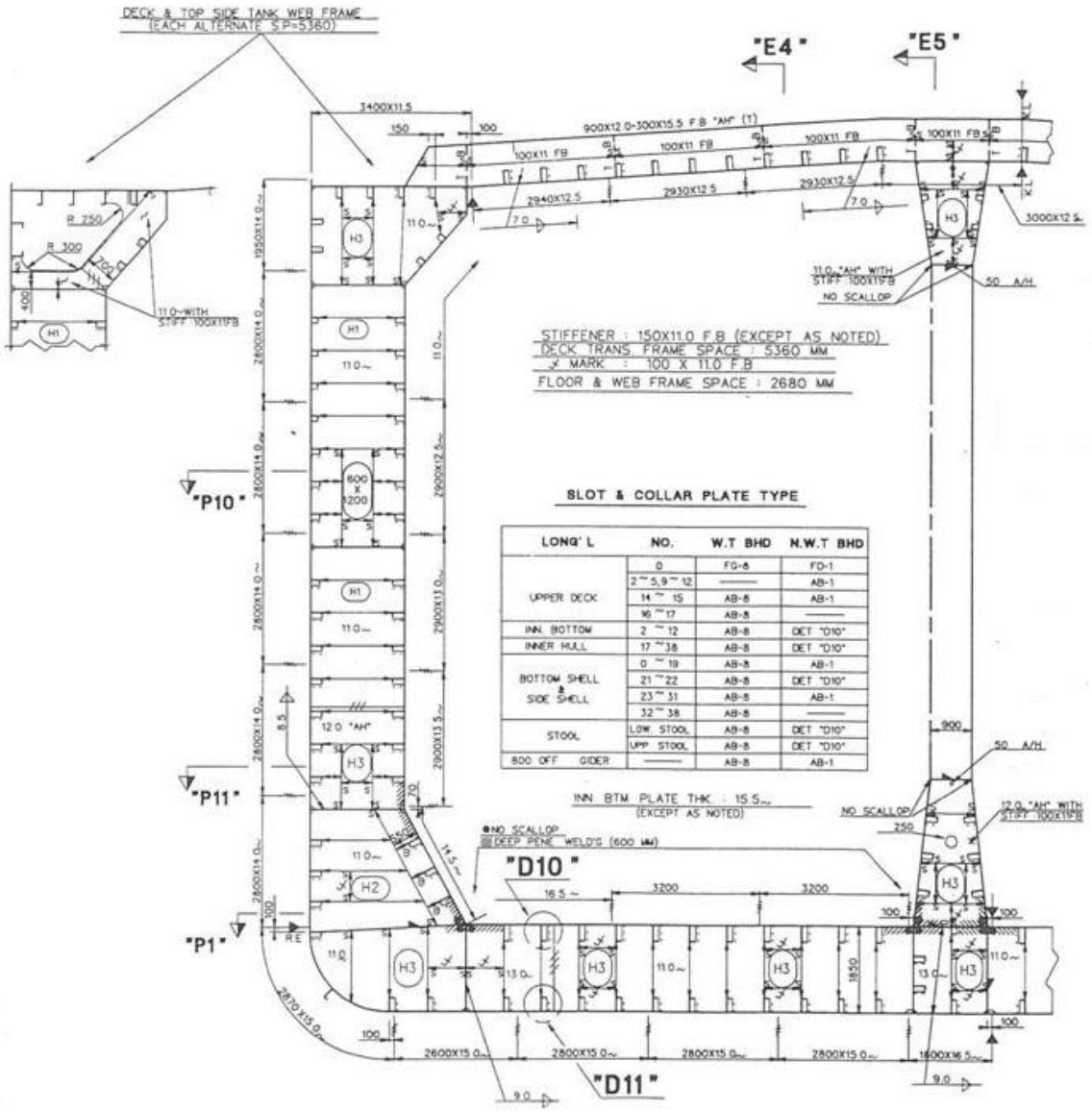

Figure 83: Web frame section

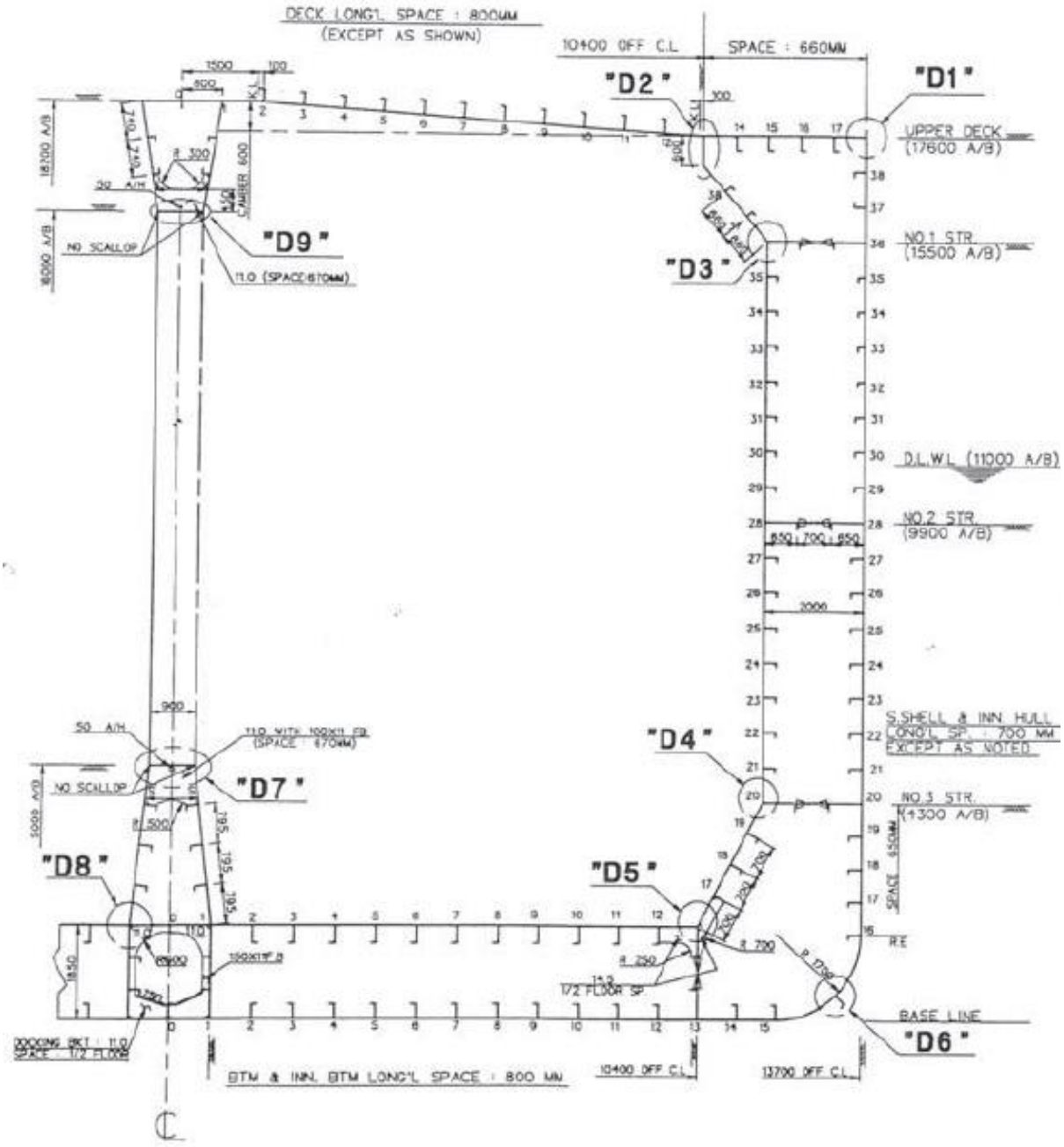

Figure 84: Ordinary section

The ship model was generated in CATIA and imported in ABAQUS in independent parts. The ship model parts were merged in ABAQUS assembly module. In some cases the merge execution did not work properly and leading to misconnected areas in the ship model. This happens due to the difference in accuracy of CATIA sketch and ABAQUS sketch. In order to avoid relative errors in the analyses, the ship model was designed also in ABAQUS part module. The man holes but also holes for water drain at the transverse frames and construction details did not included in the ship models. This is due to minimization of the computational cost but also for the increase of mesh quality. Figures 85 and 86 present 1 frame model and 3 frames model respectively, designed in ABAQUS. The 3 model frame consists of two full transverse bulkheads which is

different from the initial ship design. The 3 frame model designed in such way in order to maintain the symmetry and the results between the 1 frame and 3 frame model can be comparable. The ship consist of two types of steel, mild steel grade “A” of yield stress: 235 MPa and high tensile steel grade “AH” of yield stress 315 MPa. In Figure 87 the regions with high tensile steel are marked with red color while the regions with mild steel are marked with white color.

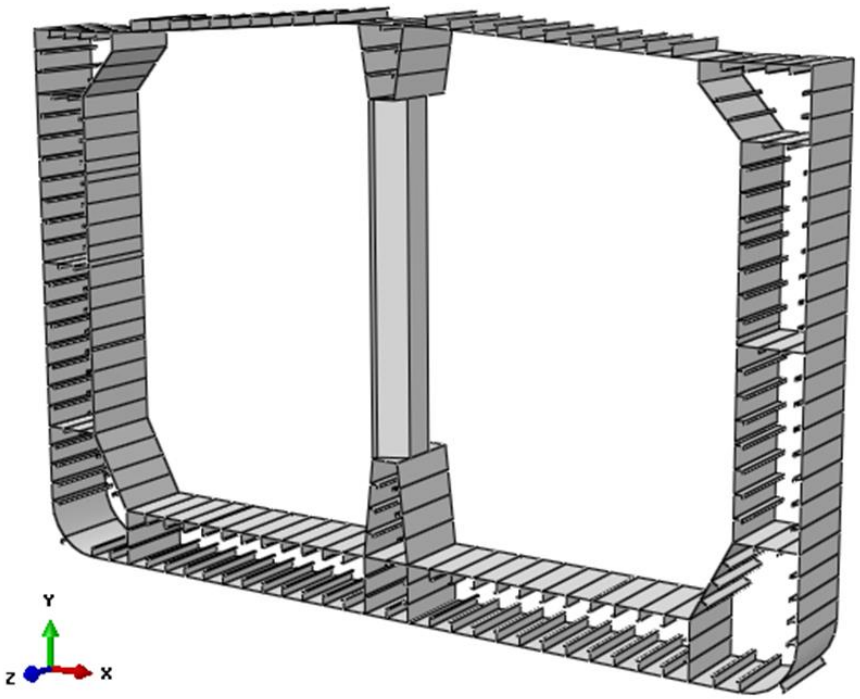

Figure 85: ABAQUS 1 frame model

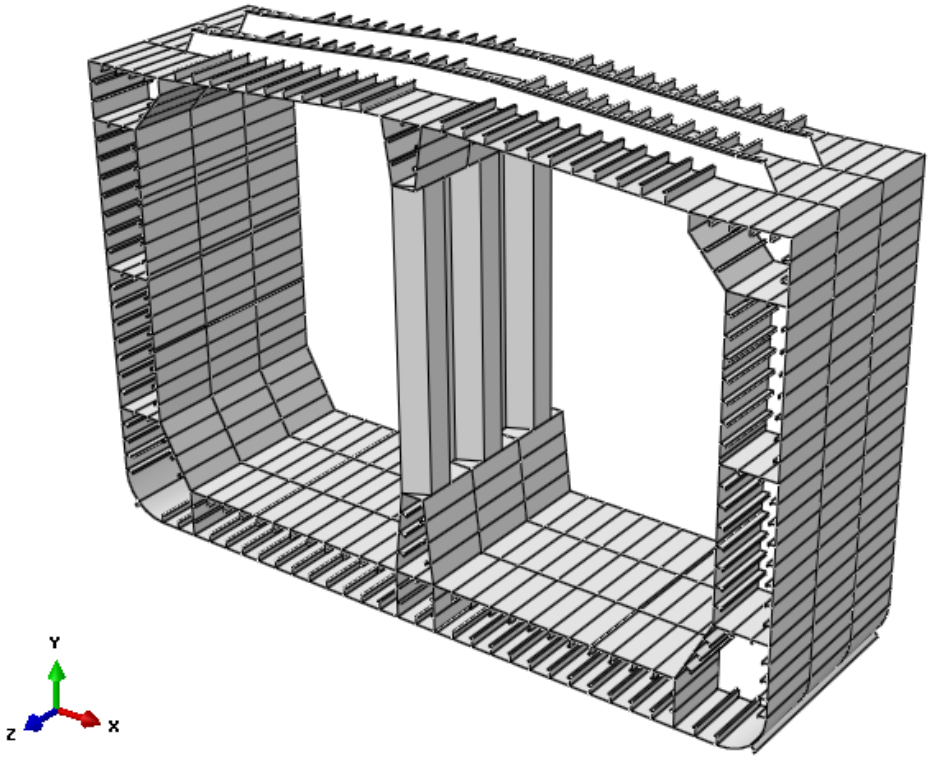

Figure 86: ABAQUS 3 frames model

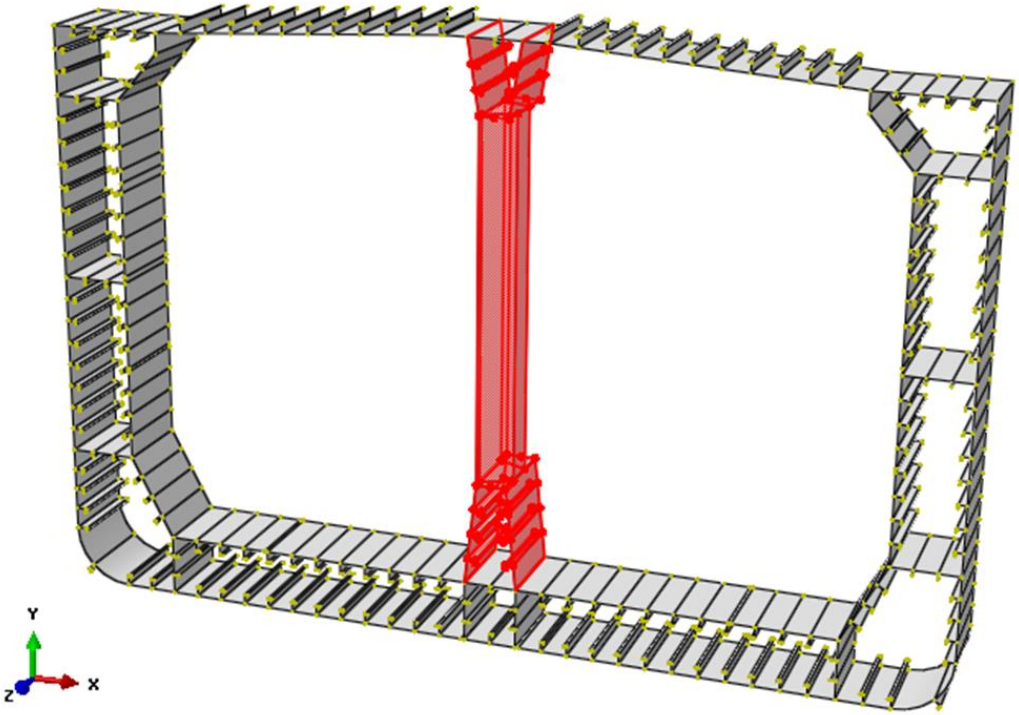

Figure 87: Material in ship transverse section (white color: mild steel, red color: high tensile steel)

5.5 Impact of Initial Geometric Imperfections in Buckling Analysis

Soares et al. studied the influence of the initial imperfections at the ultimate strength of a stiffened panel [23]. They concluded that a combination of the 3 types of imperfections (plate, beam column & sideways) leads to the minimum ultimate strength relative to the results from each type of deflection. The difference in the maximum value of ultimate strength between the results of CSR method and the NLFEA model with 3 types of imperfections is -8.17%. They also obtained that each type of initial deflection leads to the equivalent mode of failure. Based on this study, the impact of the initial geometric imperfections was examined in a stiffened panel. The examined stiffened panel is a part of the deck stiffened plate structure of the ship model presented in section 5.4. The geometric characteristic of the stiffened panel are presented in Table 8.

a (mm)	b (mm)	t_p (mm)	h_w (mm)	t_w (mm)	b_f (mm)	t_f (mm)
2680	800	10.5	300	9	90	14

Table 8: Principal dimensions of stiffened panel

The dimensions applied to the present analysis were defined by excluding the 50% corrosion margin as specified by IACS [32]. The material was assumed as elastic – perfectly plastic, with yield stress equal to 235 MPa, Young's modulus equal to 210 GPa and Poisson ratio equal to 0.3. The boundary conditions are equivalent to the benchmark analysis (Chapter 4) and they are presented in Figure 88. Three types of initial geometric imperfection were examined, plate deflection, beam column deflection and sideways deflection. The initial deflections are presented in Figure 89. The equations describing the initial deflections are the same as presented in benchmark analysis in Chapter 4. For mesh generation S4R elements were used with mesh size $40\ mm * 40\ mm$. Figure 90 presents the load – end shortening curves calculated from CSR equations, for the examined stiffened panel.

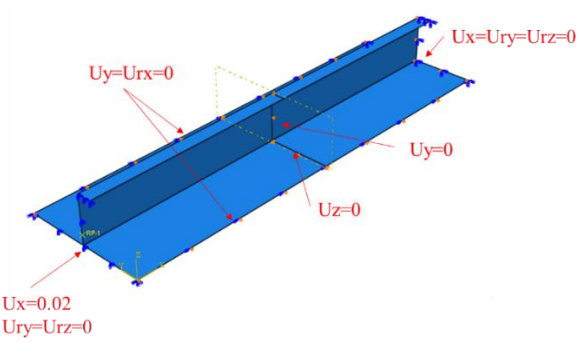

Figure 88: Boundary and loading conditions of stiffened panel

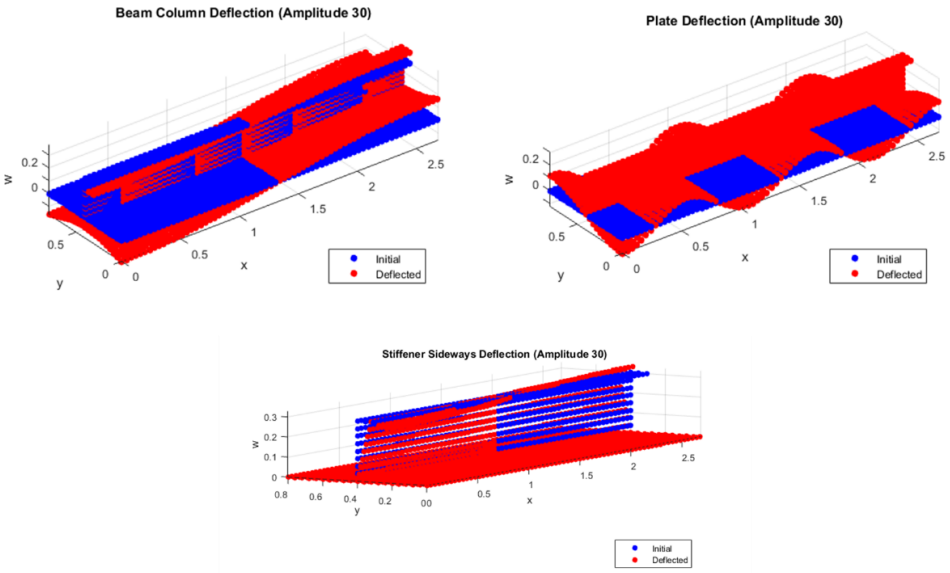

Figure 89: Initial geometric imperfection types

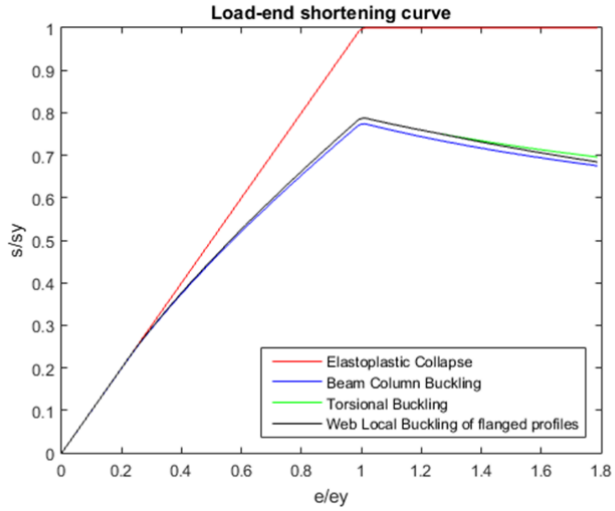

Figure 90: Load end shortening curves of stiffened panel calculated from IACS equations (MatLab code)

Figure 91 shows the comparison between the NLFEA modes and the CSR method and Table 9 presents the maximum values of stiffened panel ultimate strength of the examined cases. The ultimate strength of the stiffened panel with the three imperfection types applied simultaneously is smaller than that of each initial imperfection type. The ultimate strength of the stiffened plate with the beam column type initial deflection is the largest and its value is close to the CSR value of beam column mode of failure. The lower value of the ultimate strength predicted by the CSR (Beam Column) is larger than that of NLFEA with the three initial imperfection types. The absolute difference between the two values is 8.65%. The stress contour on the deformed stiffened panel under each of the three types of initial imperfections are shown in Figure 92. All models appear plate failure mode but in the stiffened panel under sideways initial deflection a web rotation is obtained. In all cases, the flange and the plate appear to yield.

Case (Type of initial deflection)	Maximum Ultimate Strength Value
Beam Column (NLFEA)	0.7671
Sideways (NLFEA)	0.7516
Plate (NLFEA)	0.7224
All Imperfections (NLFEA)	0.7072
Beam Column (CSR)	0.7742

Table 9: Maximum values of stiffened panel ultimate strength of the examined cases

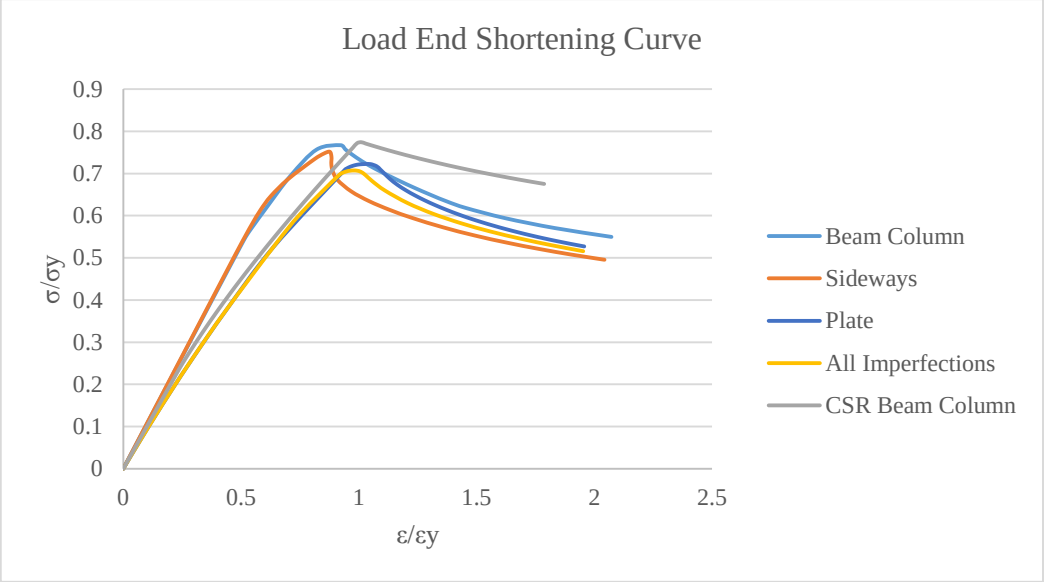

Figure 91: Load end shortening curves of stiffened panel NLFEA method compared to CSR method

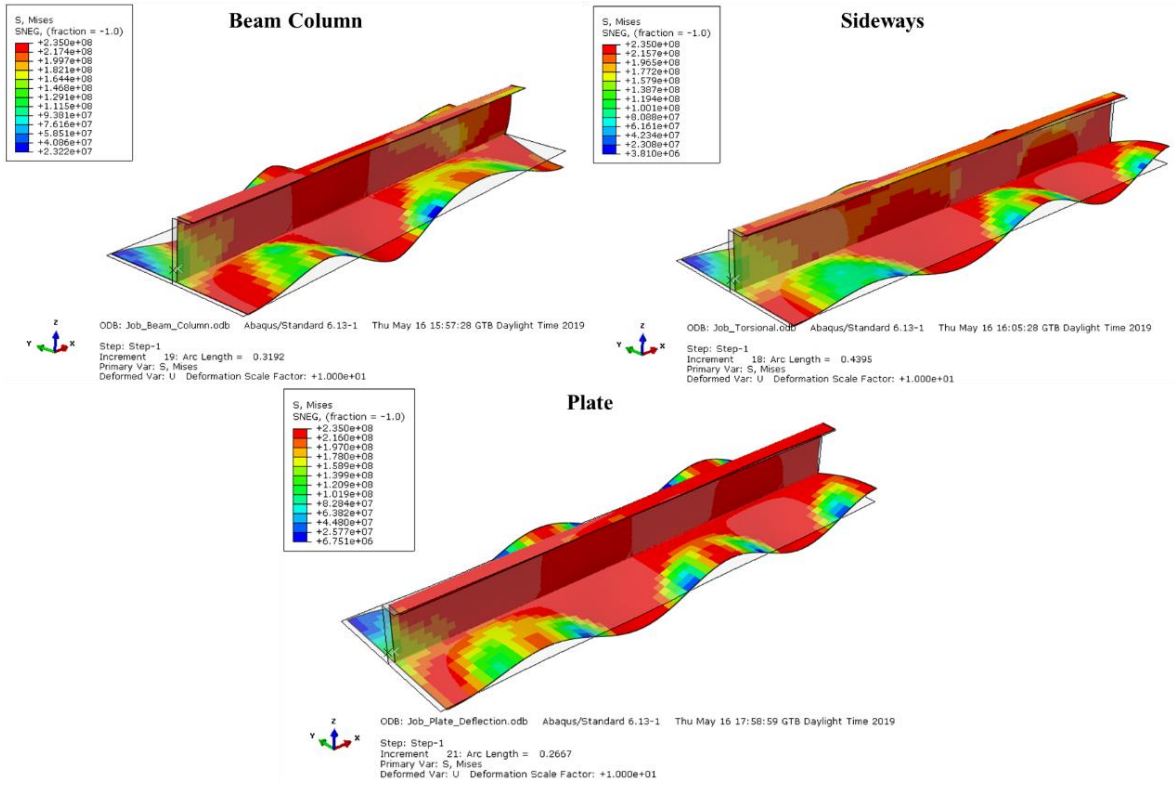

Figure 92: Stress contour on deformed stiffened panel at ultimate strength

5.6 Buckling at Elevated Temperatures

In this subchapter the examination of the ultimate strength of a stiffened plate at elevated temperatures will be presented. The examined stiffened plate geometry, boundary conditions and mesh characteristics are the same as in section 5.5. Three initial imperfection types applied simultaneously in the model as defined in section 5.5. The stiffened plate's material is described from Eurocode's relations as presented in Appendix A. Engineering stress – strain relations and no hardening effect were assumed. Static Riks step was used for the analysis. The examined temperatures vary form 20°C to 1000°C and the temperature applied as a predefined field at the initial step. Figure 93 presents the load – end shortening curves for the stiffened plate element at the different temperatures. It can be said that the shape of the load – end shortening curves at elevated temperature (above 500°C) follows the pattern of material's stress – strain curves. The decrease in the value of the ultimate strength is proportional to the reduction factors describing the yield stress of the material (Appendix A). Figure 94 presents the stress contour on the deformed stiffened panel at temperature of 100°C and 1000°C, respectively.

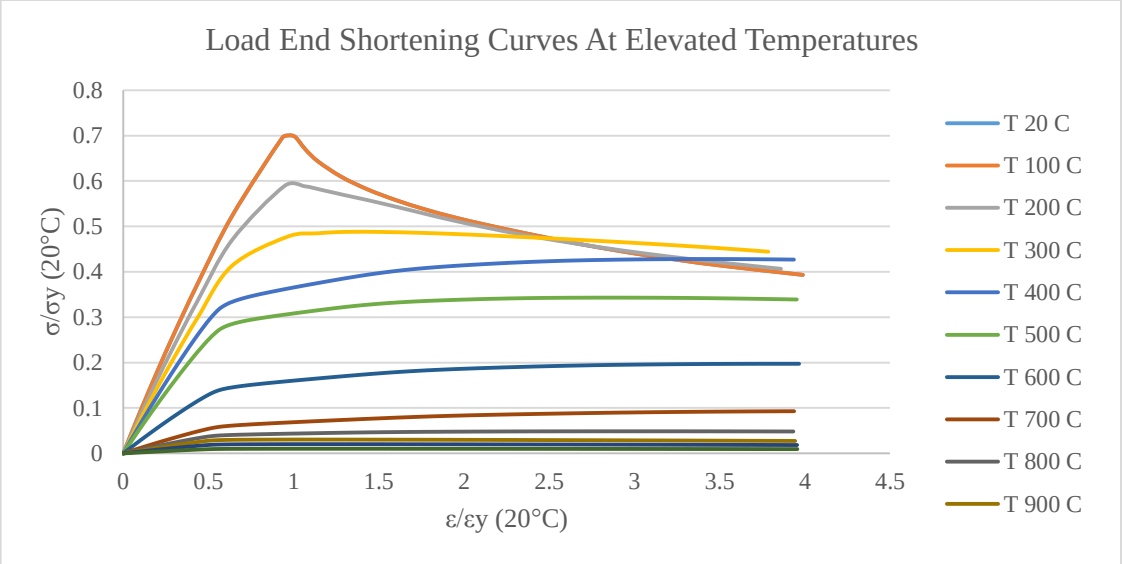

Figure 93: Load end shortening curves of stiffened panel at elevated temperatures

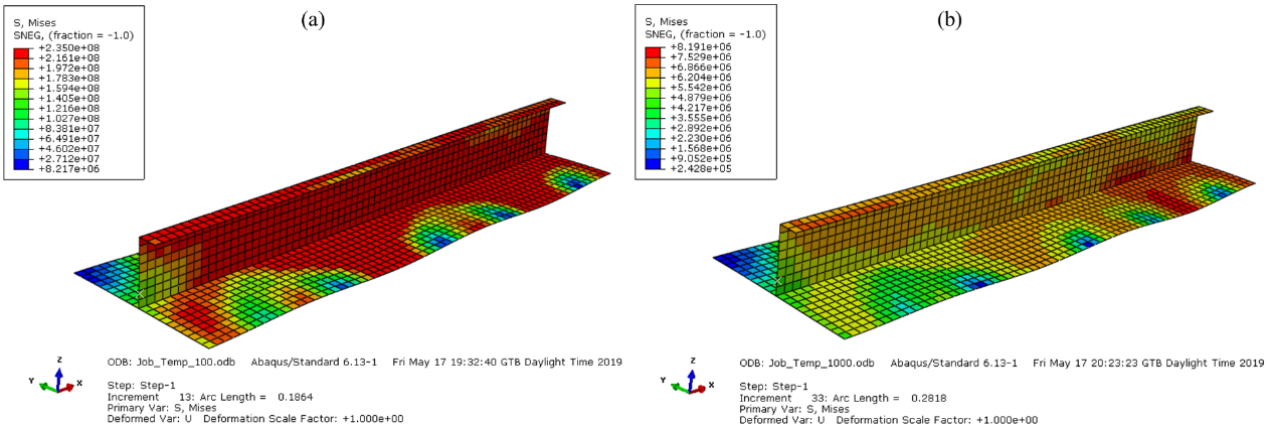

Figure 94: Stress contours on deformed stiffened panel (a) 100°C, (b) 1000°C

5.7 Mesh Convergence for Buckling Analysis

NLFEA result's accuracy is mesh characteristics dependent, so the mesh convergence study is significant in a finite element model generation. For the present study, the stiffened panel presented in section 5.5 was used. The parameters of the analysis (step, boundary conditions, material) were the same as the analysis in section 5.5. Three initial geometric imperfection types (plate deflection, beam column deflection and sideways deflection) applied simultaneously in the model. Five different mesh sizes were examined: 40 mm, 60 mm, 80 mm, 100 mm and 120 mm. Figure 95 shows the load – end shortening curves of the stiffened panel for the five different mesh sizes. It can be seen that the differences in the maximum value of ultimate strength between the different mesh sizes are small. The significant differences are obtained in the post buckling region. In post buckling region, the stiffened panel appears large topical deformations. Generally, large topical deformations can be predicted better with a finer mesh model than with a coarser mesh model.

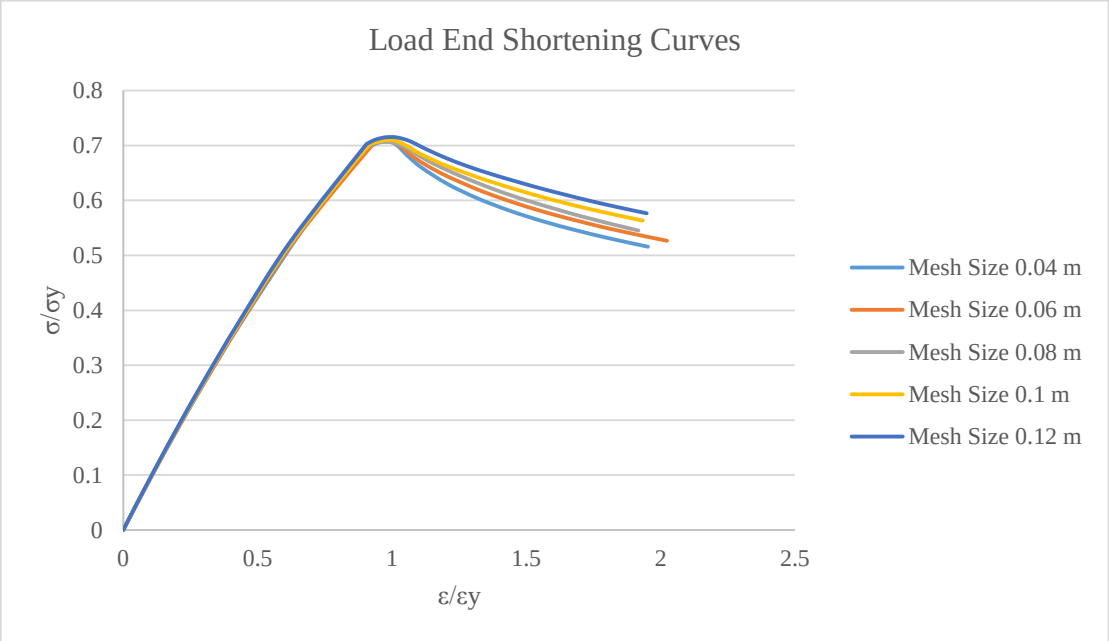

Figure 95: Load end shortening curves of stiffened panel with different mesh sizes

5.8 Thermal Analysis of Ship Frame

In order to obtain a temperature profile with known temperature boundary conditions in the ship frame, a thermal analysis was executed in ABAQUS, using Coupled Temperature – Displacement step. One frame and three frames models were used as presented in section 5.4. The structural dimension were defined by excluding 50% corrosion margin values of individual structural components as specified by IACS [32]. The nodes at both end transverse cross – section were rigidly linked to two individual master points, respectively, which locate at the center of the neutral axes of cross section. The mechanical boundary conditions at the two master (reference) points are presented in Table 10. Figure 96 shows the thermal boundary conditions. The higher temperature boundary condition (500 °C) represents a simplified temperature profile at elevated temperature conditions and

the lower temperature boundary condition (20 °C) represents the constant sea temperature. Due to the lack in the literature of ship large fires data, the determination and the evaluation of a fire case scenario was inevitably difficult. The examined thermal scenario and the higher temperature was determined based on the steel material properties. The steel's strength at 500 °C is the half than that in 20 °C. Only thermal conduction was taken into account in the analysis. Figures 97 and 98 show the temperature profile for the above thermal boundary conditions in 1 frames and 3 frames at the thermal equilibrium increment of the analysis, respectively.

RP – 1	Ux = Uy = Uz = URx = URy = URz = 0
RP – 2	Ux = Uy = URz = 0

Table 10: Mechanical boundary conditions for 1 and 3 frames model thermal analysis

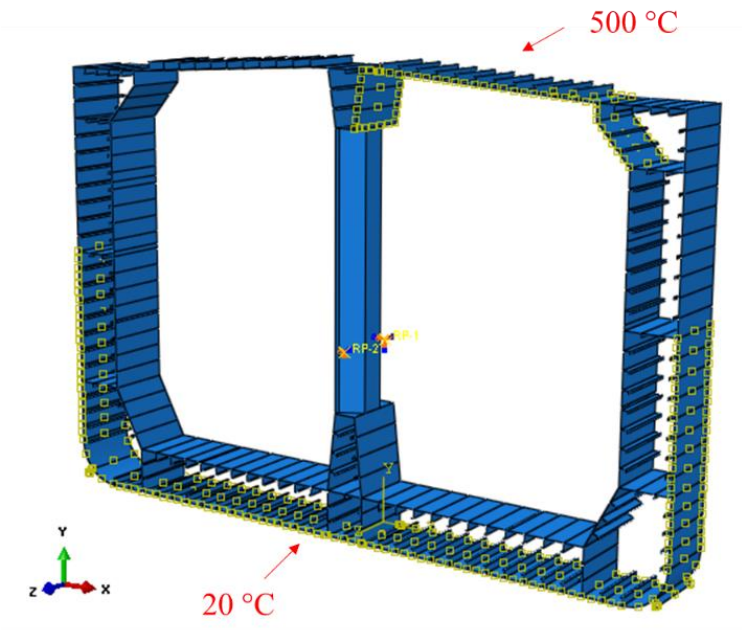

Figure 96: Thermal boundary conditions for 1 and 3 frames model thermal analysis

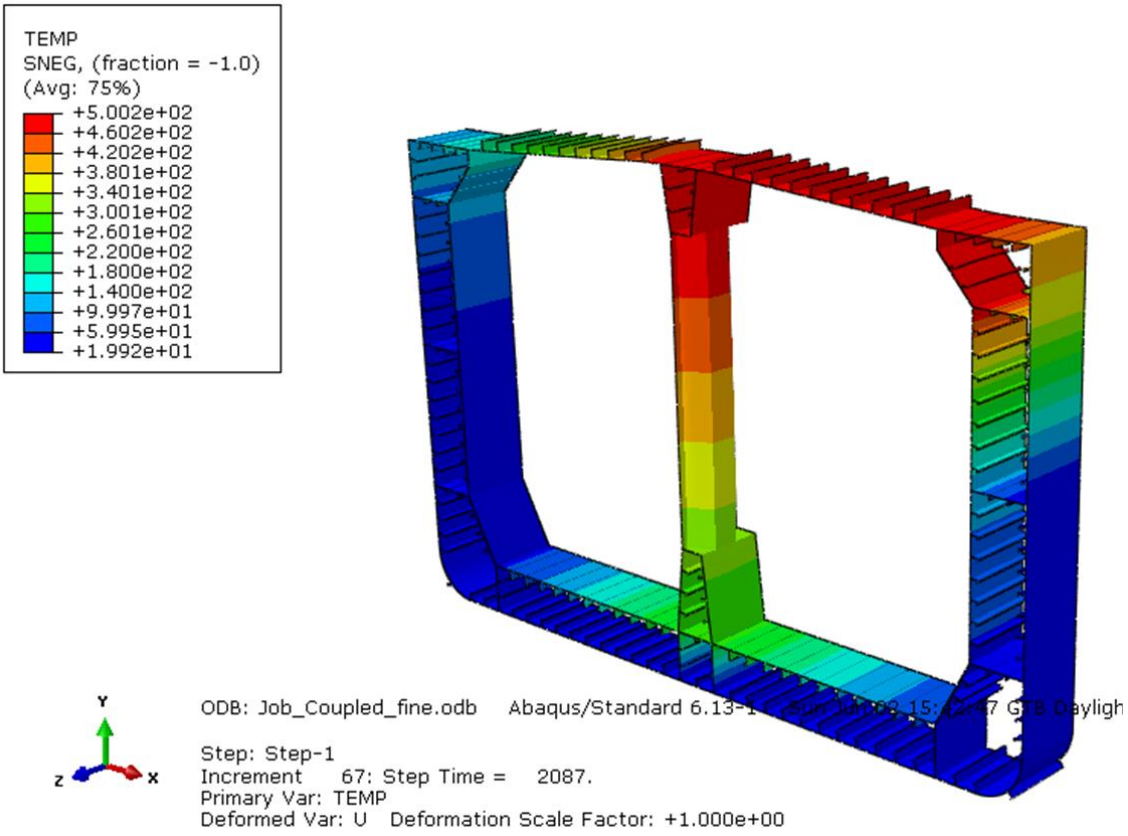

Figure 97: Temperature profile of 1 frame model thermal analysis

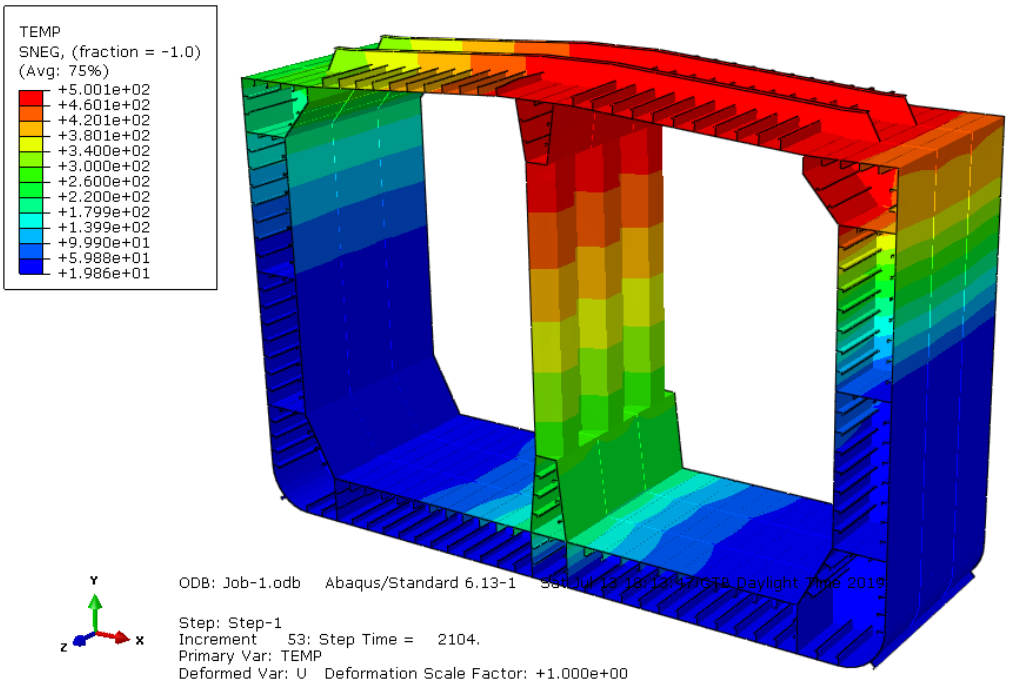

Figure 98: Temperature profile of 3 frames model thermal analysis

5.9 Effect of the Initial Geometric Imperfections Topology in Ultimate Hull Girder Strength

Two different initial geometric imperfections topologies were examined, in order to obtain the impact of the imperfection topology in the ultimate bending moment of the hull. The first topology consists of bottom surfaces and the second topology consists of bottom and side surfaces. One frame model was used for the analysis, with initial imperfections at the bottom and at the bottom and side, as presented in Figure 99. Three initial deflection types were applied simultaneously in the models (plate, beam column & sideways) [24]. The formulas describing each type of deflection are presented in Table 11 and they applied properly at each different structural element.

Plate Deflection	$w_{pl} = w_p * \sin\left(\frac{m\pi x}{a}\right) * \sin\left(\frac{\pi x}{b}\right), m = 5$
Beam Column Deflection	$w_{cl} = w_{oc} * \sin\left(\frac{\pi x}{a}\right)$
Sideways Deflection	$w_{ss} = \frac{w_o}{h_w} * z * \sin\left(\frac{\pi x}{a}\right)$

Table 11: Initial deflection formulas

The nodes at both end transverse cross – section were rigidly linked to two individual master points, respectively, which locate at the center of the neutral axes of cross section. The mechanical boundary and loading conditions at the two master (reference) points are presented in Table 12. The materials assumed as elastic – perfectly plastic. For the mesh generation S4R elements were used with mesh size $120\ mm * 120\ mm$. Static Riks step was used for the analyses.

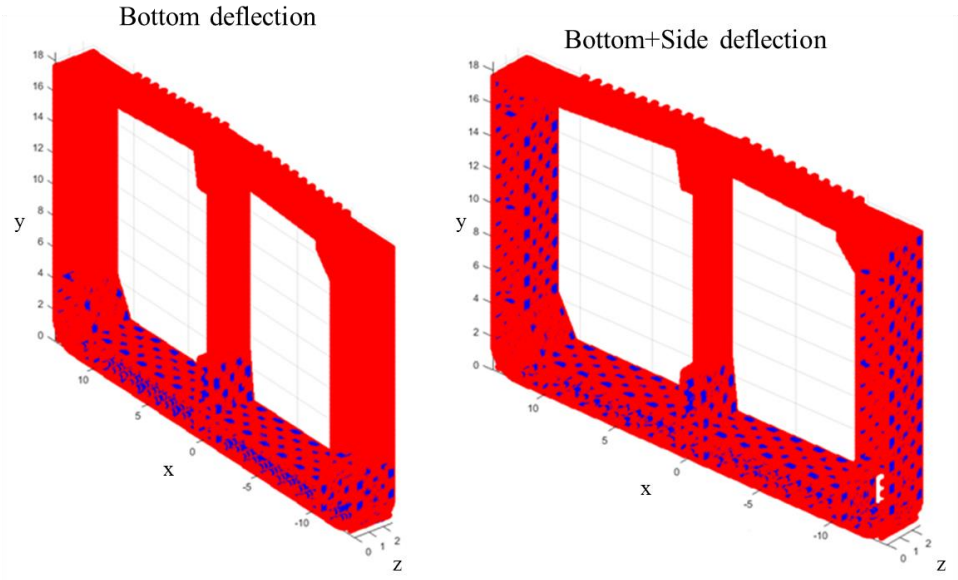

Figure 99: Initial deflection topologies

RP – 1	Ux = Uy = Uz = URx = URy = URz = 0
RP – 2	Ux = Uy = URy =URz = 0, URx = 0.003 rad

Table 12: Boundary and loading conditions at reference point of 1 frame model

Figure 100 shows the bending moment about x axis relative to curvature for the two models. The curvature was calculated from the following formula: $C = \frac{\theta_x}{Model\ Length}$. There are minor difference between the two model's results. It can be said that the initial geometric imperfections at the side of the hull do not influence the ultimate bending moment. Figure 101 shows the deformations and stresses for the two models at the maximum value of bending moment. The stress magnitude in the longitudinal bulkhead is relative small compared with the deck, bottom and stool areas.

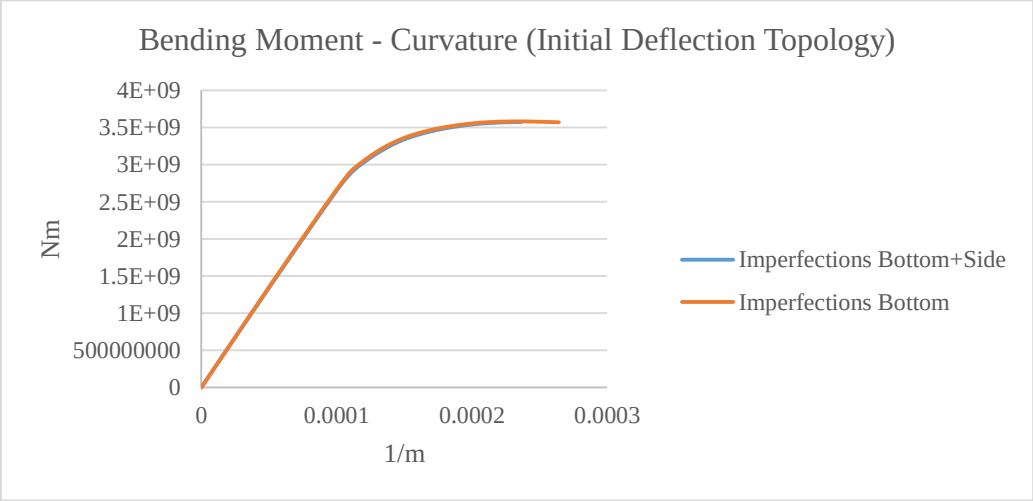

Figure 100: Bending moment versus curvature for 1 frame model at different initial deflection topologies

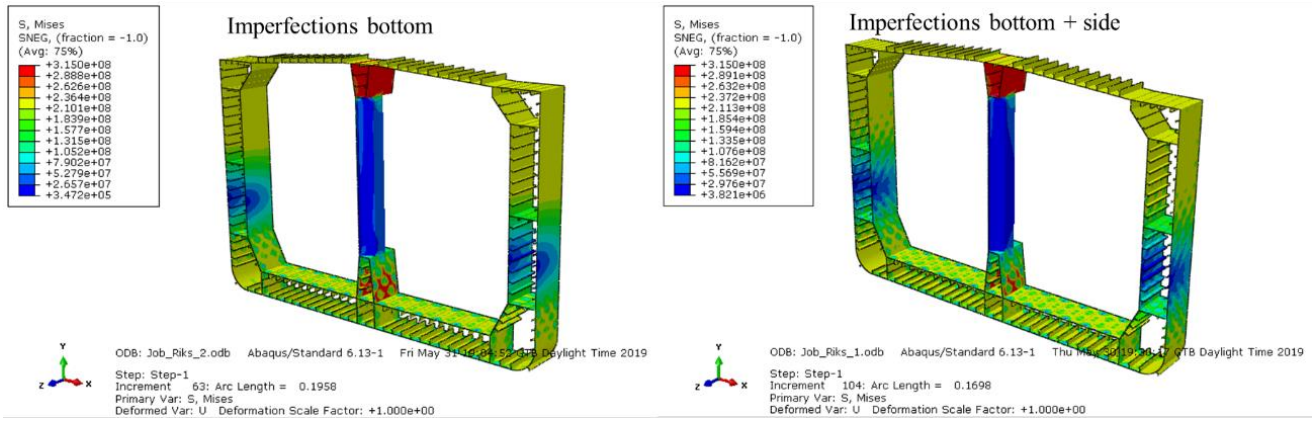

Figure 101: Stress contours on 1 frame model at different initial deflection topologies

5.10 Effect of the Longitudinal Bulkhead in Ultimate Hull Girder Strength

The results from the analyses in section 5.9 showed that the developed stresses in the longitudinal bulkhead are significant small compared to other areas of the frame. With this in mind, the ultimate bending moment of a hull girder model with and without the longitudinal bulkhead was examined. The model with the longitudinal bulkhead is the same as in section 5.9, while the meshed frame model without the longitudinal bulkhead is presented in Figure 102. For the mesh generation S4R elements were used with mesh size $120\ mm * 120\ mm$. Static Riks step was used for the analyses.

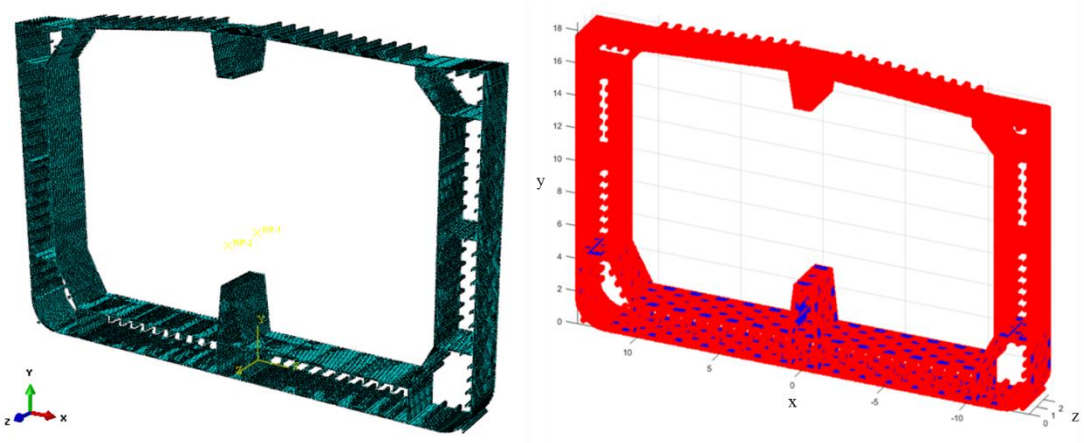

Figure 102: 1 frame model without longitudinal bulkhead

Figures 103 and 104 show the bending moment about x axis relative to curvature and the deformations and stresses for the two models, respectively. There are not any differences between the bending moment curves of the two models. Consequently, it can be said that the existence or not of a longitudinal bulkhead in the model is unrelated to the model's response. The existence of a longitudinal bulkhead may be crucial in cases of dynamic loading where the mass properties are taken into account or in more complicated and physically accurate loading cases. Generally, if a model part excluded from the analysis, equivalent boundary conditions should be applied [25], hence for following analyses the longitudinal bulkhead will be used in all presented models.

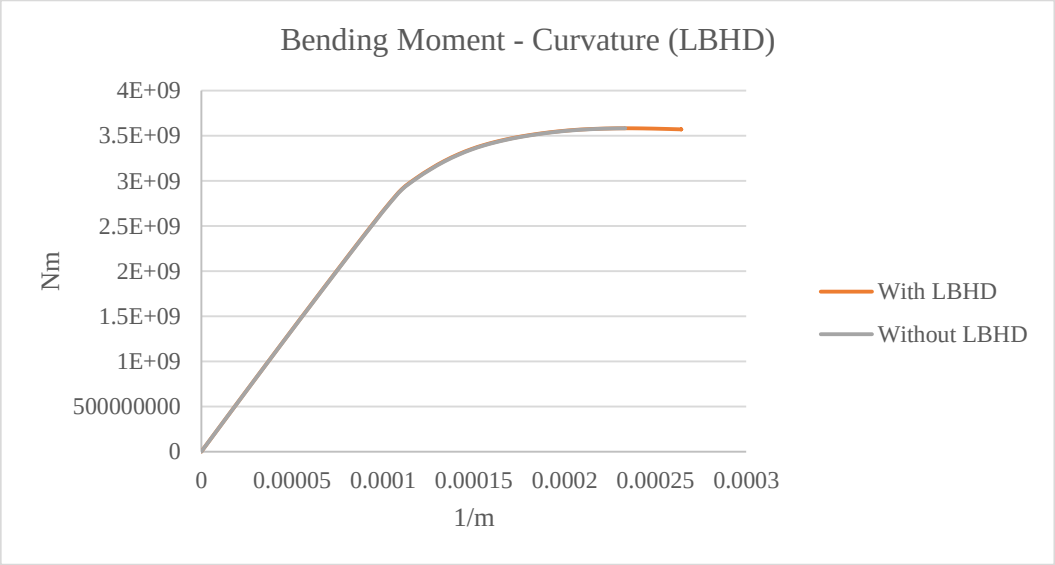

Figure 103: Bending moment versus curvature of 1 frame models with and without LBHD

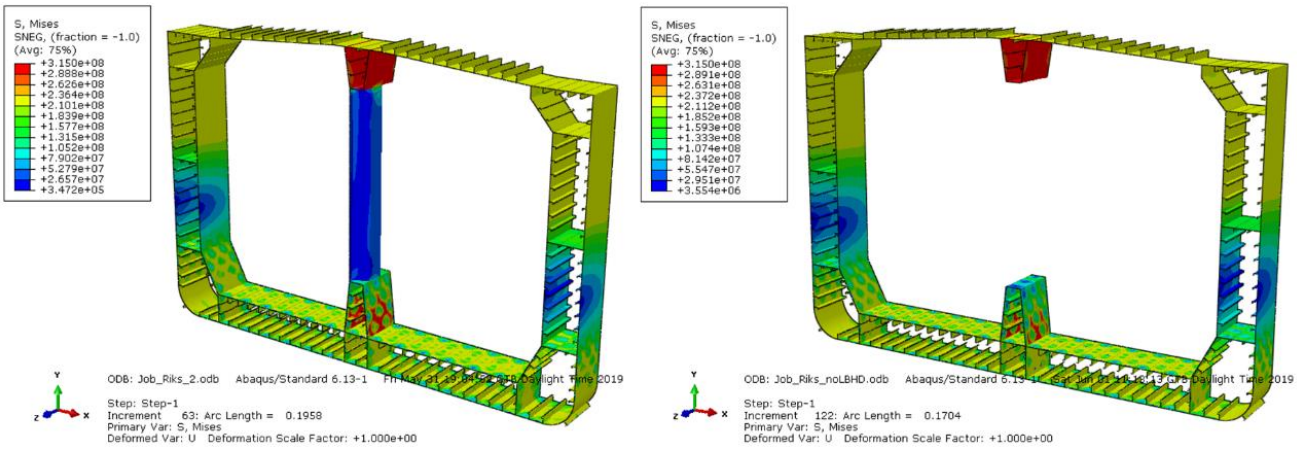

Figure 104: Stress contours on 1 frame models with and without LBHD

5.11 Effect of the Boundary Conditions in Ultimate Hull Girder Strength

Boundary conditions in ultimate hull girder strength analyses vary among the literature's studies. Three proposed boundary conditions were examined using 1 frame model. The nodes at both end transverse cross – section were rigidly linked to two individual master points, respectively, which locate at the center of the neutral axes of cross section. The examined mechanical boundary and loading conditions at the two master (reference) points are presented in Table 13. Static Riks step was used for the analyses and for the mesh generation S4R elements were used with mesh size $120\,mm * 120\,mm$. Figure 105 shows the bending moment relative to curvature for the three types of boundary conditions. The BC – 2 and BC – 3 cases did not successfully completed. According to Figure 105, there are no differences between the examined cases curves.

Name	RP – 1	RP – 2
BC – 1	Ux = Uy = Uz = 0 URx = URy = URz = 0	Ux = Uy = 0 URy = URz = 0 URx = 0.003 rad
BC – 2	Ux = Uy = Uz = 0 URx = URy = URz = 0	Ux = 0 URy = URz = 0 URx = 0.003 rad
BC – 3	Ux = Uy = Uz = 0 URx = URy = URz = 0	Ux = Uy = 0 URx = 0.003 rad

Table 13: Examined boundary and loading condition cases

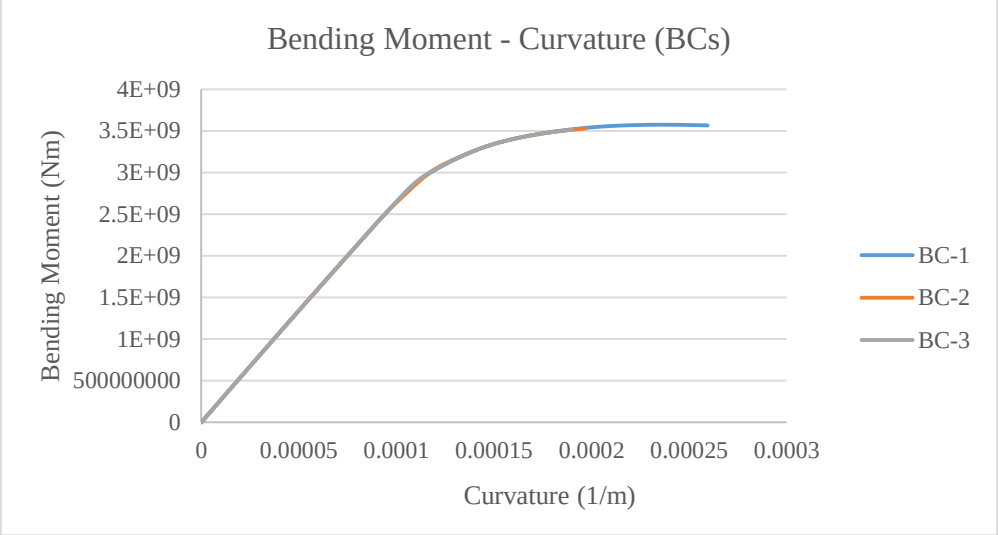

Figure 105: Bending moment versus curvature of 1 frame model at 3 examined boundary and loading condition cases

5.12 Effect of the Analysis Method in Ultimate Hull Girder Strength

The analyses in the previous section 5.11 showed that the arc length method (Static Riks) did not properly work under certain boundary conditions and the solution was interrupted. The examination of the analysis method is necessary, in order to obtain better and accurate results and more stable solution procedure. In the present analysis, three different steps were examined, Static Riks, Static General (using stabilization) and Dynamic Explicit [35]. BC – 1 boundary condition type was used for the present analyses and the mesh topology was equivalent to the previous analysis (section 5.11). For Explicit Dynamic step, total step time was equal to 1 second. Rotation about x - axis applied to one end reference point with the use of a tabular amplitude. The maximum value of x – axis rotation was equal to 0.003 rad. At analysis time 0, x – axis rotation was equal to 0 and at analysis time 1 second, x – axis rotation was equal to its maximum value. Figure 106 shows the bending moment relative to curvature for the three step types. Dynamic explicit step appears to be the more stable solution method relative to other two methods. Arc length (Static Riks) and Newton Raphson (Static General) methods did not converge at the early post buckling region. There are minor differences between the maximum values of the ultimate bending moment of the three step types. Provided the above in the following analyses Dynamic Explicit will be used.

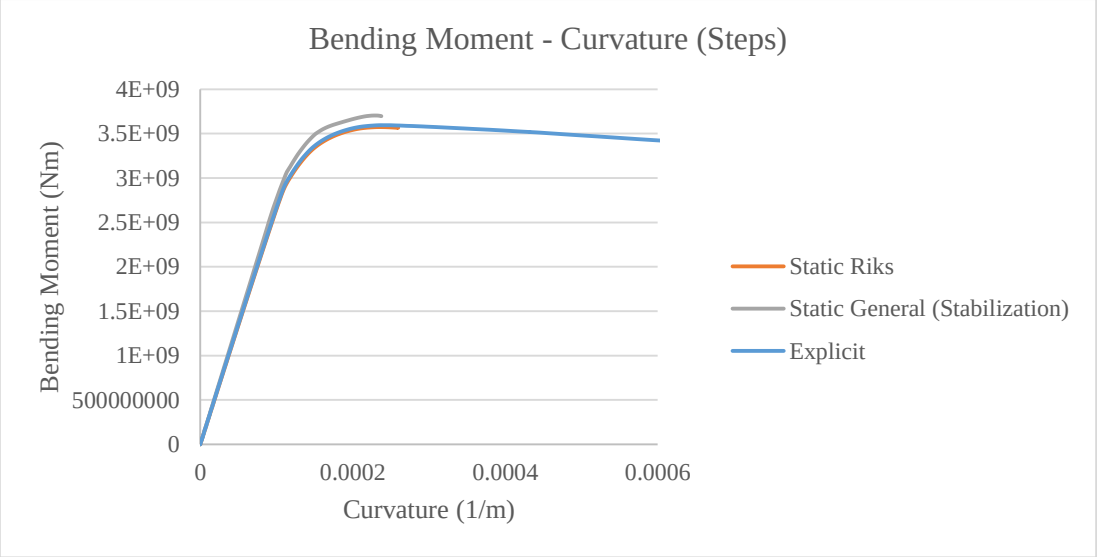

Figure 106: Bending moment versus curvature of 1 frame model at 3 examined steps

5.13 Influence of Model Geometric Range (1 Frame Model versus 3 Frames Model)

Xu et al [25] examined the hull girder geometric range in order to evaluate the appropriate hull girder model and to determine the result difference between the models. Their results showed that the two bending moment versus curvature curves are close in the pre – buckling area. The maximum ultimate bending moment in one span (1 frame) model is larger than the in three span (3 frames) model. In the post buckling area, there are significant differences in the bending moment versus curvature curve between the models. Regarding the above, the evaluation of model geometric range is very significant for the consistency and the accuracy of the results. Two models were examined: 1 frame model and 3 frames model. The models were examined for hogging condition at intact condition and at elevated temperatures according to thermal study presented in section 5.8.

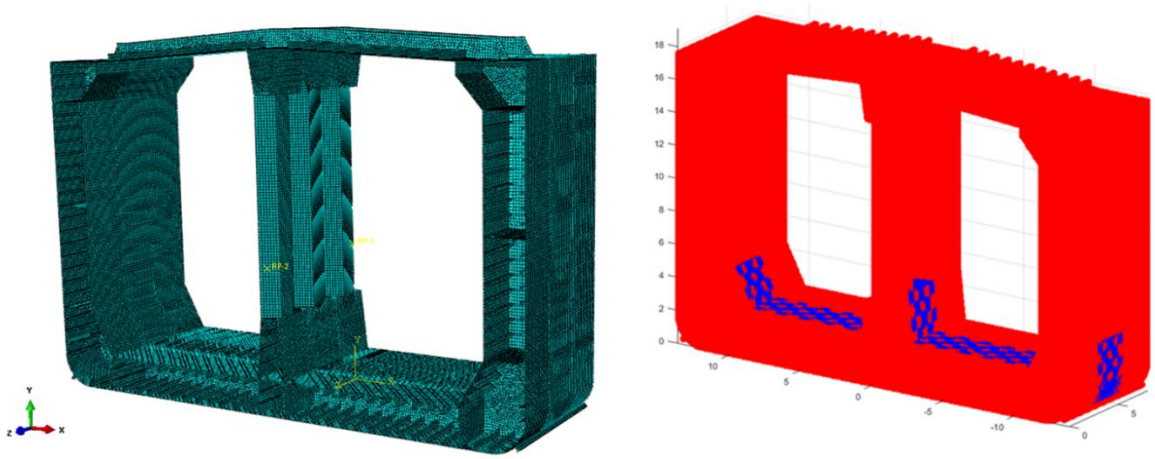

Figure 107: Meshed 3 frames model and initial deflection topology in 3 frames model

One frame model has been presented on previous sections, while the three frames model is presented in Figure 107. For the mesh generation S4R elements were used with mesh size equal to $120\ mm * 120\ mm$

and the initial geometric imperfection applied at the middle frame bottom. The formulas describing the initial geometric imperfections for the 3 frames model are the same to the formulas describing the initial geometric imperfection for 1 frame model presented in section 5.9. Explicit analysis method was used for the analyses.

5.13.1 1 Frame Model vs 3 Frame Model: Intact Condition

The two intact frame models examined for hogging condition. Boundary and loading conditions for the two models are presented in Table 14. The bending hogging moment versus curvature diagram is presented in Figure 108. In the pre – buckling area there are minor differences between the two curves. The maximum bending moment capacity for 1 frame model is 3594.96 MNm at curvature equal to $2.37 * 10^{-4}\ m^{-1}$ and for the 3 frame model is 3586.13 MNm at curvature equal to $1.95 * 10^{-4}\ m^{-1}$. In the post – buckling area there are significant differences between the two models.

RP – 1	RP – 2
Ux = Uy = Uz = URx = URy = URz = 0	Ux = Uy = URy = URz = 0 URx = 0.003 rad

Table 14: Boundary and loading conditions

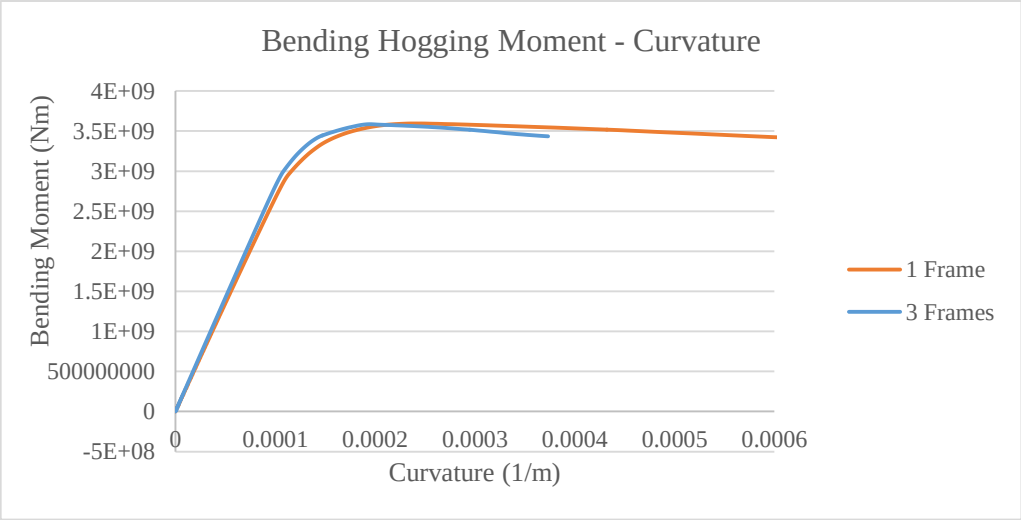

Figure 108: Bending moment versus curvature of 1 frame model and 3 frames model at intact condition

5.13.2 1 Frame Model vs 3 Frame Model: Elevated Temperature Condition

The two models were also examined for hogging condition at elevated temperatures. The examined temperature profile has been presented in section 5.8. Boundary and loading conditions for the two models are presented in Table 15. In the present analysis, reference point 2 rotation about y axis is free, in order to obtain the neutral axis rotation. The bending hogging moment versus curvature diagram is presented in Figure 109. In the pre – buckling area there are minor differences between the two curves. The maximum bending moment capacity for 1 frame model is 3112.86 MNm at curvature equal to $4.87 * 10^{-4}\ m^{-1}$ and for the 3 frame model is 3028.6 MNm at curvature equal to $4.13 * 10^{-4}\ m^{-1}$. In the post – buckling area there are significant

differences between the two models. Figures 110 show the stress contour on 1 frame model at early time and at the time of ultimate bending moment in case of elevated temperature. The neutral axis rotation can be observed from the Figures 110. Initially, the neutral axis was parallel to XZ plane, then the neutral axis rotate about z axis with curvature increase.

RP – 1	RP – 2
Ux = Uy = Uz = URx = URy = URz = 0	Ux = Uy = URz = 0 URx = 0.003 rad

Table 15: Boundary and loading conditions

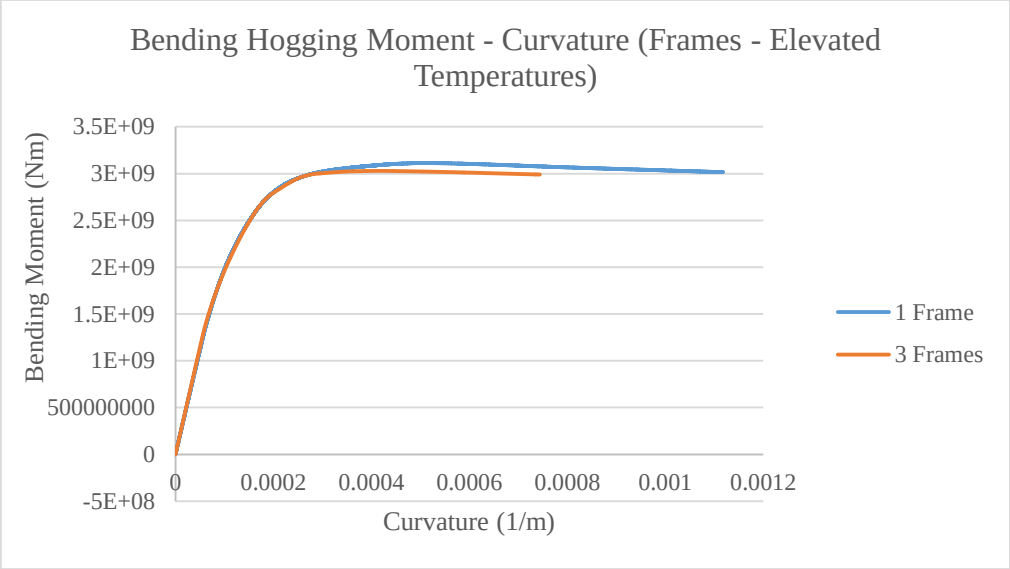

Figure 109: Bending moment versus curvature of 1 frame model and 3 frames model at elevated temperature condition

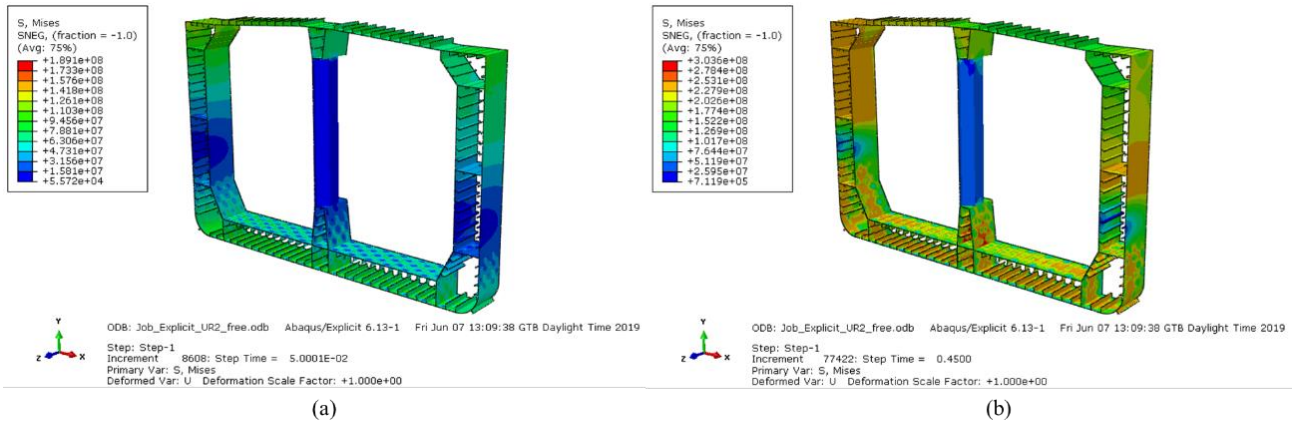

Figure 110: Stress contour on 1 frame model (a) early analysis time (b) ultimate hull girder strength

Chapter 6: Ultimate Hull Strength – NLFEA

Nonlinear finite element analysis was used for the estimation of the bending moment capacity of the chemical/oil product carrier hull girder. According to the results presented in section 5.13 and the results from the study of Xu et al. [25], a 3 frame model was used for the following analyses. The 3 frame model was examined at intact and elevated temperature states for hogging and sagging conditions. Dynamic explicit step was used for the analyses. The analysis time was 1 second for intact condition and 2 seconds for elevated temperature condition. For the applied x – axis rotation a tabular amplitude was used as described previously. In case of elevated temperature condition, the value of the applied rotation at 2 seconds was equal to 0.006 rads. Figure 111 (a) and (b) presents the initial geometric imperfection for hogging and sagging condition, respectively. The geometric imperfection formulas were introduced in section 5.9 and applied properly in the bottom areas for hogging condition and deck areas for sagging condition. For the mesh generation S4R elements where used with mesh size $120\ mm * 120\ mm$. The analyses performed on laptop computer with an Intel i7-2630QM CPU at 2.00 GHz and RAM 8.00 GB.

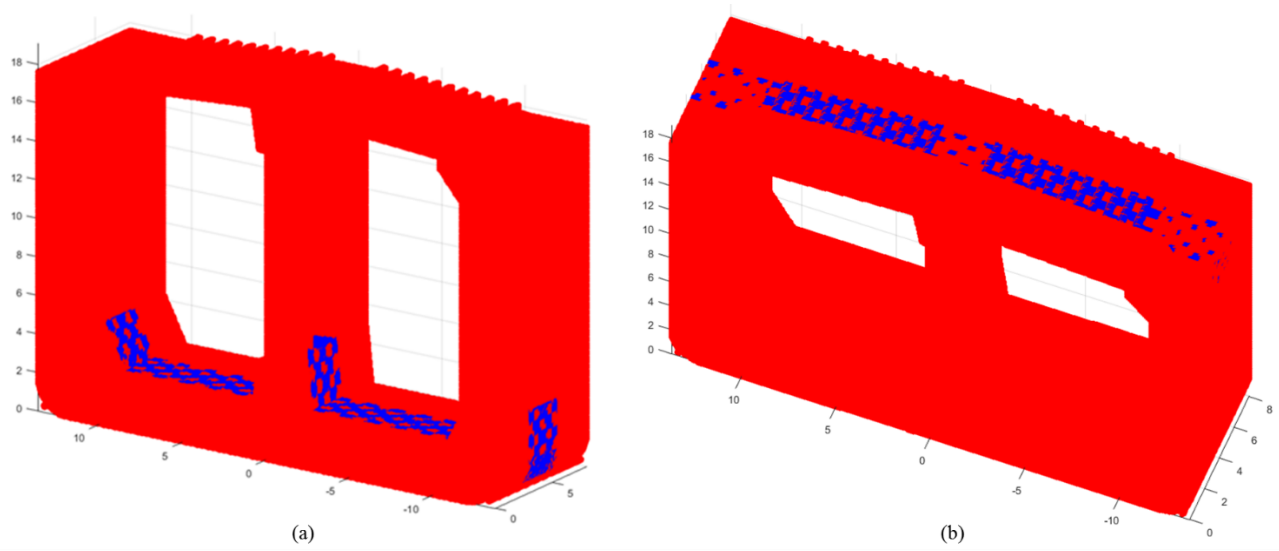

Figure 111: Initial deflection for (a) hogging condition and (b) sagging condition

6.1 Intact Condition

Hogging and sagging conditions were examined for the intact 3 frame model. The boundary and loading conditions are presented in Table 16. The total step time was equal to 1 second to minimize the computational time but also preserve the results accuracy [25].

RP – 1	RP – 2
Ux = Uy = Uz = URx = URy = URz = 0	Ux = Uy = URy = URz = 0 URx = 0.003 rad

Table 16: Boundary and loading conditions for 3 frame model at intact condition

Figures 112 and 113 show the bending moment versus curvature for hogging and sagging condition, respectively. Regarding hogging condition, the maximum bending moment is $3586.1\ MNm$ at curvature $1.95 * 10^{-4}\ m^{-1}$. On the other hand, for sagging condition the maximum bending moment is $-2472.6\ MNm$ at curvature $-2.45 * 10^{-4}\ m^{-1}$. Applying the CSR – H criterion for the two conditions, as presented in sections 2.2 and 7.3.1, we obtain the following results:

- Hogging Condition:

$$M \leq \frac{M_{U-hog}}{\gamma_R} \Rightarrow$$

$$2345533.6\ \text{kNm} \leq \frac{3586100\ \text{kNm}}{1.21} \Rightarrow 2345533.6\ \text{kNm} \leq 2963743.8\ \text{kNm}$$

- Sagging Condition:

$$M \leq \frac{M_{U-sag}}{\gamma_R} \Rightarrow$$

$$-2368953.9\ \text{kNm} \leq \frac{-2472600\ \text{kNm}}{1.1} \Rightarrow 2368953.9\ \text{kNm} \leq 2247818.2\ \text{kNm}$$

CSR – H criterion is satisfied for hogging condition but is no satisfied for sagging condition. Regarding sagging condition, the difference between the value of the vertical hull girder bending moment for the ultimate strength check and the value of the vertical hull girder ultimate bending capacity reduced by the γ_R factor, is relative small. Thus, the lack of satisfaction of the CSR – H criterion may lay on several computational reasons. Computational parameters that influence the ultimate bending moment are the boundary and loading conditions, the loading time, the mesh characteristics, the magnitude and shape of initial geometric imperfections even more the analysis method. Moreover, the examined ship was designed in 1999, when the rules did not exist or if existed, they had lesser safety factors.

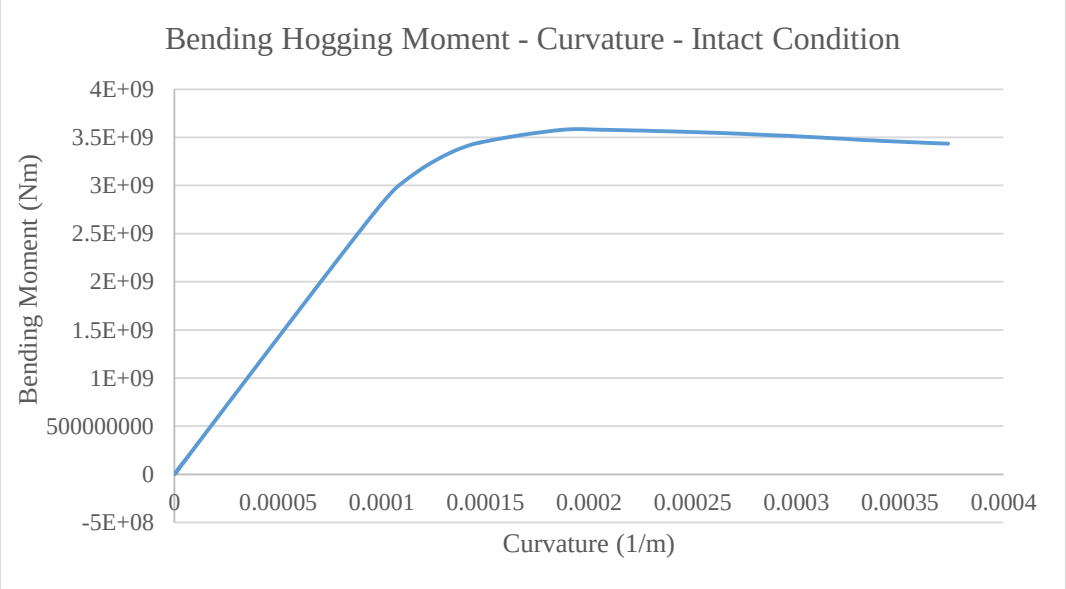

Figure 112: Bending hogging moment versus curvature of hull girder at intact condition (ABAQUS)

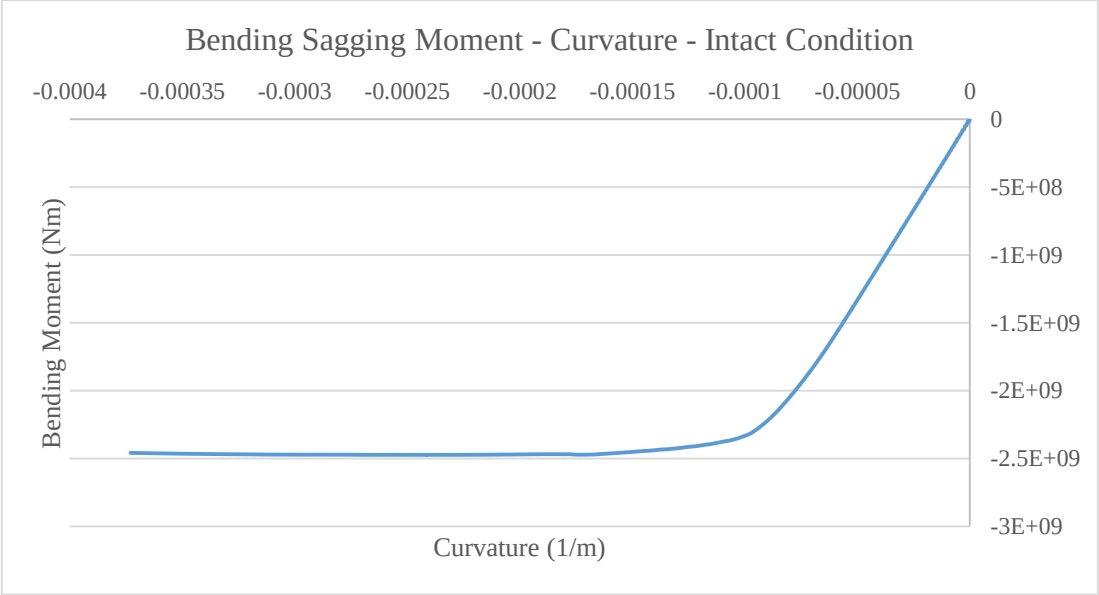

Figure 113: Bending sagging moment versus curvature of hull girder at intact condition (ABAQUS)

Figures 114 and 115 show the stress contours on deformed 3 frame model for hogging condition near the ultimate bending moment. Specifically, Figure 115 shows the outer bottom of the 3 frame model. Figures 116 and 117 show the stress contours on the deformed 3 frame model for sagging condition. It is obtained that in sagging condition average Mises stresses are greater than yield stress. This is a common error in several finite element analysis programs and is caused by post processing procedure (stress extrapolation which related to element type and mesh topology).

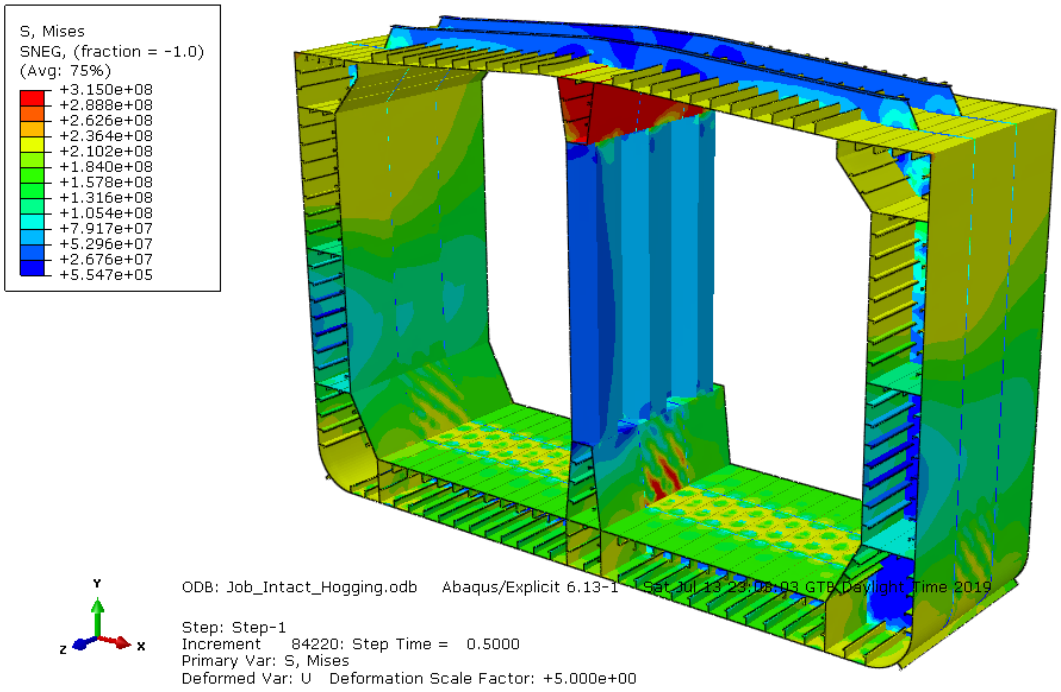

Figure 114: Stress contour on deformed 3 frame model for hogging condition

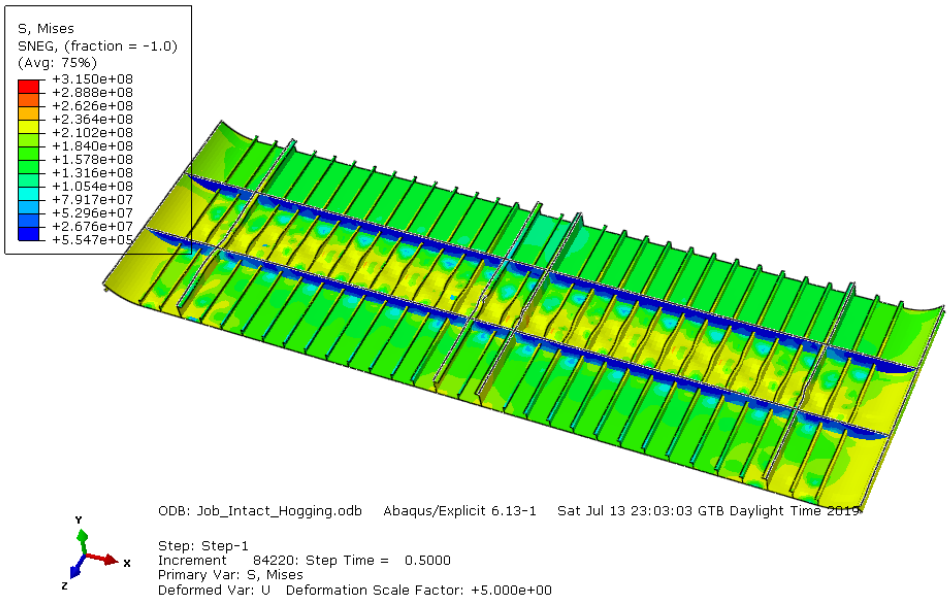

Figure 115: Stress contour on deformed 3 frame model outer bottom for hogging condition

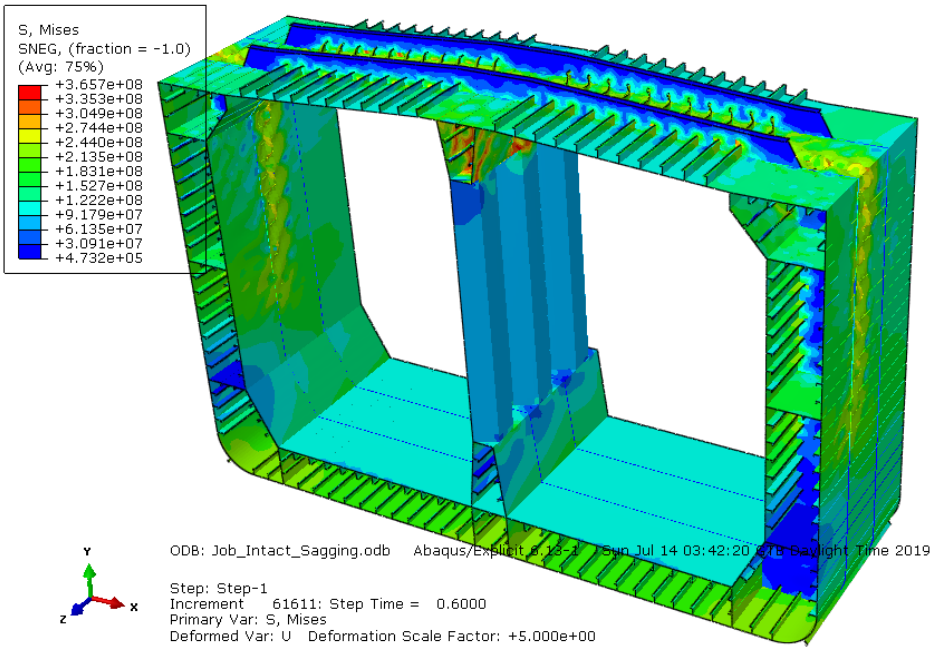

Figure 116: Stress contour on deformed 3 frame model for sagging condition

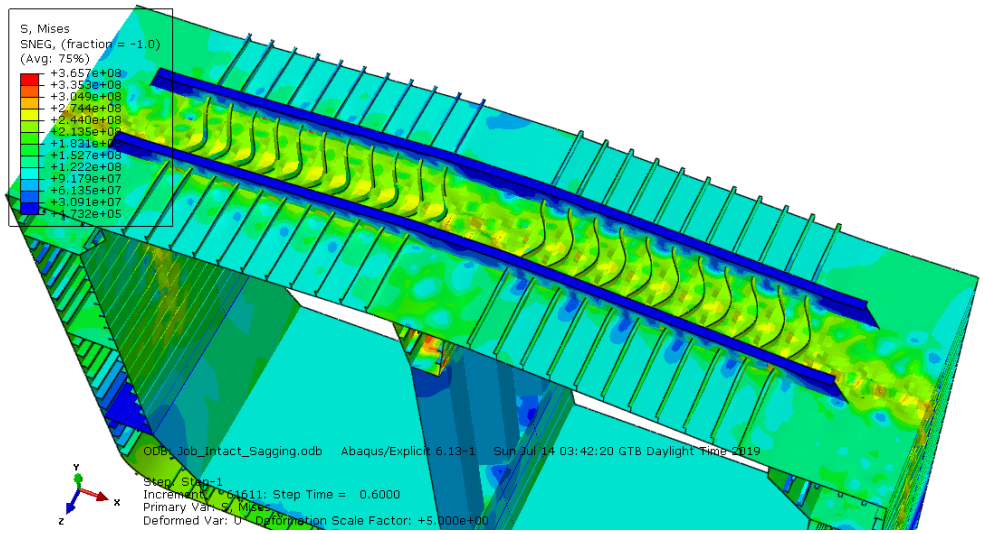

Figure 117: Stress contour on deformed 3 frame model for sagging condition

6.2 Elevated Temperature Condition

Hogging and sagging conditions were examined for the 3 frame model at elevated temperature. The boundary and loading conditions are presented in Table 17. The total step time was equal to 2 sec and the loading rate maintained the same as the analyses in intact condition.

RP – 1	RP – 2
Ux = Uy = Uz = URx = URy = URz = 0	Ux = Uy = URz = 0 URx = 0.003 rad

Table 17: Boundary and loading conditions for 3 frame model at elevated temperature condition

Figures 118 and 119 show the bending moment versus curvature for hogging and sagging condition, respectively. Regarding hogging condition, the maximum bending moment is 3028.6 MNm at curvature $4.13 * 10^{-4}\, m^{-1}$. On the other hand, for sagging condition the maximum bending moment is $-2118\, MNm$ at curvature $-2.79 * 10^{-4}\, m^{-1}$. Applying the CSR – H criterion for the two conditions, as presented in sections 2.2 and 7.3.1, we obtain the following results:

- Hogging Condition:

$$M \leq \frac{M_{U-hog}}{\gamma_R} \Rightarrow$$

$$2345533.6\ \text{kNm} \leq \frac{3028600\ \text{kNm}}{1.21} \Rightarrow 2345533.6\ \text{kNm} \leq 2502975.2\ \text{kNm}$$

- Sagging Condition:

$$M \leq \frac{M_{U-sag}}{\gamma_R} \Rightarrow$$

$$-2368953.9\ \text{kNm} \leq \frac{-2118000\ \text{kNm}}{1.1} \Rightarrow 2368953.9\ \text{kNm} \leq 1925454.5\ \text{kNm}$$

CSR – H criterion is satisfied for hogging condition but is no satisfied for sagging condition. Regarding hogging condition, the difference between the value of the vertical hull girder bending moment for the ultimate strength check and the value of the vertical hull girder ultimate bending capacity reduced by the γ_R factor, is relative small. As it has been mentioned before, computational results affected from many parameters, so the estimated result values from the analysis can be actually greater or smaller.

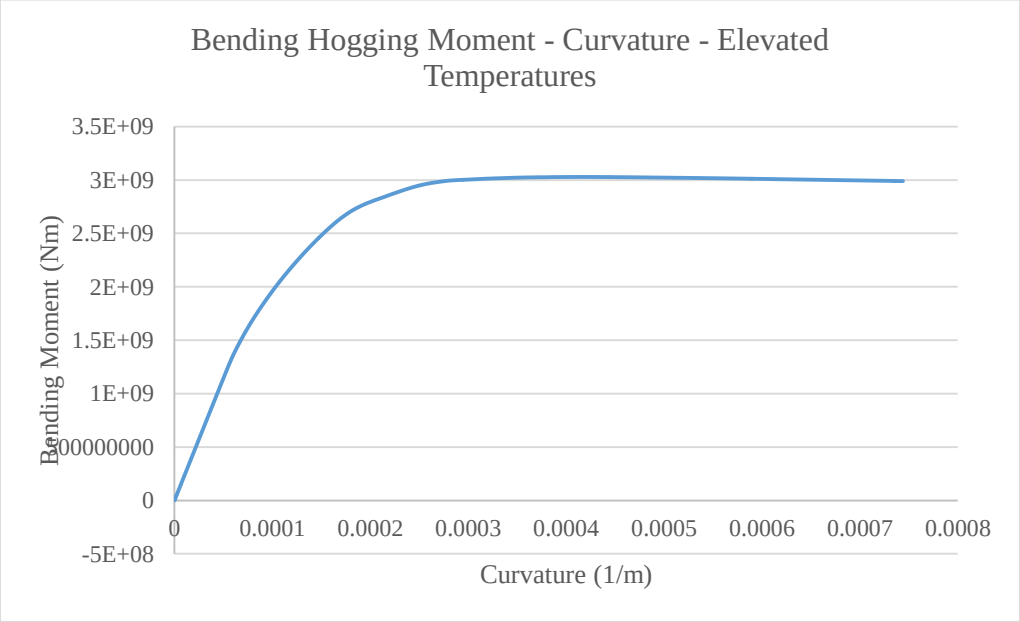

Figure 118: Bending hogging moment versus curvature of hull girder at elevated temperature condition (ABAQUS)

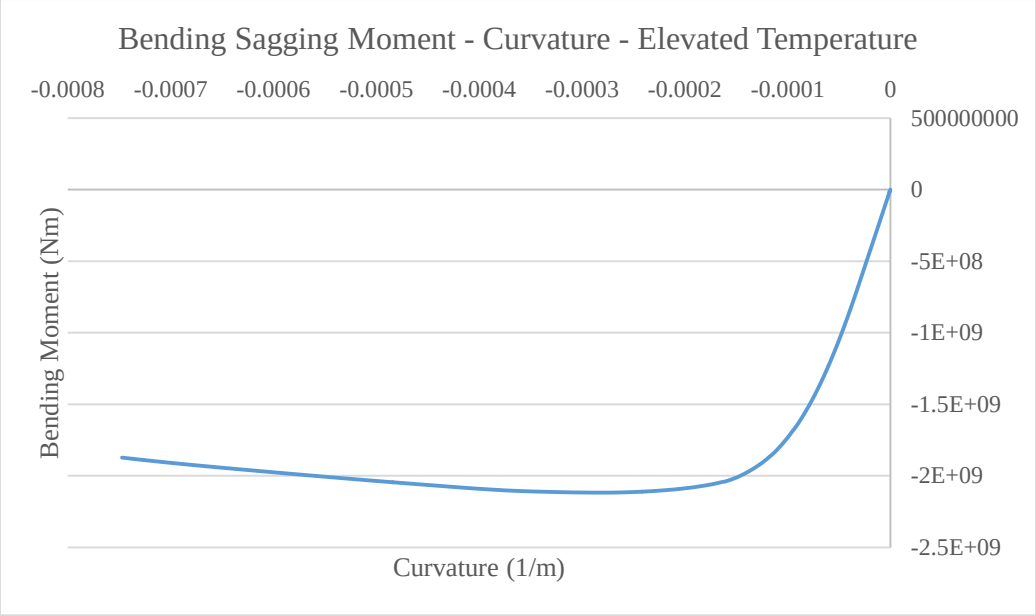

Figure 119: Bending sagging moment versus curvature of hull girder at elevated temperature condition (ABAQUS)

Figures 120 and 121 show the stress contours on the deformed 3 frame model for hogging condition near the ultimate bending moment. Specifically, Figure 121 shows the outer bottom of the 3 frame model. Figures 122 and 123 show the stress contours on the deformed 3 frame model for sagging condition. In hogging condition average Mises stresses are greater than yield stress. As it has been mention before this is a common error of finite element analysis packages caused by post processing procedure.

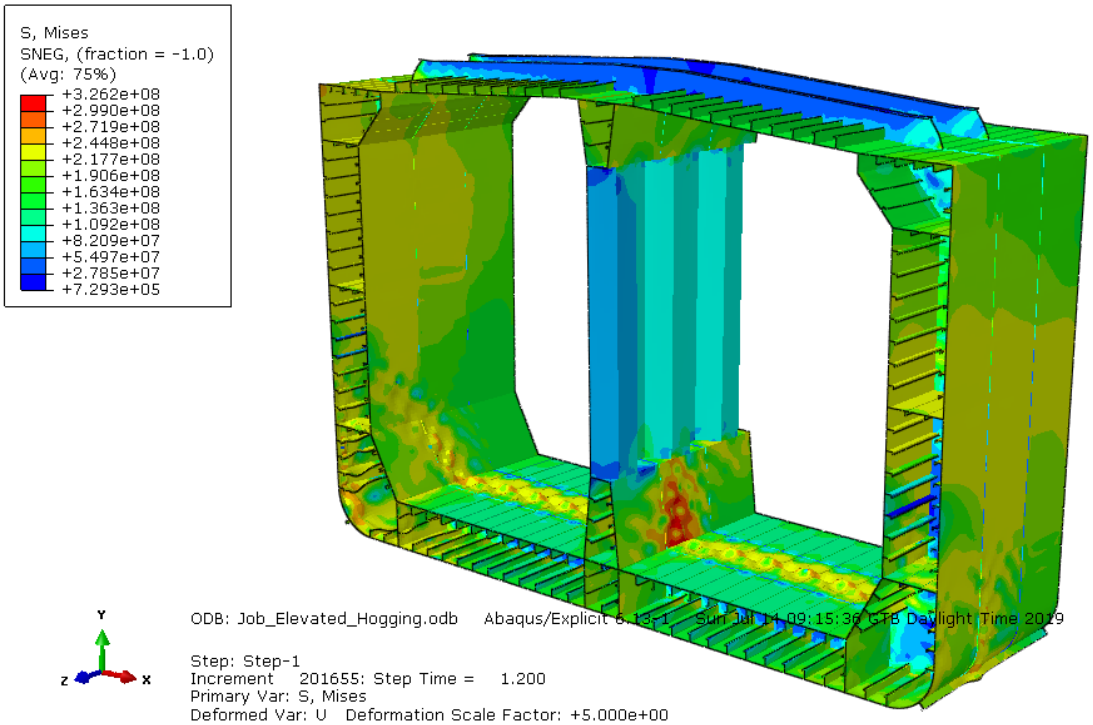

Figure 120: Stress contour on deformed 3 frame model for hogging condition

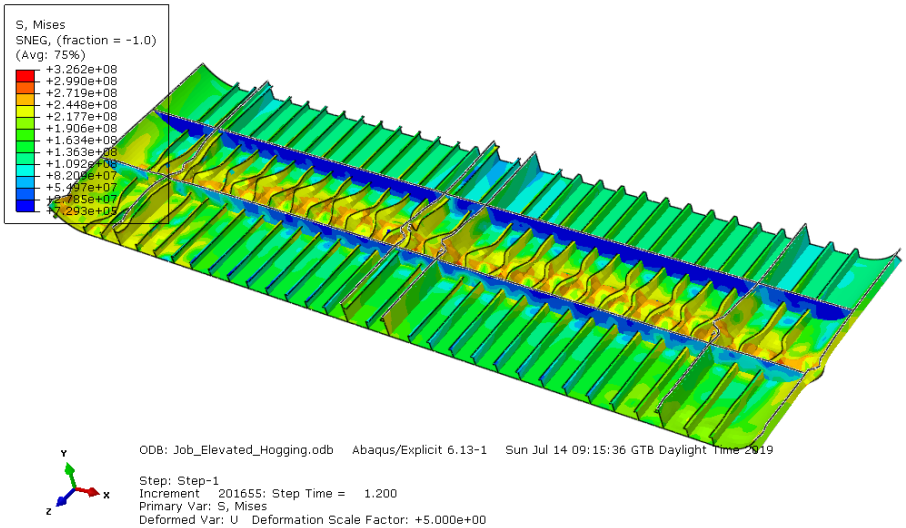

Figure 121: Stress contour on deformed 3 frame model outer bottom for hogging condition

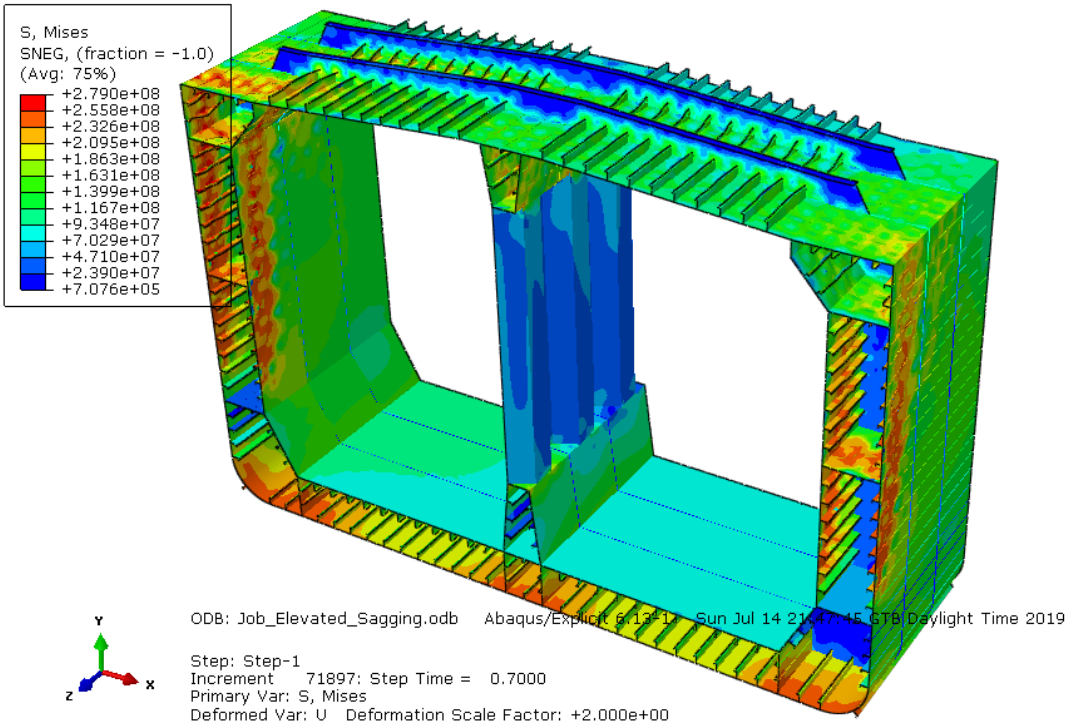

Figure 122: Stress contour on deformed 3 frame model for sagging condition

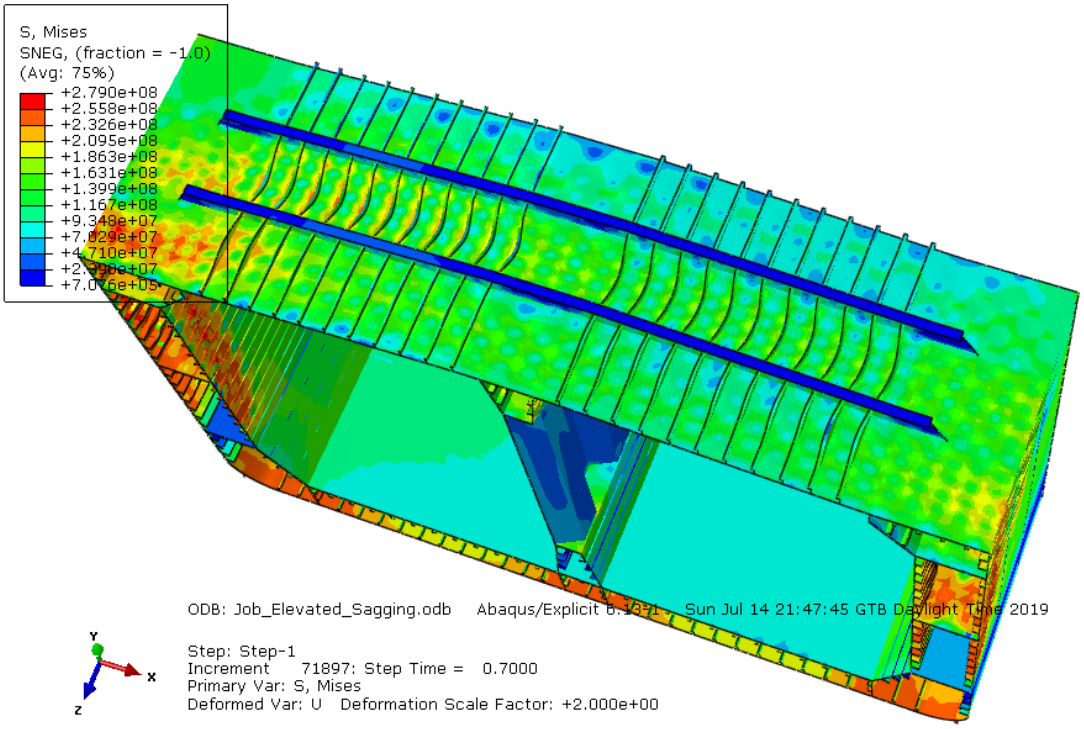

Figure 123: Stress contour on deformed 3 frame model for sagging condition

Chapter 7: Ultimate Hull Strength – Smith Method – Modified Smith Method

Smith method is an incremental – iterative process for progressive collapse analysis of hull girders structures. In present chapter, Smith method will be presented and a modified Smith method for ultimate strength at elevated temperatures will be introduced. Moreover, the analysis parameters (CSR – H criterion, hull transverse section division, primary calculations) and the results from the Smith and modified Smith methods will be presented. MatLab code development for the Smith and modified Smith methods was based on the code presented by Ioannidis [28]. Spreadsheets needed for the primary calculations of Smith method are presented in Appendix E. MatLab code for Smith and modified Smith methods are presented in Appendix F and G, respectively.

7.1 Smith Method

Common structural rules for bulk carriers and oil tankers are provided from International Association of Classification Societies in order to establish rules, methods and requirements for ship construction [32]. The rules refer to several features in ship construction such as fatigue, loads, design principles, superstructures etc.. The present study is dealing with the hull girder ultimate strength thus the chapter which describes the hull girder strength from the common structural rules will be presented.

There are three different methods to obtain the ultimate strength of a hull girder. A widely used method is the incremental – iterative process introduced in late 70s by Smith, referred as Smith method. The other two methods are the finite element method (FEM) and the idealized structural unit method (ISUM). According to Smith method the cross section of the ship is divided in three types of structural elements: hard corners, stiffener elements and stiffened plate elements. The method is based on the summation of the contributions of all elements for the calculation of the ultimate bending moment. The basic assumptions of the method are:

- plane cross section during the progressive collapse,
- no existence of interaction between the adjacent structural elements,
- the transverse frame is stocky enough such that the structural elements fail in an inter – frame mode and
- no shear stresses.

The main disadvantages of the Smith method are related to the assumptions. The cross section is studied under pure bending, without taking into account the interaction between the structural elements. Also, in Smith method there is no control of boundary conditions [28,32].The main steps of the Smith method are presented below [32]:

1) Divide the transverse section of hull into elements.
2) Define stress – strain relationships for all elements (section 7.1.1).

3) Initialize curvature and neutral axis for the first incremental step with the value of incremental curvature: $\chi_1 = \Delta\chi = 0.01\frac{R_{eH}}{E}\frac{1}{z_D - z_n}$.
4) Calculate for each element the corresponding strain ($\varepsilon_i = \chi(z_i - z_n)$) and the corresponding stress.
5) Determine the neutral axis at each incremental step by establishing force equilibrium over the whole transverse section: $\sum A_i\sigma_i = \sum A_j\sigma_j$.
6) Calculate the corresponding moment by summing the contributions of all elements as: $M_U = \sum A_i\sigma_i\,|(z_i - z_n)|$.
7) Compare the moment in the current incremental step with the moment in the previous incremental step. If the slope in moment – curvature relationship is less than a negative fixed value, terminate the process and define the peak value of the moment. Otherwise, increase the curvature by the amount of Δx and go to step 4. The iterative process is terminated when the curvature reach the critical value of: $\chi_F = \pm 0.003\frac{M_Y}{EI_Y}$.

Figure 125 presents the flow chart of the above incremental – iterative procedure. Moreover, when applying Smith method, all hull structural dimensions are defined by excluding the 50% corrosion margin as specified by IACS [32]. Figure 124 presents graphically the corrosion margin excluded from the structural elements [59].

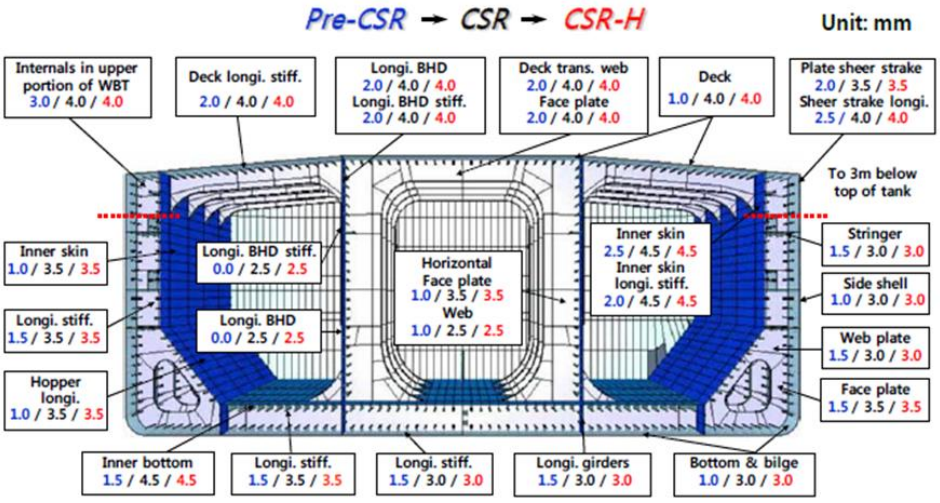

Fig. 2 Changes in corrosion addition rules for double hull oil tanker structures (DNV, 2005; IACS, 2006a; 2006b; IMO, 2012).

Figure 124: Corrosion margins [59]

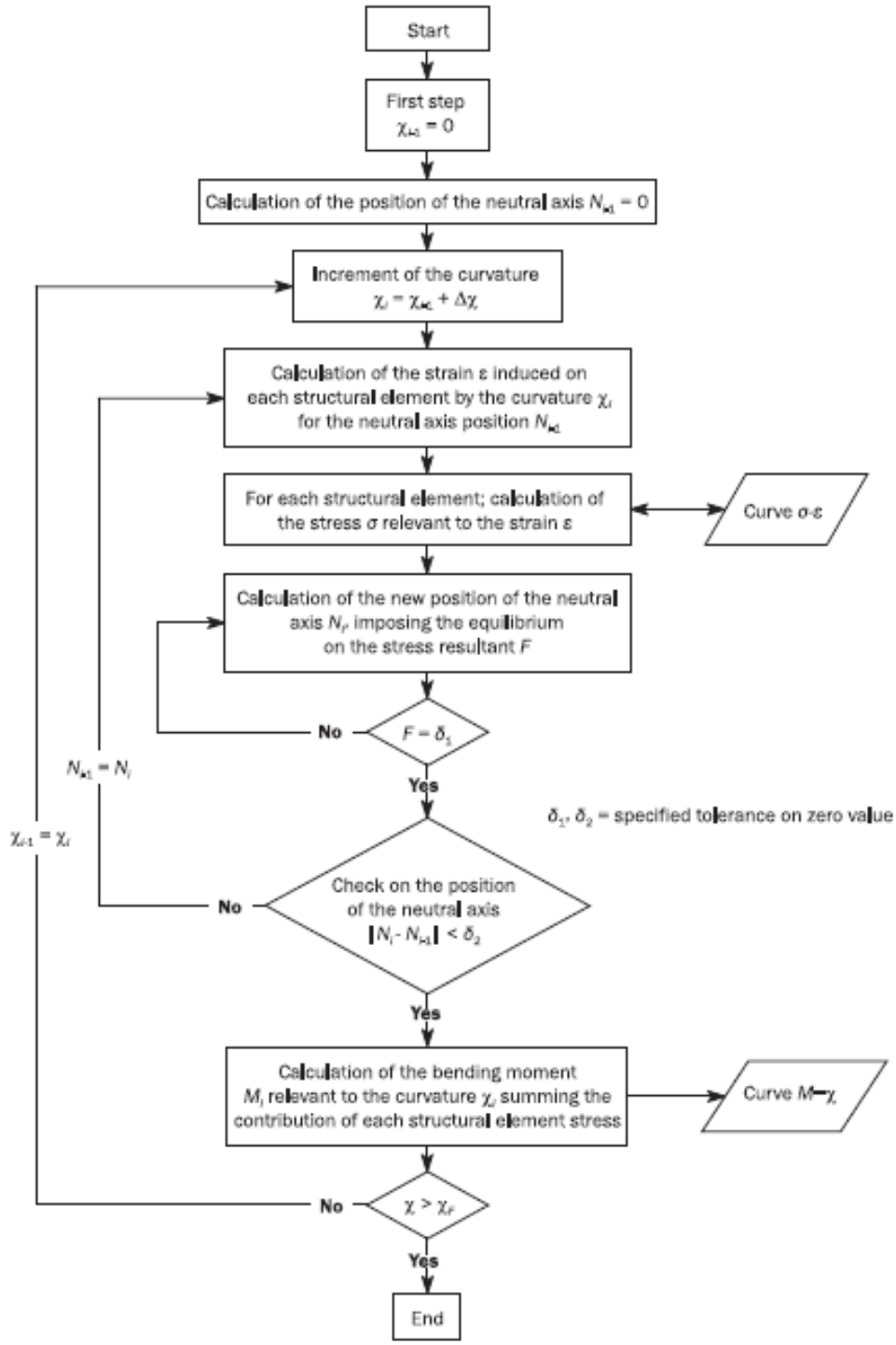

Figure 125: Flow chart for Smith method [32]

7.1.1 Load End Shortening Curves

Structural elements composing the hull girder may collapse following one of the modes of failure specified in Table 18. When an element is in tension the stress – strain curve shape is equivalent to Elasto – plastic collapse curve. In the next paragraphs there will be an extensive presentation of the equations which describing the modes of failure [32].

Hard Corner	Elasto – plastic collapse
Stiffener Element	Elasto – plastic collapse Beam Column buckling Torsional buckling Web Local buckling of flanged profiles or flat bars
Stiffened Plate Element	Plate buckling

Table 18: Structural elements modes of failure

Regarding the Elasto – plastic collapse, the equation describing the load – end shortening curve is to be obtained from the following formula:

$$\sigma = \Phi R_{eHA} \tag{65}$$

Where equivalent minimum yield stress: $R_{eHA} = \frac{R_{eHp}A_{p-n50}+R_{eHs}A_{s-n50}}{A_{p-n50}+A_{s-n50}} \left(\frac{N}{mm^2}\right)$, edge function: $\Phi = \begin{matrix} -1\,,\varepsilon < -1 \\ \varepsilon, -1 \le \varepsilon \le 1 \\ 1\,,\varepsilon > 1 \end{matrix}$, relative strain: $\varepsilon = \frac{\varepsilon_E}{\varepsilon_y}$, element strain: ε_E and strain at yield stress in the element: $\varepsilon_y = \frac{R_{eHA}}{E}$.

The equation describing the load – end shortening curve for the beam column buckling of stiffeners composing the hull girder transverse section is to be obtained from the following formula:

$$\sigma_{CR1} = \Phi\sigma_{C1}\frac{A_{s-n50} + A_{pE-n50}}{A_{s-n50} + A_{p-n50}} \tag{66}$$

Where edge function: $\Phi = \begin{matrix} -1\,,\varepsilon < -1 \\ \varepsilon, -1 \le \varepsilon \le 1 \\ 1\,,\varepsilon > 1 \end{matrix}$, critical stress: $\begin{matrix} \sigma_{C1} = \frac{\sigma_{E1}}{\varepsilon}, \gamma\iota\alpha\ \sigma_{E1} \le \frac{R_{eHB}}{2}\varepsilon \\ \sigma_{C1} = R_{eHB}\left(1 - \frac{R_{eHB}\varepsilon}{4\sigma_{E1}}\right), \gamma\iota\alpha\ \sigma_{E1} > \frac{R_{eHB}}{2}\varepsilon \end{matrix} \left(\frac{N}{mm^2}\right)$, equivalent minimum yield stress of the considered element: $R_{eHB} = \frac{R_{eHp}A_{pEI-n50}l_{pE}+R_{eHs}A_{s-n50}l_{sE}}{A_{p-n50}l_{pE}+A_{s-n50}l_{sE}} \left(\frac{N}{mm^2}\right)$, effective area: $A_{pEI-n50} = 10b_{E1}t_{n50}\ (cm^2)$, distance measured from the neutral axis of the stiffener with attached plate of width $b_{E1}$to the bottom of the attached plate: $l_{pE}\ (mm)$, distance measured from the neutral axis of the stiffener with attached plating of width $b_{E1}$to the top of the stiffener: $l_{sE}\ (mm)$, relative strain: ε, Euler column buckling stress: $\sigma_{E1} = \pi^2 E\frac{I_{E-n50}}{A_{E-n50}l^2}10^{-4} \left(\frac{N}{mm^2}\right)$, net moment of inertia of stiffeners with attached plating of width b_{E1}: $I_{E-n50}(cm^4)$, net area of stiffeners with attached plating of width b_{E1}: $A_{E-n50}\ (cm^2)$, effective width corrected for relative strain of the attached plating: $b_{E1} = \begin{matrix} \frac{s}{\beta_E}\gamma\iota\alpha\ \beta_E > 1.0 \\ s\ \gamma\iota\alpha\ \beta_E \le 1.0 \end{matrix}\ (m)$, slenderness factor: $\beta_E = 10^3\frac{s}{t_{n50}}\sqrt{\frac{\varepsilon R_{eHp}}{E}}$, net sectional area of attached plating of width b_E: $A_{pE-n50} = 10b_E t_{n50}\ (cm^2)$ and effective width of the attached plating: $b_E = \begin{matrix} \left(\frac{2.25}{\beta_E} - \frac{1.25}{\beta_E^2}\right)s, \gamma\iota\alpha\ \beta_E > 1.25 \\ s, \gamma\iota\alpha\ \beta_E \le 1.25 \end{matrix}\ (m)$.

The formula describing the load – end shortening curve for torsional buckling is presented below:

$$\sigma_{CR2} = \Phi \frac{A_{s-n50}\sigma_{C2} + A_{p-n50}\sigma_{CP}}{A_{s-n50} + A_{p-n50}} \quad (67)$$

Where edge function: $\Phi = \begin{matrix} -1\,, \varepsilon < -1 \\ \varepsilon, -1 \le \varepsilon \le 1, \\ 1\,, \varepsilon > 1 \end{matrix}$ critical stress: $\begin{matrix} \sigma_{C2} = \frac{\sigma_{E2}}{\varepsilon}, \gamma\iota\alpha\ \sigma_{E2} \le \frac{R_{eHs}}{2}\varepsilon \\ \sigma_{C2} = R_{eHs}\left(1 - \frac{R_{eHs}\varepsilon}{4\sigma_{E2}}\right), \gamma\iota\alpha\ \sigma_{E1} > \frac{R_{eHs}}{2}\varepsilon \end{matrix}$ $\left(\frac{N}{mm^2}\right)$,

Euler torsional buckling stress: $\sigma_{E2} = \frac{E}{I_p}\left(\frac{\varepsilon\pi^2 I_\omega 10^2}{l^2} + 0.385 I_T\right)$ $\left(\frac{N}{mm^2}\right)$, net polar moment of inertia of the stiffener: $I_p(cm^4)$, net St. Venant's moment of inertia of the stiffener: $I_T\ (cm^4)$, net sectional moment of inertia of the stiffener: $I_\omega(cm^6)$ (for better comprehension see Part 1, Chapter 8, Section 5, Paragraph 2.3.4 from [32]), degree of fixation: $\varepsilon = 1 + \frac{\left(\frac{l}{\pi}\right)^2 10^{-3}}{\sqrt{I_\omega\left(\frac{0.75s}{t_p^3} + \frac{e_f - 0.5t_f}{t_w^3}\right)}}$, buckling stress of the attached plating: $\sigma_{CP} = \begin{matrix} \left(\frac{2.25}{\beta_E} - \frac{1.25}{\beta_E^2}\right) R_{eHp}, \gamma\iota\alpha\ \beta_E > 1.25 \\ R_{eHp}, \gamma\iota\alpha\ \beta_E \le 1.25 \end{matrix}$ $\left(\frac{N}{mm^2}\right)$ and slenderness factor: $\beta_E = 10^3 \frac{s}{t_{n50}}\sqrt{\frac{\varepsilon R_{eHp}}{E}}$.

For the web local buckling of stiffeners made of flanged profiles the formula describing the load – end shortening curve is presented below:

$$\sigma_{CR3} = \Phi \frac{10^3 b_E t_{n50} R_{eHp} + (h_{we} t_{w-n50} + b_f t_{f-n50}) R_{eHs}}{10^3 s t_{n50} + h_w t_{w-n50} + b_f t_{f-n50}} \quad (68)$$

Where: edge function: $\Phi = \begin{matrix} -1\,, \varepsilon < -1 \\ \varepsilon, -1 \le \varepsilon \le 1, \\ 1\,, \varepsilon > 1 \end{matrix}$ effective width of the attached plating: $b_E = \begin{matrix} \left(\frac{2.25}{\beta_E} - \frac{1.25}{\beta_E^2}\right) s, \gamma\iota\alpha\ \beta_E > 1.25 \\ s, \gamma\iota\alpha\ \beta_E \le 1.25 \end{matrix}$ (m), effective height of the web: $h_{we} = \begin{matrix} \left(\frac{2.25}{\beta_w} - \frac{1.25}{\beta_w^2}\right) h_w, \gamma\iota\alpha\ \beta_w \ge 1.25 \\ h_w, \gamma\iota\alpha\ \beta_w < 1.2 \end{matrix}$ (mm) and slenderness factor: $\beta_w = \frac{h_w}{t_{w-n50}}\sqrt{\frac{\varepsilon R_{eHs}}{E}}$.

The equation describing the load – end shortening curve for the web local buckling of flat bar stiffeners composing the hull girder transverse section is to be obtained from the following formula:

$$\sigma_{CR4} = \Phi \frac{A_{p-n50}\sigma_{CP} + A_{s-n50}\sigma_{C4}}{A_{p-n50} + A_{s-n50}} \quad (69)$$

Where: edge function: $\Phi = \begin{matrix} -1\,, \varepsilon < -1 \\ \varepsilon, -1 \le \varepsilon \le 1, \\ 1\,, \varepsilon > 1 \end{matrix}$ buckling stress of the attached plating: $\sigma_{CP} = \begin{matrix} \left(\frac{2.25}{\beta_E} - \frac{1.25}{\beta_E^2}\right) R_{eHp}, \gamma\iota\alpha\ \beta_E > 1.25 \\ R_{eHp}, \gamma\iota\alpha\ \beta_E \le 1.25 \end{matrix}$ $\left(\frac{N}{mm^2}\right)$, critical stress: $\sigma_{C4} = \begin{matrix} \frac{\sigma_{E4}}{\varepsilon}, \gamma\iota\alpha\ \sigma_{E4} \le \frac{R_{eHs}}{2}\varepsilon \\ R_{eHs}\left(1 - \frac{R_{eHs}\varepsilon}{4\sigma_{E4}}\right), \gamma\iota\alpha\ \sigma_{E4} > \frac{R_{eHs}}{2}\varepsilon \end{matrix}$ $\left(\frac{N}{mm^2}\right)$ and local Euler buckling stress: $\sigma_{E4} = 160000\left(\frac{t_{w-n50}}{h_w}\right)^2$ $\left(\frac{N}{mm^2}\right)$.

For the plate buckling the formula describing the load – end shortening curve is presented below:

$$\sigma_{CR5} = \min\left\{ \begin{matrix} R_{eHp}\Phi \\ \Phi R_{eHp}\left[\frac{s}{l}\left(\frac{2.25}{\beta_E} - \frac{1.25}{\beta_E^2}\right) + 0.1\left(1 - \frac{s}{l}\right)\left(1 + \frac{1}{\beta_E^2}\right)^2\right] \end{matrix} \right\} \quad (70)$$

Where: edge function: $\Phi = \begin{matrix} -1\,, \varepsilon < -1 \\ \varepsilon, -1 \le \varepsilon \le 1 \\ 1\,, \varepsilon > 1 \end{matrix}$, slenderness factor: $\beta_E = 10^3 \frac{s}{t_{n50}}\sqrt{\frac{\varepsilon R_{eHp}}{E}}$, plate breadth taken as the spacing between the stiffeners: $s\ (m)$ and the longer side of the plate: $l\ (m)$. Figure 126 presents the load – end shortening curves for the above modes of failure.

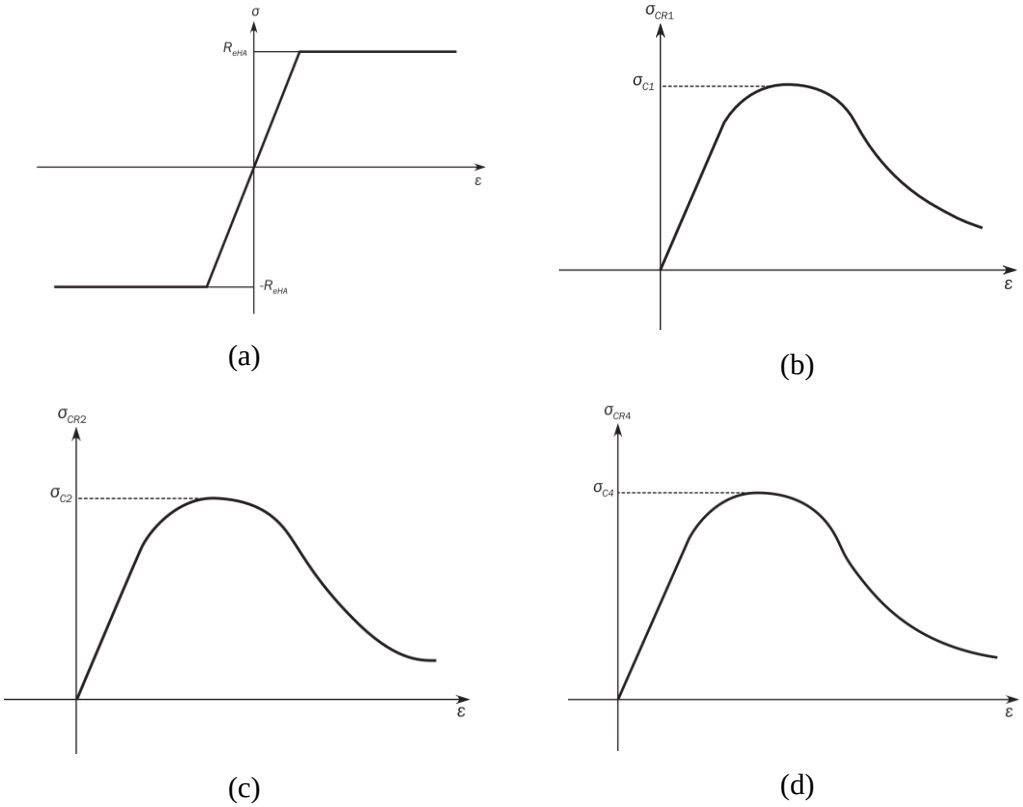

Figure 126: Load – end shortening curves of (a) Elasto – plastic collapse, (b) Beam column buckling, (c) Torsional buckling, (d) Web local buckling

7.2 Modified Smith Method

One way to investigate the ultimate bending moment capacity of a chemical/oil product carrier subjected to elevated temperatures is the use of a modified Smith method. The analysis concept for a modified Smith method is presented in Figure 127. Firstly, an ABAQUS thermal analysis is executed as presented in section 5.8, in order to obtain the hull girder temperature profile and the temperature of each element. Average element temperatures were assumed for each structural element. For instance, for element temperature equal to 436 °C, the element temperature rounded down to 400 °C and for element temperature equal to 465 °C, the element temperature rounded up to 500 °C. Consequently, a nonlinear buckling analysis was executed for each structural element at specific temperature, in order to obtain the load – end shortening curve of the element at specific temperature state. An Excel file was generated with stress – strain curves of the structural elements.

The compression stress – strain curves are described from the load – end shortening curves obtained from ABAQUS nonlinear buckling analysis while the tension stress – strain curves are described from the material's stress – strain curves described by Eurocode [60] (Appendix A). The generated Excel file consist an input parameter for the modified Smith method MatLab code (Appendix G).

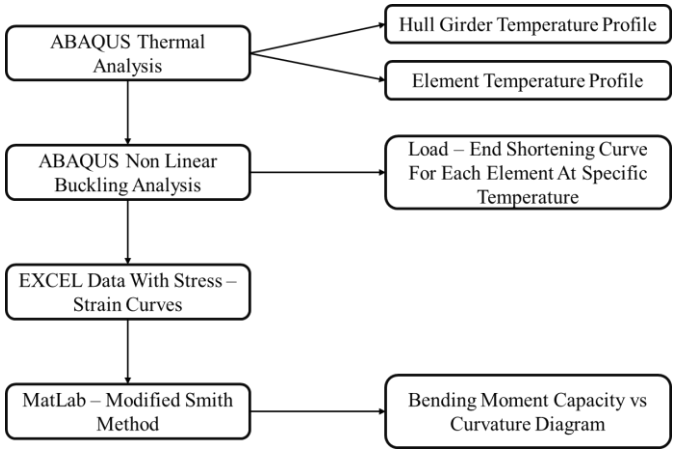

Figure 127: Analysis concept of modified Smith method

The only difference between the original and modified Smith method is the addition of a moment equilibrium in step 5 of the iterative – incremental process (see section 7.1) [28]. Except from the force equilibrium over transverse section's elements ($\sum_{elem=1}^{N} \sigma_{elem}(x) * A_{elem} = 0$), a moment equilibrium about the vertical axis is added ($\sum_{elem=1}^{N} \sigma_{elem}(x) * y_{elem} * A_{elem} = 0$). The satisfaction of the two equilibriums determines the displacement and the rotation of the neutral axis. The vertical displacement of the neutral axis is determined by the force equilibrium, while the moment equilibrium determines the rotation of the neutral axis. Element strain is calculated in code from the structural element coordinates and curvature. In order to specify the element stress, linear interpolation is performed in the stress and strain values of input Excel file.

7.3 Analysis Parameters

7.3.1 CSR – H Criterion

The geometric characteristics of the examined ship has been presented in section 5.4. The wave coefficient can be calculated from the following formula for ship lengths greater from 90 meters and smaller than 300 meters: $C_w = 10.75 - \left(\frac{300-L}{100}\right)^{1.5} = 9.31$. According to IACS [32], the vertical wave bending moment in hogging and sagging conditions can be estimated from equation (3) where $f_{nl-vh} = 1, f_{nl-vs} = 0.58\left(\frac{C_B+0.7}{C_B}\right) = 1.07$ $f_m = 1, f_p = f_{ps} = 1$:

$$M_{wv-h} = 1196375.897\ kNm$$
$$M_{wv-s} = -1280122.209\ kNm \quad (71)$$

For hogging condition, the vertical hull girder bending moment for ultimate strength check can be calculated from equation (2), where $\gamma_M = 1.1$, $\gamma_{DB} = 1.1$ thus $\gamma_R = 1.21$, $\gamma_s = 1$, $\gamma_w = 1.2$, $f_\beta = 1.05$, $M_{sw-h} = 838000\ kNm$ and $M_{wv-h} = 1196375.9\ kNm$:

$$M_h = 2345533.6\ kNm \tag{72}$$

For sagging condition, the vertical hull girder bending moment for ultimate strength check can be calculated from equation (2), where $\gamma_M = 1.1$, $\gamma_{DB} = 1.0$ thus $\gamma_R = 1.1$, $\gamma_s = 1$, $\gamma_w = 1.2$, $f_\beta = 1.05$, $M_{sw-s} = -756000\ kNm$ and $M_{wv-s} = -1280122.2\ kNm$:

$$M_s = -2368953.9 kNm \tag{73}$$

7.3.2 Structural Element Division

Figure 128 shows the division of the transverse section of hull into stiffener elements and stiffened plate element. The division was based on the IACS rules [32] and the total number of elements was 223. The elements with number 1, 61 and 112 are asymmetrical.

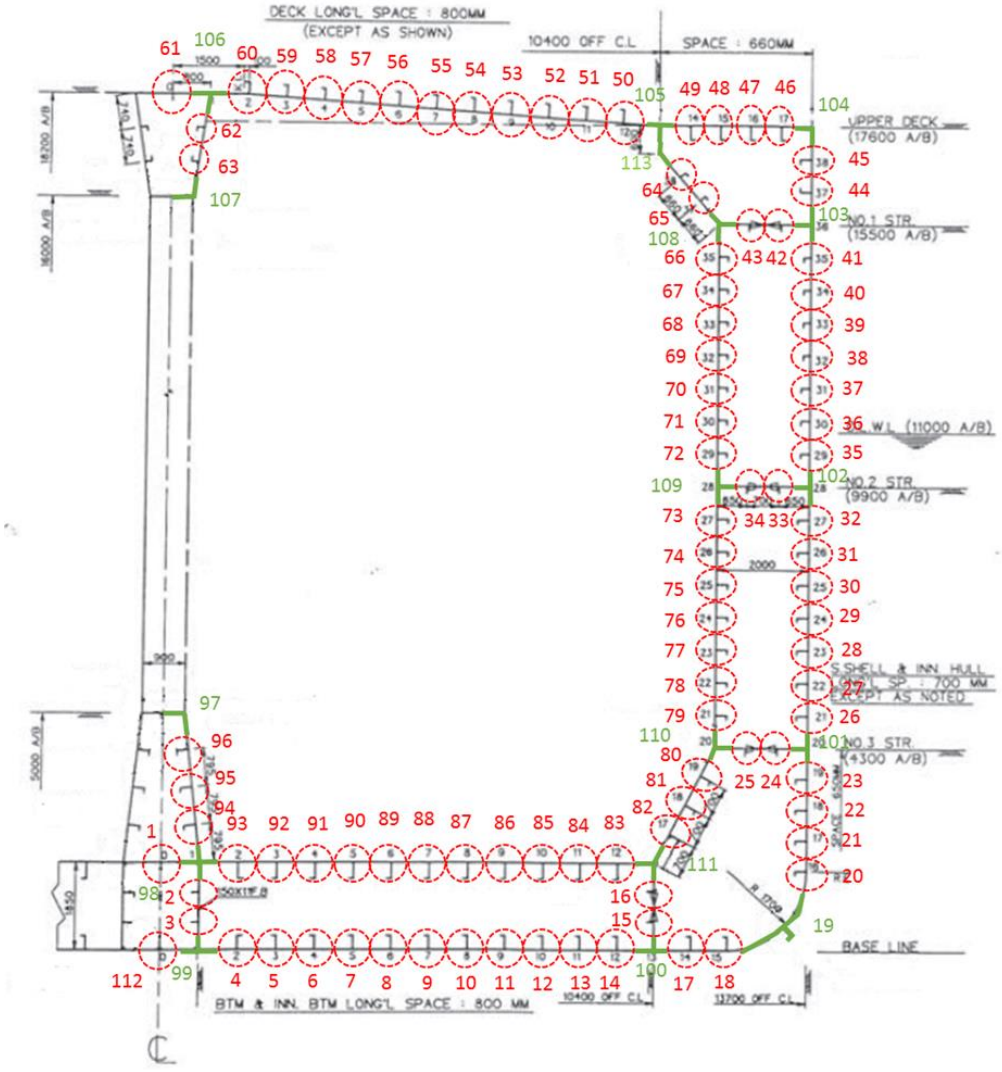

Figure 128: Element division for Smith and modified Smith method

7.3.3 Primary Calculations

The execution of Smith method in MatLab require the geometrical characteristics (dimensions, inertia moments, geometrical centroids) for the elements but also some characteristics of the hull transverse section (neutral axis position, second moment of inertia about neutral axis, section modulus at deck and bottom). The above parameters calculated in Excel and imported in MatLab codes. The generated Excel spreadsheets are presented in Appendix E. For the present analysis the 50% corrosion margin has been applied to the element's dimensions. Table 1 in Appendix E presents geometric characteristics of the attached plates in stiffener elements. Table 2 in Appendix E presents the moment of inertia of hull's plates. Table 3 in Appendix E presents geometric characteristics of the stiffeners of the stiffener elements. Table 4 in Appendix E presents the element's geometric center coordinates from the base line (z axis) and the middle vertical axis (y axis). Table 5 in Appendix E presents data for the calculation of geometric characteristics (total area, first moment of inertia from base line, second moment of inertia from base line) of the hull transverse cross section. From the previous data, the neutral axis position can be calculated. Table 6 in Appendix E consists an input file in MatLab code and it has been generated using the previous tables. It contains all the data needed by code to run properly. Table 19 presents input data for the MatLab codes calculated from the tables in Appendix E.

Total Area of Mid - Section	$\Sigma n_i A_i$	2.717	m^2
First Moment of Inertia About Base Line	$\Sigma n_i A_i z_i$	19.8225	m^3
Neutral Axis Position	Z_n	7.295	m
Second Moment About Base Line	$I_{yy,\ BL}$	283.6941	m^4
Second Moment About Neutral Axis	$I_{yy,\ NA}$	139.0749	m^4
Deck Height From Base Line	H	17.6	m
Distance From Neutral Axis to Deck	V_D	10.3042	m
Section Modulus at Bottom	Z_B	19.0625	m^3
Section Modulus at Deck	Z_D	13.4967	m^3

Table 19: Input data in MatLab code for Smith method

7.4 Smith Method Results

Smith method was applied through the MatLab code presented in Appendix F. Executing the code, the diagram of bending moment capacity versus curvature is obtained for the examined chemical/oil carrier (Figure 129). The maximum bending moment for hogging condition is equal to $3510222.6\ kNm$ at $2.837 * 10^{-4} m$ of curvature. The maximum bending moment for sagging condition is equal to $-2647417.2\ kNm$ at $-1.9707 * 10^{-4} m$ of curvature. The green line depicts the initial inclinations of the two curves, which can be calculated from the following formula: $E * I_y = 210000\ MPa * 139.0749 m^4 = 29205729\ MNm^2$.

Applying CSR – H criterion for hogging and sagging conditions, as presented in sections 2.2 and 7.3.1, we obtain the following results:

- Hogging Condition:

$$M \leq \frac{M_{U-hog}}{\gamma_R} \Rightarrow$$

$$2345533.6\ \text{kNm} \leq \frac{3510222.6\ \text{kNm}}{1.21} \Rightarrow 2345533.6\ \text{kNm} \leq 2901010.4\ \text{kNm}$$

- Sagging Condition:

$$M \leq \frac{M_{U-sag}}{\gamma_R} \Rightarrow$$

$$-2368953.9\ \text{kNm} \leq \frac{-2647417.2\ \text{kNm}}{1.1} \Rightarrow 2368953.9\ \text{kNm} \leq 2406742.9\ \text{kNm}$$

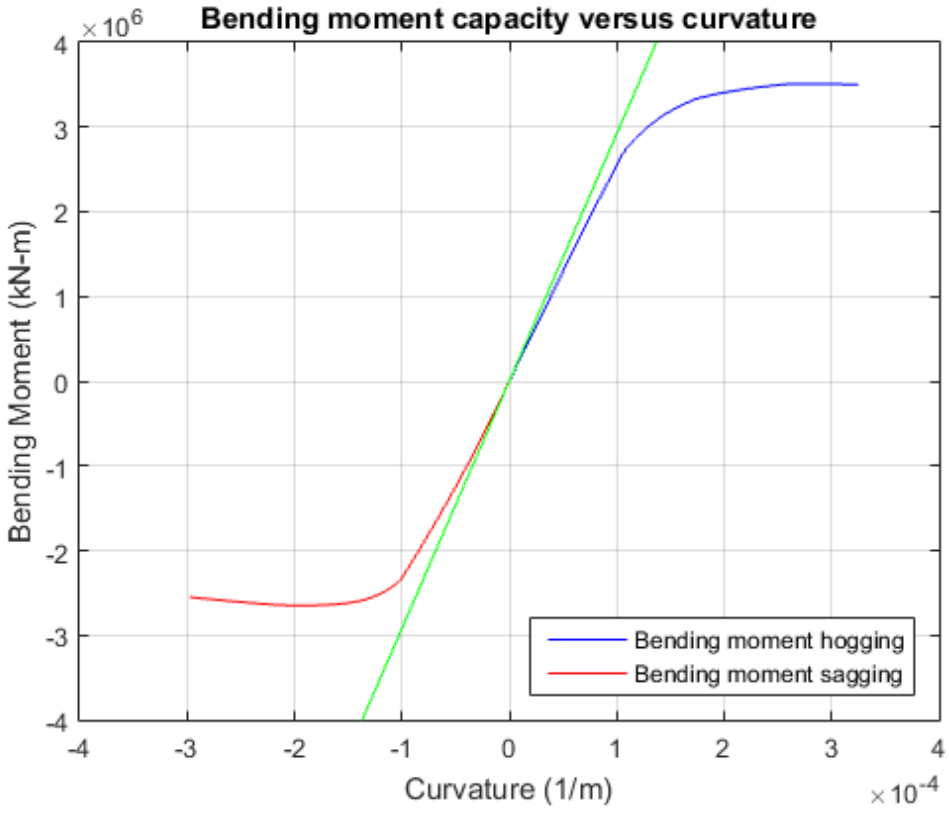

Figure 129: Bending moment capacity versus curvature of hull girder at intact condition

Consequently, the CSR – H criterion is satisfied for the two conditions. Figure 130 shows the vertical displacement of the neutral axis versus curvature for the two conditions. Figure 131 presents the bending moment capacity relative to neutral axis vertical displacement versus curvature for the two conditions ((a) Hogging, (b) Sagging).

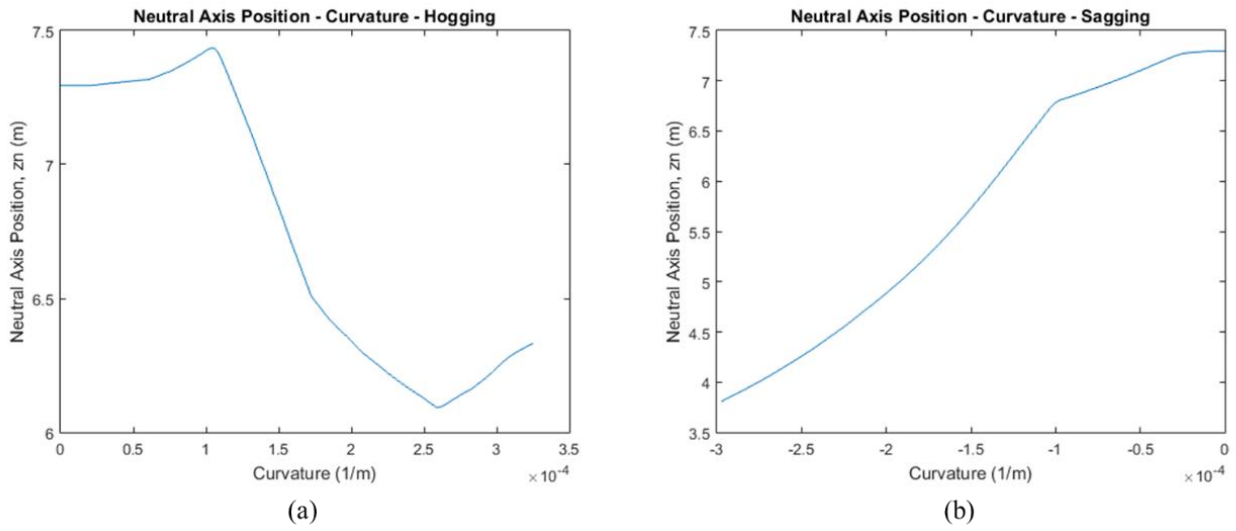

Figure 130: Vertical displacement of neutral axis for (a) hogging condition and (b) sagging condition

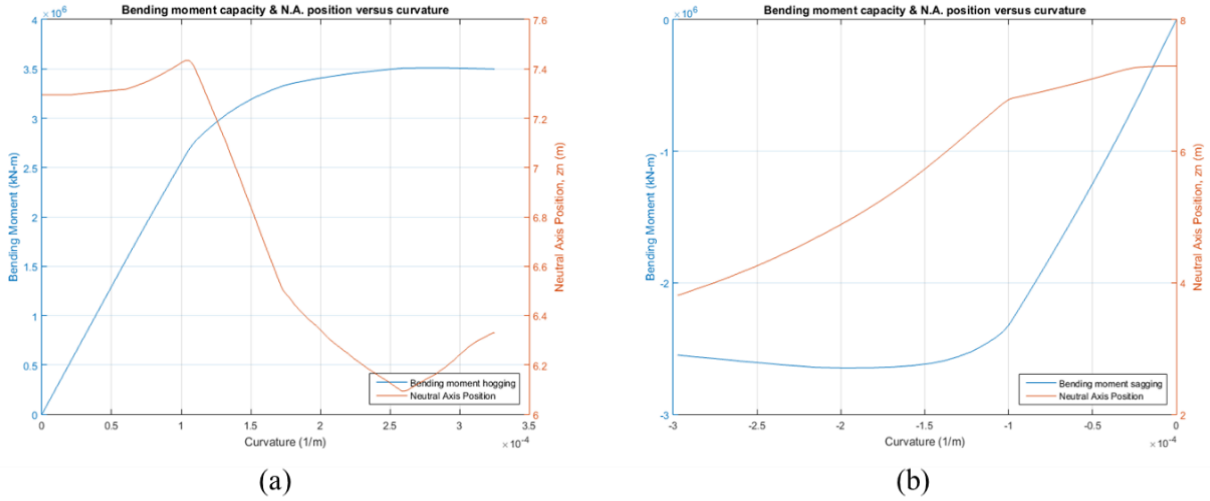

Figure 131:Bending moment and neutral axis displacement versus curvature for (a) hogging condition and (b) sagging condition

Figures 132 and 133 show the element stresses relative to element height for iterations 10, 100, 200 and 300 for hogging and sagging conditions, respectively. Regarding the hogging conditions, in the early iteration steps of the process the structural element stresses lay on a straight line which means that hull cross section is in elastic region. The diversion from the straight line of the structual element stresses indicates the plastic yield at the corresponding element of the hull cross section. A corresponding behavior is obtained in sagging condition. The difference between the two conditions is the starting yielding region. For hogging condition yielding starts from bottom elements while for sagging conditions yielding starts from deck structural elements. Figure 134 shows the load – end shortening curves for the structural elements 30, 60 and 90 for the two conditions (Hogging and Sagging). Elements 30, 60 and 90 are angle bar stiffener elements. Element 30 is located in hull side close to neutral axis, element 60 is located at the deck and element 90 is located at the bottom.

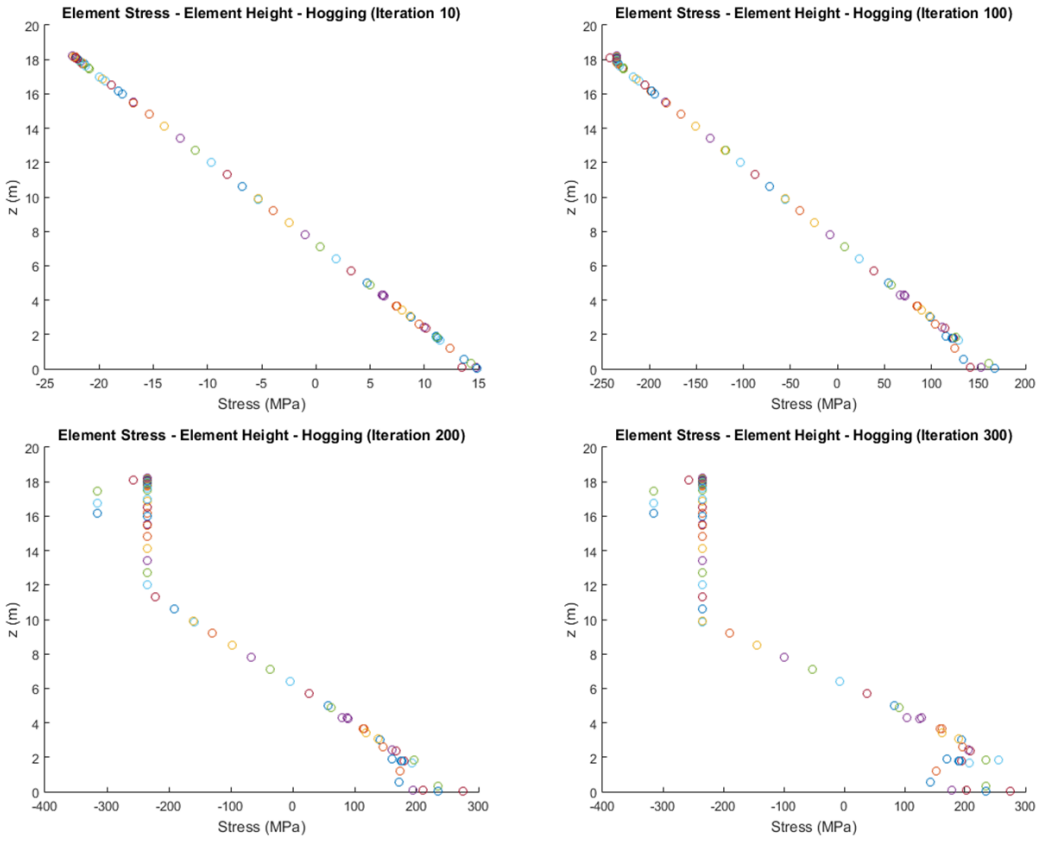

Figure 132: Element stresses relative to element height at different iterations of hogging condition

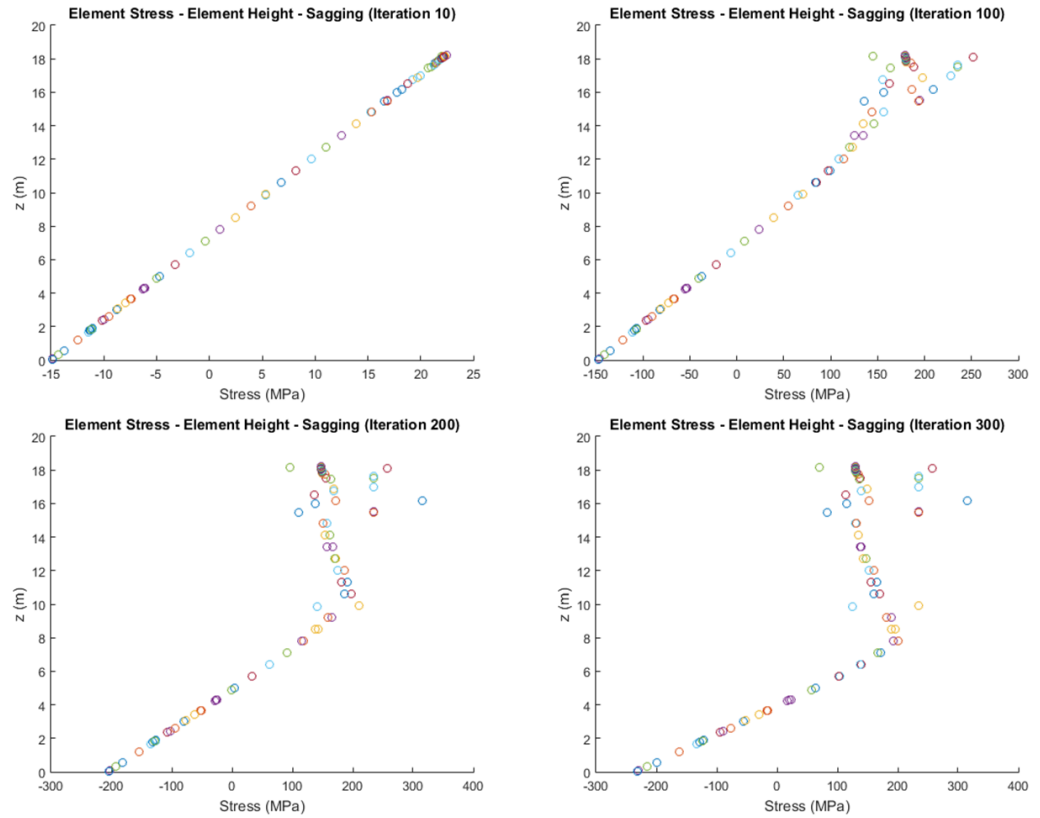

Figure 133: Element stresses relative to element height at different iterations of sagging condition

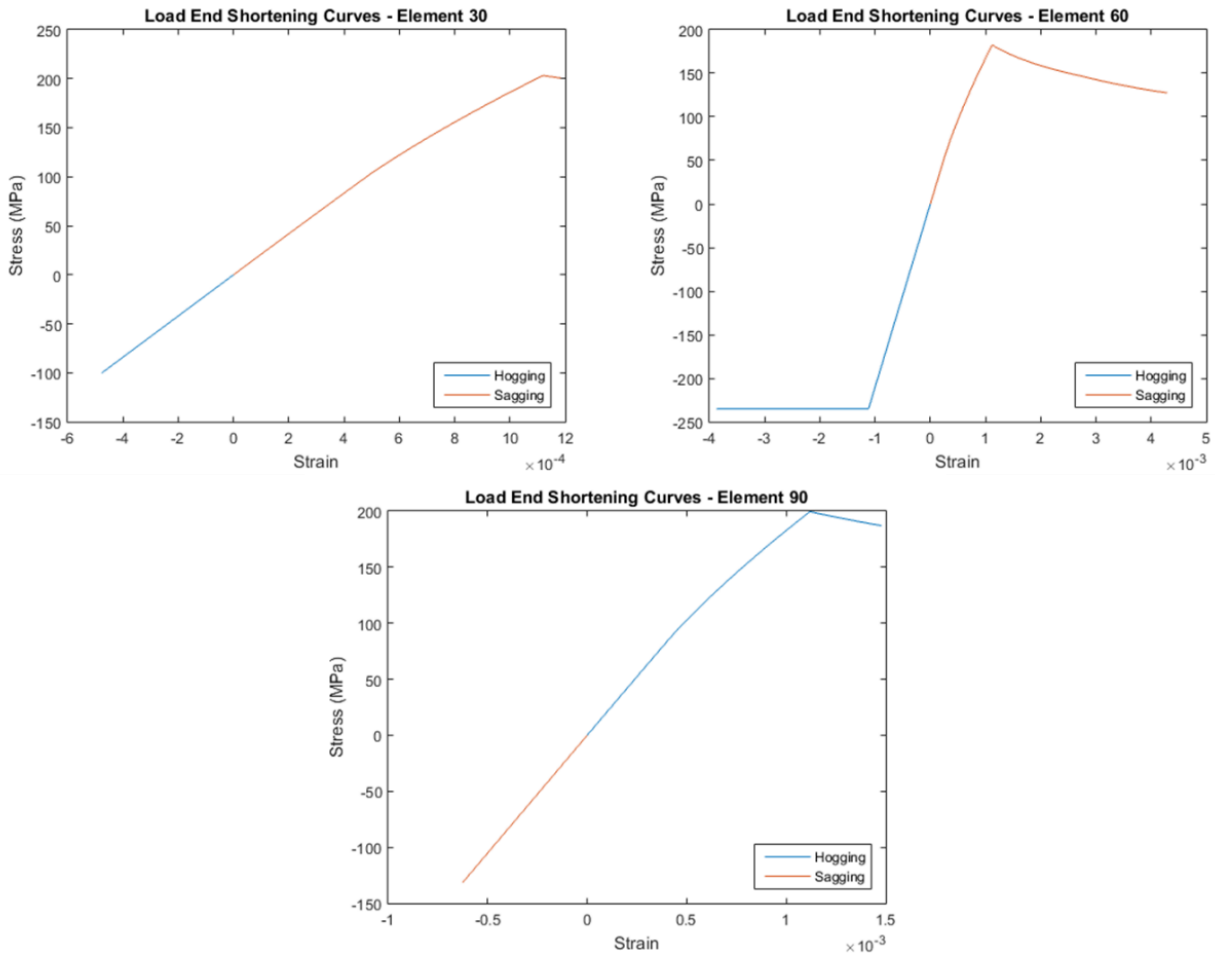

Figure 134: Load end shortening curves at hogging and sagging conditions for elements 30, 60 and 90

7.5 Modified Smith Method Results

The developed MatLab code for the modified Smith method is presented in Appendix G. The present analysis temperature profile is the same as the temperature profile presented in section 5.8. Executing the code, the diagram of bending moment capacity versus curvature is obtained for the examined chemical/oil carrier subjected to elevated temperatures (Figure 135). The maximum bending moment for hogging condition is equal to $2744739.2\ kNm$ at $3.2142 * 10^{-4} m$ of curvature. The maximum bending moment for sagging condition is equal to $-1905966.9\ kNm$ at $-2.1984 * 10^{-4} m$ of curvature.

Applying CSR – H criterion for hogging and sagging conditions, as presented in sections 2.2 and 7.3.1, we obtain the following results:

- Hogging Condition:

$$M \leq \frac{M_{U-hog}}{\gamma_R} \Rightarrow$$

$$2345533.6\ \text{kNm} \leq \frac{2744739.2\ \text{kNm}}{1.21} \Rightarrow 2345533.6\ \text{kNm} \leq 2268379.5\ \text{kNm}$$

- Sagging Condition:

$$M \leq \frac{M_{U-sag}}{\gamma_R} \Rightarrow$$

$$-2368953.9\ \text{kNm} \leq \frac{-1905966.9\ \text{kNm}}{1.1} \Rightarrow 2368953.9\ \text{kNm} \leq 1732697.2\ \text{kNm}$$

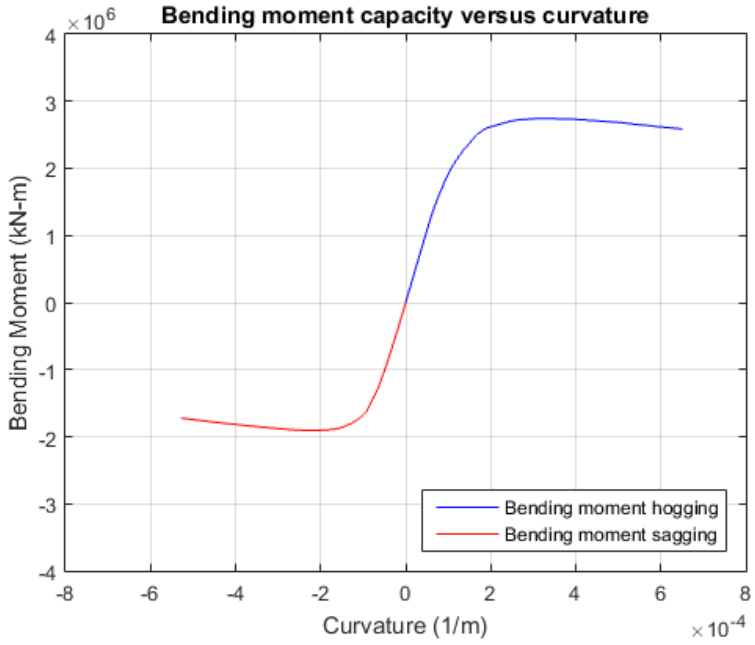

Figure 135: Bending moment capacity versus curvature of hull girder at elevated temperature condition

CSR – H criterion is not satisfied for the two conditions. Figure 136 (a) and (b) show the neutral axis vertical displacement versus curvature and the angle of neutral axis rotation versus curvature for the two conditions, hogging and sagging respectively. Figure 137 (a) and (b) present the bending moment capacity and the neutral axis position versus curvature for hogging and sagging condition, respectively. Figure 138 (a) and (b) present the bending moment capacity and the neutral axis rotation angle versus curvature for hogging and sagging condition, respectively.

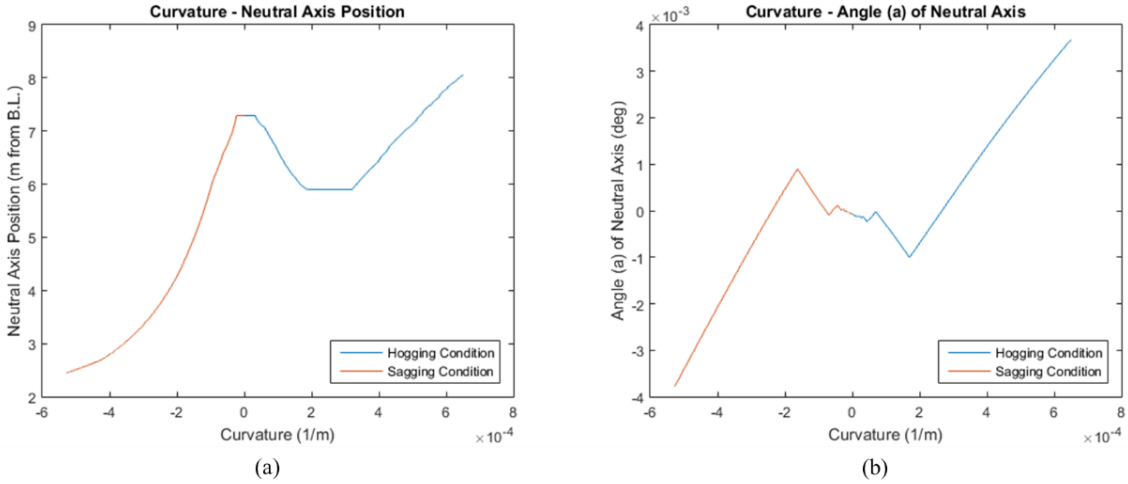

Figure 136: (a) Vertical axis displacement versus curvature, (b) vertical axis rotation versus curvature

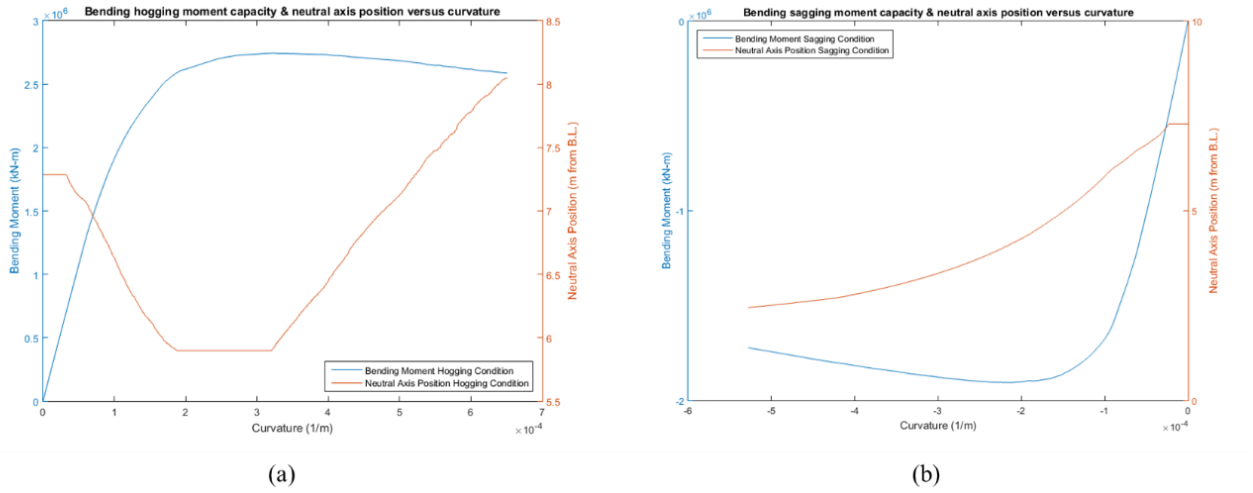

(a) (b)

Figure 137: Bending moment capacity and the neutral axis position versus curvature for (a) hogging condition and (b) sagging condition

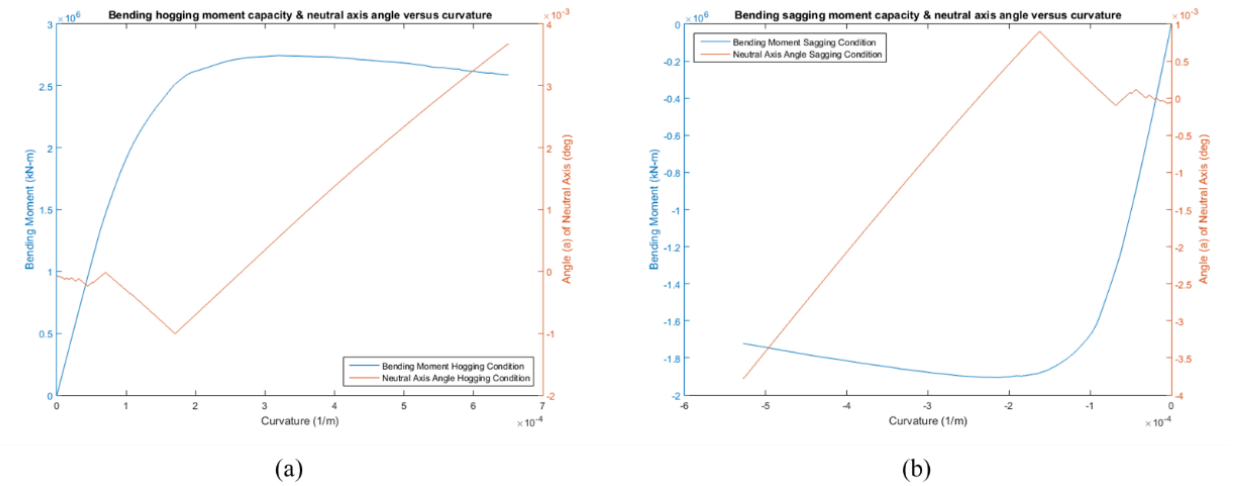

(a) (b)

Figure 138: Bending moment capacity and the neutral axis rotation angle versus curvature for (a) hogging condition and (b) sagging condition

Figures 140 and 141 present structural element stress relative to element height for iterations 10, 200, 400 and 600, for hogging and sagging condition, respectively. For hogging condition, it is initially observed that the structural element stresses lay on a line, except from stuctural elements at elevated temperature. As the iterative process continues bottom structural elements but also deck structural elements with elevated temperatures undergo yield. Further increase of curvature leads more structural elements to yield. For sagging condition, the results showed that deck structural elements undergo plastic yield while inner bottom structural elements remain in elastic region and outer bottom structural element reach yield stress. Figure 142 shows the load – end shortening curves for elements 10, 30, 60 and 90 for hogging and sagging conditions. Structural Elements 10 and 90 are located in bottom, element 30 is located at hull side close to neutral axis and element 60 is located at the deck.

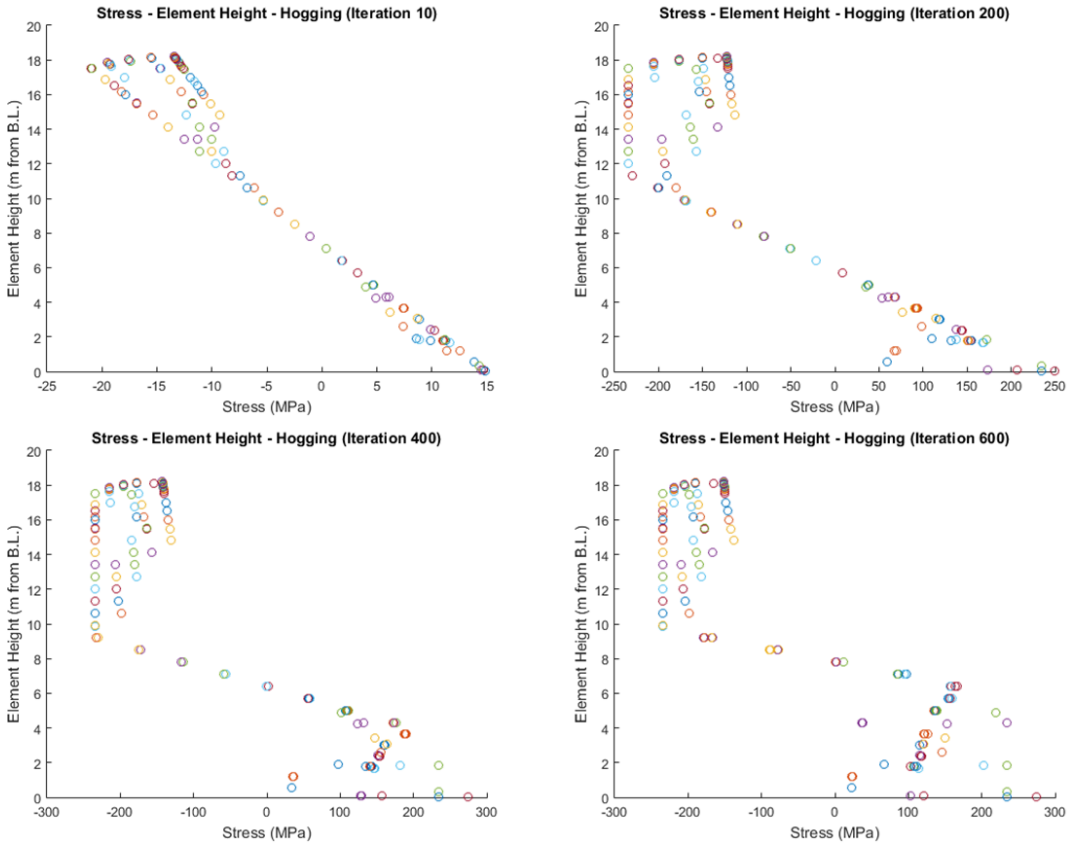

Figure 139: Element stresses relative to element height at different iterations of hogging condition

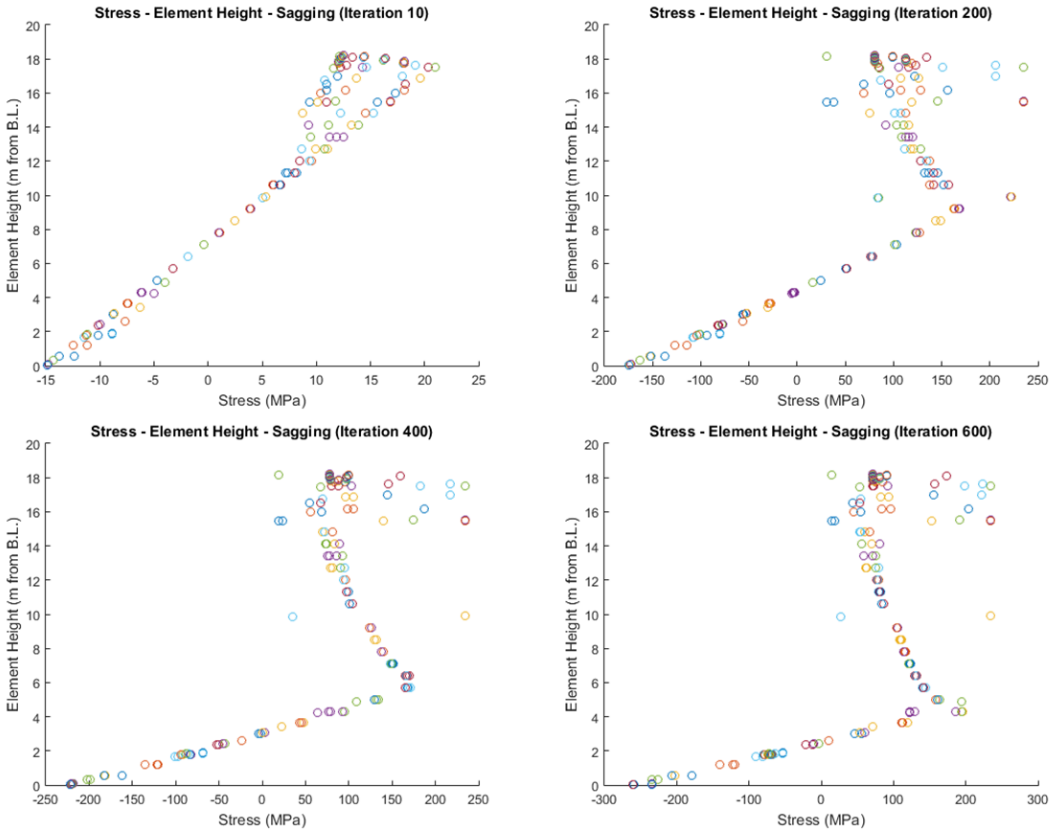

Figure 140: Element stresses relative to element height at different iterations of sagging condition

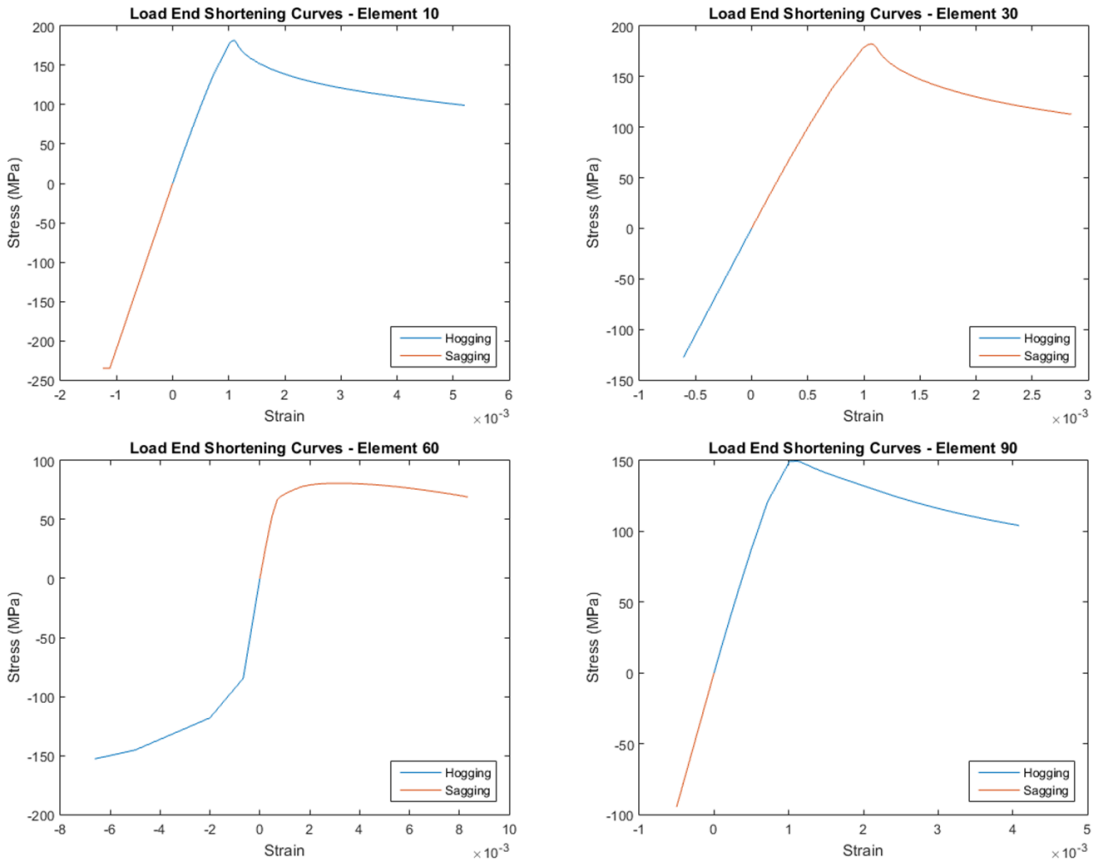

Figure 141: Load end shortening curves at hogging and sagging conditions for elements 10, 30, 60 and 90

Chapter 8: Discussion

8.1 Comparisons

In this section comparisons between the results of the examined will be presented. A brief description of the examined methods is worth mentioned for the better comprehension of the results comparison. In the present study three methods were employed for the observation of the ultimate strength of a chemical/ product oil carrier hull girder at intact and elevated temperature conditions. Intact condition refers to the undamaged hull girder state. At intact condition hull girder's temperature is equal to the ambient temperature (20°C). Elevated temperature state refers to the condition in which specific hull girder area's temperature is different from the ambient temperature (20°C) and there is no damage at the hull girder structure. As it has been mentioned before (section 5.8), the maximum temperature of the examined hull girder was 500°C and the minimum was 20°C. Material's mechanical properties change with the temperature increase and this result's to a different ultimate strength of a hull girder between intact condition and elevated temperature condition. For intact condition Smith and NLFEA (ABAQUS) methods were used while for elevated temperature condition a proposed modified Smith and NLFEA (ABAQUS) methods were used.

Figure 142 shows a comparison between Smith and modified Smith methods. As it has been mentioned before, Smith method was used for the estimation of the bending moment capacity in intact condition, while modified Smith method was used for the elevated temperature condition. According to the results, Smith method presents greater ultimate bending moment for hogging and sagging conditions than the modified Smith method for equivalent conditions. Table 20 presents the ultimate bending moment for hogging and sagging condition estimated by the two methods.

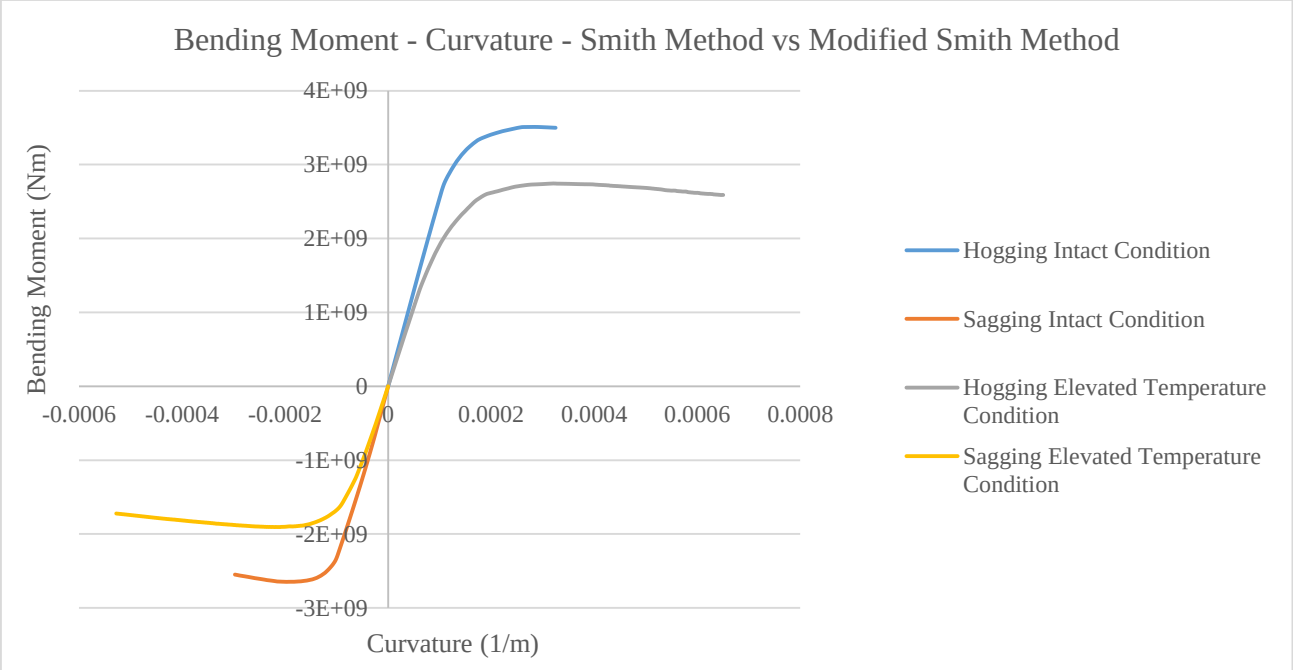

Figure 142: Bending moment versus curvature comparison between Smith method and modified Smith method

Method	Condition	Ultimate Bending Moment (kNm)	Curvature (1/m)
Smith	Hogging	3510222.6	$2.837*10^{-4}$
	Sagging	-2647417.2	$-1.9707*10^{-4}$
Modified Smith	Hogging	2744739.2	$3.2142*10^{-4}$
	Sagging	-1905966.9	$-2.1984*10^{-4}$

Table 20: Ultimate bending moment for Smith and modified Smith methods

Figure 143 shows a comparison of ABAQUS results between intact and elevated temperature state for hogging and sagging condition. Lower ultimate bending moment is observed at elevated temperature state for hogging and sagging condition. Table 21 presents the ultimate bending moment capacity of the examined cases for hogging and sagging condition.

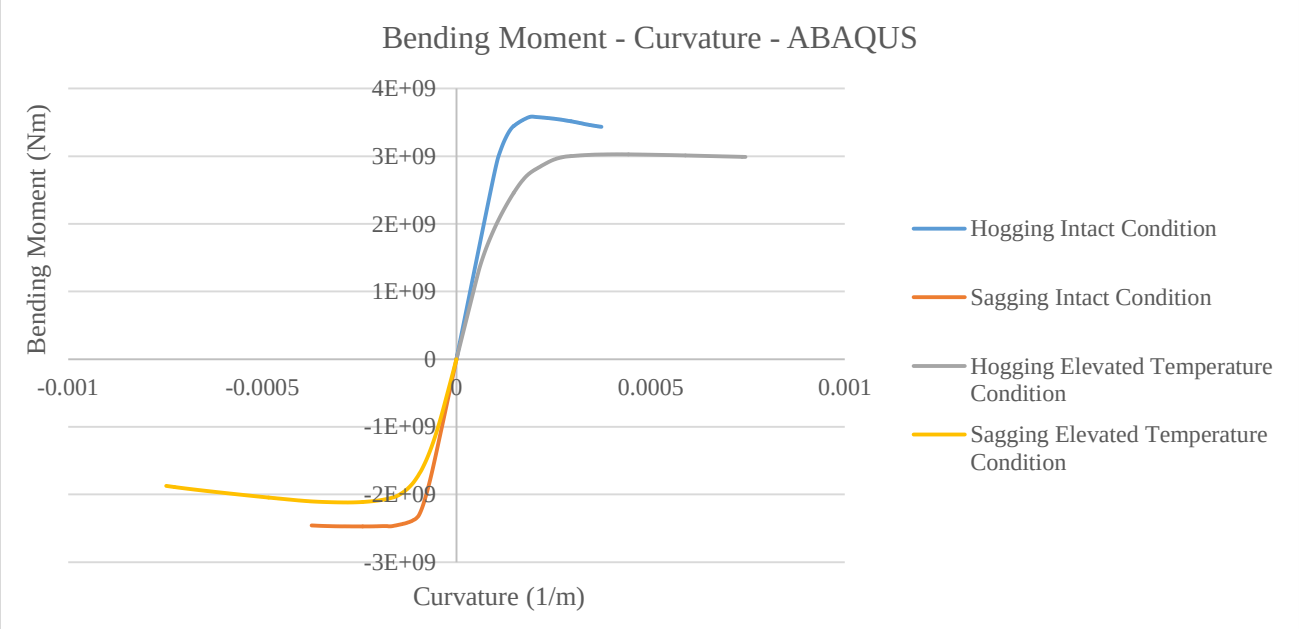

Figure 143: Bending moment versus curvature comparison between ABAQUS results of intact and elevated temperature states

Case	Condition	Ultimate Bending Moment (kNm)	Curvature (1/m)
Intact	Hogging	3586100	$1.95*10^{-4}$
	Sagging	-2472600	$-2.45*10^{-4}$
Elevated Temperature	Hogging	3028600	$4.13*10^{-4}$
	Sagging	-2118000	$-2.79*10^{-4}$

Table 21: Ultimate bending moment for ABAQUS intact and elevated temperature states

Figure 144 shows a comparison between Smith method and ABAQUS for intact condition. Regarding hogging condition, the value of ultimate bending moment obtained from ABAQUS is greater than the equivalent value computed with Smith method. Moreover, the ultimate bending moment, obtained from ABAQUS, appeared at lower curvature compared with the ultimate bending moment obtained from Smith method. At sagging condition, the value of ultimate bending moment obtained from Smith method is greater than the equivalent from ABAQUS. The ultimate bending moment, obtained from ABAQUS, appeared at greater curvature compared with the ultimate bending moment obtained from Smith method. Smith method results

satisfy the CSR – H criterion for hogging and sagging conditions (section 7.4), while ABAQUS results satisfy the CSR – H criterion for hogging condition only (section 6.1). Differences between the two methods lay on the assumptions at the implementation of the two methods. Specifically, Smith method do not take into account the interaction between the structural elements, while in NLFEA methods several computational parameters, such as mesh modelling, boundary and loading conditions, initial geometric imperfection, solution procedures etc. can affect the results accuracy and consistency.

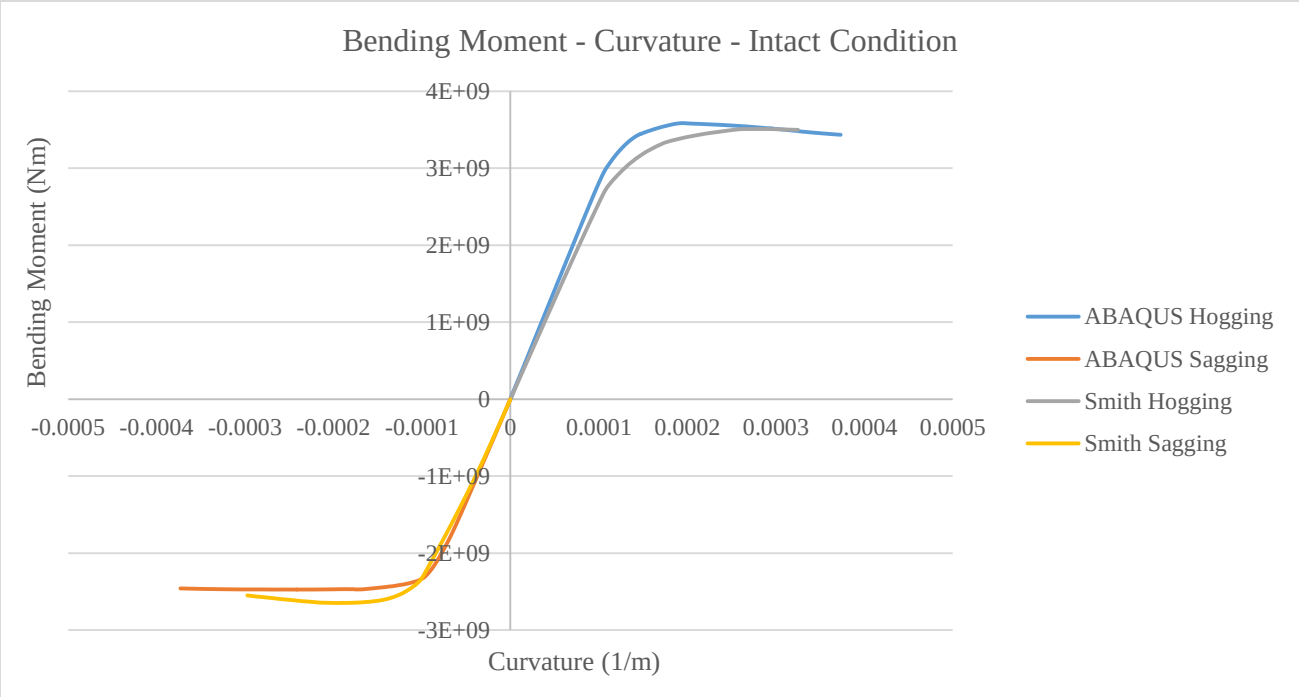

Figure 144: Bending moment versus curvature comparison between ABAQUS results of intact state and Smith method

Figure 145 shows a comparison between modified Smith method and ABAQUS for elevated temperature condition. The values of ultimate bending moment for hogging and sagging condition, obtained from ABAQUS, are greater than the corresponding values obtained from modified Smith method. Furthermore, the ultimate bending moment for hogging and sagging condition, obtained from ABAQUS, appeared at greater curvature compared with the equivalent ultimate bending moments obtained from Smith method. Modified Smith method results do not satisfy the CSR – H criterion (section 7.5), while ABAQUS results satisfy CSR – H criterion for hogging condition only (section 6.2). Differences between the two methods lay on the assumptions at the implementation of the two methods. Specifically, the proposed modified Smith method do not take into account the interaction between the structural elements and temperature rounding has been performed for element's temperature. In NLFEA methods several computational parameters, such as mesh modelling, boundary and loading conditions, initial geometric imperfection, solution procedures etc. can affect the results accuracy and consistency.

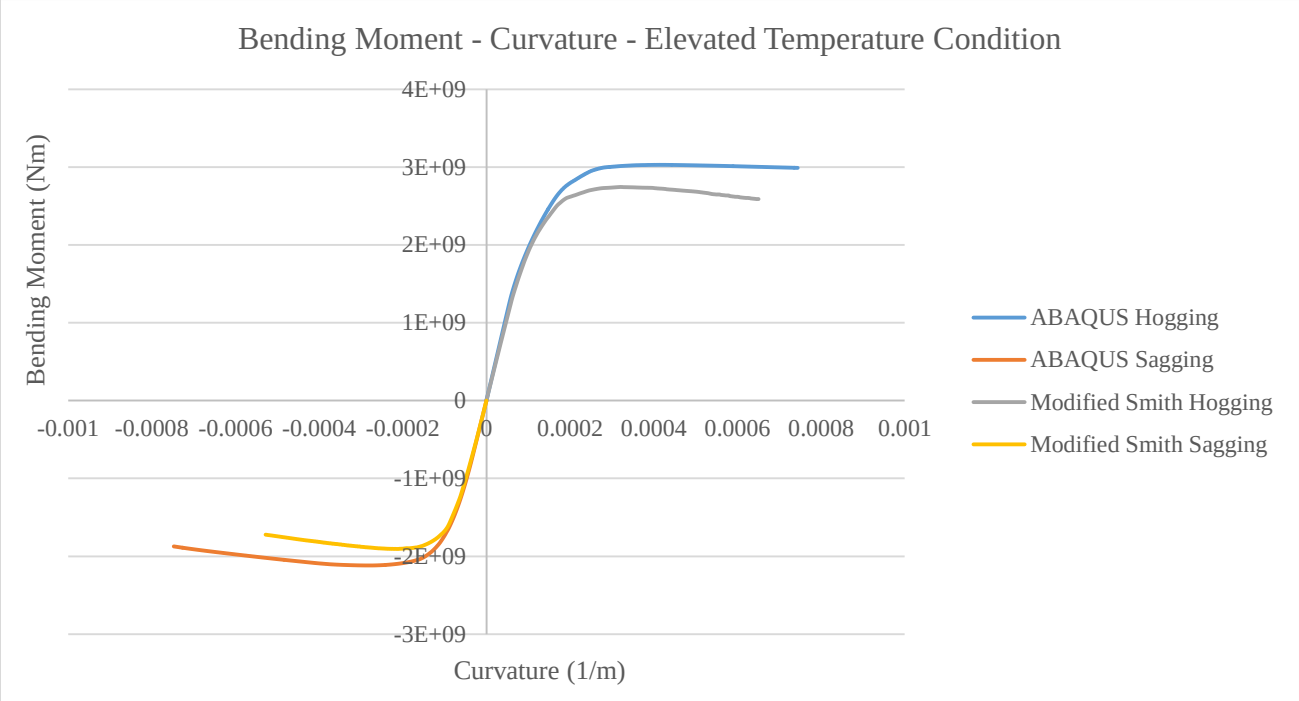

Figure 145: Bending moment versus curvature comparison between ABAQUS results of elevated temperature state and modified Smith method

8.2 Conclusions

The aim of the present study has been to evaluate the ultimate bending moment capacity of a chemical/ oil product carrier at intact and elevated temperature conditions, using nonlinear finite element analysis, Smith method and a proposed modified Smith method. Intact condition refers to the undamaged hull girder state at ambient temperature, while elevated temperature condition refers to the undamaged hull girder state at greater temperature than the ambient temperature. As it has been presented before (sections 6.1, 6.2, 7.4 and 7.5) the results from the examined methods were evaluated with CSR – H criterion. CSR – H criterion is generally used to evaluate the results from methods used for the ultimate hull girder strength assessment at intact condition and damaged condition (section 2.2) ignoring temperature effects on the material properties and structural response. CSR – H criterion was used also for the elevated temperature condition's results evaluation.

The bending moment capacity versus curvature curves of the above examined methods (Smith, Modified Smith and ABAQUS), at equivalent conditions, are very similar. In particular, for hogging and sagging conditions, they initially present a steady increase in the bending moment values with the increase of curvature with steady inclination value close to the value of $E * I_y$ followed by a decrease in the inclination. After reaching the maximum value of the bending moment capacity the curves present a decrease in bending moment values with the increasing curvature. Smith method presents lower ultimate bending moment for hogging condition and greater for sagging condition compared to ABAQUS corresponding results. Modified Smith method presents lower ultimate bending moment for hogging and sagging conditions compared to ABAQUS corresponding results. Finite element modelling parameters such as boundary and loading conditions,

shape and magnitude of initial geometric imperfections, model geometric range and analysis method etc., but also the assumptions of the examined methods lead to the differences between the examined methods (section 8.1). Differences obtained between ABAQUS and Modified Smith method are due to the finite element modelling parameters, such as boundary and loading conditions, shape and magnitude of initial imperfections, model geometric range and analysis method etc., for ABAQUS and the implementation of the Modified Smith method (section 7.2). Moreover, the implementation of rounding at the structural element temperature's values on the Modified Smith method can lead to significant differences between the two examined methods.

The differences in the ultimate capacity of the hull girded according to the numerical simulations on one hand and the Smith/ modified Smith on the other, influence the assessment of the ultimate capacity of the hull versus the demand as required by CSR – H. In particular:

- According to ABAQUS results for intact ship state, it was obtained that the CSR – H criterion is satisfied for hogging condition only. Finite element parameters and the age of the subject ship design are the main reasons related to the lack of CSR – H criterion satisfaction for sagging conditions. For sagging condition the margin of the compared bending moment values is significant small.
- ABAQUS results of ultimate bending moment capacity at elevated temperatures satisfy the CSR – H criterion for hogging condition only. The margin of the compared bending moment values is significant small.
- Smith method results for ultimate bending moment capacity satisfy the CSR – H criterion. Smith method was used in case of intact ship. For hogging condition the margin between the compared ultimate bending moment values from Smith method and CSR – H criterion is significant large.
- Modified Smith method results for ultimate bending moment capacity does not satisfy the CSR – H criterion. The proposed modified Smith method was used in case of elevated temperature condition. For hogging condition the margin between the compared ultimate bending moment values from modified Smith method and CSR – H criterion is relative small while for sagging condition the equivalent margin is significant large.
- The examined thermal scenario lead to lack of satisfaction of the CSR – H criterion. This means that the examination of greater temperatures with the same thermal boundary conditions topology will lead to the same results.
- With the proposed modified Smith method, it is possible to determine the maximum temperature for which the hull girder satisfies the CSR – H criterion.

Except from the above principal results of the study, some useful and worth mentioned observations have been made during the finite element modelling. It was observed that for greater than 1000 seconds analysis time, heat transfer phenomena can be neglected, while for smaller analysis time heat transfer phenomena are significant. More specifically, Static General step and Coupled Temperature – Displacement step presents the same results for greater analysis time. Static General step solves steady states of mechanical loading with specific temperature. Boundary conditions can affect the structural response under the thermal loading.

Moreover, initial deflections characteristics can affect the ultimate strength of the structure. Mesh size mainly affects post buckling response of the structure. Finally, it was obtained that solution procedures are strongly related not only to the results accuracy and consistency but also to the solution stability.

8.3 Future Work

The present study was carried out with taking into account some assumptions. The assumptions were made due to lack in literature for related studies on ultimate hull girder strength at elevated temperature condition. Future works should be based on the following proposals, in order to realistic describe the bending moment capacity of a hull girder subjected to elevated temperatures. The present study pointed out the need of a realistic thermal scenario, which will represent temperatures and heat fluxes from a ship fire incident. The extensive literature research, carried out in the present study, was unable to come up with a realistic fire/thermal scenario. Except from the fire/thermal scenario, the examination of temperature profiles with different thermal boundary conditions is also proposed. In addition to that, fire modelling is proposed using commercial CFD packages such us Fire Dynamic Simulator (FDS), Kameleon FireEx (KFX), OpenFOAM and ANSYS CFX/Fluent. A common problem in the above CFD programs is the modelling of large scale fires (pool fires), but for small scale fires the results lead to good approximation of the physical problem. Moreover, studies with Thermal Fluid Structure Interaction (TFSI) have been carried out (section 1.2). ABAQUS co – simulation does not support displacement exchange through the codes (FEM, CFD) for 2 – way TFSI. So an external script for displacement exchange between the codes is needed. 1 – way TFSI could be also realistic in case of relative small displacements.

Regarding nonlinear finite element analysis further examination of boundary and loading conditions and of model geometric range is proposed. Also, material characteristics and constitutive model is an important parameter in nonlinear finite element analysis. The assumption of material behavior as elastic – perfectly plastic or with the stress – strain curves proposed by Eurocode is far from the actual material's behavior. The hardening phenomenon influence the post buckling behavior of a structure, as it has been shown by [24]. Except from the use of hardening phenomenon, the use of Johnson – Cook constitutive model is also proposed. Several studies have attempt to evaluate the Johnson – Cook model's parameters at elevated temperatures for mild steel or high tensile steel [61–64]. It was observed that Johnson – Cook model presents reliable results when is used closed to reference temperature. For smaller or greater temperatures than reference temperature, there is a significant difference between the Johnson – Cook and experimental results. This implies the necessity of experiments at interested temperatures for material properties characterization. Moreover, initial imperfections shape and size has to be further examined as is not clear yet how they affect the buckling capacity. In addition to that, a crucial parameter in ultimate compressive strength of ship shaped structures are the residual stresses from the welding procedures, which usually neglected from the finite element simulations. The way of influence of residual stresses on the ultimate strength is also proposed for examination.

As it has been mention before the proposed methodology for the modified Smith method can be used for the estimation of the ultimate bending moment capacity of a hull girder subjected to elevated temperatures. The proposed method was significantly time consuming. Therefore, the development of analytical formulas for load – end shortening curves at elevated temperatures is proposed. Finally, experimental results are needed in order to evaluate and compare the results obtained from Smith method, modified Smith method and ABAQUS nonlinear analysis.

Bibliography

[1] Allianz Global Corporate & Specialty. SAFETY AND SHIPPING REVIEW 2018, An annual review of trends and developments in shipping losses and safety. 2018.

[2] Baalisampang T, Abbassi R, Garaniya V, Khan F. Review and analysis of fire and explosion accidents in maritime transportation. Ocean Eng 2018;158:350–66. doi:10.1016/j.oceaneng.2018.04.022.

[3] Kim JH, Kim DC, Kim CK, Islam MS, Paik JK. NONLINEAR STRUCTURAL CONSEQUENCE ANALYSIS OF FPSO TOPSIDES. 31st Int. Conf. Ocean. Offshore Arct. Eng., OMAE; 2016, p. 1–10.

[4] Lien KH, Chiou YJ, Wang RZ, Hsiao PA. Nonlinear behavior of steel structures considering the cooling phase of a fire. J Constr Steel Res 2009;65:1776–86. doi:10.1016/j.jcsr.2009.03.015.

[5] Gillie M. Analysis of heated structures : Nature and modelling benchmarks. Fire Saf J 2009;44:673–80. doi:10.1016/j.firesaf.2009.01.003.

[6] Soares CG, Teixeira AP. Strength of plates subjected to localised heat loads. J Constr Steel Res 2000;53:335–58.

[7] Sohn JM, Kim SJ, Kim BH, Islam CK, Paik JK, Katsaounis GM, et al. COMPUTATIONAL MODELLING OF INTERACTION BETWEEN CFD AND FEA SIMULATIONS UNDER GAS EXPLOSION LOADS. Dev Fixed Float Offshore Struct 2012:23–4.

[8] Kim JH, Kim DC, Kim CK, Islam MS, Paik JK, Katsaounis GM, et al. DEVELOPMENT OF AN INTERFACE PROGRAM FOR THE INTERACTION BETWEEN ACTIONS AND ACTION EFFECTS OF STEEL STRUCTURES SUBJECT TO FIRE. Dev Fixed Float Offshore Struct 2012:23–4.

[9] Katsaounis GM, Katsourinis D, Samuelides MS, Founti M, Paik JK, Kim BJ. COMPUTATIONAL MODELING OF INTERACTION BETWEEN ACTIONS AND ACTION EFFECTS OF FPSO TOPSIDE STRUCTURES SUBJECT TO JET FIRE. Int. Conf. Ocean. Offshore, Arct. Eng., OMAE; 2010, p. 1–8.

[10] Jin S, Lee J, Hwan S, Kwan J, Ju B, Chul Y, et al. Nonlinear structural response in jet fire in association with the interaction between fire loads and time-variant geometry and material properties. Ocean Eng 2017;144:118–34. doi:10.1016/j.oceaneng.2017.08.028.

[11] Hofmeyer IH, Feenstra IJA, Herpen IRAP, Mahendram M. Automated two-way CFD fire-FEM thermo-mechanical coupling for global modelling of building structures under fire. n.d.

[12] Paajanen A, Hostikka S, Matala A, Gutkin R. CFD-FEA SIMULATION FRAMEWORK FOR COMPOSITE STRUCTURES IN FIRE. 16TH Eur. Conf. Compos. Mater., ECCM; 2014.

[13] Malendowski M, Glema A. Development and Implementation of Coupling Method for CFD-FEM Analyses of Steel Structures in Natural Fire. Procedia Eng 2017;172:692–700. doi:10.1016/j.proeng.2017.02.082.

[14] Nariman NA. Thermal fluid-structure interaction and coupled thermal- stress analysis in a cable stayed bridge exposed to fire. Front Struct Civ Eng 2018:1–20.

[15] Kang HJ, Choi J, Lee D, Park BJ. A framework for using computational fire simulations in early phases of ship design. Ocean Eng 2017;129:335–42. doi:10.1016/j.oceaneng.2016.11.018.

[16] Hulin T, Karatzas V, Mindykowski P, Jomaas G, Berggreen C, Lauridsen D, et al. Experimental assessment of the robustness in fire of lightweight ship bulkheads. Mar Struct 2019;64:161–73. doi:10.1016/j.marstruc.2018.11.005.

[17] Hakkarainen T, Hietaniemi J, Hostikka S, Karhula T, Kling T, Mangs J, et al. Survivability for ships in case of fire Final report of SURSHIP-FIRE project. 2009.

[18] Paik JK, Kim BJ, Seo JK. Methods for ultimate limit state assessment of ships and ship-shaped offshore structures : Part I — Unstiffened plates 2008;35:261–70. doi:10.1016/j.oceaneng.2007.08.004.

[19] Paik JK, Kim BJ, Seo JK. Methods for ultimate limit state assessment of ships and ship-shaped offshore structures : Part II stiffened panels 2008;35:271–80. doi:10.1016/j.oceaneng.2007.08.004.

[20] Paik JK, Kim BJ, Seo JK. Methods for ultimate limit state assessment of ships and ship-shaped offshore structures : Part III hull girders 2008;35:281–6. doi:10.1016/j.oceaneng.2007.08.008.

[21] Jose Manuel Gordo. Effect of Initial Imperfections on the Strength of Restrained Plates. J Offshore Mech

Arct Eng 2015. doi:10.1115/1.4030927.
[22] Soares CG, Parunov J. Advanced Ship Design for Pollution Prevention. Taylor & Francis Group; 2009.
[23] Soares CG, Santos TA. Maritime Technology and Engineering. Taylor & Francis Group; 2015.
[24] Branner K, Czujko J, Fujikubo M. " Committee III . 1 - Ultimate Strength ", Proceedings of the 17th International Ship and Offshore Structures Congress (ISSC), 2009.
[25] Cai M, Jun Z, Pan J. Study on influence of nonlinear finite element method models on ultimate bending moment for hull girder. Thin-Walled Struct 2017;119:282–95.
[26] Mohammed EA, Benson SD, Hirdaris SE, Dow RS. Design safety margin of a 10 , 000 TEU container ship through ultimate hull girder load combination analysis. Mar Struct 2016;46:78–101. doi:10.1016/j.marstruc.2015.12.003.
[27] Estefen SF, Chujutalli JH, Soares CG. Influence of geometric imperfections on the ultimate strength of the double bottom of a Suezmax tanker. Eng Struct 2016;127:287–303. doi:10.1016/j.engstruct.2016.08.036.
[28] Δημήτριος Ι. Μέγιστη Αντοχή Bulk Carrier σε Άθικτη και Βεβλαμμένη Κατάσταση. NTUA, 2017.
[29] Πολλάλης Χ. Προσομοίωση πειραμάτων προσδιορισμού μέγιστης αντοχής με τη χρήση του κώδικα Abaqus Implicit. NTUA, 2012.
[30] Hughes OF., Paik JK, Béghin D, Caldwell JB, Payer HG, Schellin TE. SHIP STRUCTURAL ANALYSIS AND DESIGN. SNAME; 2010.
[31] Σαμουηλίδης Μ. Αντοχή Πλοίου. Εθνικό Μετσόβιο Πολυτεχνείο; 2010.
[32] IACS. Common Structural Rules for Bulk Carriers and Oil Tankers. 2017.
[33] Chandrupatla T, Belegundu A. Introduction to Finite Elements in Engineering. Third. Prentice Hall Inc.; 2002.
[34] Σαραβάνος Δ. Εισαγωγή στην Μέθοδο των Πεπερασμένων Στοιχείων, Πανεπιστημιακές Παραδόσεις. Πάτρα: 2008.
[35] Systemes D. Abaqus Documentation 6.13 n.d. http://dsk.ippt.pan.pl/docs/abaqus/v6.13/index.html.
[36] Bathe KJ 1996. K.-J. - Finite Element Procedures - 1996 - Prentice-Hall - ISBN 0133014584 - 1052s.pdf. 1996.
[37] Τσαμασφύρος Γ, Θεοτόκογλου Ε. Μέθοδος των Πεπερασμένων Στοιχείων Ι. Αθήνα: Συμμετρία; 2005.
[38] Τσαμασφύρος Γ, Θεοτόκογλου Ε. Μέθοδος των Πεπερασμένων Στοιχείων ΙΙ. Αθήνα: Συμμετρία; 2005.
[39] Vasios N. Nonlinear Analysis of Structures. Harvard, 2015.
[40] Systemes D. Abaqus 6.14 Documentation. Http://AbaqusSoftwarePolimiIt/v614/IndexHtml 2014.
[41] Sun EQ. Shear Locking and Hourglassing in MSC Nastran , ABAQUS , and ANSYS Shear Locking. n.d.
[42] Παντελάκης Σ, Τσερπές Κ. Μηχανική Συμπεριφορά Υλικών. Εκδόσεις Τζίολα; 2016.
[43] Kelly P. Mechanics Lecture Notes: An introduction to Solid Mechanics. Auckland: 2012.
[44] Κερμανίδης Θ. Αντοχή Υλικών, Τόμος 2. Πάτρα: Πανεπιστήμιο Πατρών; 2009.
[45] Κερμανίδης Θ. Αντοχή Υλικών, Τόμος 1. Πάτρα: Πανεπιστήμιο Πατρών; 2009.
[46] Beer F, Johnston R, DeWolf J, Mazurek D. Mechanics of Materials. Sixth. Mc Graw - Hill; 2012.
[47] Stamatelos DG, Labeas GN, Tserpes KI. Analytical calculation of local buckling and post-buckling behavior of isotropic and orthotropic stiffened panels. Thin Walled Struct 2011;49:422–30. doi:10.1016/j.tws.2010.11.008.
[48] Yao T, Fujikubo M. Buckling and Ultimate Strength of Ship and Ship-like Floating Structures. Elsevier Ltd; 2016.
[49] Timoshenko SP, Gere JM. Theory of Elastic Stability. McGraw - Hill; 1963.
[50] Cengel YA. HEAT TRANSFER, A Practical Approach. Second. McGraw - Hill; 2002.
[51] Ebbing DD, Gammon SD. General Chemistry. Ninth. Houghton Mifflin Company; 2009.
[52] Glassman I, Yetter R. Combustion. Fourth. Elsevier Ltd; 2008.
[53] Engineering ToolBox 2001. https://www.engineeringtoolbox.com/.
[54] Steinhaus T, Welch S, Carvel RO, Torero JL. LARGE-SCALE POOL FIRES. Therm Sci 2007;11:101–

18. doi:10.2298/TSCI0702101S.

[55] DiNenno PJ, Beyler CL, Drysdale D, Walton WD, Custer RLP, Hall JR, et al. SFPE Handbook of Fire Protection Engineering. National Fire Protection Association; 2002.

[56] Shokri M, Beyler CL. Radiation from Large Pool Fires. J Fire Prot Eng 1989;1. doi:10.1177/104239158900100404.

[57] Babrauskas V. Estimating Large Pool Fire Burning Rates. Fire Technol 1983;19:251–61.

[58] U S Nuclear Regulatory. Fire Dynamics Tools, Quantitative Fire Hazard Analysis Methods for the. 2004.

[59] Kim DK, Kim HB, Zhang X, Li CG, Paik JK. Ultimate strength performance of tankers associated with industry corrosion addition practices. Int J Nav Archit Ocean Eng 2014;6:507–28. doi:10.2478/IJNAOE-2013-0196.

[60] European Committee for Standardization. Eurocode 3: Design of steel structures. 2005.

[61] Ying H, Feng X, Ying J, Jiao J. A modified Johnson Cook model for elevated temperature flow behavior of T24 steel. Mater Sci Eng A 2013;577:138–46. doi:10.1016/j.msea.2013.04.041.

[62] Lin YC, Chen X, Liu G. A modified Johnson – Cook model for tensile behaviors of typical high-strength alloy steel. Mater Sci Eng A 2010;527:6980–6. doi:10.1016/j.msea.2010.07.061.

[63] He J, Chen F, Wang B, Bei L. A modified Johnson-Cook model for 10 % Cr steel at elevated temperatures and a wide range of strain rates. Mater Sci Eng A 2018;715:1–9. doi:10.1016/j.msea.2017.10.037.

[64] Iqbal MA, Senthil K, Bhargava P, Gupta NK. The characterization and ballistic evaluation of mild steel. Int J Impact Eng 2015;78:98–113. doi:10.1016/j.ijimpeng.2014.12.006.

[65] European Committee for Standardization. Eurocode 1: Actions on structures. vol. 2. 2002.

[66] Promat International N.V. Promat Fire curves 2019. https://www.promat-tunnel.com/en/advices/fire-protection/fire curves.

Appendix A: Material Properties

To evaluate the thermal and structural response analyses of structures due to fire, the involved properties must be known. The material thermal and mechanical properties of carbon steel are stated in EN 1993 – 1 – 2 [60]. Thermal properties such as specific heat, thermal conductivity and thermal elongation are important parameters in a thermal response analysis. Generally, the mechanical properties of steel, such as strength and stiffness, in relation to increasing temperature decreases.

A.1 Thermal Properties

The specific heat of carbon steel C_a (J/kgK) should be determined from the following equations (74). Figure 147 illustrates the variations of the specific heat with temperature.

$$C_a = \begin{cases} 425 + 7.73 * 10^{-1}\theta_\alpha - 1{,}69 * 10^{-3}\theta_\alpha + 2{,}22 * 10^{-6}\theta_\alpha, (20°C \leq \theta_\alpha < 600°C) \\ 666 + \dfrac{13002}{738 - \theta_\alpha}, (600°C \leq \theta_\alpha < 735°C) \\ 545 + \dfrac{17820}{\theta_\alpha - 731}, (735°C \leq \theta_\alpha < 900°C) \\ 650, (900°C \leq \theta_\alpha < 1200°C) \end{cases} \quad (74)$$

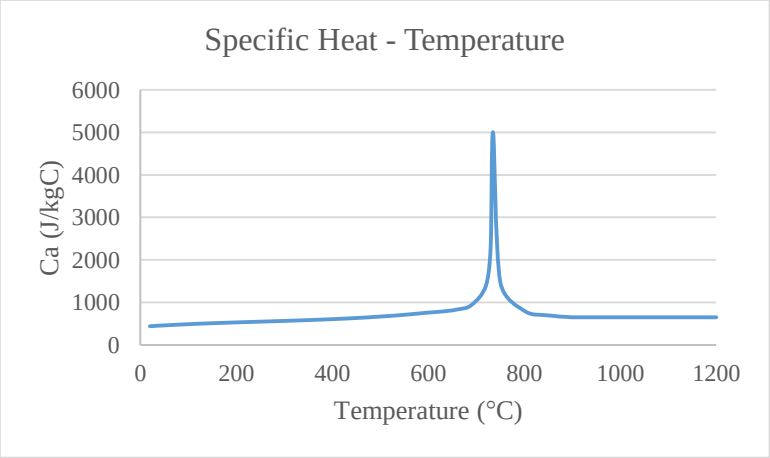

Figure 146: Specific heat – temperature

The thermal conductivity of carbon steel λ_a (W/mK) should be determined from the following equations (75). Figure 148 illustrates the variations of thermal conductivity with temperature.

$$\lambda_a = \begin{cases} 54 - 3.33 * 10^{-2}\theta_\alpha, (20°C \leq \theta_\alpha < 800°C) \\ 27.3, (800°C \leq \theta_\alpha < 1200°C) \end{cases} \quad (75)$$

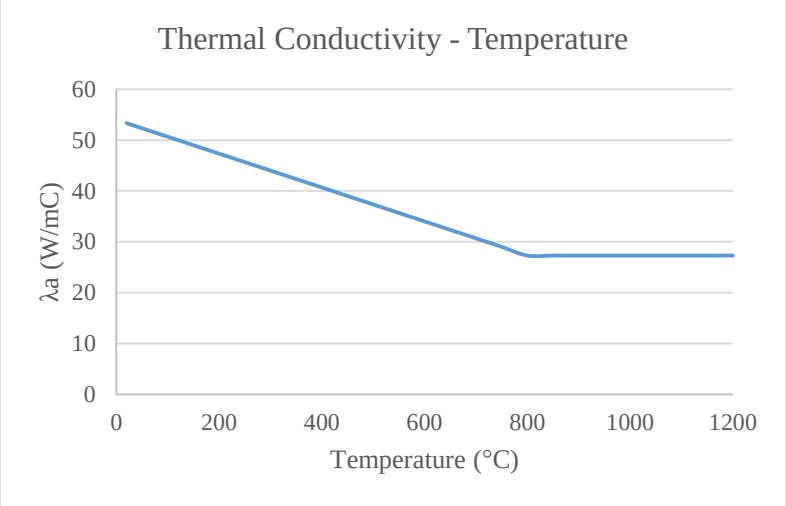

Figure 147: Thermal conductivity – temperature

The thermal elongation of carbon steel Δl/l should be determined from the following equations (76). Figure 149 illustrates the variations of thermal elongation with temperature.

$$\frac{\Delta l}{l} = \begin{Bmatrix} 1.2 * 10^{-5}\theta_\alpha + 0.4 * 10^{-8}\theta_\alpha^2 - 2.419 * 10^{-4}, (20°C \leq \theta_\alpha < 750°C) \\ 1.1 * 10^{-2}, (750°C \leq \theta_\alpha < 860°C) \\ 2 * 10^{-5}\theta_\alpha - 6.2 * 10^{-3}, (860°C \leq \theta_\alpha < 1200°C) \end{Bmatrix} \quad (76)$$

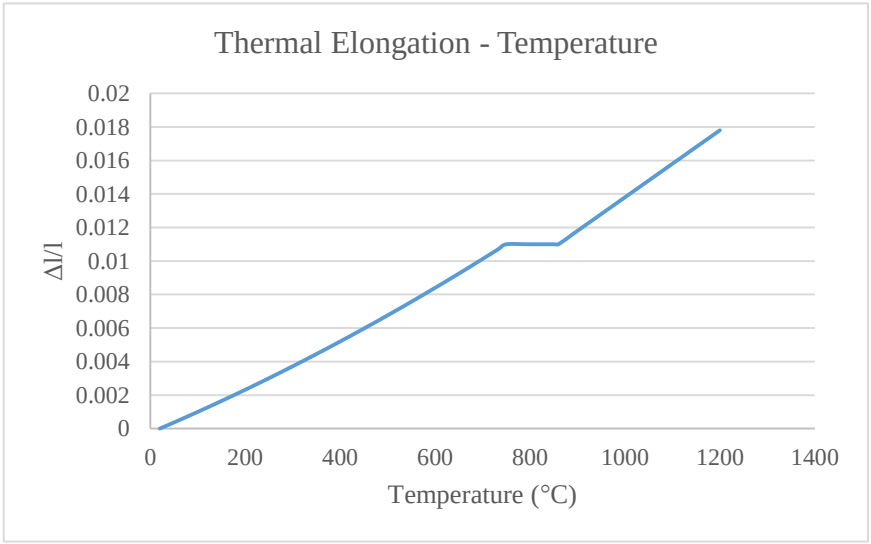

Figure 148: Thermal elongation – temperature

A.2 Mechanical Properties

The yield stress and elastic modulus of carbon steel at ambient temperature is 330 MPa and 210 GPa, respectively. Elevated temperatures on steel structures results in a decrease in Young's modulus, yield stress and proportional limit as mentioned before. The unit mass of steel ρ_a may be considered to be independent of steel temperature and the value is equal to 7850 kg/m^3. For heating rates between 2 and 50 K/min, the stress – strain relationship is given by Figure 150 and the reduction factors for the stress – strain relationship for steel are given by Figure 151 [60].

Strain range	Stress σ	Tangent modulus
$\varepsilon \le \varepsilon_{p,\theta}$	$\varepsilon E_{a,\theta}$	$E_{a,\theta}$
$\varepsilon_{p,\theta} < \varepsilon < \varepsilon_{y,\theta}$	$f_{p,\theta} - c + (b/a)\left[a^2 - (\varepsilon_{y,\theta} - \varepsilon)^2\right]^{0,5}$	$\frac{b(\varepsilon_{y,\theta} - \varepsilon)}{a\left[a^2 - (\varepsilon_{y,\theta} - \varepsilon)^2\right]^{0,5}}$
$\varepsilon_{y,\theta} \le \varepsilon \le \varepsilon_{t,\theta}$	$f_{y,\theta}$	0
$\varepsilon_{t,\theta} < \varepsilon < \varepsilon_{u,\theta}$	$f_{y,\theta}\left[1 - (\varepsilon - \varepsilon_{t,\theta})/(\varepsilon_{u,\theta} - \varepsilon_{t,\theta})\right]$	-
$\varepsilon = \varepsilon_{u,\theta}$	0,00	-
Parameters	$\varepsilon_{p,\theta} = f_{p,\theta}/E_{a,\theta}$ $\varepsilon_{y,\theta} = 0,02$	$\varepsilon_{t,\theta} = 0,15$ $\varepsilon_{u,\theta} = 0,20$
Functions	$a^2 = (\varepsilon_{y,\theta} - \varepsilon_{p,\theta})(\varepsilon_{y,\theta} - \varepsilon_{p,\theta} + c/E_{a,\theta})$ $b^2 = c(\varepsilon_{y,\theta} - \varepsilon_{p,\theta})E_{a,\theta} + c^2$ $c = \frac{(f_{y,\theta} - f_{p,\theta})^2}{(\varepsilon_{y,\theta} - \varepsilon_{p,\theta})E_{a,\theta} - 2(f_{y,\theta} - f_{p,\theta})}$	

Figure 149: Stress – strain relationship at elevated temperature [60]

Steel Temperature θ_a	Reduction factors at temperature θ_a relative to the value of f_y or E_a at 20°C		
	Reduction factor (relative to f_y) for effective yield strength $k_{y,\theta} = f_{y,\theta}/f_y$	Reduction factor (relative to f_y) for proportional limit $k_{p,\theta} = f_{p,\theta}/f_y$	Reduction factor (relative to E_a) for the slope of the linear elastic range $k_{E,\theta} = E_{a,\theta}/E_a$
20°C	1,000	1,000	1,000
100°C	1,000	1,000	1,000
200°C	1,000	0,807	0,900
300°C	1,000	0,613	0,800
400°C	1,000	0,420	0,700
500°C	0,780	0,360	0,600
600°C	0,470	0,180	0,310
700°C	0,230	0,075	0,130
800°C	0,110	0,050	0,090
900°C	0,060	0,0375	0,0675
1000°C	0,040	0,0250	0,0450
1100°C	0,020	0,0125	0,0225
1200°C	0,000	0,0000	0,0000
NOTE: For intermediate values of the steel temperature, linear interpolation may be used.			

Figure 150: Reduction factor at elevated temperatures [60]

Using the above relationships and reduction factors the stress – strain diagram for carbon steel, at elevated temperatures, can be generated (Figure 152). The figure shows the relationship until the strain reaches yield strain value. The above modelling method does not include material hardening and can be referred as engineering stress – strain relationships. The material's plasticity model is called elastic – perfectly plastic.

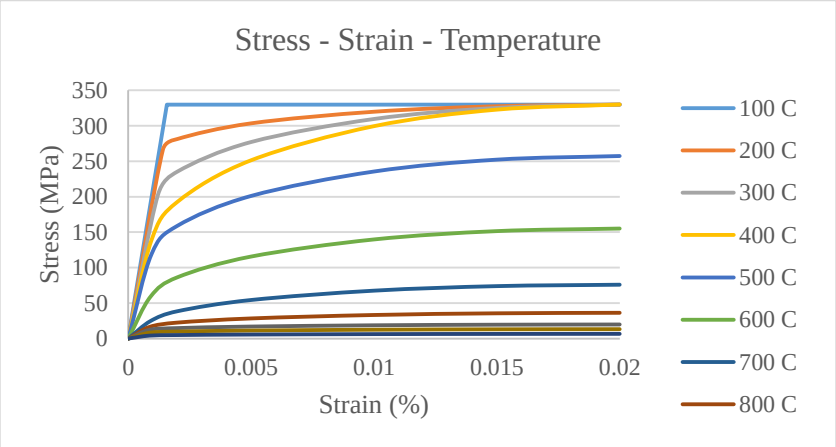

Figure 151: Stress – strain diagram at elevated temperatures

Appendix B: Temperature Profiles

EN 1991 – 1 – 2 [65] presents temperature profiles for fire modelling related to nominal and physically based thermal actions. The methods given by EN 1991 – 1 – 2 are applicable to buildings, with fire load related to the building and its occupancy. EN 1991 – 1 – 2 presents three nominal temperature – time curves, the standard temperature – time curve, the external fire curve and the hydrocarbon curve.

Standard (ISO 834) temperature – time curve is given by equation (77), where Θ_g is the gas temperature in the fire compartment and t is the time. The coefficient of heat transfer by convection is $a_c = 25\ W/m^2K$ [65].

$$\Theta_g = 20 + 345 * log(8 * t + 1) \quad (77)$$

External fire curve is given by equation (78),where Θ_g is the gas temperature near the member and t is the time. The coefficient of heat transfer by convection is $a_c = 25\ W/m^2K$ [65].

$$\Theta_g = 660 * (1 - 0{,}687e^{-0{,}32*t} - 0{,}313 * e^{-3{,}8*t}) + 20 \quad (78)$$

Hydrocarbon (HC) temperature – time curve is given by equation (79), where Θ_g is the gas temperature in the fire compartment and t is the time. The coefficient of heat transfer by convection is $a_c = 50\ W/m^2K$ [65].

$$\Theta_g = 1080 * (1 - 0{,}325e^{-0{,}167*t} - 0{,}675e^{-2{,}5*t}) + 20 \quad (79)$$

Figure 153 presents the three temperature – time curves which mentioned above. In recent years more temperature – time curves have been developed for better description of fire cases [66].

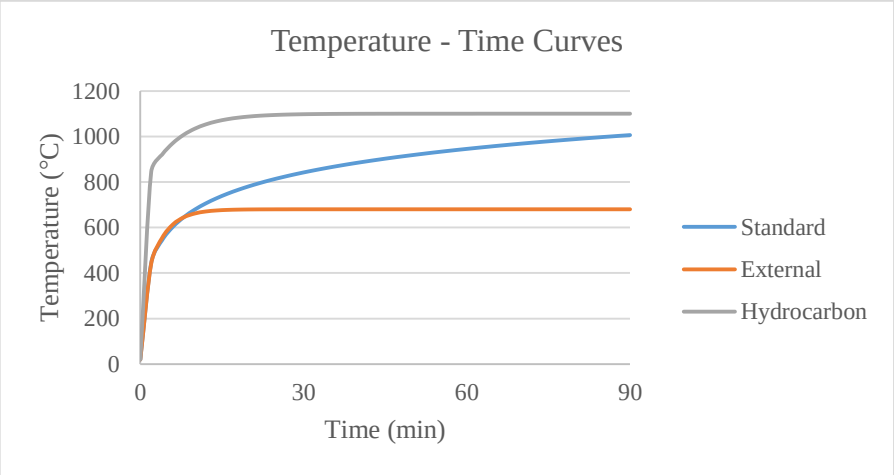

Figure 152: Temperature – time curves

Appendix C: MatLab Code for Initial Geometric Imperfections

```
%%%%% INITIAL IMPERFECTION %%%%%
%%%%% STIFFENED PLATE %%%%%
%%%%% Nodes from input file %%%%%
close all
clear all
clc
%% EXCEL DATA GLOBAL COORDINATES %%
Nodes_Data=xlsread('Point_Data');
Node_Number=Nodes_Data(:,1);
x_coors=Nodes_Data(:,2);
y_coors=Nodes_Data(:,3);
z_coors=Nodes_Data(:,4);
%% EXCEL DATA LOCAL COORDINATES %%
% Plate
PN = xlsread('Point_Data','Plate','A1:P144');    % reading data from excel
PNr=reshape(PN,[],1);                            % matrix to column
PNs=sort(PNr);                                   % sorting numbers with asceding order
PNn=PNs(~isnan(PNs));                            % deleting NaNs/zeros
PNu=unique(PNn);                                 % keeping the unique numbers
% Web
WN = xlsread('Point_Data','Web','A1:P89');       % reading data from excel
WNr=reshape(WN,[],1);                            % matrix to column
WNs=sort(WNr);                                   % sorting numbers with asceding order
WNn=WNs(~isnan(WNs));                            % deleting NaNs/zeros
WNu=unique(WNn);                                 % keeping the unique numbers
% Flange
FN = xlsread('Point_Data','Flange','A1:P35');    % reading data from excel
FNr=reshape(FN,[],1);                            % matrix to column
FNs=sort(FNr);                                   % sorting numbers with asceding order
FNn=FNs(~isnan(FNs));                            % deleting NaNs/zeros
FNu=unique(FNn);                                 % keeping the unique numbers
% Web & Flange
WFN = xlsread('Point_Data','Web_Flange','A1:P124');   % reading data from excel
WFNr=reshape(WFN,[],1);                               % matrix to column
WFNs=sort(WFNr);                                      % sorting numbers with asceding order
WFNn=WFNs(~isnan(WFNs));                              % deleting NaNs/zeros
WFNu=unique(WFNn);                                    % keeping the unique numbers
% Middle Region Nodes (Nodes to be constrained)
MR = xlsread('Point_Data','Middle_Region','A1:P3');   % reading data from excel
MRr=reshape(MR,[],1);                                 % matrix to column
MRs=sort(MRr);                                        % sorting numbers with asceding order
MRn=MRs(~isnan(MRs));                                 % deleting NaNs/zeros
MRu=unique(MRn);                                      % keeping the unique numbers
%% INPUT DATA %%
% Plate dimensions (m)
xmin = 0;
xmax = 4.3;  % a
ymin = 0;
ymax = 0.815; % b
a = xmax-xmin;
b = ymax-ymin;
hw = 0.463;
%% SOLUTION %%
% Plate applied to local plate nodes
dz_plate = zeros(length(Node_Number),1);
mp = 5;
np = 1;
wp= b/200;
for i = 1:length(PNu)
dz_plate(PNu(i)) = 1*wp*sin(mp*pi*(x_coors(PNu(i))+a/10)/a)*sin(np*pi*(y_coors(PNu(i))-
b/2)/b);
end
% Beam Column applied to global nodes
dz_beam_column = zeros(length(Node_Number),1);
```

```
woc=a/1000;
mbz = 1;
nbz = 1;
for i = 1:length(Node_Number)
dz_beam_column(i) = 1*2*woc*sin(mbz*pi*(x_coors(i)-
a/2)/a)+1*woc*sin(mbz*pi*(x_coors(i)+a/2)/a)*sin(nbz*pi*(y_coors(i))/b);
end
% Web - Flange Sideways applied to local web & flange nodes
dy_web_flange_sideways = zeros(length(Node_Number),1);
dz_web_flange_sideways = zeros(length(Node_Number),1);
wos=a/1000;
mw = 1;
for i = 1:length(WFNu)
dy_web_flange_sideways(WFNu(i)) = 1*wos/hw*sin(mw*pi*(x_coors(WFNu(i))-
a/2)/a)*(z_coors(WFNu(i)));
end
mf = 1;
for i = 1:length(FNu)
dz_web_flange_sideways(FNu(i)) =
1*wos/hw*sin(mf*pi*(x_coors(FNu(i))+a/2)/a)*((y_coors(FNu(i))-b/2)/b);
end
% Web Hollow applied to local web nodes
dy_web_hollow = zeros(length(Node_Number),1);
wow=hw/200;
mw = 5;
nw = 1;
for i = 1:length(WNu)
dy_web_hollow(WNu(i)) = 1*wow*sin(mw*pi*(x_coors(WNu(i)))/a)*sin(-
nw*pi*(z_coors(WNu(i)))/hw);
end
%% BOUNDARY CONDITION %%
% Middle Region's nodes do not have any displacement on z & y axis
for i = 1:length(MRu)
dy_web_flange_sideways(MRu(i)) = 0;
dy_web_hollow(MRu(i)) = 0;
dz_beam_column(MRu(i)) = 0;
dz_plate(MRu(i)) = 0;
dz_web_flange_sideways(MRu(i)) = 0;
end
%% FINAL COORDINATES %%
x_coors_final = x_coors;
y_coors_final = y_coors+dy_web_flange_sideways;              %   ;
z_coors_final = z_coors+dz_beam_column+dz_plate+dz_web_flange_sideways;    %
%% WRITTING TXT FILE WITH COORDINATES %%
coordinates(:,1)=Node_Number;
coordinates(:,2)=x_coors_final;
coordinates(:,3)=y_coors_final;
coordinates(:,4)=z_coors_final;
dlmwrite('Deformed_Coordinates.txt',coordinates);
%% PLOT INITIAL & DEFORMED %%
figure (1)
scatter3(x_coors,y_coors,z_coors,'filled','b')
hold on
scatter3(x_coors_final,y_coors_final,z_coors_final,'filled','r')
hold off
axis('equal')
xlabel('x')
ylabel('y')
zlabel('w')
title('Initial Deflection')
legend('Initial','Deflected','location','southeast')
```

Appendix D: MatLab Code for Load End Shortening Curves of Angle Bar Stiffener Element

```
%%%%%%%%% STIFFENER ELEMENT WITH ANGLE BAR %%%%%%%%
%%%%%%%%% LOAD END SHORRENING CURVES %%%%%%
clc
clear all
close all

%% DATA FOR ANGLE BAR (INPUTS)%%

t_p=17.5;         % (mm) Equivalent net thickness of plate
s=0.82;           % (m) Equivalent plate's width
Ap=t_p*s*10;   % (cm^2) Net area of plate
R_eHp=315;        % (MPa) Plate's yield stress
t_w=11;           % (mm) Thichness of stiffener's web
h_w=223.2;        % (mm) Height of stiffener's web
b_f=50.8;         % (mm) Width of stiffener's flange
t_f=28.4;                       % (mm) Thickness of stiffener's flange
As=(t_w*h_w+b_f*t_f)*0.01;      % (cm^2) Net area of stiffener
R_eHs=315;         % (MPa) Stiffener's yield stress
cg_s=158.1618;     % (mm) Vertical distance of stiffener's centre of gravity from its
bottom
I_stiff=2467.1054; % (cm^4) Moment of inertia through stiffeners centroid (y axis)
l=3.84;            % (m) Element length (unsupported)
A=Ap+As;          % (cm^2) Total area of element
E=205800;          % (MPa) Young's modulus

%% STRAIN VECTORS CREATION %%
strain_values=linspace(0,0.002,100); % Input
strain=strain_values;

for i=1:100
%% LOAD END SHORTENING CURVES %%

% Elasto-plastic collapse of structural element %

R_eHa=(R_eHp*Ap+R_eHs*As)/(Ap+As);     % (MPa) Equivalent minimum yield stress
strain_yield=R_eHa/E;                  % Strain at yield stress in the element
e(i)=strain(i)/strain_yield;           % Relative strain of element
    if e(i)<-1                         % Edge function
    F(i)=-1;
    elseif (e(i)>=-1) && (e(i)<=1)
    F(i)=e(i);
    else
    F(i)=1;
    end
stress(i)=F(i)*R_eHa;                  % (MPa)Stress formula

% Beam Column Buckling %

vita_e(i)=10^3*(s/t_p)*sqrt(e(i)*R_eHp/E);      % Coefficient

if vita_e(i)>1.25        % Effective width of the attached plating
b_e(i)=(2.25/vita_e(i)-1.25/vita_e(i)^2)*s;
else
b_e(i)=s;
end

if vita_e(i)>1           % Effective width corrected for relative strain of the attached
plating
b_e1(i)=s/vita_e(i);
else
```

```
b_e1(i)=s;
end

A_pEI(i)=10*b_e1(i)*t_p;     % (cm^2) Effective area
A_E1(i)=A_pEI(i)+As;         % (cm^2) Effective area of stiffeners with attached plating
A_pE(i)=10*b_e(i)*t_p;       % (cm^2) Net sectional area of attached plating of width be
A_E(i)=A_pE(i)+As;           % (cm^2) Net area of stiffeners with attached plating of width
be

l_pE(i)=(A_pEI(i)*t_p/2+As*(cg_s+t_p))/A_E1(i);     % (mm) Distance: neutral axis of the
stiffener with attached plate of width b_e1 to the bottom of the attached plate
l_sE(i)=(t_p+h_w+t_f)-l_pE(i);                      % (mm) Distance: neutral axis of the
stiffener with attached plate of width b_e1 to the top of the stiffener

I_E1(i)=1/12*(t_p/10)^3*(b_e1(i)*100)+A_pEI(i)*(t_p/20)^2+I_stiff+As*(cg_s/10+t_p/10)^2;
% (cm^4) Moment of inertia of stiffener relative to the base of plate
I_E(i)=I_E1(i)-A_E1(i)*(l_pE(i)*0.1)^2;
% (cm^4) Net moment of inertia of stiffeners with attached plating of width be1

stress_E1(i)=pi^2*E*I_E(i)*10^(-4)/(A_E(i)*l^2);                                  % (MPa)
Euler column buckling stress
R_eHB(i)=(R_eHp*A_pEI(i)*l_pE(i)+R_eHs*As*l_sE(i))/(A_pEI(i)*l_pE(i)+As*l_sE(i)); % (MPa)
Equivalne minimum yield stress of the correspoding element

if stress_E1(i)<=(R_eHB(i)/2)*e(i)       % (MPa) Critical stress
stress_C1(i)=stress_E1(i)/e(i);
else
stress_C1(i)=R_eHB(i)*(1-R_eHB(i)*e(i)/(4*stress_E1(i)));
end

stress_CR1(i)=F(i)*stress_C1(i)*(As+A_pE(i))/(As+Ap);    % (MPa) Stress formula

% Torsional Buckling %

if vita_e(i)>1.25                                        % (MPa) Buckling stress of the
attached plating
stress_CP(i)=(2.25/vita_e(i)-1.25/vita_e(i)^2)*R_eHp;
else
stress_CP(i)=R_eHp;
end

e_f=h_w+0.5*t_f;         % (mm) Distance from point C
A_w=h_w*t_w;             % (mm^2) Net web area
A_f=As*100*t_f;          % (mm^2) Net flange area
I_P=(A_w*((e_f-0.5*t_f)^2)/3+A_f*e_f^2)*10^(-4);                % (cm^4) Net polar moment
of inertia of the stiffener
I_T=((e_f-0.5*t_f)*t_w^3/(3*10^4))*(1-0.63*t_w/(e_f-0.5*t_f))+(b_f*t_f^3/(3*10^4)*(1-
0.6*t_f/b_f)); % (cm^4) Net St. Venant's moment of inertia of the stiffener
I_w=(A_f*e_f^2*b_f^2/(12*10^6))*((A_f+2.6*A_w)/(A_f+A_w));      % (cm^6) Net sectional
moment of inertia of the stiffener
epsilon=1+((l/pi)^2*10^(-3))/sqrt(I_w*(0.75*s/t_p^3+(e_f-0.5*t_f)/t_w^3));      % Degree
of fixation
stress_E2(i)=E/I_P*(epsilon*pi^2*I_w*10^2/l^2+0.385*I_T);                       % (MPa)
Euler torsional buckling

if (stress_E2(i)<=R_eHs/2*e(i))             % (MPa) Critical stress
stress_C2(i)=stress_E2(i)/e(i);
else
stress_C2(i)=R_eHs*(1-R_eHs*e(i)/(4*stress_E2(i)));
end

stress_CR2(i)=F(i)*(As*stress_C2(i)+Ap*stress_CP(i))/(As+Ap);   % (MPa) Stress formula

% Web local buckling of stiffeners made of flanged profiles %
```

```
vita_w(i)=h_w/t_w*sqrt(e(i)*R_eHs/E);           % Coefficient
if vita_w(i)>=1.25                              % (mm) Sffective heigth of the web
h_we(i)=(2.25/vita_w(i)-1.25/vita_w(i)^2)*h_w;
else
h_we(i)=h_w;
end

stress_CR3(i)=F(i)*((10^3*b_e(i)*t_p*R_eHp+(h_we(i)*t_w+b_f*t_f)*R_eHs)/(10^3*s*t_p+h_w*t_
w+b_f*t_f));   % (MPa) Stress formula
end

% Dimensionless Stress
s_sy_stress=stress/R_eHa;
s_sy_stress_CR1=stress_CR1/R_eHa;
s_sy_stress_CR2=stress_CR2/R_eHa;
s_sy_stress_CR3=stress_CR3/R_eHa;

% Row to Column
s_sy_stress_col=s_sy_stress';
s_sy_stress_CR1_col=s_sy_stress_CR1';
s_sy_stress_CR2_col=s_sy_stress_CR2';
s_sy_stress_CR3_col=s_sy_stress_CR3';
e_col=e';

stress_strain(:,1)=e_col;
stress_strain(:,2)=s_sy_stress_CR1_col;
dlmwrite('Stress_Strain.txt',stress_strain)

%% PLOTS %%

figure(1)
plot(e,s_sy_stress,'r')
hold on
plot(e,s_sy_stress_CR1,'b')
hold on
plot(e,s_sy_stress_CR2,'g')
hold on
plot(e,s_sy_stress_CR3,'k')
hold off
legend('Elastoplastic Collapse','Beam Column Buckling','Torsional Buckling','Web Local
Buckling of flanged profiles','location','southeast')
xlabel('Relative Strain')
ylabel('σ/σy')
title('Load-end shortening curve')
```

Appendix E: Spreadsheets for Smith Method

Table 1: Attached Plates

Num of Elem	t1-g	t2-g	t3-g	t4-g	0.5tc1	0.5tr2	0.5tc3	0.5tc4	s1	s2	s3	s4	t1-n50	t2-n50	t3-n50	t4-n50	ReHp1	ReHp2	ReHp3	ReHp4	s	tp-n50	Ap-n50	Ap-n50	ReHp
-	mm	mm	mm	mm	mm	mm	mm	mm	mm	mm	mm	mm	mm	mm	mm	mm	MPa	MPa	MPa	MPa	mm	mm	mm^2	cm^2	MPa
1	15.5				2.25				800				13.25				235				400	13.25	5300	53	235
2	14.5				1.5				630				13				235				630	13.00	8190	81.9	235
3	14.5				1.5				630				13				235				630	13.00	8190	81.9	235
4	15				1.5				800				13.5				235				800	13.50	10800	108	235
5	15				1.5				800				13.5				235				800	13.50	10800	108	235
6	15				1.5				800				13.5				235				800	13.50	10800	108	235
7	15				1.5				800				13.5				235				800	13.50	10800	108	235
8	15				1.5				800				13.5				235				800	13.50	10800	108	235
9	15				1.5				800				13.5				235				800	13.50	10800	108	235
10	15				1.5				800				13.5				235				800	13.50	10800	108	235
11	15				1.5				800				13.5				235				800	13.50	10800	108	235
12	15				1.5				800				13.5				235				800	13.50	10800	108	235
13	15				1.5				800				13.5				235				800	13.50	10800	108	235
14	15				1.5				800				13.5				235				800	13.50	10800	108	235
15	14.5				1.5				630				13				235				630	13.00	8190	81.9	235
16	14.5				1.5				630				13				235				630	13.00	8190	81.9	235
17	15				1.5				800				13.5				235				800	13.50	10800	108	235
18	15				1.5				800				13.5				235				800	13.50	10800	108	235
19	15	12	16		1.5	1.5	1.5		1945.35	250	90		13.5	10.5	14.5	0	235	235	235		2285.35	13.21	30192.225	301.92225	235
20	15	14			1.5	1.5			475	175			13.5	12.5			235	235			650	13.23	8600	86	235
21	14				1.5				650				12.5				235				650	12.50	8125	81.25	235
22	14				1.5				650				12.5				235				650	12.50	8125	81.25	235
23	14				1.5				650				12.5				235				650	12.50	8125	81.25	235
24	11				1.5				700				9.5				235				700	9.50	6650	66.5	235
25	11				1.5				700				9.5				235				700	9.50	6650	66.5	235
26	14				1.5				700				12.5				235				700	12.50	8750	87.5	235
27	14				1.5				700				12.5				235				700	12.50	8750	87.5	235
28	14				1.5				700				12.5				235				700	12.50	8750	87.5	235
29	14				1.5				700				12.5				235				700	12.50	8750	87.5	235
30	14				1.5				700				12.5				235				700	12.50	8750	87.5	235
31	14				1.5				700				12.5				235				700	12.50	8750	87.5	235
32	14				1.5				700				12.5				235				700	12.50	8750	87.5	235
33	11				1.5				700				9.5				235				700	9.50	6650	66.5	235
34	11				1.5				700				9.5				235				700	9.50	6650	66.5	235
35	14				1.5				700				12.5				235				700	12.50	8750	87.5	235
36	14				1.5				700				12.5				235				700	12.50	8750	87.5	235
37	14				1.5				700				12.5				235				700	12.50	8750	87.5	235
38	14				1.5				700				12.5				235				700	12.50	8750	87.5	235
39	14				1.5				700				12.5				235				700	12.50	8750	87.5	235
40	14				1.5				700				12.5				235				700	12.50	8750	87.5	235
41	14				1.5				700				12.5				235				700	12.50	8750	87.5	235
42	11				1.5				700				9.5				235				700	9.50	6650	66.5	235
43	11				1.5				700				9.5				235				700	9.50	6650	66.5	235
44	14				1.5				700				12.5				235				700	12.50	8750	87.5	235
45	14				1.5				700				12.5				235				700	12.50	8750	87.5	235
46	11.5				2				660				9.5				235				660	9.50	6270	62.7	235
47	11.5				2				660				9.5				235				660	9.50	6270	62.7	235
48	11.5				2				660				9.5				235				660	9.50	6270	62.7	235
49	11.5				2				660				9.5				235				660	9.50	6270	62.7	235
50	12.5				2				800				10.5				235				800	10.50	8400	84	235
51	12.5				2				800				10.5				235				800	10.50	8400	84	235
52	12.5				2				800				10.5				235				800	10.50	8400	84	235
53	12.5				2				800				10.5				235				800	10.50	8400	84	235
54	12.5				2				800				10.5				235				800	10.50	8400	84	235
55	12.5				2				800				10.5				235				800	10.50	8400	84	235
56	12.5				2				800				10.5				235				800	10.50	8400	84	235
57	12.5				2				800				10.5				235				800	10.50	8400	84	235
58	12.5				2				800				10.5				235				800	10.50	8400	84	235
59	12.5				2				800				10.5				235				800	10.50	8400	84	235
60	12.5				2				800				10.5				235				800	10.50	8400	84	235
61	12.5				2				800				10.5				235				800	10.50	8400	84	235
62	11				2.25				740				8.75				315				740	8.75	6475	64.75	315
63	11				2.25				740				8.75				315				740	8.75	6475	64.75	315
64	11				2.25				660				8.75				235				660	8.75	5775	57.75	235
65	11				2.25				660				8.75				235				660	8.75	5775	57.75	235
66	11				1.75				700				9.25				235				700	9.25	6475	64.75	235
67	11				1.75				700				9.25				235				700	9.25	6475	64.75	235
68	11				1.75				700				9.25				235				700	9.25	6475	64.75	235
69	11	12.5			1.75	1.75			50	650			9.25	10.75			235	235			700	10.64	7450	74.5	235
70	12.5				1.75				700				10.75				235				700	10.75	7525	75.25	235
71	12.5				1.75				700				10.75				235				700	10.75	7525	75.25	235
72	12.5				1.75				700				10.75				235				700	10.75	7525	75.25	235
73	13				1.75				700				11.25				235				700	11.25	7875	78.75	235
74	13				1.75				700				11.25				235				700	11.25	7875	78.75	235
75	13				1.75				700				11.25				235				700	11.25	7875	78.75	235
76	13	13.5			1.75	1.75			250	450			11.25	11.75			235	235			700	11.57	8100	81	235
77	13.5				1.75				700				11.75				235				700	11.75	8225	82.25	235
78	13.5				1.75				700				11.75				235				700	11.75	8225	82.25	235
79	13.5				1.75				700				11.75				235				700	11.75	8225	82.25	235
80	14.5				1.75				700				12.75				235				700	12.75	8925	89.25	235
81	14.5				1.75				700				12.75				235				700	12.75	8925	89.25	235
82	14.5				1.75				700				12.75				235				700	12.75	8925	89.25	235
83	16.5				2.25				800				14.25				235				800	14.25	11400	114	235
84	16.5				2.25				800				14.25				235				800	14.25	11400	114	235
85	16.5				2.25				800				14.25				235				800	14.25	11400	114	235
86	16.5	15.5			2.25	2.25			300	500			14.25	13.25			235				800	13.63	10900	109	235
87	15.5				2.25				800				13.25				235				800	13.25	10600	106	235
88	15.5				2.25				800				13.25				235				800	13.25	10600	106	235
89	15.5				2.25				800				13.25				235				800	13.25	10600	106	235
90	15.5				2.25				800				13.25				235				800	13.25	10600	106	235
91	15.5				2.25				800				13.25				235				800	13.25	10600	106	235
92	15.5				2.25				800				13.25				235				800	13.25	10600	106	235
93	15.5				2.25				800				13.25				235				800	13.25	10600	106	235
94	14.5				1.75				795				12.75				315				795	12.75	10136.25	101.3625	315
95	14.5				1.75				795				12.75				315				795	12.75	10136.25	101.3625	315
96	14.5				1.75				795				12.75				315				795	12.75	10136.25	101.3625	315
97	14.5	14.5			1.75	1.75			397.5	225			12.75	12.75	0	0	315	315			622.5	12.75	7936.875	79.36875	315.00
98	15.5	14.5	15.5	14.5	2.25	1.5	2.25	1.75	400	320	400	397.5	13.25	13	13.25	12.75	235	235	235	315	1517.5	13.06630972	19828.125	198.28125	255.45
99	16.5	16.5	15	14.5	1.5	1.5	1.5	1.5	330	100	300	270	15	15	13.5	13	315	315	235	235	1000	14.01	14010	140.1	271.83
100	15	15	14.5		1.5	1.5	1.5		400	400	270		13.5	13.5	13	0	235	235	235		1070	13.37383178	14310	143.1	235.00
101	14	14	11		1.5	1.5	1.5		325	350	300		12.5	12.5	9.5	0	235	235	235		975	11.57692308	11287.5	112.875	235.00
102	14	14	11		1.5	1.5	1.5		350	350	300		12.5	12.5	9.5	0	235	235	235		1000	11.6	11600	116	235.00
103	14	14	11		1.5	1.75	1.5		350	350	300		12.5	12.25	9.5	0	235	235	235		1000	11.5125	11512.5	115.125	235.00
104	14	11.5			1.75	2			350	330			12.25	9.5	0	0	235	235			680	10.91544118	7422.5	74.225	235.00
105	11.5	12.5	11		2	2	2.25		330	400	300		9.5	10.5	8.75	0	235	235	235		1030	9.669902913	9960	99.6	235.00
106	12.5	12.5	11		2	2	2.25		400	400	370		10.5	10.5	8.75	0	235	235	315		1170	9.946581197	11637.5	116.375	257.26
107	11.5	11			2.25	2.25			225	370			9.25	8.75	0	0	315	315			595	8.93907563	5318.75	53.1875	315
108	11	11	11		2.25	1.75	1.5		330	350	300		8.75	9.25	9.5	0	235	235	235		980	9.158163265	8975	89.75	235
109	11	13	13	12.5	1.5	1.75	1.75	1.75	300	200	350	150	9.5	11.25	11.25	10.75	235	235	235	235	1000	10.65	10650	106.5	235
110	11	13.5	14.5		1.5	1.75	1.75		300	350	350		9.5	11.75	12.75	0	235	235	235		1000	11.425	11425	114.25	235
111	14.5	14.5	16.5		1.5	1.75	2.25		320	350	400		13	12.75	14.25	0	235	235	235		1070	13.38551402	14322.5	143.225	235
112	16.5				1.5				800				15				235				800	15	12000	120	235
113	11	11			2.25	2.25			330	300			8.75	8.75	0	0	235	235	0	0	630	8.75	5512.5	55.125	235

Table 2: Total moment of inertia of plates												
Location	**Characteristic**	**Quantity**	**Length**	**t-g**	**tn-50**	**Net Area**	**θ**	**θ**	**sinθ**	**Length*sinθ**	**Moment of inertia**	**Total moment of inertia**
-	**-**	**-**	**m**	**m**	**m**	**m^2**	**degrees**	**rad**	**-**	**m**	**m^4**	**m^4**
Outer Bottom	0-900	2	0.9	0.0165	0.015	0.0135	0	0	0	0	2.53125E-07	5.0625E-07
Outer Bottom	900-12000	2	11.1	0.015	0.0135	0.14985	0	0	0	0	2.27585E-06	4.55169E-06
Bilge		2	2.6703	0.015	0.0135	0.03604905					3.16	6.32
Side Shell	1700-17600	2	15.9	0.014	0.0125	0.19875	90	1.570796327	1	15.9	4.187165625	8.37433125
Upper Deck	10400-13700	2	3.3	0.0115	0.0095	0.03135	0	0	0	0	2.35778E-07	4.71556E-07
Upper Deck	Inclined	2	8.9202	0.0125	0.0105	0.0936621	-3.857	-0.067317349	-0.067266518	-0.600030793	0.002810151	0.005620303
Upper Deck	0-1500	2	1.5	0.0125	0.0105	0.01575	0	0	0	0	1.44703E-07	2.89406E-07
Inner Hull	17000-17600	2	0.6	0.011	0.00875	0.00525	90	1.570796327	1	0.6	0.0001575	0.000315
Inner Hull	Inclined Upper	2	1.9849	0.011	0.00875	0.017367875	130.9144	2.284887318	0.755688891	1.49996688	0.003256333	0.006512666
Inner Hull	11 thick	2	2.5	0.011	0.00925	0.023125	90	1.570796327	1	2.5	0.012044271	0.024088542
Inner Hull	12.5 thick	2	2.9	0.0125	0.01075	0.031175	90	1.570796327	1	2.9	0.021848479	0.043696958
Inner Hull	13 thick	2	2.9	0.013	0.01125	0.032625	90	1.570796327	1	2.9	0.022864688	0.045729375
Inner Hull	13.5 thick	2	2.9	0.0135	0.01175	0.034075	90	1.570796327	1	2.9	0.023880896	0.047761792
Inner Hull	Inclined Lower	2	2.7735	0.0145	0.01275	0.035362125	62.049	1.082959348	0.883348767	2.449967806	0.017687965	0.035375929
Inner Bottom	0-7300	2	7.3	0.0155	0.01325	0.096725	0	0	0	0	1.41511E-06	2.83021E-06
Inner Bottom	7300-10400	2	3.1	0.0165	0.01425	0.044175	0	0	0	0	7.47524E-07	1.49505E-06
Upper Stool	Inclined	2	2.2276	0.011	0.00875	0.0194915	80.9605	1.413027289	0.987580259	2.199933785	0.007861098	0.015722197
Upper Stool	horizontal	2	0.45	0.0115	0.00925	0.0041625	0	0	0	0	2.96795E-08	5.9359E-08
Lower Stool	Inclined	2	3.1693	0.0145	0.01275	0.040408575	96.3401	1.681451947	0.993883912	3.149916281	0.033411064	0.066822129
Lower Stool	horizontal	2	0.45	0.0145	0.01275	0.0057375	0	0	0	0	7.77252E-08	1.5545E-07
Grider	bottom 1	2	1.85	0.0145	0.013	0.02405	90	1.570796327	1	1.85	0.00685926	0.013718521
Grider	bottom 2	2	1.85	0.0145	0.013	0.02405	90	1.570796327	1	1.85	0.00685926	0.013718521
Grider	side 1	2	2	0.011	0.0095	0.019	0	0	0	0	1.42896E-07	2.85792E-07
Grider	side 2	2	2	0.011	0.0095	0.019	0	0	0	0	1.42896E-07	2.85792E-07
Grider	side 3	2	2	0.011	0.0095	0.019	0	0	0	0	1.42896E-07	2.85792E-07

Table 3: Stiffener's Geometric Characteristics

Num of Elem	hw	tw	bf	tf	θ	sinθ	cosθ	0.5tcor	tw-n50	tf-n50	Aw-n50	Af-n50	Zg	Yg	Iyy	Izz	As-n50	Iyy/YY	Iyy/YY
-	mm	mm	mm	mm	degrees	-	-	mm	mm	mm	mm^2	mm^2	mm	mm	cm^4	cm^4	cm^2	cm^4	m^4
1	150	12	90	12	180	0.0000	-1.0000	1.75	10.25	10.25	1537.5	922.5	105.046875	20.078125	659.24294	154.07442	24.6	659.2429438	6.59243E-06
2	150	11			270	-1.0000	0.0000	1.75	9.2500		1387.5		75	4.625	260.15625	0.1069531	13.875	0.106953125	1.06953E-09
3	150	11			270	-1.0000	0.0000	1.75	9.2500		1387.5		75	4.625	260.15625	0.1069531	13.875	0.106953125	1.06953E-09
4	300	13	90	17	0	0.0000	1.0000	1.5	11.5	15.5	3450	1395	195.4202786	17.051084	5062.2348	247.52392	48.45	5062.234796	5.06223E-05
5	300	13	90	17	0	0.0000	1.0000	1.5	11.5	15.5	3450	1395	195.4202786	17.051084	5062.2348	247.52392	48.45	5062.234796	5.06223E-05
6	300	13	90	17	0	0.0000	1.0000	1.5	11.5	15.5	3450	1395	195.4202786	17.051084	5062.2348	247.52392	48.45	5062.234796	5.06223E-05
7	300	13	90	17	0	0.0000	1.0000	1.5	11.5	15.5	3450	1395	195.4202786	17.051084	5062.2348	247.52392	48.45	5062.234796	5.06223E-05
8	300	13	90	17	0	0.0000	1.0000	1.5	11.5	15.5	3450	1395	195.4202786	17.051084	5062.2348	247.52392	48.45	5062.234796	5.06223E-05
9	300	13	90	17	0	0.0000	1.0000	1.5	11.5	15.5	3450	1395	195.4202786	17.051084	5062.2348	247.52392	48.45	5062.234796	5.06223E-05
10	300	13	90	17	0	0.0000	1.0000	1.5	11.5	15.5	3450	1395	195.4202786	17.051084	5062.2348	247.52392	48.45	5062.234796	5.06223E-05
11	300	13	90	17	0	0.0000	1.0000	1.5	11.5	15.5	3450	1395	195.4202786	17.051084	5062.2348	247.52392	48.45	5062.234796	5.06223E-05
12	300	13	90	17	0	0.0000	1.0000	1.5	11.5	15.5	3450	1395	195.4202786	17.051084	5062.2348	247.52392	48.45	5062.234796	5.06223E-05
13	300	13	90	17	0	0.0000	1.0000	1.5	11.5	15.5	3450	1395	195.4202786	17.051084	5062.2348	247.52392	48.45	5062.234796	5.06223E-05
14	300	13	90	17	0	0.0000	1.0000	1.5	11.5	15.5	3450	1395	195.4202786	17.051084	5062.2348	247.52392	48.45	5062.234796	5.06223E-05
15	150	11			270	-1.0000	0.0000	1.75	9.2500		1387.5		75	4.625	260.15625	0.1069531	13.875	0.106953125	1.06953E-09
16	150	11			270	-1.0000	0.0000	1.75	9.2500		1387.5		75	4.625	260.15625	0.1069531	13.875	0.106953125	1.06953E-09
17	300	13	90	17	0	0.0000	1.0000	1.5	11.5	15.5	3450	1395	195.4202786	17.051084	5062.2348	247.52392	48.45	5062.234796	5.06223E-05
18	300	13	90	17	0	0.0000	1.0000	1.5	11.5	15.5	3450	1395	195.4202786	17.051084	5062.2348	247.52392	48.45	5062.234796	5.06223E-05
20	300	11	90	16	270	-1.0000	0.0000	1.75	9.25	14.25	2775	1282.5	199.6642791	17.386784	4248.8914	229.76648	40.575	229.7664788	2.29766E-06
21	300	11	90	16	270	-1.0000	0.0000	1.75	9.25	14.25	2775	1282.5	199.6642791	17.386784	4248.8914	229.76648	40.575	229.7664788	2.29766E-06
22	250	10	90	15	270	-1.0000	0.0000	1.75	8.25	13.25	2062.5	1192.5	173.2220622	19.099942	2385.0794	206.88133	32.55	206.8813308	2.06881E-06
23	250	10	90	15	270	-1.0000	0.0000	1.75	8.25	13.25	2062.5	1192.5	173.2220622	19.099942	2385.0794	206.88133	32.55	206.8813308	2.06881E-06
24	150	11			180	0.0000	-1.0000	1.75	9.25		1387.5		75	4.625	260.15625	0.1069531	13.875	260.15625	2.60156E-06
25	150	11			180	0.0000	-1.0000	1.75	9.25		1387.5		75	4.625	260.15625	0.1069531	13.875	260.15625	2.60156E-06
26	250	10	90	15	270	-1.0000	0.0000	1.75	8.25	13.25	2062.5	1192.5	173.2220622	19.099942	2385.0794	206.88133	32.55	206.8813308	2.06881E-06
27	250	10	90	15	270	-1.0000	0.0000	1.75	8.25	13.25	2062.5	1192.5	173.2220622	19.099942	2385.0794	206.88133	32.55	206.8813308	2.06881E-06
28	250	10	90	15	270	-1.0000	0.0000	1.75	8.25	13.25	2062.5	1192.5	173.2220622	19.099942	2385.0794	206.88133	32.55	206.8813308	2.06881E-06
29	250	10	90	15	270	-1.0000	0.0000	1.75	8.25	13.25	2062.5	1192.5	173.2220622	19.099942	2385.0794	206.88133	32.55	206.8813308	2.06881E-06
30	250	10	90	15	270	-1.0000	0.0000	1.75	8.25	13.25	2062.5	1192.5	173.2220622	19.099942	2385.0794	206.88133	32.55	206.8813308	2.06881E-06
31	250	10	90	15	270	-1.0000	0.0000	1.75	8.25	13.25	2062.5	1192.5	173.2220622	19.099942	2385.0794	206.88133	32.55	206.8813308	2.06881E-06
32	250	10	90	15	270	-1.0000	0.0000	1.75	8.25	13.25	2062.5	1192.5	173.2220622	19.099942	2385.0794	206.88133	32.55	206.8813308	2.06881E-06
33	150	11			180	0.0000	-1.0000	1.75	9.25		1387.5		75	4.625	260.15625	0.1069531	13.875	260.15625	2.60156E-06
34	150	11			180	0.0000	-1.0000	1.75	9.25		1387.5		75	4.625	260.15625	0.1069531	13.875	260.15625	2.60156E-06
35	200	9	90	14	270	-1.0000	0.0000	1.75	7.25	12.25	1450	1102.5	145.8385162	21.496082	1190.0808	181.72168	25.525	181.7216784	1.81722E-06
36	200	9	90	14	270	-1.0000	0.0000	1.75	7.25	12.25	1450	1102.5	145.8385162	21.496082	1190.0808	181.72168	25.525	181.7216784	1.81722E-06
37	200	9	90	14	270	-1.0000	0.0000	1.75	7.25	12.25	1450	1102.5	145.8385162	21.496082	1190.0808	181.72168	25.525	181.7216784	1.81722E-06
38	150	12	90	12	270	-1.0000	0.0000	1.75	10.25	10.25	1537.5	922.5	105.046875	20.078125	659.24294	154.07442	24.6	154.0744165	1.54074E-06
39	150	12	90	12	270	-1.0000	0.0000	1.75	10.25	10.25	1537.5	922.5	105.046875	20.078125	659.24294	154.07442	24.6	154.0744165	1.54074E-06
40	150	12	90	12	270	-1.0000	0.0000	1.75	10.25	10.25	1537.5	922.5	105.046875	20.078125	659.24294	154.07442	24.6	154.0744165	1.54074E-06
41	150	12	90	12	270	-1.0000	0.0000	1.75	10.25	10.25	1537.5	922.5	105.046875	20.078125	659.24294	154.07442	24.6	154.0744165	1.54074E-06
42	150	11			180	0.0000	-1.0000	1.75	9.25		1387.5		75	4.625	260.15625	0.1069531	13.875	260.15625	2.60156E-06
43	150	11			180	0.0000	-1.0000	1.75	9.25		1387.5		75	4.625	260.15625	0.1069531	13.875	260.15625	2.60156E-06
44	250	12	90	16	270	-1.0000	0.0000	2	10	14	2500	1260	169.2340426	18.404255	2763.8647	219.30089	37.6	219.3008865	2.19301E-06
45	250	12	90	16	270	-1.0000	0.0000	2	10	14	2500	1260	169.2340426	18.404255	2763.8647	219.30089	37.6	219.3008865	2.19301E-06
46	250	10	90	15	180	0.0000	-1.0000	2	8	13	2000	1170	173.5347003	19.132492	2319.777	203.19477	31.7	2319.777035	2.31978E-05
47	250	10	90	15	180	0.0000	-1.0000	2	8	13	2000	1170	173.5347003	19.132492	2319.777	203.19477	31.7	2319.777035	2.31978E-05
48	250	10	90	15	180	0.0000	-1.0000	2	8	13	2000	1170	173.5347003	19.132492	2319.777	203.19477	31.7	2319.777035	2.31978E-05
49	250	10	90	15	180	0.0000	-1.0000	2	8	13	2000	1170	173.5347003	19.132492	2319.777	203.19477	31.7	2319.777035	2.31978E-05
50	350	12	100	17	3.857	0.0673	0.9977	2	10	15	3500	1500	229.75	18.5	7072.8854	337.91667	50	7042.411135	7.04241E-05
51	350	12	100	17	3.857	0.0673	0.9977	2	10	15	3500	1500	229.75	18.5	7072.8854	337.91667	50	7042.411135	7.04241E-05
52	300	11	90	16	3.857	0.0673	0.9977	2	9	14	2700	1260	199.9545455	17.386364	4144.6312	226.16489	39.6	4126.900967	4.1269E-05
53	300	11	90	16	3.857	0.0673	0.9977	2	9	14	2700	1260	199.9545455	17.386364	4144.6312	226.16489	39.6	4126.900967	4.1269E-05
54	300	11	90	16	3.857	0.0673	0.9977	2	9	14	2700	1260	199.9545455	17.386364	4144.6312	226.16489	39.6	4126.900967	4.1269E-05
55	300	11	90	16	3.857	0.0673	0.9977	2	9	14	2700	1260	199.9545455	17.386364	4144.6312	226.16489	39.6	4126.900967	4.1269E-05
56	300	11	90	16	3.857	0.0673	0.9977	2	9	14	2700	1260	199.9545455	17.386364	4144.6312	226.16489	39.6	4126.900967	4.1269E-05
57	300	11	90	16	3.857	0.0673	0.9977	2	9	14	2700	1260	199.9545455	17.386364	4144.6312	226.16489	39.6	4126.900967	4.1269E-05
58	300	11	90	16	3.857	0.0673	0.9977	2	9	14	2700	1260	199.9545455	17.386364	4144.6312	226.16489	39.6	4126.900967	4.1269E-05
59	300	11	90	16	3.857	0.0673	0.9977	2	9	14	2700	1260	199.9545455	17.386364	4144.6312	226.16489	39.6	4126.900967	4.1269E-05
60	300	11	90	16	3.857	0.0673	0.9977	2	9	14	2700	1260	199.9545455	17.386364	4144.6312	226.16489	39.6	4126.900967	4.1269E-05
61	150	14			180	0.0000	-1.0000	2	12		1800		75	6	337.5	0.18	18	337.5	0.000003375
62	150	12	90	12	279.03948	-0.9876	0.1571	2	10	10	1500	900	105	20	642	150.875	24	162.9984887	1.62998E-06
63	150	12	90	12	279.03948	-0.9876	0.1571	2	10	10	1500	900	105	20	642	150.875	24	162.9984887	1.62998E-06
64	150	12	90	12	40.914384	0.6549	0.7557	2	10	10	1500	900	105	20	642	150.875	24	431.3397776	4.3134E-06
65	150	12	90	12	40.914384	0.6549	0.7557	2	10	10	1500	900	105	20	642	150.875	24	431.3397776	4.3134E-06
66	200	9	90	14	90	1.0000	0.0000	1.75	7.25	12.25	1450	1102.5	145.8385162	21.496082	1190.0808	181.72168	25.525	181.7216784	1.81722E-06
67	200	9	90	14	90	1.0000	0.0000	1.75	7.25	12.25	1450	1102.5	145.8385162	21.496082	1190.0808	181.72168	25.525	181.7216784	1.81722E-06
68	200	9	90	14	90	1.0000	0.0000	1.75	7.25	12.25	1450	1102.5	145.8385162	21.496082	1190.0808	181.72168	25.525	181.7216784	1.81722E-06
69	200	9	90	14	90	1.0000	0.0000	1.75	7.25	12.25	1450	1102.5	145.8385162	21.496082	1190.0808	181.72168	25.525	181.7216784	1.81722E-06
70	200	9	90	14	90	1.0000	0.0000	1.75	7.25	12.25	1450	1102.5	145.8385162	21.496082	1190.0808	181.72168	25.525	181.7216784	1.81722E-06
71	200	9	90	14	90	1.0000	0.0000	1.75	7.25	12.25	1450	1102.5	145.8385162	21.496082	1190.0808	181.72168	25.525	181.7216784	1.81722E-06
72	200	9	90	14	90	1.0000	0.0000	1.75	7.25	12.25	1450	1102.5	145.8385162	21.496082	1190.0808	181.72168	25.525	181.7216784	1.81722E-06
73	250	10	90	15	90	1.0000	0.0000	1.75	8.25	13.25	2062.5	1192.5	173.2220622	19.099942	2385.0794	206.88133	32.55	206.8813308	2.06881E-06
74	250	10	90	15	90	1.0000	0.0000	1.75	8.25	13.25	2062.5	1192.5	173.2220622	19.099942	2385.0794	206.88133	32.55	206.8813308	2.06881E-06
75	250	10	90	15	90	1.0000	0.0000	1.75	8.25	13.25	2062.5	1192.5	173.2220622	19.099942	2385.0794	206.88133	32.55	206.8813308	2.06881E-06
76	250	10	90	15	90	1.0000	0.0000	1.75	8.25	13.25	2062.5	1192.5	173.2220622	19.099942	2385.0794	206.88133	32.55	206.8813308	2.06881E-06
77	250	10	90	15	90	1.0000	0.0000	1.75	8.25	13.25	2062.5	1192.5	173.2220622	19.099942	2385.0794	206.88133	32.55	206.8813308	2.06881E-06
78	250	10	90	15	90	1.0000	0.0000	1.75	8.25	13.25	2062.5	1192.5	173.2220622	19.099942	2385.0794	206.88133	32.55	206.8813308	2.06881E-06
79	250	10	90	15	90	1.0000	0.0000	1.75	8.25	13.25	2062.5	1192.5	173.2220622	19.099942	2385.0794	206.88133	32.55	206.8813308	2.06881E-06
80	300	11	90	16	117.95097	0.8833	-0.4687	1.75	9.25	14.25	2775	1282.5	199.6642791	17.386784	4248.8914	229.76648	40.575	1112.746157	1.11275E-05
81	300	11	90	16	117.95097	0.8833	-0.4687	1.75	9.25	14.25	2775	1282.5	199.6642791	17.386784	4248.8914	229.76648	40.575	1112.746157	1.11275E-05
82	300	11	90	16	117.95097	0.8833	-0.4687	1.75	9.25	14.25	2775	1282.5	199.6642791	17.386784	4248.8914	229.76648	40.575	1112.746157	1.11275E-05
83	300	12	90	17	180	0.0000	-1.0000	1.75	10.25	15.25	3075	1372.5	198.6431282	17.430438	4666.6272	243.79031	44.475	4666.627155	4.66663E-05
84	300	12	90	17	180	0.0000	-1.0000	1.75	10.25	15.25	3075	1372.5	198.6431282	17.430438	4666.6272	243.79031	44.475	4666.627155	4.66663E-05
85	300	12	90	17	180	0.0000	-1.0000	1.75	10.25	15.25	3075	1372.5	198.6431282	17.430438	4666.6272	243.79031	44.475	4666.627155	4.66663E-05
86	300	12	90	17	180	0.0000	-1.0000	1.75	10.25	15.25	3075	1372.5	198.6431282	17.430438	4666.6272	243.79031	44.475	4666.627155	4.66663E-05
87	300	12	90	17	180	0.0000	-1.0000	1.75	10.25	15.25	3075	1372.5	198.6431282	17.430438	4666.6272	243.79031	44.475	4666.627155	4.66663E-05
88	300	12	90	17	180	0.0000	-1.0000	1.75	10.25	15.25	3075	1372.5	198.6431282	17.430438	4666.6272	243.79031	44.475	4666.627155	4.66663E-05
89	300	12	90	17	180	0.0000	-1.0000	1.75	10.25	15.25	3075	1372.5	198.6431282	17.430438	4666.6272	243.79031	44.475	4666.627155	4.66663E-05
90	300	12	90	17	180	0.0000	-1.0000	1.75	10.25	15.25	3075	1372.5	198.6431282	17.430438	4666.6272	243.79031	44.475	4666.627155	4.66663E-05
91	300	12	90	17	180	0.0000	-1.0000	1.75	10.25	15.25	3075	1372.5	198.6431282	17.430438	4666.6272	243.79031	44.475	4666.627155	4.66663E-05
92	300	12	90	17	180	0.0000	-1.0000	1.75	10.25	15.25	3075	1372.5	198.6431282	17.430438	4666.6272	243.79031	44.475	4666.627155	4.66663E-05
93	300	12	90	17	180	0.0000	-1.0000	1.75	10.25	15.25	3075	1372.5	198.6431282	17.430438	4666.6272	243.79031	44.475	4666.627155	4.66663E-05
94	250	12	90	16	263.65981	-0.9939	-0.1104	1.75	10.25	14.25	2562.5	1282.5	169.0703023	18.425309	2828.8953	222.68977	38.45	254.4727635	2.54473E-06
95	250	12	90	16	263.65981	-0.9939	-0.1104	1.75	10.25	14.25	2562.5	1282.5	169.0703023	18.425309	2828.8953	222.68977	38.45	254.4727635	2.54473E-06
96	250	12	90	16	263.65981	-0.9939	-0.1104	1.75	10.25	14.25	2562.5	1282.5	169.0703023	18.425309	2828.8953	222.68977	38.45	254.4727635	2.54473E-06
112	300	13	90	17	0	0.0000	1.0000	1.5	11.5	15.5	3450	1395	195.4202786	17.051084	5062.2348	247.52392	48.45	5062.234796	0.000151867

Table 4: Element's Global Coordinates

Num of Elem	A1p-n50	s1	t1p-n50	A2p-n50	s2	t2p-n50	A3p-n50	s3	t3p-n50	A4p-n50	s4	t4p-n50	z topical	y topical	z ref	y ref	z global	y global
-	m^2	m	m	m^2	m	m	m^2	m	m	m^2	m	m	m	m	m	m	m	m
1	0.0053	0.4	0.01325	0.0015375	0.01025	0.15	0.0009225	0.01025	0.09				0.042026136	0.204740295	1.85	-0.2	1.892026136	0.004740295
2	0.00819	0.63	0.013	0.0013875	0.00925	0.15							0.018306969	0.315	0.9	0.8	1.215	0.781693031
3	0.00819	0.63	0.013	0.0013875	0.00925	0.15							0.018306969	0.315	0.27	0.8	0.585	0.781693031
4	0.0108	0.8	0.0135	0.00345	0.0115	0.3	0.001395	0.0155	0.09				0.069358821	0.40349976	0	1.2	0.069358821	2.4
5	0.0108	0.8	0.0135	0.00345	0.0115	0.3	0.001395	0.0155	0.09				0.069358821	0.40349976	0	2.8	0.069358821	2.39650024
6	0.0108	0.8	0.0135	0.00345	0.0115	0.3	0.001395	0.0155	0.09				0.069358821	0.40349976	0	3.6	0.069358821	3.19650024
7	0.0108	0.8	0.0135	0.00345	0.0115	0.3	0.001395	0.0155	0.09				0.069358821	0.40349976	0	4.4	0.069358821	3.99650024
8	0.0108	0.8	0.0135	0.00345	0.0115	0.3	0.001395	0.0155	0.09				0.069358821	0.40349976	0	5.2	0.069358821	4.79650024
9	0.0108	0.8	0.0135	0.00345	0.0115	0.3	0.001395	0.0155	0.09				0.069358821	0.40349976	0	6	0.069358821	5.59650024
10	0.0108	0.8	0.0135	0.00345	0.0115	0.3	0.001395	0.0155	0.09				0.069358821	0.40349976	0	6.8	0.069358821	6.39650024
11	0.0108	0.8	0.0135	0.00345	0.0115	0.3	0.001395	0.0155	0.09				0.069358821	0.40349976	0	7.6	0.069358821	7.19650024
12	0.0108	0.8	0.0135	0.00345	0.0115	0.3	0.001395	0.0155	0.09				0.069358821	0.40349976	0	8.4	0.069358821	7.99650024
13	0.0108	0.8	0.0135	0.00345	0.0115	0.3	0.001395	0.0155	0.09				0.069358821	0.40349976	0	9.2	0.069358821	8.79650024
14	0.0108	0.8	0.0135	0.00345	0.0115	0.3	0.001395	0.0155	0.09				0.069358821	0.40349976	0	10	0.069358821	9.59650024
15	0.00819	0.63	0.013	0.0013875	0.00925	0.15							0.018306969	0.315	0.27	10.4	0.585	10.38169303
16	0.00819	0.63	0.013	0.0013875	0.00925	0.15							0.018306969	0.315	0.9	10.4	1.215	10.38169303
17	0.0108	0.8	0.0135	0.00345	0.0115	0.3	0.001395	0.0155	0.09				0.069358821	0.40349976	0	11.6	0.069358821	11.19650024
18	0.0108	0.8	0.0135	0.00345	0.0115	0.3	0.001395	0.0155	0.09				0.069358821	0.40349976	0	12.4	0.069358821	11.99650024
19	0.026262225	1.94535	0.0135	0.002625	0.25	0.0105	0.001305	0.09	0.0145				0.891436879	0.319404149	0	12.4	0.319404149	13.29143688
20	0.0086	0.65	0.013230769	0.002775	0.00925	0.3	0.0012825	0.01425	0.09				0.072740586	0.329090929	2.025	13.7	1.695909071	13.62725941
21	0.008125	0.65	0.0125	0.002775	0.00925	0.3	0.0012825	0.01425	0.09				0.074831751	0.329250436	2.675	13.7	2.345749564	13.62516825
22	0.008125	0.65	0.0125	0.0020625	0.00825	0.25	0.0011925	0.01325	0.09				0.057584056	0.329283255	3.325	13.7	2.995716745	13.64241594
23	0.008125	0.65	0.0125	0.0020625	0.00825	0.25	0.0011925	0.01325	0.09				0.057584056	0.329283255	3.975	13.7	3.645716745	13.64241594
24	0.00665	0.7	0.0095	0.0013875	0.00925	0.15							0.018517107	0.35	4.3	13.4	4.281482893	13.05
25	0.00665	0.7	0.0095	0.0013875	0.00925	0.15							0.018517107	0.35	4.3	12.7	4.281482893	12.35
26	0.00875	0.7	0.0125	0.0020625	0.00825	0.25	0.0011925	0.01325	0.09				0.054911521	0.354060261	5.35	13.7	4.995939739	13.64508848
27	0.00875	0.7	0.0125	0.0020625	0.00825	0.25	0.0011925	0.01325	0.09				0.054911521	0.354060261	6.05	13.7	5.695939739	13.64508848
28	0.00875	0.7	0.0125	0.0020625	0.00825	0.25	0.0011925	0.01325	0.09				0.054911521	0.354060261	6.75	13.7	6.395939739	13.64508848
29	0.00875	0.7	0.0125	0.0020625	0.00825	0.25	0.0011925	0.01325	0.09				0.054911521	0.354060261	7.45	13.7	7.095939739	13.64508848
30	0.00875	0.7	0.0125	0.0020625	0.00825	0.25	0.0011925	0.01325	0.09				0.054911521	0.354060261	8.15	13.7	7.795939739	13.64508848
31	0.00875	0.7	0.0125	0.0020625	0.00825	0.25	0.0011925	0.01325	0.09				0.054911521	0.354060261	8.85	13.7	8.495939739	13.64508848
32	0.00875	0.7	0.0125	0.0020625	0.00825	0.25	0.0011925	0.01325	0.09				0.054911521	0.354060261	9.55	13.7	9.195939739	13.64508848
33	0.00665	0.7	0.0095	0.0013875	0.00925	0.15							0.018517107	0.35	9.9	13.4	9.881482893	13.05
34	0.00665	0.7	0.0095	0.0013875	0.00925	0.15							0.018517107	0.35	9.9	12.7	9.881482893	12.35
35	0.00875	0.7	0.0125	0.00145	0.00725	0.2	0.0011025	0.01225	0.09				0.040596909	0.354035916	10.95	13.7	10.59596408	13.65940309
36	0.00875	0.7	0.0125	0.00145	0.00725	0.2	0.0011025	0.01225	0.09				0.040596909	0.354035916	11.65	13.7	11.29596408	13.65940309
37	0.00875	0.7	0.0125	0.00145	0.00725	0.2	0.0011025	0.01225	0.09				0.040596909	0.354035916	12.35	13.7	11.99596408	13.65940309
38	0.00875	0.7	0.0125	0.0015375	0.01025	0.15	0.0009225	0.01025	0.09				0.030673757	0.353281417	13.05	13.7	12.69671858	13.66932624
39	0.00875	0.7	0.0125	0.0015375	0.01025	0.15	0.0009225	0.01025	0.09				0.030673757	0.353281417	13.75	13.7	13.39671858	13.66932624
40	0.00875	0.7	0.0125	0.0015375	0.01025	0.15	0.0009225	0.01025	0.09				0.030673757	0.353281417	14.45	13.7	14.09671858	13.66932624
41	0.00875	0.7	0.0125	0.0015375	0.01025	0.15	0.0009225	0.01025	0.09				0.030673757	0.353281417	15.15	13.7	14.79671858	13.66932624
42	0.00665	0.7	0.0095	0.0013875	0.00925	0.15							0.018517107	0.35	15.5	13.4	15.48148289	13.05
43	0.00665	0.7	0.0095	0.0013875	0.00925	0.15							0.018517107	0.35	15.5	12.7	15.48148289	12.35
44	0.00875	0.7	0.0125	0.0025	0.01	0.25	0.00126	0.014	0.09				0.058993405	0.354028777	16.55	13.7	16.19597122	13.64100659
45	0.00875	0.7	0.0125	0.0025	0.01	0.25	0.00126	0.014	0.09				0.058993405	0.354028777	17.25	13.7	16.89597122	13.64100659
46	0.00627	0.66	0.0095	0.002	0.008	0.25	0.00117	0.013	0.09				0.064618909	0.335081568	17.6	12.71	17.53538109	13.04508157
47	0.00627	0.66	0.0095	0.002	0.008	0.25	0.00117	0.013	0.09				0.064618909	0.335081568	17.6	12.05	17.53538109	12.38508157
48	0.00627	0.66	0.0095	0.002	0.008	0.25	0.00117	0.013	0.09				0.064618909	0.335081568	17.6	11.39	17.53538109	11.72508157
49	0.00627	0.66	0.0095	0.002	0.008	0.25	0.00117	0.013	0.09				0.064618909	0.335081568	17.6	10.73	17.53538109	11.06508157
50	0.0084	0.8	0.0105	0.0035	0.01	0.35	0.0015	0.015	0.1				0.092936567	0.405037313	17.62690661	10	17.71984317	9.594962687
51	0.0084	0.8	0.0105	0.0035	0.01	0.35	0.0015	0.015	0.1				0.092936567	0.405037313	17.68071982	9.2	17.77365639	8.794962687
52	0.0084	0.8	0.0105	0.0027	0.009	0.3	0.00126	0.014	0.09				0.070995146	0.404128641	17.73453304	8.4	17.80552818	7.995871359
53	0.0084	0.8	0.0105	0.0027	0.009	0.3	0.00126	0.014	0.09				0.070995146	0.404128641	17.78834625	7.6	17.8593414	7.195871359
54	0.0084	0.8	0.0105	0.0027	0.009	0.3	0.00126	0.014	0.09				0.070995146	0.404128641	17.84215946	6.8	17.91315461	6.395871359
55	0.0084	0.8	0.0105	0.0027	0.009	0.3	0.00126	0.014	0.09				0.070995146	0.404128641	17.89597268	6	17.96696782	5.595871359
56	0.0084	0.8	0.0105	0.0027	0.009	0.3	0.00126	0.014	0.09				0.070995146	0.404128641	17.94978589	5.2	18.02078104	4.795871359
57	0.0084	0.8	0.0105	0.0027	0.009	0.3	0.00126	0.014	0.09				0.070995146	0.404128641	18.00359911	4.4	18.07459425	3.995871359
58	0.0084	0.8	0.0105	0.0027	0.009	0.3	0.00126	0.014	0.09				0.070995146	0.404128641	18.05741232	3.6	18.12840747	3.195871359
59	0.0084	0.8	0.0105	0.0027	0.009	0.3	0.00126	0.014	0.09				0.070995146	0.404128641	18.11122554	2.8	18.18222068	2.395871359
60	0.0084	0.8	0.0105	0.0027	0.009	0.3	0.00126	0.014	0.09				0.070995146	0.404128641	18.16503875	2	18.2360339	1.595871359
61	0.0084	0.8	0.0105	0.0018	0.012	0.15							0.019411765	0.4	18.2	0.4	18.18058824	0
62	0.006475	0.74	0.00875	0.0015	0.01	0.15	0.0009	0.01	0.09				0.033952465	0.374056338	17.83459529	0.841867432	17.46518461	0.836532989
63	0.006475	0.74	0.00875	0.0015	0.01	0.15	0.0009	0.01	0.09				0.033952465	0.374056338	17.10872376	0.726387871	16.73931309	0.721053428
64	0.005775	0.66	0.00875	0.0015	0.01	0.15	0.0009	0.01	0.09				0.036485092	0.33440367	16.74688699	9.319364612	16.49418178	9.295469411
65	0.005775	0.66	0.00875	0.0015	0.01	0.15	0.0009	0.01	0.09				0.036485092	0.33440367	16.24813219	9.751618767	15.99542699	9.727723666
66	0.006475	0.7	0.00925	0.00145	0.00725	0.2	0.0011025	0.01225	0.09				0.047168132	0.355052998	15.15	11.7	14.794947	11.74716813
67	0.006475	0.7	0.00925	0.00145	0.00725	0.2	0.0011025	0.01225	0.09				0.047168132	0.355052998	14.45	11.7	14.094947	11.74716813
68	0.006475	0.7	0.00925	0.00145	0.00725	0.2	0.0011025	0.01225	0.09				0.047168132	0.355052998	13.75	11.7	13.394947	11.74716813
69	0.00745	0.7	0.010642857	0.00145	0.00725	0.2	0.0011025	0.01225	0.09				0.043895361	0.354560454	13.05	11.7	12.69543955	11.74389536
70	0.007525	0.7	0.01075	0.00145	0.00725	0.2	0.0011025	0.01225	0.09				0.043675422	0.354526513	12.35	11.7	11.99547349	11.74367542
71	0.007525	0.7	0.01075	0.00145	0.00725	0.2	0.0011025	0.01225	0.09				0.043675422	0.354526513	11.65	11.7	11.29547349	11.74367542
72	0.007525	0.7	0.01075	0.00145	0.00725	0.2	0.0011025	0.01225	0.09				0.043675422	0.354526513	10.95	11.7	10.59547349	11.74367542
73	0.007875	0.7	0.01125	0.0020625	0.00825	0.25	0.0011925	0.01325	0.09				0.05792933	0.354379464	9.55	11.7	9.195620536	11.75792933
74	0.007875	0.7	0.01125	0.0020625	0.00825	0.25	0.0011925	0.01325	0.09				0.05792933	0.354379464	8.85	11.7	8.495620536	11.75792933
75	0.007875	0.7	0.01125	0.0020625	0.00825	0.25	0.0011925	0.01325	0.09				0.05792933	0.354379464	8.15	11.7	7.795620536	11.75792933
76	0.0081	0.7	0.011571429	0.0020625	0.00825	0.25	0.0011925	0.01325	0.09				0.0570997	0.354292685	7.45	11.7	7.095707315	11.7570997
77	0.008225	0.7	0.01175	0.0020625	0.00825	0.25	0.0011925	0.01325	0.09				0.056655569	0.354245944	6.75	11.7	6.395754056	11.75665557
78	0.008225	0.7	0.01175	0.0020625	0.00825	0.25	0.0011925	0.01325	0.09				0.056655569	0.354245944	6.05	11.7	5.695754056	11.75665557
79	0.008225	0.7	0.01175	0.0020625	0.00825	0.25	0.0011925	0.01325	0.09				0.056655569	0.354245944	5.35	11.7	4.995754056	11.75665557
80	0.008925	0.7	0.01275	0.002775	0.00925	0.3	0.0012825	0.01425	0.09				0.070769714	0.353988518	3.990827843	11.53594947	3.678132432	11.50277858
81	0.008925	0.7	0.01275	0.002775	0.00925	0.3	0.0012825	0.01425	0.09				0.070769714	0.353988518	3.372483528	11.2078484	3.059788117	11.17467752
82	0.008925	0.7	0.01275	0.002775	0.00925	0.3	0.0012825	0.01425	0.09				0.070769714	0.353988518	2.754139214	10.87974734	2.441443803	10.84657645
83	0.0114	0.8	0.01425	0.003075	0.01025	0.3	0.0013725	0.01525	0.09				0.064872515	0.403453443	1.85	10	1.785127485	9.596546557
84	0.0114	0.8	0.01425	0.003075	0.01025	0.3	0.0013725	0.01525	0.09				0.064872515	0.403453443	1.85	9.2	1.785127485	8.796546557
85	0.0114	0.8	0.01425	0.003075	0.01025	0.3	0.0013725	0.01525	0.09				0.064872515	0.403453443	1.85	8.4	1.785127485	7.996546557
86	0.0109	0.8	0.013625	0.003075	0.01025	0.3	0.0013725	0.01525	0.09				0.06635079	0.403565951	1.85	7.6	1.78364921	7.196434049
87	0.0106	0.8	0.01325	0.003075	0.01025	0.3	0.0013725	0.01525	0.09				0.067294879	0.403637045	1.85	6.8	1.782705121	6.396362955
88	0.0106	0.8	0.01325	0.003075	0.01025	0.3	0.0013725	0.01525	0.09				0.067294879	0.403637045	1.85	6	1.782705121	5.596362955
89	0.0106	0.8	0.01325	0.003075	0.01025	0.3	0.0013725	0.01525	0.09				0.067294879	0.403637045	1.85	5.2	1.782705121	4.796362955
90	0.0106	0.8	0.01325	0.003075	0.01025	0.3	0.0013725	0.01525	0.09				0.067294879	0.403637045	1.85	4.4	1.782705121	3.996362955
91	0.0106	0.8	0.01325	0.003075	0.01025	0.3	0.0013725	0.01525	0.09				0.067294879	0.403637045	1.85	3.6	1.782705121	3.196362955
92	0.0106	0.8	0.01325	0.003075	0.01025	0.3	0.0013725	0.01525	0.09				0.067294879	0.403637045	1.85	2.8	1.782705121	2.396362955
93	0.0106	0.8	0.01325	0.003075	0.01025	0.3	0.0013725	0.01525	0.09				0.067294879	0.403637045	1.85	1.2	1.782705121	1.603637045
94	0.01013625	0.795	0.01275	0.0025625	0.01025	0.25	0.0012825	0.01425	0.09				0.054624419	0.401157734	3.035206354	0.668310405	2.636502207	0.662278147
95	0.01013625	0.795	0.01275	0.0025625	0.01025	0.25	0.0012825	0.01425	0.09				0.054624419	0.401157734	3.825343923	0.580517342	3.426639776	0.574485084
96	0.01013625	0.795	0.01275	0.0025625	0.01025	0.25	0.0012825	0.01425	0.09				0.054624419	0.401157734	4.615481492	0.492724279	4.216777345	0.486692021
97	0.005068125	0.3975	0.01275	0.00286875	0.225	0.01275							0.19857685	-0.123832249	5	0	4.876167751	0.19857685
98	0.0053	0.4	0.01325	0.00416	0.32	0.013	0.0053	0.4	0.01325	0.005068125	0.3975	0.01275	0.39557391	0.023850315	1.85	0.4	1.873850315	0.79557391
99	0.00495	0.33	0.015	0.0015	0.1	0.015	0.00405	0.3	0.0135	0.00351	0.27	0.013	0.347697002	0.042984475	0	0.47	0.042984475	0.817697002
100	0.0054	0.4	0.0135	0.0054	0.4	0.0135	0.00351	0.27	0.013				0.38840566	0.041518868	0	10	0.041518868	10.39840566
101	0.0040625	0.325	0.0125	0.0043875	0.35	0.0125	0.00285	0.3	0.0095				0.266798173	0.012384275	4.3	13.4	4.312384275	13.41238427
102	0.004375	0.35	0.0125	0.0043875	0.35	0.0125	0.00285	0.3	0.0095				0.267860991	0.002958513	9.9	13.4	9.902958513	13.40295851
103	0.004375	0.35	0.0125	0.0042875	0.35	0.01225	0.00285	0.3	0.0095				0.267522666	0.001614821	15.5	13.4	15.50161482	13.40161482
104	0.0042875	0.35	0.01225	0.003135	0.33	0.0095							0.256771851	-0.099079993	17.6	13.37	17.50092001	13.62677185
105	0.003135	0.33	0.0095	0.0042	0.4	0.0105	0.002625	0.3	0.00875				-0.363364138	0.048910159	17.6	10.73	17.64891016	10.36663586
106	0.0042	0.4	0.0105	0.0042	0.4	0.0105	0.0032375	0.37	0.00875				0.383826864	-0.097864323	18.2	0.4	18.10213568	0.783826864
107	0.00208125	0.225	0.00925	0.0032375	0.37	0.00875							0.198671785	0.153647424	16	0	16.15364742	0.198671785
108	0.0028875	0.33	0.00875	0.0032375	0.35	0.00925	0.00285	0.3	0.0095				-0.190202107	-0.018446629	15.5	12	15.48155337	11.80979789
109	0.00285	0.3	0.0095	0.00225	0.2	0.01125	0.0039375	0.35	0.01125	0.0016125	0.15	0.01075	-0.255777289	0.00277993	9.9	12	9.90277993	11.74422271
110	0.00285	0.3	0.0095	0.0041125	0.35	0.01175	0.0044625	0.35	0.01275				-0.292505662	0.007216943	4.3	12	4.307216943	11.70749434
111	0.00416	0.32	0.013	0.0044625	0.35	0.01275	0.0057	0.4	0.01425	0			0.344073878	0.008967939	1.85	10	1.858967939	10.34407388
112	0.012	0.8	0.015	0.00345	0.0115	0.3	0.001395	0.0155	0.09				0.065864426	0.403726625	0	-0.4	0.065864426	0.003726625
113	0.0028875	0.33	0.00875	0.002625	0.3	0.00875							0.158689168	-0.293883947	17.3	10.4	17.00611605	10.55868917

Table 5: Element's Geometric Characteristics						
Num of Ele	Quantity (ni)	Ai	niAi	zi	Ai*zi	Ai*zi^2
-	-	m^2	m^2	m	m^3	m^4
1	1	0.01306	0.01306	1.8776597	0.0245222	0.0460444
2	2	0.0095775	0.019155	1.215	0.0232733	0.0282771
3	2	0.0095775	0.019155	0.585	0.0112057	0.0065553
4	2	0.015645	0.03129	0.0693588	0.0021702	0.0001505
5	2	0.015645	0.03129	0.0693588	0.0021702	0.0001505
6	2	0.015645	0.03129	0.0693588	0.0021702	0.0001505
7	2	0.015645	0.03129	0.0693588	0.0021702	0.0001505
8	2	0.015645	0.03129	0.0693588	0.0021702	0.0001505
9	2	0.015645	0.03129	0.0693588	0.0021702	0.0001505
10	2	0.015645	0.03129	0.0693588	0.0021702	0.0001505
11	2	0.015645	0.03129	0.0693588	0.0021702	0.0001505
12	2	0.015645	0.03129	0.0693588	0.0021702	0.0001505
13	2	0.015645	0.03129	0.0693588	0.0021702	0.0001505
14	2	0.015645	0.03129	0.0693588	0.0021702	0.0001505
15	2	0.0095775	0.019155	0.585	0.0112057	0.0065553
16	2	0.0095775	0.019155	1.215	0.0232733	0.0282771
17	2	0.015645	0.03129	0.0693588	0.0021702	0.0001505
18	2	0.015645	0.03129	0.0693588	0.0021702	0.0001505
19	2	0.0301922	0.0603845	0.3194041	0.019287	0.0061604
20	2	0.0126575	0.025315	1.6959091	0.0429319	0.0728087
21	2	0.0121825	0.024365	2.3457496	0.0571542	0.1340694
22	2	0.01138	0.02276	2.9957167	0.0681825	0.2042555
23	2	0.01138	0.02276	3.6457167	0.0829765	0.3025089
24	2	0.0080375	0.016075	4.2814829	0.0688248	0.2946724
25	2	0.0080375	0.016075	4.2814829	0.0688248	0.2946724
26	2	0.012005	0.02401	4.9959397	0.1199525	0.5992755
27	2	0.012005	0.02401	5.6959397	0.1367595	0.7789739
28	2	0.012005	0.02401	6.3959397	0.1535665	0.9822022
29	2	0.012005	0.02401	7.0959397	0.1703735	1.2089602
30	2	0.012005	0.02401	7.7959397	0.1871805	1.459248
31	2	0.012005	0.02401	8.4959397	0.2039875	1.7330656
32	2	0.012005	0.02401	9.1959397	0.2207945	2.030413
33	2	0.0080375	0.016075	9.8814829	0.1588448	1.5696225
34	2	0.0080375	0.016075	9.8814829	0.1588448	1.5696225
35	2	0.0113025	0.022605	10.595964	0.2395218	2.5379641
36	2	0.0113025	0.022605	11.295964	0.2553453	2.884371
37	2	0.0113025	0.022605	11.995964	0.2711688	3.2529308
38	2	0.01121	0.02242	12.696719	0.2846604	3.6142534
39	2	0.01121	0.02242	13.396719	0.3003544	4.0237638
40	2	0.01121	0.02242	14.096719	0.3160484	4.4552458
41	2	0.01121	0.02242	14.796719	0.3317424	4.9086994
42	2	0.0080375	0.016075	15.481483	0.2488648	3.8527967
43	2	0.0080375	0.016075	15.481483	0.2488648	3.8527967
44	2	0.01251	0.02502	16.195971	0.4052232	6.5629833
45	2	0.01251	0.02502	16.895971	0.4227372	7.1425556
46	2	0.00944	0.01888	17.535381	0.331068	5.8054035
47	2	0.00944	0.01888	17.535381	0.331068	5.8054035
48	2	0.00944	0.01888	17.535381	0.331068	5.8054035
49	2	0.00944	0.01888	17.535381	0.331068	5.8054035
50	2	0.0134	0.0268	17.719843	0.4748918	8.4150082
51	2	0.0134	0.0268	17.773656	0.476334	8.4661967
52	2	0.01236	0.02472	17.805528	0.4401527	7.8371505
53	2	0.01236	0.02472	17.859341	0.4414829	7.8845942
54	2	0.01236	0.02472	17.913155	0.4428132	7.932181
55	2	0.01236	0.02472	17.966968	0.4441434	7.979911
56	2	0.01236	0.02472	18.020781	0.4454737	8.0277841
57	2	0.01236	0.02472	18.074594	0.446804	8.0758005
58	2	0.01236	0.02472	18.128407	0.4481342	8.12396
59	2	0.01236	0.02472	18.182221	0.4494645	8.1722626
60	2	0.01236	0.02472	18.236034	0.4507948	8.2207085
61	2	0.0102	0.0204	18.180588	0.370884	6.7428893
62	1	0.008875	0.008875	17.465185	0.1550035	2.707165
63	2	0.008875	0.01775	16.739313	0.2971228	4.9736317
64	2	0.008175	0.01635	16.494182	0.2696799	4.4481488
65	2	0.008175	0.01635	15.995427	0.2615252	4.1832077
66	2	0.0090275	0.018055	14.794947	0.2671228	3.9520672
67	2	0.0090275	0.018055	14.094947	0.2544843	3.5869423
68	2	0.0090275	0.018055	13.394947	0.2418458	3.2395112
69	2	0.0100025	0.020005	12.69544	0.2539723	3.2242896
70	2	0.0100775	0.020155	11.995473	0.2417688	2.9001308
71	2	0.0100775	0.020155	11.295473	0.2276603	2.5715305
72	2	0.0100775	0.020155	10.595473	0.2135518	2.2626821
73	2	0.01113	0.02226	9.1956205	0.2046945	1.8822931
74	2	0.01113	0.02226	8.4956205	0.1891125	1.6066282
75	2	0.01113	0.02226	7.7956205	0.1735305	1.352778
76	2	0.011355	0.02271	7.0957073	0.1611435	1.1434272
77	2	0.01148	0.02296	6.3957541	0.1468465	0.9391942
78	2	0.01148	0.02296	5.6957541	0.1307745	0.7448595
79	2	0.01148	0.02296	4.9957541	0.1147025	0.5730255
80	2	0.0129825	0.025965	3.6781324	0.0955027	0.3512716
81	2	0.0129825	0.025965	3.0597881	0.0794474	0.2430922
82	2	0.0129825	0.025965	2.4414438	0.0633921	0.1547682
83	2	0.0158475	0.031695	1.7851275	0.0565796	0.1010018
84	2	0.0158475	0.031695	1.7851275	0.0565796	0.1010018
85	2	0.0158475	0.031695	1.7851275	0.0565796	0.1010018
86	2	0.0153475	0.030695	1.7836492	0.0547491	0.0976532
87	2	0.0150475	0.030095	1.7827051	0.0536505	0.095643
88	2	0.0150475	0.030095	1.7827051	0.0536505	0.095643
89	2	0.0150475	0.030095	1.7827051	0.0536505	0.095643
90	2	0.0150475	0.030095	1.7827051	0.0536505	0.095643
91	2	0.0150475	0.030095	1.7827051	0.0536505	0.095643
92	2	0.0150475	0.030095	1.7827051	0.0536505	0.095643
93	2	0.0150475	0.030095	1.7827051	0.0536505	0.095643
94	2	0.0139813	0.0279625	2.6365022	0.0737232	0.1943714
95	2	0.0139813	0.0279625	3.4266398	0.0958174	0.3283318
96	2	0.0139813	0.0279625	4.2167773	0.1179116	0.4972071
97	2	0.0079369	0.0158738	4.8761678	0.0774031	0.3774303
98	2	0.0198281	0.0396563	1.8738503	0.0743099	0.1392456
99	2	0.01506	0.03012	0.0405105	0.0012202	4.943E-05
100	2	0.01431	0.02862	0.0415189	0.0011883	4.934E-05
101	2	0.0112875	0.022575	4.3123843	0.0973521	0.4198196
102	2	0.0116	0.0232	9.9029585	0.2297486	2.2751912
103	2	0.0115125	0.023025	15.501615	0.3569247	5.5329089
104	2	0.0074225	0.014845	17.50092	0.2598012	4.5467593
105	2	0.00996	0.01992	17.64891	0.3515663	6.2047619
106	2	0.0116375	0.023275	18.102136	0.4213272	7.6269223
107	2	0.0053188	0.0106375	16.153647	0.1718344	2.7757527
108	2	0.008975	0.01795	15.481553	0.2778939	4.302229
109	2	0.01065	0.0213	9.9027799	0.2109292	2.0887856
110	2	0.011425	0.02285	4.3072169	0.0984199	0.4239159
111	2	0.0143225	0.028645	1.8589679	0.0532501	0.0989903
112	1	0.016845	0.016845	0.0658644	0.0011095	7.308E-05
113	2	0.0055125	0.011025	17.006116	0.1874924	3.188518

Table 6: Input Data for MatLab Smith Method Code

Num of Elem	Type of Elem	tp-n50	s	Ap-n50	ReHp	Type of Stiffener	tw-n50	hw	bf	tf	As-n50	ReHs	Zg-stif	Iy-stiff	A-n50	L	Zg-Elem	Yg-Elem
-	-	mm	m	cm^2	N/mm^2	-	mm	mm	mm	mm	cm^2	N/mm^2	mm	cm^4	cm^2	m	m	m
1	Stiffener Element	13.25	0.8	106	235	L Type	10.25	150	90	10.25	24.6	235	105.04688	659.24294	130.6	2.68	1.87765967	0.202817
2	Stiffener Element	13.00	0.63	81.9	235	Flat Bar	9.25	150	0	0	13.875	235	75	260.15625	95.775	2.68	1.215	0.781693
3	Stiffener Element	13	0.63	81.9	235	Flat Bar	9.25	150	0	0	13.875	235	75	260.15625	95.775	2.68	0.585	0.781693
4	Stiffener Element	13.50	0.8	108	235	L Type	11.5	300	90	15.5	48.45	235	195.42028	5062.2348	156.45	2.68	0.06935882	2.4
5	Stiffener Element	13.50	0.8	108	235	L Type	11.5	300	90	15.5	48.45	235	195.42028	5062.2348	156.45	2.68	0.06935882	2.3965
6	Stiffener Element	13.50	0.8	108	235	L Type	11.5	300	90	15.5	48.45	235	195.42028	5062.2348	156.45	2.68	0.06935882	3.1965
7	Stiffener Element	13.50	0.8	108	235	L Type	11.5	300	90	15.5	48.45	235	195.42028	5062.2348	156.45	2.68	0.06935882	3.9965
8	Stiffener Element	13.50	0.8	108	235	L Type	11.5	300	90	15.5	48.45	235	195.42028	5062.2348	156.45	2.68	0.06935882	4.7965
9	Stiffener Element	13.50	0.8	108	235	L Type	11.5	300	90	15.5	48.45	235	195.42028	5062.2348	156.45	2.68	0.06935882	5.5965
10	Stiffener Element	13.50	0.8	108	235	L Type	11.5	300	90	15.5	48.45	235	195.42028	5062.2348	156.45	2.68	0.06935882	6.3965
11	Stiffener Element	13.50	0.8	108	235	L Type	11.5	300	90	15.5	48.45	235	195.42028	5062.2348	156.45	2.68	0.06935882	7.1965
12	Stiffener Element	13.50	0.8	108	235	L Type	11.5	300	90	15.5	48.45	235	195.42028	5062.2348	156.45	2.68	0.06935882	7.9965
13	Stiffener Element	13.50	0.8	108	235	L Type	11.5	300	90	15.5	48.45	235	195.42028	5062.2348	156.45	2.68	0.06935882	8.7965
14	Stiffener Element	13.50	0.8	108	235	L Type	11.5	300	90	15.5	48.45	235	195.42028	5062.2348	156.45	2.68	0.06935882	9.5965
15	Stiffener Element	13.00	0.63	81.9	235	Flat Bar	9.25	150	0	0	13.875	235	75	260.15625	95.775	2.68	0.585	10.38169
16	Stiffener Element	13.00	0.63	81.9	235	Flat Bar	9.25	150	0	0	13.875	235	75	260.15625	95.775	2.68	1.215	10.38169
17	Stiffener Element	13.50	0.8	108	235	L Type	11.5	300	90	15.5	48.45	235	195.42028	5062.2348	156.45	2.68	0.06935882	11.1965
18	Stiffener Element	13.50	0.8	108	235	L Type	11.5	300	90	15.5	48.45	235	195.42028	5062.2348	156.45	2.68	0.06935882	11.9965
19	Hard Corner	0.00	0	301.92225	235	-	0	0	0	0	0	0	0	0	301.92225	0	0.31940415	13.29144
20	Stiffener Element	13.23	0.65	86	235	L Type	9.25	300	90	14.25	40.575	235	199.66428	4248.8914	126.575	2.68	1.69590907	13.62726
21	Stiffener Element	12.5	0.65	81.25	235	L Type	9.25	300	90	14.25	40.575	235	199.66428	4248.8914	121.825	2.68	2.34574956	13.62517
22	Stiffener Element	12.50	0.65	81.25	235	L Type	8.25	250	90	13.25	32.55	235	173.22206	2385.0794	113.8	2.68	2.99571675	13.64242
23	Stiffener Element	12.50	0.65	81.25	235	L Type	8.25	250	90	13.25	32.55	235	173.22206	2385.0794	113.8	2.68	3.64571675	13.64242
24	Stiffener Element	9.50	0.7	66.5	235	Flat Bar	9.25	150	0	0	13.875	235	75	260.15625	80.375	2.68	4.28148289	13.05
25	Stiffener Element	9.50	0.7	66.5	235	Flat Bar	9.25	150	0	0	13.875	235	75	260.15625	80.375	2.68	4.28148289	12.35
26	Stiffener Element	12.50	0.7	87.5	235	L Type	8.25	250	90	13.25	32.55	235	173.22206	2385.0794	120.05	2.68	4.99593974	13.64509
27	Stiffener Element	12.50	0.7	87.5	235	L Type	8.25	250	90	13.25	32.55	235	173.22206	2385.0794	120.05	2.68	5.69593974	13.64509
28	Stiffener Element	12.50	0.7	87.5	235	L Type	8.25	250	90	13.25	32.55	235	173.22206	2385.0794	120.05	2.68	6.39593974	13.64509
29	Stiffener Element	12.50	0.7	87.5	235	L Type	8.25	250	90	13.25	32.55	235	173.22206	2385.0794	120.05	2.68	7.09593974	13.64509
30	Stiffener Element	12.50	0.7	87.5	235	L Type	8.25	250	90	13.25	32.55	235	173.22206	2385.0794	120.05	2.68	7.79593974	13.64509
31	Stiffener Element	12.50	0.7	87.5	235	L Type	8.25	250	90	13.25	32.55	235	173.22206	2385.0794	120.05	2.68	8.49593974	13.64509
32	Stiffener Element	12.50	0.7	87.5	235	L Type	8.25	250	90	13.25	32.55	235	173.22206	2385.0794	120.05	2.68	9.19593974	13.64509
33	Stiffener Element	9.50	0.7	66.5	235	Flat Bar	9.25	150	0	0	13.875	235	75	260.15625	80.375	2.68	9.88148289	13.05
34	Stiffener Element	9.50	0.7	66.5	235	Flat Bar	9.25	150	0	0	13.875	235	75	260.15625	80.375	2.68	9.88148289	12.35
35	Stiffener Element	12.50	0.7	87.5	235	L Type	7.25	200	90	12.25	25.525	235	145.83852	1190.0808	113.025	2.68	10.5959641	13.6594
36	Stiffener Element	12.50	0.7	87.5	235	L Type	7.25	200	90	12.25	25.525	235	145.83852	1190.0808	113.025	2.68	11.2959641	13.6594
37	Stiffener Element	12.50	0.7	87.5	235	L Type	7.25	200	90	12.25	25.525	235	145.83852	1190.0808	113.025	2.68	11.9959641	13.6594
38	Stiffener Element	12.50	0.7	87.5	235	L Type	10.25	150	90	10.25	24.6	235	105.04688	659.24294	112.1	2.68	12.6967186	13.66933
39	Stiffener Element	12.50	0.7	87.5	235	L Type	10.25	150	90	10.25	24.6	235	105.04688	659.24294	112.1	2.68	13.3967186	13.66933
40	Stiffener Element	12.50	0.7	87.5	235	L Type	10.25	150	90	10.25	24.6	235	105.04688	659.24294	112.1	2.68	14.0967186	13.66933
41	Stiffener Element	12.50	0.7	87.5	235	L Type	10.25	150	90	10.25	24.6	235	105.04688	659.24294	112.1	2.68	14.7967186	13.66933
42	Stiffener Element	9.50	0.7	66.5	235	Flat Bar	9.25	150	0	0	13.875	235	75	260.15625	80.375	2.68	15.4814829	13.05
43	Stiffener Element	9.50	0.7	66.5	235	Flat Bar	9.25	150	0	0	13.875	235	75	260.15625	80.375	2.68	15.4814829	12.35
44	Stiffener Element	12.50	0.7	87.5	235	L Type	10	250	90	14	37.6	235	169.23404	2763.8647	125.1	2.68	16.1959712	13.64101
45	Stiffener Element	12.50	0.7	87.5	235	L Type	10	250	90	14	37.6	235	169.23404	2763.8647	125.1	2.68	16.8959712	13.64101
46	Stiffener Element	9.50	0.66	62.7	235	L Type	8	250	90	13	31.7	235	173.5347	2319.777	94.4	2.68	17.5353811	13.04508
47	Stiffener Element	9.50	0.66	62.7	235	L Type	8	250	90	13	31.7	235	173.5347	2319.777	94.4	2.68	17.5353811	12.38508
48	Stiffener Element	9.50	0.66	62.7	235	L Type	8	250	90	13	31.7	235	173.5347	2319.777	94.4	2.68	17.5353811	11.72508
49	Stiffener Element	9.50	0.66	62.7	235	L Type	8	250	90	13	31.7	235	173.5347	2319.777	94.4	2.68	17.5353811	11.06508
50	Stiffener Element	10.50	0.8	84	235	L Type	10	350	100	15	50	235	229.75	7072.8854	134	2.68	17.7198432	9.594963
51	Stiffener Element	10.50	0.8	84	235	L Type	10	350	100	15	50	235	229.75	7072.8854	134	2.68	17.7736564	8.794963
52	Stiffener Element	10.50	0.8	84	235	L Type	9	300	90	14	39.6	235	199.95455	4144.6312	123.6	2.68	17.8055282	7.995871
53	Stiffener Element	10.50	0.8	84	235	L Type	9	300	90	14	39.6	235	199.95455	4144.6312	123.6	2.68	17.8593414	7.195871
54	Stiffener Element	10.50	0.8	84	235	L Type	9	300	90	14	39.6	235	199.95455	4144.6312	123.6	2.68	17.9131546	6.395871
55	Stiffener Element	10.50	0.8	84	235	L Type	9	300	90	14	39.6	235	199.95455	4144.6312	123.6	2.68	17.9669678	5.595871
56	Stiffener Element	10.50	0.8	84	235	L Type	9	300	90	14	39.6	235	199.95455	4144.6312	123.6	2.68	18.020781	4.795871
57	Stiffener Element	10.50	0.8	84	235	L Type	9	300	90	14	39.6	235	199.95455	4144.6312	123.6	2.68	18.0745943	3.995871
58	Stiffener Element	10.50	0.8	84	235	L Type	9	300	90	14	39.6	235	199.95455	4144.6312	123.6	2.68	18.1284075	3.195871
59	Stiffener Element	10.50	0.8	84	235	L Type	9	300	90	14	39.6	235	199.95455	4144.6312	123.6	2.68	18.1822207	2.395871
60	Stiffener Element	10.50	0.8	84	235	L Type	9	300	90	14	39.6	235	199.95455	4144.6312	123.6	2.68	18.2360339	1.595871
61	Stiffener Element	10.50	0.8	84	235	Flat Bar	12	150	0	0	18	235	75	337.5	102	2.68	18.1805882	0
62	Stiffener Element	8.75	0.74	64.75	315	L Type	10	150	90	10	24	315	105	642	88.75	2.68	17.4651846	0.836533
63	Stiffener Element	8.75	0.74	64.75	315	L Type	10	150	90	10	24	315	105	642	88.75	2.68	16.7393131	0.721053
64	Stiffener Element	8.75	0.66	57.75	235	L Type	10	150	90	10	24	235	105	642	81.75	2.68	16.4941818	9.295469
65	Stiffener Element	8.75	0.66	57.75	235	L Type	10	150	90	10	24	235	105	642	81.75	2.68	15.995427	9.727724
66	Stiffener Element	9.25	0.7	64.75	235	L Type	7.25	200	90	12.25	25.525	235	145.83852	1190.0808	90.275	2.68	14.794947	11.74717
67	Stiffener Element	9.25	0.7	64.75	235	L Type	7.25	200	90	12.25	25.525	235	145.83852	1190.0808	90.275	2.68	14.094947	11.74717
68	Stiffener Element	9.25	0.7	64.75	235	L Type	7.25	200	90	12.25	25.525	235	145.83852	1190.0808	90.275	2.68	13.394947	11.74717
69	Stiffener Element	10.64	0.7	74.5	235	L Type	7.25	200	90	12.25	25.525	235	145.83852	1190.0808	100.025	2.68	12.6954395	11.7439
70	Stiffener Element	10.75	0.7	75.25	235	L Type	7.25	200	90	12.25	25.525	235	145.83852	1190.0808	100.775	2.68	11.9954735	11.74368
71	Stiffener Element	10.75	0.7	75.25	235	L Type	7.25	200	90	12.25	25.525	235	145.83852	1190.0808	100.775	2.68	11.2954735	11.74368
72	Stiffener Element	10.75	0.7	75.25	235	L Type	7.25	200	90	12.25	25.525	235	145.83852	1190.0808	100.775	2.68	10.5954735	11.74368
73	Stiffener Element	11.25	0.7	78.75	235	L Type	8.25	250	90	13.25	32.55	235	173.22206	2385.0794	111.3	2.68	9.19562054	11.75793

74	Stiffener Element	11.25	0.7	78.75	235	L Type	8.25	250	90	13.25	32.55	235	173.22206	2385.0794	111.3	2.68	8.49562054	11.75793
75	Stiffener Element	11.25	0.7	78.75	235	L Type	8.25	250	90	13.25	32.55	235	173.22206	2385.0794	111.3	2.68	7.79562054	11.75793
76	Stiffener Element	11.57	0.7	81	235	L Type	8.25	250	90	13.25	32.55	235	173.22206	2385.0794	113.55	2.68	7.09570732	11.7571
77	Stiffener Element	11.75	0.7	82.25	235	L Type	8.25	250	90	13.25	32.55	235	173.22206	2385.0794	114.8	2.68	6.39575406	11.75666
78	Stiffener Element	11.75	0.7	82.25	235	L Type	8.25	250	90	13.25	32.55	235	173.22206	2385.0794	114.8	2.68	5.69575406	11.75666
79	Stiffener Element	11.75	0.7	82.25	235	L Type	8.25	250	90	13.25	32.55	235	173.22206	2385.0794	114.8	2.68	4.99575406	11.75666
80	Stiffener Element	12.75	0.7	89.25	235	L Type	9.25	300	90	14.25	40.575	235	199.66428	4248.8914	129.825	2.68	3.67813243	11.50278
81	Stiffener Element	12.75	0.7	89.25	235	L Type	9.25	300	90	14.25	40.575	235	199.66428	4248.8914	129.825	2.68	3.05978812	11.17468
82	Stiffener Element	12.75	0.7	89.25	235	L Type	9.25	300	90	14.25	40.575	235	199.66428	4248.8914	129.825	2.68	2.4414438	10.84658
83	Stiffener Element	14.25	0.8	114	235	L Type	10.25	300	90	15.25	44.475	235	198.64313	4666.6272	158.475	2.68	1.78512748	9.596547
84	Stiffener Element	14.25	0.8	114	235	L Type	10.25	300	90	15.25	44.475	235	198.64313	4666.6272	158.475	2.68	1.78512748	8.796547
85	Stiffener Element	14.25	0.8	114	235	L Type	10.25	300	90	15.25	44.475	235	198.64313	4666.6272	158.475	2.68	1.78512748	7.996547
86	Stiffener Element	13.63	0.8	109	235	L Type	10.25	300	90	15.25	44.475	235	198.64313	4666.6272	153.475	2.68	1.78364921	7.196434
87	Stiffener Element	13.25	0.8	106	235	L Type	10.25	300	90	15.25	44.475	235	198.64313	4666.6272	150.475	2.68	1.78270512	6.396363
88	Stiffener Element	13.25	0.8	106	235	L Type	10.25	300	90	15.25	44.475	235	198.64313	4666.6272	150.475	2.68	1.78270512	5.596363
89	Stiffener Element	13.25	0.8	106	235	L Type	10.25	300	90	15.25	44.475	235	198.64313	4666.6272	150.475	2.68	1.78270512	4.796363
90	Stiffener Element	13.25	0.8	106	235	L Type	10.25	300	90	15.25	44.475	235	198.64313	4666.6272	150.475	2.68	1.78270512	3.996363
91	Stiffener Element	13.25	0.8	106	235	L Type	10.25	300	90	15.25	44.475	235	198.64313	4666.6272	150.475	2.68	1.78270512	3.196363
92	Stiffener Element	13.25	0.8	106	235	L Type	10.25	300	90	15.25	44.475	235	198.64313	4666.6272	150.475	2.68	1.78270512	2.396363
93	Stiffener Element	13.25	0.8	106	235	L Type	10.25	300	90	15.25	44.475	235	198.64313	4666.6272	150.475	2.68	1.78270512	1.603637
94	Stiffener Element	12.75	0.795	101.3625	315	L Type	10.25	250	90	14.25	38.45	315	169.0703	2828.8953	139.8125	2.68	2.63650221	0.662278
95	Stiffener Element	12.75	0.795	101.3625	315	L Type	10.25	250	90	14.25	38.45	315	169.0703	2828.8953	139.8125	2.68	3.42663978	0.574485
96	Stiffener Element	12.75	0.795	101.3625	315	L Type	10.25	250	90	14.25	38.45	315	169.0703	2828.8953	139.8125	2.68	4.21677735	0.486692
97	Hard Corner	0.00	0	79.36875	315	-	0	0	0	0	0	0	0	0	79.36875	0	4.87616775	0.198577
98	Hard Corner	0.00	0	198.28125	255.448227	-	0	0	0	0	0	0	0	0	198.28125	0	1.87385031	0.795574
99	Hard Corner	0.00	0	150.6	274.8406375	-	0	0	0	0	0	0	0	0	150.6	0	0.04051046	0.861015
100	Hard Corner	0.00	0	143.1	235	-	0	0	0	0	0	0	0	0	143.1	0	0.04151887	10.39841
101	Hard Corner	0.00	0	112.875	235	-	0	0	0	0	0	0	0	0	112.875	0	4.31238427	13.41238
102	Hard Corner	0.00	0	116	235	-	0	0	0	0	0	0	0	0	116	0	9.90295851	13.40296
103	Hard Corner	0.00	0	115.125	235	-	0	0	0	0	0	0	0	0	115.125	0	15.5016148	13.40161
104	Hard Corner	0.00	0	74.225	235	-	0	0	0	0	0	0	0	0	74.225	0	17.50092	13.62677
105	Hard Corner	0.00	0	99.6	235	-	0	0	0	0	0	0	0	0	99.6	0	17.6489102	10.36664
106	Hard Corner	0.00	0	116.375	257.2556391	-	0	0	0	0	0	0	0	0	116.375	0	18.1021357	0.783827
107	Hard Corner	0.00	0	53.1875	315	-	0	0	0	0	0	0	0	0	53.1875	0	16.1536474	0.198672
108	Hard Corner	0.00	0	89.75	235	-	0	0	0	0	0	0	0	0	89.75	0	15.4815534	11.8098
109	Hard Corner	0.00	0	106.5	235	-	0	0	0	0	0	0	0	0	106.5	0	9.90277993	11.74422
110	Hard Corner	0.00	0	114.25	235	-	0	0	0	0	0	0	0	0	114.25	0	4.30721694	11.70749
111	Hard Corner	0.00	0	143.225	235	-	0	0	0	0	0	0	0	0	143.225	0	1.85896794	10.34407
112	Stiffener Element	15.00	0.8	120	315	L Type	11.5	300	90	15.5	48.45	235	195.42028	5062.2348	168.45	2.68	0.06586443	0.003727
113	Hard Corner	0.00	0	55.125	235	-	0	0	0	0	0	0	0	0	55.125	0	17.0061161	10.55869
114	Stiffener Element	13.00	0.63	81.9	235	Flat Bar	9.25	150	0	0	13.875	235	75	260.15625	95.775	2.68	1.215	0.781693
115	Stiffener Element	13.00	0.63	81.9	235	Flat Bar	9.25	150	0	0	13.875	235	75	260.15625	95.775	2.68	0.585	0.781693
116	Stiffener Element	13.50	0.8	108	235	L Type	11.5	300	90	15.5	48.45	235	195.42028	5062.2348	156.45	2.68	0.06935882	2.4
117	Stiffener Element	13.50	0.8	108	235	L Type	11.5	300	90	15.5	48.45	235	195.42028	5062.2348	156.45	2.68	0.06935882	2.3965
118	Stiffener Element	13.50	0.8	108	235	L Type	11.5	300	90	15.5	48.45	235	195.42028	5062.2348	156.45	2.68	0.06935882	3.1965
119	Stiffener Element	13.50	0.8	108	235	L Type	11.5	300	90	15.5	48.45	235	195.42028	5062.2348	156.45	2.68	0.06935882	3.9965
120	Stiffener Element	13.50	0.8	108	235	L Type	11.5	300	90	15.5	48.45	235	195.42028	5062.2348	156.45	2.68	0.06935882	4.7965
121	Stiffener Element	13.50	0.8	108	235	L Type	11.5	300	90	15.5	48.45	235	195.42028	5062.2348	156.45	2.68	0.06935882	5.5965
122	Stiffener Element	13.50	0.8	108	235	L Type	11.5	300	90	15.5	48.45	235	195.42028	5062.2348	156.45	2.68	0.06935882	6.3965
123	Stiffener Element	13.50	0.8	108	235	L Type	11.5	300	90	15.5	48.45	235	195.42028	5062.2348	156.45	2.68	0.06935882	7.1965
124	Stiffener Element	13.50	0.8	108	235	L Type	11.5	300	90	15.5	48.45	235	195.42028	5062.2348	156.45	2.68	0.06935882	7.9965
125	Stiffener Element	13.50	0.8	108	235	L Type	11.5	300	90	15.5	48.45	235	195.42028	5062.2348	156.45	2.68	0.06935882	8.7965
126	Stiffener Element	13.50	0.8	108	235	L Type	11.5	300	90	15.5	48.45	235	195.42028	5062.2348	156.45	2.68	0.06935882	9.5965
127	Stiffener Element	13.00	0.63	81.9	235	Flat Bar	9.25	150	0	0	13.875	235	75	260.15625	95.775	2.68	0.585	10.38169
128	Stiffener Element	13.00	0.63	81.9	235	Flat Bar	9.25	150	0	0	13.875	235	75	260.15625	95.775	2.68	1.215	10.38169
129	Stiffener Element	13.50	0.8	108	235	L Type	11.5	300	90	15.5	48.45	235	195.42028	5062.2348	156.45	2.68	0.06935882	11.1965
130	Stiffener Element	13.50	0.8	108	235	L Type	11.5	300	90	15.5	48.45	235	195.42028	5062.2348	156.45	2.68	0.06935882	11.9965
131	Hard Corner	0.00	0	301.92225	235	-	0	0	0	0	0	0	0	0	301.92225	0	0.31940415	13.29144
132	Stiffener Element	13.23	0.65	86	235	L Type	9.25	300	90	14.25	40.575	235	199.66428	4248.8914	126.575	2.68	1.69590907	13.62726
133	Stiffener Element	12.50	0.65	81.25	235	L Type	9.25	300	90	14.25	40.575	235	199.66428	4248.8914	121.825	2.68	2.34574956	13.62517
134	Stiffener Element	12.50	0.65	81.25	235	L Type	8.25	250	90	13.25	32.55	235	173.22206	2385.0794	113.8	2.68	2.99571675	13.64242
135	Stiffener Element	12.50	0.65	81.25	235	L Type	8.25	250	90	13.25	32.55	235	173.22206	2385.0794	113.8	2.68	3.64571675	13.64242
136	Stiffener Element	9.50	0.7	66.5	235	Flat Bar	9.25	150	0	0	13.875	235	75	260.15625	80.375	2.68	4.28148289	13.05
137	Stiffener Element	9.50	0.7	66.5	235	Flat Bar	9.25	150	0	0	13.875	235	75	260.15625	80.375	2.68	4.28148289	12.35
138	Stiffener Element	12.50	0.7	87.5	235	L Type	8.25	250	90	13.25	32.55	235	173.22206	2385.0794	120.05	2.68	4.99593974	13.64509
139	Stiffener Element	12.50	0.7	87.5	235	L Type	8.25	250	90	13.25	32.55	235	173.22206	2385.0794	120.05	2.68	5.69593974	13.64509
140	Stiffener Element	12.50	0.7	87.5	235	L Type	8.25	250	90	13.25	32.55	235	173.22206	2385.0794	120.05	2.68	6.39593974	13.64509
141	Stiffener Element	12.50	0.7	87.5	235	L Type	8.25	250	90	13.25	32.55	235	173.22206	2385.0794	120.05	2.68	7.09593974	13.64509
142	Stiffener Element	12.50	0.7	87.5	235	L Type	8.25	250	90	13.25	32.55	235	173.22206	2385.0794	120.05	2.68	7.79593974	13.64509
143	Stiffener Element	12.50	0.7	87.5	235	L Type	8.25	250	90	13.25	32.55	235	173.22206	2385.0794	120.05	2.68	8.49593974	13.64509
144	Stiffener Element	12.50	0.7	87.5	235	L Type	8.25	250	90	13.25	32.55	235	173.22206	2385.0794	120.05	2.68	9.19593974	13.64509
145	Stiffener Element	9.50	0.7	66.5	235	Flat Bar	9.25	150	0	0	13.875	235	75	260.15625	80.375	2.68	9.88148289	13.05
146	Stiffener Element	9.50	0.7	66.5	235	Flat Bar	9.25	150	0	0	13.875	235	75	260.15625	80.375	2.68	9.88148289	12.35
147	Stiffener Element	12.50	0.7	87.5	235	L Type	7.25	200	90	12.25	25.525	235	145.83852	1190.0808	113.025	2.68	10.5959641	13.6594
148	Stiffener Element	12.50	0.7	87.5	235	L Type	7.25	200	90	12.25	25.525	235	145.83852	1190.0808	113.025	2.68	11.2959641	13.6594
149	Stiffener Element	12.50	0.7	87.5	235	L Type	7.25	200	90	12.25	25.525	235	145.83852	1190.0808	113.025	2.68	11.9959641	13.6594

150	Stiffener Element	12.50	0.7	87.5	235	L Type	10.25	150	90	10.25	24.6	235	105.04688	659.24294	112.1	2.68	12.6967186	13.66933
151	Stiffener Element	12.50	0.7	87.5	235	L Type	10.25	150	90	10.25	24.6	235	105.04688	659.24294	112.1	2.68	13.3967186	13.66933
152	Stiffener Element	12.50	0.7	87.5	235	L Type	10.25	150	90	10.25	24.6	235	105.04688	659.24294	112.1	2.68	14.0967186	13.66933
153	Stiffener Element	12.50	0.7	87.5	235	L Type	10.25	150	90	10.25	24.6	235	105.04688	659.24294	112.1	2.68	14.7967186	13.66933
154	Stiffener Element	9.50	0.7	66.5	235	Flat Bar	9.25	150	0	0	13.875	235	75	260.15625	80.375	2.68	15.4814829	13.05
155	Stiffener Element	9.50	0.7	66.5	235	Flat Bar	9.25	150	0	0	13.875	235	75	260.15625	80.375	2.68	15.4814829	12.35
156	Stiffener Element	12.50	0.7	87.5	235	L Type	10	250	90	14	37.6	235	169.23404	2763.8647	125.1	2.68	16.1959712	13.64101
157	Stiffener Element	12.50	0.7	87.5	235	L Type	10	250	90	14	37.6	235	169.23404	2763.8647	125.1	2.68	16.8959712	13.64101
158	Stiffener Element	9.50	0.66	62.7	235	L Type	8	250	90	13	31.7	235	173.5347	2319.777	94.4	2.68	17.5353811	13.04508
159	Stiffener Element	9.50	0.66	62.7	235	L Type	8	250	90	13	31.7	235	173.5347	2319.777	94.4	2.68	17.5353811	12.38508
160	Stiffener Element	9.50	0.66	62.7	235	L Type	8	250	90	13	31.7	235	173.5347	2319.777	94.4	2.68	17.5353811	11.72508
161	Stiffener Element	9.50	0.66	62.7	235	L Type	8	250	90	13	31.7	235	173.5347	2319.777	94.4	2.68	17.5353811	11.06508
162	Stiffener Element	10.50	0.8	84	235	L Type	10	350	100	15	50	235	229.75	7072.8854	134	2.68	17.7198432	9.594963
163	Stiffener Element	10.50	0.8	84	235	L Type	10	350	100	15	50	235	229.75	7072.8854	134	2.68	17.7736564	8.794963
164	Stiffener Element	10.50	0.8	84	235	L Type	9	300	90	14	39.6	235	199.95455	4144.6312	123.6	2.68	17.8055282	7.995871
165	Stiffener Element	10.50	0.8	84	235	L Type	9	300	90	14	39.6	235	199.95455	4144.6312	123.6	2.68	17.8593414	7.195871
166	Stiffener Element	10.50	0.8	84	235	L Type	9	300	90	14	39.6	235	199.95455	4144.6312	123.6	2.68	17.9131546	6.395871
167	Stiffener Element	10.50	0.8	84	235	L Type	9	300	90	14	39.6	235	199.95455	4144.6312	123.6	2.68	17.9669678	5.595871
168	Stiffener Element	10.50	0.8	84	235	L Type	9	300	90	14	39.6	235	199.95455	4144.6312	123.6	2.68	18.020781	4.795871
169	Stiffener Element	10.50	0.8	84	235	L Type	9	300	90	14	39.6	235	199.95455	4144.6312	123.6	2.68	18.0745943	3.995871
170	Stiffener Element	10.50	0.8	84	235	L Type	9	300	90	14	39.6	235	199.95455	4144.6312	123.6	2.68	18.1284075	3.195871
171	Stiffener Element	10.50	0.8	84	235	L Type	9	300	90	14	39.6	235	199.95455	4144.6312	123.6	2.68	18.1822207	2.395871
172	Stiffener Element	10.50	0.8	84	235	L Type	9	300	90	14	39.6	235	199.95455	4144.6312	123.6	2.68	18.2360339	1.595871
173	Stiffener Element	8.75	0.74	64.75	315	L Type	10	150	90	10	24	315	105	642	88.75	2.68	17.4651846	0.836533
174	Stiffener Element	8.75	0.74	64.75	315	L Type	10	150	90	10	24	315	105	642	88.75	2.68	16.7393131	0.721053
175	Stiffener Element	8.75	0.66	57.75	235	L Type	10	150	90	10	24	235	105	642	81.75	2.68	16.4941818	9.295469
176	Stiffener Element	8.75	0.66	57.75	235	L Type	10	150	90	10	24	235	105	642	81.75	2.68	15.995427	9.727724
177	Stiffener Element	9.25	0.7	64.75	235	L Type	7.25	200	90	12.25	25.525	235	145.83852	1190.0808	90.275	2.68	14.794947	11.74717
178	Stiffener Element	9.25	0.7	64.75	235	L Type	7.25	200	90	12.25	25.525	235	145.83852	1190.0808	90.275	2.68	14.094947	11.74717
179	Stiffener Element	9.25	0.7	64.75	235	L Type	7.25	200	90	12.25	25.525	235	145.83852	1190.0808	90.275	2.68	13.394947	11.74717
180	Stiffener Element	10.64	0.7	74.5	235	L Type	7.25	200	90	12.25	25.525	235	145.83852	1190.0808	100.025	2.68	12.6954395	11.7439
181	Stiffener Element	10.75	0.7	75.25	235	L Type	7.25	200	90	12.25	25.525	235	145.83852	1190.0808	100.775	2.68	11.9954735	11.74368
182	Stiffener Element	10.75	0.7	75.25	235	L Type	7.25	200	90	12.25	25.525	235	145.83852	1190.0808	100.775	2.68	11.2954735	11.74368
183	Stiffener Element	10.75	0.7	75.25	235	L Type	7.25	200	90	12.25	25.525	235	145.83852	1190.0808	100.775	2.68	10.5954735	11.74368
184	Stiffener Element	11.25	0.7	78.75	235	L Type	8.25	250	90	13.25	32.55	235	173.22206	2385.0794	111.3	2.68	9.19562054	11.75793
185	Stiffener Element	11.25	0.7	78.75	235	L Type	8.25	250	90	13.25	32.55	235	173.22206	2385.0794	111.3	2.68	8.49562054	11.75793
186	Stiffener Element	11.25	0.7	78.75	235	L Type	8.25	250	90	13.25	32.55	235	173.22206	2385.0794	111.3	2.68	7.79562054	11.75793
187	Stiffener Element	11.57	0.7	81	235	L Type	8.25	250	90	13.25	32.55	235	173.22206	2385.0794	113.55	2.68	7.09570732	11.7571
188	Stiffener Element	11.75	0.7	82.25	235	L Type	8.25	250	90	13.25	32.55	235	173.22206	2385.0794	114.8	2.68	6.39575406	11.75666
189	Stiffener Element	11.75	0.7	82.25	235	L Type	8.25	250	90	13.25	32.55	235	173.22206	2385.0794	114.8	2.68	5.69575406	11.75666
190	Stiffener Element	11.75	0.7	82.25	235	L Type	8.25	250	90	13.25	32.55	235	173.22206	2385.0794	114.8	2.68	4.99575406	11.75666
191	Stiffener Element	12.75	0.7	89.25	235	L Type	9.25	300	90	14.25	40.575	235	199.66428	4248.8914	129.825	2.68	3.67813243	11.50278
192	Stiffener Element	12.75	0.7	89.25	235	L Type	9.25	300	90	14.25	40.575	235	199.66428	4248.8914	129.825	2.68	3.05978812	11.17468
193	Stiffener Element	12.75	0.7	89.25	235	L Type	9.25	300	90	14.25	40.575	235	199.66428	4248.8914	129.825	2.68	2.4414438	10.84658
194	Stiffener Element	14.25	0.8	114	235	L Type	10.25	300	90	15.25	44.475	235	198.64313	4666.6272	158.475	2.68	1.78512748	9.596547
195	Stiffener Element	14.25	0.8	114	235	L Type	10.25	300	90	15.25	44.475	235	198.64313	4666.6272	158.475	2.68	1.78512748	8.796547
196	Stiffener Element	14.25	0.8	114	235	L Type	10.25	300	90	15.25	44.475	235	198.64313	4666.6272	158.475	2.68	1.78512748	7.996547
197	Stiffener Element	13.63	0.8	109	235	L Type	10.25	300	90	15.25	44.475	235	198.64313	4666.6272	153.475	2.68	1.78364921	7.196434
198	Stiffener Element	13.25	0.8	106	235	L Type	10.25	300	90	15.25	44.475	235	198.64313	4666.6272	150.475	2.68	1.78270512	6.396363
199	Stiffener Element	13.25	0.8	106	235	L Type	10.25	300	90	15.25	44.475	235	198.64313	4666.6272	150.475	2.68	1.78270512	5.596363
200	Stiffener Element	13.25	0.8	106	235	L Type	10.25	300	90	15.25	44.475	235	198.64313	4666.6272	150.475	2.68	1.78270512	4.796363
201	Stiffener Element	13.25	0.8	106	235	L Type	10.25	300	90	15.25	44.475	235	198.64313	4666.6272	150.475	2.68	1.78270512	3.996363
202	Stiffener Element	13.25	0.8	106	235	L Type	10.25	300	90	15.25	44.475	235	198.64313	4666.6272	150.475	2.68	1.78270512	3.196363
203	Stiffener Element	13.25	0.8	106	235	L Type	10.25	300	90	15.25	44.475	235	198.64313	4666.6272	150.475	2.68	1.78270512	2.396363
204	Stiffener Element	13.25	0.8	106	235	L Type	10.25	300	90	15.25	44.475	235	198.64313	4666.6272	150.475	2.68	1.78270512	1.603637
205	Stiffener Element	12.75	0.795	101.3625	315	L Type	10.25	250	90	14.25	38.45	315	169.0703	2828.8953	139.8125	2.68	2.63650221	0.662278
206	Stiffener Element	12.75	0.795	101.3625	315	L Type	10.25	250	90	14.25	38.45	315	169.0703	2828.8953	139.8125	2.68	3.42663978	0.574485
207	Stiffener Element	12.75	0.795	101.3625	315	L Type	10.25	250	90	14.25	38.45	315	169.0703	2828.8953	139.8125	2.68	4.21677735	0.486692
208	Hard Corner	0.00	0	79.36875	315	-	0	0	0	0	0	0	0	0	79.36875	0	4.87616775	0.198577
209	Hard Corner	0.00	0	198.28125	255.448227	-	0	0	0	0	0	0	0	0	198.28125	0	1.87385031	0.795574
210	Hard Corner	0.00	0	150.6	274.8406375	-	0	0	0	0	0	0	0	0	150.6	0	0.04051046	0.861015
211	Hard Corner	0.00	0	143.1	235	-	0	0	0	0	0	0	0	0	143.1	0	0.04151887	10.39841
212	Hard Corner	0.00	0	112.875	235	-	0	0	0	0	0	0	0	0	112.875	0	4.31238427	13.41238
213	Hard Corner	0.00	0	116	235	-	0	0	0	0	0	0	0	0	116	0	9.90295851	13.40296
214	Hard Corner	0.00	0	115.125	235	-	0	0	0	0	0	0	0	0	115.125	0	15.5016148	13.40161
215	Hard Corner	0.00	0	74.225	235	-	0	0	0	0	0	0	0	0	74.225	0	17.50092	13.62677
216	Hard Corner	0.00	0	99.6	235	-	0	0	0	0	0	0	0	0	99.6	0	17.6489102	10.36664
217	Hard Corner	0.00	0	116.375	257.2556391	-	0	0	0	0	0	0	0	0	116.375	0	18.1021357	0.783827
218	Hard Corner	0.00	0	53.1875	315	-	0	0	0	0	0	0	0	0	53.1875	0	16.1536474	0.198672
219	Hard Corner	0.00	0	89.75	235	-	0	0	0	0	0	0	0	0	89.75	0	15.4815534	11.8098
220	Hard Corner	0.00	0	106.5	235	-	0	0	0	0	0	0	0	0	106.5	0	9.90277993	11.74422
221	Hard Corner	0.00	0	114.25	235	-	0	0	0	0	0	0	0	0	114.25	0	4.30721694	11.70749
222	Hard Corner	0	0	143.225	235	-	0	0	0	0	0	0	0	0	143.225	0	1.85896794	10.34407
223	Hard Corner	0	0	55.125	235	-	0	0	0	0	0	0	0	0	55.125	0	17.0061161	10.55869

Appendix F: Smith Method (MatLab Code)

```
%%%%% Smith's Method 35000 DWT Oil/Chemical Carrier
%%%%% Ship DATA: LOA = 183m, LBP = 174.5m, Lscant = 172.66m, B = 27.4m,
%%%%% DEPTH = 17.6m, DRAFTdesign = 9.8m, DRAFTscant = 11m, CB = 0.828, V = 14.2kn

clear all
close all
clc

%-------------------------------------------------------------------------%
%% INPUT DATA %%
%-------------------------------------------------------------------------%
% Geometry
zdeck=17.6;        % (m) Deck position relative to base line
zn(1,1)=0;
zn(1,2)=0;
zn(2,1)=7.295;     % (m) Initial position of neutral axis for hogging
zn(2,2)=7.295;     % (m) Initial position of neutral axis for sagging
IyyNA=139.0749;    % (m^4) Moment of inertia about neutral axis
ZB=19.06;          % Section Modulus at bottom in m^3
ZD=13.49;          % Section Modulus at deck in m^3

% Material
E=210000;          % (MPa) Young's Modulus (MPa)
ReH=235;           % (MPa) Minimum yield stress

%-------------------------------------------------------------------------%
%% INPUT DATA - EXCEL FILE READING FOR ELEMENTS %%
%-------------------------------------------------------------------------%
% EXCEL file contains the data of midship elements
% ALL elements of section are inserted
% Total number of elements = 223
% ALL thicknesses and areas refer to net thickness/areas

[num,txt]=xlsread('ShipElements.xlsx'); % Reading Excel file
NoE=num(:,1);                           % Number of element
ToE=txt(4:226,2);                       % Type of element
tp=num(:,3);                            % (mm) Plate's thickness
s=num(:,4);                             % (m) Plate's width
Ap=num(:,5);                            % (cm^2) Plate's area
ReHp=num(:,6);                          % (MPa) Plate's yield stress
ToS=txt(4:226,7);                       % Type of stiffener
tw=num(:,8);                            % (mm) Web's thickness
hw=num(:,9);                            % (mm) Web's height
bf=num(:,10);                           % (mm) Flange's width
tf=num(:,11);                           % (mm) Flange's thickness
As=num(:,12);                           % (cm^2) Stiffener's area
ReHs=num(:,13);                         % (MPa) Stiffener's yield stress
zsc=num(:,14);                          % (mm) Vertical distance of stiffener CG from its
bottom
IyyS=num(:,15);                         % (cm^4) Stiffener's second moment of inertia
A=num(:,16);                            % (cm^2) element's total area
l=num(:,17);                            % (m) Element's unsupported length
z=num(:,18);                            % (m) Distance from BL to element's CG

%-------------------------------------------------------------------------%
%% INITIALIZATION OF PARAMETERS & PRIMARY CAlCULATIONS %%
%-------------------------------------------------------------------------%
% Initializations
i = 2;
x(1,1)=0;              % First curvature step for hooging
x(1,2)=0;              % First curvature step for sagging
Mhog(1)=0;             % Initialization of hogging moment
Msag(1)=0;             % Initialization of sagging moment
```

```
% Primary Calculations
My1=10^3*ReH*ZB;                                % (kNm) Yield moment bottom
My2=10^3*ReH*ZD;                                % (kNm) Yield moment deck
My=min(My1,My2);                                % (kNm) Yield moment, lesser of the values My1
& My2
xFhog=0.003*My/(E*IyyNA);       % Curvature's critical value of termination for hogging
xFsag=-0.003*My/(E*IyyNA);      % Curvature's critical value of termination for sagging
dxhog=0.01*(ReH/E)*(1/(zdeck-zn(2,1)));     % Initial incremental step of curvature for
hogging
dxsag=0.01*(ReH/E)*(1/(zdeck-zn(2,2)));     % Initial incremental step of curvature for
sagging

%-------------------------------------------------------------------------%
%% ITERATIVE RPOCESS INITIALIZATION %%
%-------------------------------------------------------------------------%
% While loop for curvature (update/termination)
while (x(i-1,1)+dxhog<=xFhog) && (x(i-1,2)-dxsag>=xFsag)

    % Curvature increment and for loop for the 2 states (hogging, sagging)
    for j=1:2                    % j=1 refers to hogging, j=2 refers to sagging
    if j==1 && (x(i-1,1)+dxhog<=xFhog)
    x(i,j)=x(i-1,j)+dxhog;       % Curvature increment for hogging
    elseif j==2 && (x(i-1,2)-dxsag>=xFsag)
    x(i,j)=x(i-1,j)-dxsag ;      % Curvature increment for sagging
    else
        if j==1
        j=2;
        x(i,j)=x(i-1,j)-dxsag;
        else
        break
        end
    end

% Initial values for the forces over & under the NA
force_over=1000;
force_under=0;

% While loop for force equilibrium (termination)
while abs(force_over-force_under)>=10

    % Calculation for each element the corresponding strain
    for k=1:1:size(NoE,1)
    eE(i,j,k)=-x(i,j)*(z(k)-zn(i,j));
    end

%-------------------------------------------------------------------------%
%% STRESS - STRAIN CURVE FOR EACH STRUCTURAL ELEMENT %%
%-------------------------------------------------------------------------%

% Element type
for k=1:1:size(NoE,1)
HARD_CORNER = strcmp(ToE(k),'Hard Corner');
STIFFENER_ELEMENT = strcmp(ToE(k),'Stiffener Element');
L_TYPE = strcmp(ToS(k),'L Type');
FLAT_BAR = strcmp(ToS(k),'Flat Bar');
STIFFENED_PLATE_ELEMENT = strcmp(ToE(k),'Stiffened Plate Element');

%%%%%%%%%%%%%%%%%%%%%%%%%%%%%%%%%%%%%%%%%%%%%%%%%%%%%%%%%%%%%%%%%%%%%%%%%%%%
if HARD_CORNER==1             % HARD CORNER %
%%%%%%%%%%%%%%%%%%%%%%%%%%%%%%%%%%%%%%%%%%%%%%%%%%%%%%%%%%%%%%%%%%%%%%%%%%%%

%----- Elasto-plastic collapse of hard corners (structural elements) ------%
%-------------------------------------------------------------------------%

ey(k)=ReHp(k)/E;             % Strain at yield stress in the element
```

```
e(k)=eE(i,j,k)/ey(k);       % Relative strain of element
    if e(k)<-1              % Edge function
    F(k)=-1;
    elseif (e(k)>=-1) && (e(k)<=1)
    F(k)=e(k);
    else
    F(k)=1;
    end
stress(i,j,k)=F(k)*ReHp(k); % (MPa) Stress formula


%%%%%%%%%%%%%%%%%%%%%%%%%%%%%%%%%%%%%%%%%%%%%%%%%%%%%%%%%%%%%%%%%%%%%%%%%%%%%%%
elseif STIFFENER_ELEMENT==1 % STIFFENER ELEMENT %
%%%%%%%%%%%%%%%%%%%%%%%%%%%%%%%%%%%%%%%%%%%%%%%%%%%%%%%%%%%%%%%%%%%%%%%%%%%%%%%

%------------ Elasto-plastic collapse of structural elements --------------%
%--------------------------------------------------------------------------%
% When element in tension

ReHA(k)=(ReHp(k)*Ap(k)+ReHs(k)*As(k))/(Ap(k)+As(k)); % (MPa) Equivalent minimum yield
stress
ey(k)=ReHA(k)/E;                                     % Strain at yield stress in the
element
e(k)=eE(i,j,k)/ey(k);                                % Relative strain of element
    if e(k)<-1                                       % Edge function
    F(k)=-1;
    elseif (e(k)>=-1) && (e(k)<=1)
    F(k)=e(k);
    else
    F(k)=1;
    end
stress(i,j,k)=F(k)*ReHA(k);                          % (MPa) Stress formula

% When element in compression
if stress(i,j,k)>0

%------------------------ Beam Column Buckling ----------------------------%
%--------------------------------------------------------------------------%

vitaE(k)=10^3*(s(k)/tp(k))*sqrt(e(k)*ReHp(k)/E);     % factor βE (slenderness)

if vitaE(k)>1.25 % (m) Effective width of the attached plating
bE(k)=(2.25/vitaE(k)-1.25/vitaE(k)^2)*s(k);
else
bE(k)=s(k);
end

if vitaE(k)>1    % (m) Effective width corrected for relative strain of the attached
plating
bE1(k)=s(k)/vitaE(k);
else
bE1(k)=s(k);
end

ApE(k)=10*bE(k)*tp(k);      % (cm^2) Net sectional area of attached plating width bE
AE(k)=ApE(k)+As(k);         % (cm^2) Net area of stiffeners with attached plating of width
bE
ApEI(k)=10*bE1(k)*tp(k);    % (cm^2) Effective area
AE1(k)=ApEI(k)+As(k);       % (cm^2) Total effective area

% (mm) Distance measured from the NA of the stiffener with attached plate of width bE1 to
the bottom of the attached plate
lpE(k)=(ApEI(k)*tp(k)/2+As(k)*(zsc(k)+tp(k)))/AE1(k);
% (mm) Distance measured  from the neutral axis of the stiffener with attached plate of
width bE1 to the top of the stiffener
lsE(k)=(tp(k)+hw(k)+tf(k))-lpE(k);
```

```
% (cm^4) Moment of inertia of stiffener about the bottom of the plate
IE1(k)=1/12*(tp(k)/10)^3*(bE1(k)*100)+ApEI(k)*(tp(k)/20)^2+IyyS(k)+As(k)*(zsc(k)/10+tp(k)/
10)^2;
% (cm^4) Net moment of inertia of stiffeners with attacjed plating of width bE1
IE(k)=IE1(k)-AE1(k)*(lpE(k)*0.1)^2;

% (MPa) Euler column buckling stress
stressE1(k)=pi^2*E*(IE(k)/(AE(k)*l(k)^2))*10^(-4);
% (MPa) Equivalent minimum yield stress of the considered element
ReHB(k)=(ReHp(k)*ApEI(k)*lpE(k)+ReHs(k)*As(k)*lsE(k))/(ApEI(k)*lpE(k)+As(k)*lsE(k));

if stressE1<=(ReHB(k)/2)*e(k)  % (MPa) Critical stress C1
stressC1(k)=stressE1(k)/e(k);
else
stressC1(k)=ReHB(k)*(1-(ReHB(k)*e(k)/(4*stressE1(k))));
end

% (MPa) Stress formula for beam column buckling
stressCR1(i,j,k)=F(k)*stressC1(k)*(As(k)+ApE(k))/(As(k)+Ap(k));


%-------------------------- Torsional Buckling ----------------------------%
%--------------------------------------------------------------------------%

if vitaE(k)>1.25        % (MPa) Buckling stress of the attached plating
stressCP(k)=(2.25/vitaE(k)-1.25/vitaE(k)^2)*ReHp(k);
else
stressCP(k)=ReHp(k);
end

%%%%%%%%%%%%%%%%%%%%%%%%%%%%%%%%%%%%%%%%%%%%%%%%%%%%%%%%%%%%%%%%%%%%%%%%%%%%%%%
if (L_TYPE ==1)                % L TYPE %

ef(k)=hw(k)+0.5*tf(k);      % (mm) Distance from point C to middle of flange
Aw(k)=hw(k)*tw(k);          % (mm^2) Net web area
Af(k)=As(k)*100*tf(k);      % (mm^2) Net flange area
% (cm^4) Net polar moment of inertia of the stiffener about C
IP(k)=(Aw(k)*((ef(k)-0.5*tf(k))^2)/3+Af(k)*ef(k)^2)*10^(-4);
% (cm^4) Net St. Venant's moment of inertia of the stiffener
IT(k)=((ef(k)-0.5*tf(k))*tw(k)^3/(3*10^4))*(1-0.63*tw(k)/(ef(k)-
0.5*tf(k)))+(bf(k)*tf(k)^3/(3*10^4)*(1-0.6*tf(k)/bf(k)));
% (cm^6) Net sectional moment of inertia of the stiffener about point C
IW(k)=(Af(k)*ef(k)^2*bf(k)^2/(12*10^6))*((Af(k)+2.6*Aw(k))/(Af(k)+Aw(k)));

%%%%%%%%%%%%%%%%%%%%%%%%%%%%%%%%%%%%%%%%%%%%%%%%%%%%%%%%%%%%%%%%%%%%%%%%%%%%%%%
elseif (FLAT_BAR == 1)       % FLAT BAR %

ef(k)=hw(k);                % (mm) Distance from point C to top of web
% (cm^4) Net polar moment of inertia of the stiffener about C
IP(k)=hw(k)^3*tw(k)/(3*10^4);
% (cm^4) Net St. Venant's moment of inertia of the stiffener
IT(k)=hw(k)*tw(k)^3/(3*10^4)*(1-0.63*tw(k)/hw(k));
% (cm^6) Net sectional moment of inertia of the stiffener about point C
IW(k)=hw(k)^3*tw(k)^3/(36*10^6);
end

% Degree of fixation
epsilon(k)=1+((l(k)/pi)^2*10^(-3))/sqrt(IW(k)*((0.75*s(k)/tp(k)^3)+((ef(k)-
0.5*tf(k))/tw(k)^3)));
% (MPa) Euler torsional buckling stress/ Reference stress for torsional buckling
stressE2(k)=E/IP(k)*((epsilon(k)*pi^2*IW(k)*10^2/l(k)^2)+0.385*IT(k));  % Euler torsional
buckling

if (stressE2(k)<=ReHs(k)/2*e(k))      % (MPa) Critical stress
```

```
stressC2(k)=stressE2(k)/e(k);
else
stressC2(k)=ReHs(k)*(1-ReHs(k)*e(k)/(4*stressE2(k)));
end

% (MPa) Stress formula for the flexural-torsional buckling of stiffeners
stressCR2(i,j,k)=F(k)*(As(k)*stressC2(k)+Ap(k)*stressCP(k))/(As(k)+Ap(k));   % stress
formula

%-------- Web local buckling of stiffeners made of flanged profiles -------%
%--------------------------------------------------------------------------%

%%%%%%%%%%%%%%%%%%%%%%%%%%%%%%%%%%%%%%%%%%%%%%%%%%%%%%%%%%%%%%%%%%%%%%%%%%%
if (L_TYPE ==1)              % L TYPE %

vitaW(k)=hw(k)/tw(k)*sqrt(e(k)*ReHs(k)/E);      % Factor βw
if vitaW(k)>=1.25                               % (mm) Effective heigth of the web
hwe(k)=(2.25/vitaW(k)-1.25/vitaW(k)^2)*hw(k);
else
hwe(k)=hw(k);
end

% (MPa) Stress formula for the web local buckling of flanged stiffeners
stressCR3(i,j,k)=F(k)*((10^3*bE(k)*tp(k)*ReHp(k)+(hwe(k)*tw(k)+bf(k)*tf(k))*ReHs(k))/(10^3
*s(k)*tp(k)+hw(k)*tw(k)+bf(k)*tf(k)));


%----------- Web local buckling of stiffeners made of flat bars -----------%
%--------------------------------------------------------------------------%

%%%%%%%%%%%%%%%%%%%%%%%%%%%%%%%%%%%%%%%%%%%%%%%%%%%%%%%%%%%%%%%%%%%%%%%%%%%
elseif (FLAT_BAR == 1)      % FLAT BAR %

stressE4(k)=160000*(tw(k)/hw(k))^2;      % (MPa) Local Euler buckling stress
if (stressE4(k)<=ReHs(k)/2*e(k))         % (MPa) Critical stress
stressC4(k)=stressE4(k)/e(k);
else
stressC4(k)=ReHs(k)*(1-(ReHs(k)*e(k)/(4*stressE4(k))));
end
stressCR3(i,j,k)=F(k)*(Ap(k)*stressCP(k)+As(k)*stressC4(k))/(Ap(k)+As(k)); % stress
formula σcr4

end

stress(i,j,k)=min([stress(i,j,k),stressCR1(i,j,k),stressCR2(i,j,k),stressCR3(i,j,k)]); %
taking the minimum of the stresses ,stressCR4(i,j,k)
end

%%%%%%%%%%%%%%%%%%%%%%%%%%%%%%%%%%%%%%%%%%%%%%%%%%%%%%%%%%%%%%%%%%%%%%%%%%%
else            % STIFFENED PLATE ELEMENT %
%%%%%%%%%%%%%%%%%%%%%%%%%%%%%%%%%%%%%%%%%%%%%%%%%%%%%%%%%%%%%%%%%%%%%%%%%%%

%------------- Elasto-plastic collapse of structural elements -------------%
%--------------------------------------------------------------------------%
% When plate in tension
ey(k)=ReHp(k)/E;                % Strain at yield stress in the element
e(k)=eE(i,j,k)/ey(k);           % Relative strain
if e(k)<-1                      % Edge function
F(k)=-1;
elseif (e(k)>=-1) && (e(k)<=1)
F(k)=e(k);
else
F(k)=1;
end
```

```
stress(i,j,k)=F(k)*ReHp(k);     % (MPa) Stress formula

%---------------------------- Plate buckling -----------------------------%
%-------------------------------------------------------------------------%
% When plate in compression
if stress(i,j,k)>0

vitaE(k)=10^3*s(k)/tp(k)*sqrt(e(k)*ReHp(k)/E); % factor βE
stressCR5_1=ReHp(k)*F(k);
stressCR5_2=F(k)*ReHp(k)*((s(k)/l(k))*(2.25/vitaE(k)-1.25/vitaE(k)^2)+0.1*(1-
(s(k)/l(k)))*(1+(1/vitaE(k)^2))^2);

% (MPa) Stress formula for the bcukling of transversely stiffened panels
stressCR5(i,j,k)=min(abs(stressCR5_1),abs(stressCR5_2));

stress(i,j,k)=stressCR5(i,j,k);

end
end
end

%-------------------------------------------------------------------------%
%% FORCE EQUILIBRIUM %%
%-------------------------------------------------------------------------%
force_over=0;         % Force over neutral axis
force_under=0;        % Force under neutral axis

for k=1:1:size(NoE,1)
if z(k)>zn(i,j)
  force_over=force_over+abs(stress(i,j,k))*A(k)*0.01;     % (N) Force summation for non-
symmetrical elements
else
   force_under=force_under+abs(stress(i,j,k))*A(k)*0.01;    % (N) Force summation for non-
symmetrical elements
end
end

%-------------------------------------------------------------------------%
%% NEUTRAL AXIS POSITION UPDATE %%
%-------------------------------------------------------------------------%
if force_over>force_under && abs(force_over-force_under) >= 10
zn(i,j)=zn(i,j)+0.001;              % updated position of NA to positive
elseif force_over<force_under && abs(force_over-force_under) >= 10
zn(i,j)=zn(i,j)-0.001;              % updated position of NA to negative
end
end

%-------------------------------------------------------------------------%
%% BENDING MOMENT CALCULATION RELATIVE TO CURVATURE %%
%-------------------------------------------------------------------------%
% Hogging Bending Moment
if j==1
Mhog(i)=0;
for k=1:size(NoE,1)
Mhog(i)=Mhog(i)+abs(stress(i,j,k))*A(k)*abs(z(k)-zn(i,j))*0.1;      % (kNm) Correspoding
moment of symmetrical elements
end

% Sagging Bending Moment
else
Msag(i)=0;
for k=1:size(NoE,1)
Msag(i)=Msag(i)-abs(stress(i,j,k))*A(k)*abs(z(k)-zn(i,j))*0.1;      % (kNm) Correspoding
moment of symmetrical elements
end
end
```

```
end

%-------------------------------------------------------------------------%
%% CURVATURE & i UPDATE %%
%-------------------------------------------------------------------------%
% Curvature update
dxhog=0.01*(ReH/E)*(1/(zdeck-zn(i,1)));    % Incremental step of curvature for hogging
dxsag=0.01*(ReH/E)*(1/(zdeck-zn(i,2)));    % Incremental step of curvature for sagging

% i update
if (x(i-1,1)+dxhog<=xFhog) && (x(i-1,2)-dxsag>=xFsag)  % termination control
i=i+1;                      % i update
zn(i,1)=zn(i-1,1);          % zn position update hogging
zn(i,2)=zn(i-1,2);          % zn position update sagging
else
i=i+1;
end
%     if i==15;
%         break
%     end
end

%-------------------------------------------------------------------------%
%% PRINTING RESULTS %%
%-------------------------------------------------------------------------%
% Maximum values of bending moment for sagging & hogging
MAX_Mhog = max(Mhog)
MAX_Msag = min(Msag)
Mhog_column=Mhog';
Msag_column=Msag';
results(:,1)=x(:,1);
results(:,2)=Mhog_column;
dlmwrite('Smith_Results',results);

%-------------------------------------------------------------------------%
%% PLOTTING RESULTS %%
%-------------------------------------------------------------------------%
% Bending Moments
figure (1)
plot(x(:,1),Mhog(:),'b')
hold on
plot(x(:,2),Msag(:),'r')
hold off
grid on
hold on
plot(x(:,1),(210*10^6*IyyNA).*x(:,1),'g');
plot(x(:,2),(210*10^6*IyyNA).*x(:,2),'g');
xlabel('Curvature (1/m)')
ylabel('Bending Moment (kN-m)')
axis([-4*10^(-4) 4*10^(-4) -4*10^6 4*10^6])
title('Bending moment capacity versus curvature')
legend('Bending moment hogging','Bending moment sagging','Location','southeast')

% Stress vs Element height (z axis)
% Hogging Condition
figure(2)               % iteration i = 10
for k=1:(size(NoE,1))
scatter(stress(10,1,k),z(k))
hold on
end
hold off
xlabel('Stress (MPa)')
ylabel('z (m)')
title('Element Stress - Element Height - Hogging (Iteration 10)')

figure(3)               % iteration i = 100
for k=1:(size(NoE,1))
```

```
scatter(stress(100,1,k),z(k))
hold on
end
hold off
xlabel('Stress (MPa)')
ylabel('z (m)')
title('Element Stress - Element Height - Hogging (Iteration 100)')

figure(4)                % iteration i = 200
for k=1:(size(NoE,1))
scatter(stress(200,1,k),z(k))
hold on
end
hold off
xlabel('Stress (MPa)')
ylabel('z (m)')
title('Element Stress - Element Height - Hogging (Iteration 200)')

figure(5)                % iteration i = 300
for k=1:(size(NoE,1))
scatter(stress(300,1,k),z(k))
hold on
end
hold off
xlabel('Stress (MPa)')
ylabel('z (m)')
title('Element Stress - Element Height - Hogging (Iteration 300)')

% Sagging Condition
figure(6)                % iteration i = 10
for k=1:(size(NoE,1))
scatter(stress(10,2,k),z(k))
hold on
end
hold off
xlabel('Stress (MPa)')
ylabel('z (m)')
title('Element Stress - Element Height - Sagging (Iteration 10)')

figure(7)                % iteration i = 100
for k=1:(size(NoE,1))
scatter(stress(100,2,k),z(k))
hold on
end
hold off
xlabel('Stress (MPa)')
ylabel('z (m)')
title('Element Stress - Element Height - Sagging (Iteration 100)')

figure(8)                % iteration i = 200
for k=1:(size(NoE,1))
scatter(stress(200,2,k),z(k))
hold on
end
hold off
xlabel('Stress (MPa)')
ylabel('z (m)')
title('Element Stress - Element Height - Sagging (Iteration 200)')

figure(9)                % iteration i = 300
for k=1:(size(NoE,1))
scatter(stress(300,2,k),z(k))
hold on
end
hold off
xlabel('Stress (MPa)')
ylabel('z (m)')
```

```
title('Element Stress - Element Height - Sagging (Iteration 300)')

% Neutral Axis Position Relative to curvature
figure(10)
plot(x(:,1),zn(2:317,1))
ylabel('Neutral Axis Position, zn (m)')
xlabel('Curvature (1/m)')
title('Neutral Axis Position - Curvature - Hogging')

figure(11)
plot(x(:,2),zn(2:317,2))
ylabel('Neutral Axis Position, zn (m)')
xlabel('Curvature (1/m)')
title('Neutral Axis Position - Curvature - Sagging')

% Load End Shortening Curves

figure(12)                  % Element 30
plot(eE(:,1,30),stress(:,1,30))
hold on
plot(eE(:,2,30),stress(:,2,30))
hold off
ylabel('Stress (MPa)')
xlabel('Strain')
title('Load End Shortening Curves - Element 30')
legend('Hogging','Sagging','Location','southeast')

figure(13)                  % Element 60
plot(eE(:,1,60),stress(:,1,60))
hold on
plot(eE(:,2,60),stress(:,2,60))
hold off
ylabel('Stress (MPa)')
xlabel('Strain')
title('Load End Shortening Curves - Element 60')
legend('Hogging','Sagging','Location','southeast')

figure(14)                  % Element 90
plot(eE(:,1,90),stress(:,1,90))
hold on
plot(eE(:,2,90),stress(:,2,90))
hold off
ylabel('Stress (MPa)')
xlabel('Strain')
title('Load End Shortening Curves - Element 90')
legend('Hogging','Sagging','Location','southeast')

figure(15)
curve1=plotyy(x(:,1),Mhog(:),x(:,1),zn(2:317,1))
grid on
xlabel('Curvature (1/m)')
ylabel(curve1(1),'Bending Moment (kN-m)');
ylabel(curve1(2),'Neutral Axis Position, zn (m)');
title('Bending moment capacity & N.A. position versus curvature')
legend('Bending moment hogging','Neutral Axis Position','Location','southeast')

figure(16)
curve2=plotyy(x(:,2),Msag(:),x(:,2),zn(2:317,2))
grid on
xlabel('Curvature (1/m)')
ylabel(curve2(1),'Bending Moment (kN-m)');
ylabel(curve2(2),'Neutral Axis Position, zn (m)');
title('Bending moment capacity & N.A. position versus curvature')
legend('Bending moment sagging','Neutral Axis Position','Location','southeast')
```

Appendix G: Modified Smith Method (MatLab Code)

```
%%%%% Modified Smith's Method 35000 DWT Oil/Chemical Carrier
%%%%% Ship DATA: LOA = 183m, LBP = 174.5m, Lscant = 172.66m, B = 27.4m,
%%%%% DEPTH = 17.6m, DRAFTdesign = 9.8m, DRAFTscant = 11m, CB = 0.828, V = 14.2kn
clear all
close all
clc

%-------------------------------------------------------------------------%
%% INPUT DATA %%
%-------------------------------------------------------------------------%
% Geometry
zdeck=17.6;        % (m) Deck position relative to base line
IyyNA=139.0749;    % (m^4) Moment of inertia about neutral axis
ZB=19.06;          % Section Modulus at bottom in m^3
ZD=13.49;          % Section Modulus at deck in m^3

% Material
E=210000;          % (MPa) Young's Modulus (MPa)
ReH=235;           % (MPa) Minimum yield stress

%-------------------------------------------------------------------------%
%% INPUT DATA - EXCEL FILE READING FOR ELEMENTS %%
%-------------------------------------------------------------------------%
% EXCEL file contains the data of midship elements
% ALL elements of section are inserted
% Total number of elements = 223
[num,txt]=xlsread('ShipElements.xlsx'); % Reading Excel file
NoE=num(:,1);                           % Number of element
A=num(:,16);                            % (cm^2) element's total area
z=num(:,18);                            % (m) Distance from BL to element's CG
y=num(:,19);                            % (m) Distance from Middle axis to element's CG

%-------------------------------------------------------------------------%
%% INPUT DATA - EXCEL FILE READING FOR LOAD END SHORTENING CURVES %%
%-------------------------------------------------------------------------%
% Tension Curves
strain_tension=xlsread('Curves_Tension_500.xlsx','strain','A2:HO10');
stress_tension_Pa=xlsread('Curves_Tension_500.xlsx','stress','A2:HO10');
strain_tension(isnan(strain_tension))=0;
stress_tension_Pa(isnan(stress_tension_Pa))=0;
stress_tension=stress_tension_Pa*10^(-6);

% Compression Curves
strain_compression=xlsread('Curves_Compression_500.xlsx','Strain','A2:HO179');
stress_compression_Pa=xlsread('Curves_Compression_500.xlsx','Stress','A2:HO179');
strain_compression(isnan(strain_compression))=0;
stress_compression_Pa(isnan(stress_compression_Pa))=0;
stress_compression=stress_compression_Pa*10^(-6);

%-------------------------------------------------------------------------%
%% INITIALIZATION OF PARAMETERS & PRIMARY CAlCULATIONS %%
%-------------------------------------------------------------------------%
% Initializations
i = 2;
x(1,1)=0;               % First curvature step for hooging
x(1,2)=0;               % First curvature step for sagging
Mhog(1)=0;              % Initialization of hogging moment
Msag(1)=0;              % Initialization of sagging moment

% Primary Calculations
My1=10^3*ReH*ZB;                % (kNm) Yield moment bottom
My2=10^3*ReH*ZD;                % (kNm) Yield moment deck
My=min(My1,My2);                % (kNm) Yield moment, lesser of the values My1 & My2
```

```
xFhog=0.006*My/(E*IyyNA);   % Curvature's critical value of termination for hogging
xFsag=-0.006*My/(E*IyyNA);  % Curvature's critical value of termination for sagging
dxhog=0.01*(ReH/E)*(1/(zdeck-7.29));   % Initial incremental step of curvature for hogging
dxsag=0.01*(ReH/E)*(1/(zdeck-7.29));   % Initial incremental step of curvature for sagging

% Definition of Geometry Parameters
A1=0;A2=0;A3=0;A4=0;A5=0;A6=0;
for k=1:1:size(NoE,1)
    A1=A1+A(k);
    A2=A2+A(k)*z(k);
    A3=A3+A(k)*y(k);
end
z_G=A2/A1;y_G=A3/A1;
for k=1:1:size(NoE,1)
    A4=A4+A(k)*(y(k)-y_G)^2;            % I_z0
    A5=A5+A(k)*(z(k)-z_G)^2;            % I_y0
    A6=A6+A(k)*(y(k)-y_G)*(z(k)-z_G);   % I_y0z0
end

% Extra Initialization for Parameters
tan_a(i,1)=A6/A4;
tan_a(i,2)=A6/A4;
z_CL(i,1)=z_G-y_G*tan_a(i,1);
z_CL(i,2)=z_G-y_G*tan_a(i,2);
a(i,1)=atan(tan_a(i,1));
a(i,2)=atan(tan_a(i,2));

%-------------------------------------------------------------------------%
%% ITERATIVE RPOCESS INITIALIZATION %%
%-------------------------------------------------------------------------%
% While loop for curvature (update/termination)
while (x(i-1,1)+dxhog<=xFhog) && (x(i-1,2)-dxsag>=xFsag)
    % Curvature increment and for loop for the 2 states (hogging, sagging)
    for j=1:2                   % j=1 refers to hogging, j=2 refers to sagging
    if j==1 && (x(i-1,1)+dxhog<=xFhog)
    x(i,j)=x(i-1,j)+dxhog;      % Curvature increment for hogging
    elseif j==2 && (x(i-1,2)-dxsag>=xFsag)
    x(i,j)=x(i-1,j)-dxsag ;     % Curvature increment for sagging
    else
        if j==1
        j=2;
        x(i,j)=x(i-1,j)-dxsag;
        else
        break
        end
    end

% Initial values for moments and forces over & under the NA
M1=10000;
M2=0;
force_over=10000;
force_under=0;

% While loop for moment equilibrium (termination)
while abs(force_over-force_under)>=1000 && abs(abs(M1)-abs(M2))>=100
% While loop for force equilibrium (termination)
while abs(force_over-force_under)>=1000

    % Calculation for each element the corresponding strain
    for k=1:1:size(NoE,1)
    zn(i,j,k)=z_CL(i,j)+y(k)*tan_a(i,j);
    eE(i,j,k)=-x(i,j)*(z(k)-zn(i,j,k))*cos(a(i,j)); % (-) for tension, (+) for compression
    end

%-------------------------------------------------------------------------%
%% STRESS - STRAIN CURVE FOR EACH STRUCTURAL ELEMENT %%
```

```
%-------------------------------------------------------------------------%
for k=1:1:size(NoE,1)
    if eE(i,j,k)<0  % tension
    stress(i,j,k)=-
interp1(strain_tension(:,k),stress_tension(:,k),abs(eE(i,j,k)),'linear');
    elseif eE(i,j,k)>0     % compression

stress(i,j,k)=interp1(strain_compression(:,k),stress_compression(:,k),abs(eE(i,j,k)),'line
ar');
    elseif eE(i,j,k)==0
    stress(i,j,k)=0;
    end

end

%-------------------------------------------------------------------------%
%% FORCE EQUILIBRIUM %%
%-------------------------------------------------------------------------%
force_over=0;         % Force over neutral axis
force_under=0;        % Force under neutral axis

for k=1:1:size(NoE,1)
if z(k)>zn(i,j,k)
  force_over=force_over+abs(stress(i,j,k))*A(k)*0.01;     % (N) Force summation for non-
symmetrical elements
else
   force_under=force_under+abs(stress(i,j,k))*A(k)*0.01;    % (N) Force summation for non-
symmetrical elements
end
end

%-------------------------------------------------------------------------%
%% NEUTRAL AXIS VERTICAL POSITION UPDATE %%
%-------------------------------------------------------------------------%
if force_over>force_under && abs(force_over-force_under) >= 1000
z_CL(i,j)=z_CL(i,j)+0.01;              % updated position of NA to positive
elseif force_over<force_under && abs(force_over-force_under) >= 1000
z_CL(i,j)=z_CL(i,j)-0.01;              % updated position of NA to negative
end
end

%-------------------------------------------------------------------------%
% EXTRA CONDITION FOR BENDING MOMENT %
%-------------------------------------------------------------------------%
    M1=0;   % initialization of moments
    M2=0;

    for k=1:1:size(NoE,1)
        if y(k)<=0       %%% AYTO NA TSEKARW %%%
               M1=M1+stress(k)*(y(k)-0)*A(k)*10^(-2); %N*m
        else
               M2=M2+stress(k)*(y(k)-0)*A(k)*10^(-2); %N*m
        end
    end
        if abs(M1)>abs(M2) & abs(abs(M1)-abs(M2))>=100 & M1<0 & j==1 % hogging
            a(i,j)=a(i,j)+10^(-5);
        elseif abs(M1)>abs(M2) & abs(abs(M1)-abs(M2))>=100 & M1>0  & j==1 % hogging
            a(i,j)=a(i,j)-10^(-5);
        elseif abs(M2)>abs(M1) & abs(abs(M1)-abs(M2))>=100 & M2<0 & j==1 %hogging
            a(i,j)=a(i,j)+10^(-5);
        elseif abs(M2)>abs(M1) & abs(abs(M1)-abs(M2))>=100 & M2>0 & j==1 %hogging
            a(i,j)=a(i,j)-10^(-5);
        elseif abs(M1)>abs(M2) & abs(abs(M1)-abs(M2))>=100 & M1<0 & j==2  % sagging
            a(i,j)=a(i,j)-10^(-5);
         elseif abs(M1)>abs(M2) & abs(abs(M1)-abs(M2))>=100 & M1>0 & j==2  % sagging
            a(i,j)=a(i,j)+10^(-5);
        elseif abs(M2)>abs(M1) & abs(abs(M1)-abs(M2))>=100 & M2<0 & j==2 %sagging
```

```
            a(i,j)=a(i,j)-10^(-5);
        elseif abs(M2)>abs(M1) & abs(abs(M1)-abs(M2))>=100 & M2>0 & j==2 %sagging
            a(i,j)=a(i,j)+10^(-5);
        end
        tan_a(i,j)=tan(a(i,j));
end

%-------------------------------------------------------------------------%
%% BENDING MOMENT CALCULATION RELATIVE TO CURVATURE %%
%-------------------------------------------------------------------------%
% Hogging Bending Moment
if j==1
Mhog(i)=0;
for k=1:size(NoE,1)
Mhog(i)=Mhog(i)+abs(stress(i,j,k))*A(k)*abs(z(k)-zn(i,j))*0.1;      % (kNm) Correspoding
moment of symmetrical elements
end

% Sagging Bending Moment
else
Msag(i)=0;
for k=1:size(NoE,1)
Msag(i)=Msag(i)-abs(stress(i,j,k))*A(k)*abs(z(k)-zn(i,j))*0.1;      % (kNm) Correspoding
moment of symmetrical elements
end
end
end

%-------------------------------------------------------------------------%
%% CURVATURE & i UPDATE %%
%-------------------------------------------------------------------------%
% Curvature update
dxhog=0.01*(ReH/E)*(1/(zdeck-z_CL(i,1)));    % Incremental step of curvature for hogging
dxsag=0.01*(ReH/E)*(1/(zdeck-z_CL(i,2)));    % Incremental step of curvature for sagging

% i update
if (x(i-1,1)+dxhog<=xFhog) && (x(i-1,2)-dxsag>=xFsag)  % termination control
i=i+1;                      % i update
tan_a(i,1)=tan_a(i-1,1);
tan_a(i,2)=tan_a(i-1,2);
a(i,1)=a(i-1,1);
a(i,2)=a(i-1,2);
z_CL(i,1)=z_CL(i-1,1);        % zn position update hogging
z_CL(i,2)=z_CL(i-1,2);        % zn position update sagging
else
i=i+1;
end
    end

%-------------------------------------------------------------------------%
%% PRINTING RESULTS %%
%-------------------------------------------------------------------------%
% Maximum values of bending moment for sagging & hogging
MAX_Mhog = max(Mhog)
MAX_Msag = min(Msag)
Mhog_col = Mhog';
Msag_col = Msag';

%-------------------------------------------------------------------------%
%% PLOTTING RESULTS %%
%-------------------------------------------------------------------------%
% Bending Moment - Curvature
figure (1)
plot(x(:,1),Mhog(:),'b')
hold on
plot(x(:,2),Msag(:),'r')
hold off
```

```
grid on
xlabel('Curvature (1/m)')
ylabel('Bending Moment (kN-m)')
axis([-8*10^(-4) 8*10^(-4) -4*10^6 4*10^6])
title('Bending moment capacity versus curvature')
legend('Bending moment hogging','Bending moment sagging','Location','southeast')

% Neutral axis position update and angle (a) of neutral axis
figure(2)
plot(x(:,1),z_CL(2:636,1))
hold on
plot(x(:,2),z_CL(2:636,2))
hold off
xlabel('Curvature (1/m)')
ylabel('Neutral Axis Position (m from B.L.)')
title('Curvature - Neutral Axis Position')
legend('Hogging Condition','Sagging Condition','Location','southeast')

figure(3)
plot(x(:,1),a(2:636,1))
hold on
plot(x(:,2),a(2:636,2))
hold off
xlabel('Curvature (1/m)')
ylabel('Angle (a) of Neutral Axis (deg)')
title('Curvature - Angle (a) of Neutral Axis')
legend('Hogging Condition','Sagging Condition','Location','southeast')

% Stresses relative to element height
% Hogging Condition
figure(4)                   % iteration 10
for k=1:size(NoE,1)
scatter(stress(10,1,k),z(k))
hold on
end
hold off
xlabel('Stress (MPa)')
ylabel('Element Height (m from B.L.)')
title('Stress - Element Height - Hogging (Iteration 10)')

figure(5)                   % iteration 200
for k=1:size(NoE,1)
scatter(stress(200,1,k),z(k))
hold on
end
hold off
xlabel('Stress (MPa)')
ylabel('Element Height (m from B.L.)')
title('Stress - Element Height - Hogging (Iteration 200)')

figure(6)                   % iteration 400
for k=1:size(NoE,1)
scatter(stress(400,1,k),z(k))
hold on
end
hold off
xlabel('Stress (MPa)')
ylabel('Element Height (m from B.L.)')
title('Stress - Element Height - Hogging (Iteration 400)')

figure(7)                   % iteration 600
for k=1:size(NoE,1)
scatter(stress(600,1,k),z(k))
hold on
end
hold off
xlabel('Stress (MPa)')
```

```
ylabel('Element Height (m from B.L.)')
title('Stress - Element Height - Hogging (Iteration 600)')
% Sagging Condition
figure(8)                % iteration 10
for k=1:size(NoE,1)
scatter(stress(10,2,k),z(k))
hold on
end
hold off
xlabel('Stress (MPa)')
ylabel('Element Height (m from B.L.)')
title('Stress - Element Height - Sagging (Iteration 10)')

figure(9)                % iteration 200
for k=1:size(NoE,1)
scatter(stress(200,2,k),z(k))
hold on
end
hold off
xlabel('Stress (MPa)')
ylabel('Element Height (m from B.L.)')
title('Stress - Element Height - Sagging (Iteration 200)')

figure(10)                % iteration 400
for k=1:size(NoE,1)
scatter(stress(400,2,k),z(k))
hold on
end
hold off
xlabel('Stress (MPa)')
ylabel('Element Height (m from B.L.)')
title('Stress - Element Height - Sagging (Iteration 400)')

figure(11)                % iteration 600
for k=1:size(NoE,1)
scatter(stress(600,2,k),z(k))
hold on
end
hold off
xlabel('Stress (MPa)')
ylabel('Element Height (m from B.L.)')
title('Stress - Element Height - Sagging (Iteration 600)')

% Load End Shortening Curves for elements 10,30,60

figure(12)              % Element 10
plot(eE(:,1,10),stress(:,1,10));
hold on
plot(eE(:,2,10),stress(:,2,10));
hold off
ylabel('Stress (MPa)')
xlabel('Strain')
title('Load End Shortening Curves - Element 10')
legend('Hogging','Sagging','Location','southeast')

figure(13)              % Element 30
plot(eE(:,1,30),stress(:,1,30));
hold on
plot(eE(:,2,30),stress(:,2,30));
hold off
ylabel('Stress (MPa)')
xlabel('Strain')
title('Load End Shortening Curves - Element 30')
legend('Hogging','Sagging','Location','southeast')

figure(14)              % Element 60
```

```
plot(eE(:,1,60),stress(:,1,60));
hold on
plot(eE(:,2,60),stress(:,2,60));
hold off
ylabel('Stress (MPa)')
xlabel('Strain')
title('Load End Shortening Curves - Element 60')
legend('Hogging','Sagging','Location','southeast')

figure(15)              % Element 90
plot(eE(:,1,90),stress(:,1,90));
hold on
plot(eE(:,2,90),stress(:,2,90));
hold off
ylabel('Stress (MPa)')
xlabel('Strain')
title('Load End Shortening Curves - Element 90')
legend('Hogging','Sagging','Location','southeast')

figure(16)
plot(x(:,1),a(2:636,1))
hold on
plot(x(:,2),a(2:636,2))
hold on
scatter(x(:,1),a(2:636,1))
hold on
scatter(x(:,2),a(2:636,2))
hold off
xlabel('Curvature (1/m)')
ylabel('Angle (a) of Neutral Axis (deg)')
title('Curvature - Angle (a) of Neutral Axis')
legend('Hogging Condition','Sagging Condition','Location','southeast')

figure(17)
curve1=plotyy(x(:,1),Mhog(:),x(:,1),z_CL(2:636,1))
xlabel('Curvature (1/m)')
ylabel(curve1(1),'Bending Moment (kN-m)')
ylabel(curve1(2),'Neutral Axis Position (m from B.L.)')
title('Bending hogging moment capacity & neutral axis position versus curvature')
legend('Bending Moment Hogging Condition','Neutral Axis Position Hogging
Condition','Location','southeast')

figure(18)
curve2=plotyy(x(:,2),Msag(:),x(:,2),z_CL(2:636,2))
xlabel('Curvature (1/m)')
ylabel(curve2(1),'Bending Moment (kN-m)')
ylabel(curve2(2),'Neutral Axis Position (m from B.L.)')
title('Bending sagging moment capacity & neutral axis position versus curvature')
legend('Bending Moment Sagging Condition','Neutral Axis Position Sagging
Condition','Location','northwest')

figure(19)
curve1=plotyy(x(:,1),Mhog(:),x(:,1),a(2:636,1))
xlabel('Curvature (1/m)')
ylabel(curve1(1),'Bending Moment (kN-m)')
ylabel(curve1(2),'Angle (a) of Neutral Axis (deg)')
title('Bending hogging moment capacity & neutral axis angle versus curvature')
legend('Bending Moment Hogging Condition','Neutral Axis Angle Hogging
Condition','Location','southeast')
figure(20)
curve2=plotyy(x(:,2),Msag(:),x(:,2),a(2:636,2))
xlabel('Curvature (1/m)')
ylabel(curve2(1),'Bending Moment (kN-m)')
ylabel(curve2(2),'Angle (a) of Neutral Axis (deg)')
title('Bending sagging moment capacity & neutral axis angle versus curvature')
legend('Bending Moment Sagging Condition','Neutral Axis Angle Sagging
Condition','Location','northwest')
```